Evolution of multi-arc accretion systems: A case study from the southern Beishan Orogen, Central Asian Orogenic Belt, NW China

by

Tong Hong

A thesis

presented to the University of Waterloo

in fulfillment of the

thesis requirement for the degree of

Doctor in Philosophy

in

Earth Sciences

Waterloo, Ontario, Canada, 2023

© Tong Hong 2023

Examining Committee Membership

The following served on the Examining Committee for this thesis. The decision of the Examining Committee is by majority vote.

External Examiner	MIN SUN Professor University of Hong Kong
Supervisor(s)	CEES VAN STAAL Adjunct Professor Earth and Environmental Sciences
	SHOUFA LIN Professor Earth and Environmental Sciences
Internal Member	CHRIS YAKYMCHUK Associate Professor Earth and Environmental Sciences
Internal Member	DON DAVIS Adjunct Professor Earth and Environmental Sciences
Internal-external Member	BRIAN KENDALL Associate Professor Earth and Environmental Sciences
Other Member(s)	N/A

Author's Declaration

This thesis consists of material all of which I authored or co-authored: see Statement of Contributions included in the thesis. This is a true copy of the thesis, including any required final revisions, as accepted by my examiners.

I understand that my thesis may be made electronically available to the public.

Statement of Contributions

Tong Hong was the sole author for Chapters 1, 2, and 5 which were written under the supervision of Drs. Cees van Staal and Shoufa Lin and were not written for publication.

Chapters of this thesis along with a related map have been submitted for publication. Chapter 2 has been condensed into a brief perspective and published in the National Science Review, Volume 10, Issue 2, as part of a special topic on Altaids, continental growth, and metallogeny. The remaining part of Chapter 2, along with the entire mapping work, has published as part of a map by the China Geological Survey at a scale of 1:25,000. Chapter 3 has been published in the Geological Society, London, Special Publication, Volume 542, a special publication on supercontinents, orogenesis and magmatism. Chapter 4 is currently in preparation for publication and will be submitted soon.

This thesis consists in part of three manuscripts written for publication. Exceptions to sole authorship of material are as follows:

Research presented in Chapters 2:

Tong Hong: Investigation, Writing–Original Draft, Writing–Review and Editing. Gabrial S. Santos: Investigation. Cees R. van Staal: Supervision, Investigation, Writing–Review and Editing. Wenhua Ji: Investigation, Project Administration, Funding Acquisition. Shoufa Lin: Investigation, Supervision, Conceptualization, Writing–Review & Editing, Project Administration, Funding Acquisition.

Citations:

Hong, T., Santos, G.S., van Staal, C., Ji, W.H., Lin, S., Mapping uncovered a multi-phase arc–back-arc system in the southern Beishan during the Permian, National Science Review, Volume 10, Issue 2, February 2023, nwac204, DOI: 10.1093/nsr/nwac204.

Research presented in Chapters 3:

Tong Hong: conceptualization, investigation, methodology, visualization, writing – original draft, writing – review & editing. Cees R. van Staal: conceptualization, investigation, methodology, co-supervision, writing – review & editing, funding acquisition. Shoufa Lin: conceptualization, investigation, methodology, co-supervision, writing – review & editing, project administration, funding acquisition. Gabriel S. Santos: conceptualization, investigation, methodology, writing – review & editing. Kai Wang: funding acquisition, investigation, project administration.

Citations:

Hong, T., van Staal, C., Lin, S., Santos, G.S., Wang, K. (2023). Evolving Permian magmatism associated with arc migration in the southern Beishan Orogenic Collage, Central Asian orogenic belt, NW China. Geological Society, London, Special Publications. DOI: 10.1144/SP542-2022-346.

Research presented in Chapter 4:

Tong Hong: Conceptualization, Investigation – Fieldwork & Sampling, Methodology, Formal analyses, Data curation and Interpretation, Visualization, Writing - Original Draft, Writing - Review & Editing. Cees R. van Staal: Conceptualization, Investigation – Fieldwork, Sampling & Mapping, Data Interpretation, Writing - Review & Editing, Supervision. Shoufa Lin: Conceptualization, Investigation – Fieldwork & Sampling, Data Interpretation, Writing - Review & Editing, Supervision, Project administration, Funding acquisition. Don Davis: Methodology, Data Interpretation, Writing – Review & Editing. Gabriel Santos: Data Interpretation, Writing - Review & Editing. Chris Yakymchuk: Resources - Laboratory Instrumentation & Analyses, Writing – Review & Editing. Chris McFarlane: Resources - Laboratory Instrumentation & Analyses, Writing – Review. Kai Wang: Project administration, Funding acquisition.

Research presented in the geological mapping:

Geological mapping and interpretation by Cees R. van Staal, Tong Hong, Shoufa Lin, and Wenhua Ji. Structural analysis and interpretation by Cees R. van Staal, Tong Hong and Shoufa Lin. GIS compilation and data curation by Tong Hong. Project administration and funding acquisition by Wenhua Ji and Shoufa Lin. Cartography by Étienne Girard, Tong Hong, Shuping Wang and Bo Yang. Field assistance by Changcheng Li, Chaoyang Wang, Jia Hongyuan, Jiangyu Li, Kai Wang, Lamei Feng, Lingchao He, Meiling Wu, Tianyu Ma, Xiqin Chen, Yanfei Xia.

Citations:

van Staal, C.R., Hong, T., Lin, S., Ji, W.H, 2021. Bedrock Geological Map of the Baidunzi-Heishankou Area, Guazhou, Gansu, China, scale 1:25,000: China Geological Survey, DOI: 10.35080/data.C.2021.P01.

Geochronology and geochemistry analyses presented in the Chapters 3 and 4:

Geochronology and geochemistry samples were collected during fieldwork by Cees van Staal, Shoufa Lin, and Tong Hong. Sample curation and documentation were conducted by Tong

Hong. For the geochronology SHRIMP samples mentioned in chapters 3 and 4, laboratory work was conducted in three rounds. The first round involved samples H3009, H3090A, S85, V1082, V1096, V1097, V1106, V1109, V163, V176, V233, V266, and V385. The analysis for these samples was carried out by Tong Hong, with assistance from Dr. Lamei Feng (Hefei University of Technology) in January 2018. Their work was supervised by Drs. Shoujie Liu and Peng Ren at the Beijing SHRIMP center. Initial data processing was performed by Dr. Shoujie Liu. The second round comprised samples H3025, V161, and V1109. Analysis for these samples was conducted by Tong Hong, with assistance from Chaoyang Wang and Dr. Lamei Feng in September 2018. Dr. Chunyan Dong from the Beijing SHRIMP center supervised the analysis lab work and performed the initial data processing. The third round involved samples H3345, S5136, S5137, S5143, S5145, S5146, V1384, and V1385. Analysis for these samples was conducted by graduate students in March 2019, under the supervision of Drs. Peizhi Wang and Zhemin Bao from the Beijing SHRIMP center, who also performed the initial data processing work. Oxygen analyses were conducted at Beijing SHRIMP center by Dr. Peizhi Wang. Hf isotope analysis and data processing were performed by Tong Hong at Nanjing FocuMS Technology Co. Ltd, under supervision of Dr. Liang Li.

Drs. Don Davis and Chris Yakymchuk of University of Toronto and University of Waterloo assisted Tong Hong to conduct and provide laboratory results for all LA-ICP-MS detrital zircon geochronology analyses presented. Dr. Chris McFarlane of University of New Brunswick conducted and provided laboratory results for LA-ICP-MS titanite geochronology analyses presented in Chapter Four.

As lead author of these four chapters, I was responsible for contributing to conceptualizing study design, carrying out data collection and analysis, and drafting and submitting manuscripts. My coauthors provided guidance during each step of the research and provided feedback on draft manuscripts.

Abstract

The Central Asian Orogenic Belt (CAOB) is characterized as an accretionary orogen, evolved for ca. 800 m.y from late Mesoproterozoic to early Mesozoic. Its terminal collision and accretion generally commenced in the west and terminated in the east, creating the Tien Shan suture and Solonker suture, respectively. The Beishan Orogen is a southern-central segment of the Central Asian Orogenic Belt, located in Northwest China. It connects the two sutures and contains some of the youngest ophiolitic complexes, arc terranes, and sedimentary basins in the CAOB. Hence, investigations of the southern Beishan Orogen can contribute to correlating the geology on both sides and establishing an integrated tectonic history of the Paleo-Asian Ocean's closure.

Through detailed mapping at 1:25000 scale in southern Beishan, five distinctive tectono-stratigraphic packages have been identified, from south to north, including the Shiyaozi Complex, the Baidunzi Complex, the Ganquan Complex, the Liuyuan Complex, and a cover sequence forming the Heishankou Basin. The Baidunzi Complex comprises a mixture of sheared and transposed metasedimentary and syn-kinematic meta-plutonic rocks, ranging from greenschist to amphibolite facies. The metasedimentary sequences contain Carboniferous-Permian marble and meta-calcareous clastic rocks, which were intruded by syn-tectonic arc magmatic rocks (Baidunzi Intrusive Suite). Collectively these rocks represent a continental arc setting. A massive sheet of bedded quartzite in this complex, displaying no age signatures younger than 1.0 Ga, stands as the most probable candidate for Precambrian basement, with an inferred affinity to the Tarim Craton.

The Baidunzi Complex was overthrusted by the Ganquan Complex, which primarily consists of two sequences separated by unconformities and thrust faults. The lower sequence exhibits minimal reworking and lacks continent-derived materials in its stratigraphy. U-Pb zircon dating of this sequence yielded ages ranging from 295 to 285 Ma, without zircon inheritance. In contrast, the upper

sequence is dominated by epiclastic sedimentary rocks, structurally and/or unconformably overlying rocks of the lower sequence. Both sequences display geochemical characteristics typical of island arcs, with an increase of εHf values over time. They correlate temporally and tectonically with the adjacent back-arc ophiolitic rocks within the Liuyuan Complex, an ophiolite mélange formed in a backarc setting. Together they represent an arc-backarc system, with arc-trench migration leading to the progressive incorporation of juvenile components in the source.

A cover sequence forming a Permian foreland basin, with typical fold-and-thrust style deformation, developed unconformably on the Ganquan and Liuyuan Complexes. From bottom to top, it consists of black shale, an unconformably overlying flysch-like sedimentary unit, and a syn-orogenic conglomerate with clasts of rocks from all the underlying sequences. The sedimentary record and structural analyses of this basin suggest south-verging deformation, associated with a collisional event involving the Ganquan arc-Liuyuan Backarc system over the Baidunzi Complex. Subsequently, this thrust-and-fold belt experienced a phase of north-verging deformation, aligning with the amalgamation of the Shiyaozi Complex from the southernmost region toward the Baidunzi Complex.

The overall field relationships record a transition from a passive to an active margin (Baidunzi Complex), formation and accretion of a relatively juvenile arc, and collision during the Permian.

Acknowledgements

I would like to acknowledge Dr. Shoufa Lin and the China Geological Survey for providing me the opportunity to pursue the PhD program and engage in the mapping project. I want to express my deepest appreciation to my co-supervisor, Dr. Cees van Staal, whose role as my mentor and educator has been truly influential. His unwavering support, guidance, patience, integrity, and vast knowledge have been instrumental in the successful completion of this project. His presence in the field, coupled with his profound insights and expertise, significantly contributed to its accomplishment.

The 6-year fast-tracked PhD program has been an incredible adventure and an immense challenge. I owe a tremendous debt of gratitude to our Beishan gang—Dr. Gabriel dos Santos, Jordy de Vires, and Jiangyu Li. They are more than just colleagues; they are my cherished friends and nearly family. Their unwavering presence by my side, both in and out of the field, has been a constant source of support, inspiration, and encouragement throughout these years.

My deepest regards go to my committee members – Drs. Don W. Davis and Chris Yakymchuk for sharing extensive comments and critical insights on my thesis. I would also like to thank the rest instructors and professors – Drs. Jen Parks, Changcheng Li, John Johnson, and Brian Kendall from the Dept. of Environmental and Earth Sciences at University of Waterloo, who are greatly acknowledged for sharing their passion and knowledge on geology with me. Many thanks go to my beloved grad crew – Ameerah, Nanqin, Quinn, Ludo, Grant, Jill, Zach, Sophie, Katia, Alex, Carson, Ivan, Boyao, Natascia, and Sebastien – for creating a lovely and dynamic atmosphere on campus and gave me the best school memories.

Finally, I am deeply grateful to my family – my mother Xinli, my sister Evie, and my partner Miguel for their unwavering patience, understanding, and support throughout my journey – to celebrate my successes and stand by me during my hardships. I owe the greatest debt of gratitude to my late father, Dan Hong, whose love and support made my comfortable and joyful life in Canada possible. His encouragement and belief in me were a constant source of inspiration and motivation, and I dedicate this thesis to his memory.

Table of Contents

Examining Committee Membership ii
Author's Declaration iii
Statement of Contributions iv
Abstract vii
Acknowledgements ix
List of Figures xiii
Chapter 1 Introduction 1
1.1 Introduction 1
1.2 The Central Asian Orogenic Belt (CAOB) 2
1.3 The Beishan Orogen 5
1.4 Thesis objectives 7
1.5 Organization of the thesis 8
1.6 Figures and captions 10
Chapter 2 Detailed geological mapping uncovered complex arc-arc accretions and progressive tectonic stacking during Permian to Triassic in the southern Beishan Orogen, southern Central Asian Orogenic Belt 13
2.1 Introduction 13
2.2 Geological background 14
2.3 Tectono-stratigraphic divisions uncovered by bedrock mapping 16
2.3.1 Structural panel division and deformation history 16
2.3.2 The Shiyaozi Complex 18
2.3.3 The Baidunzi Complex 19
2.3.4 The Ganquan Complex 21
2.3.5 Liuyuan Complex 23
2.3.6 The Heishankou Basin 24
2.4 Discussion 25
2.4.1 Reconstructions of regional Upper Paleozoic stratigraphy 25
2.4.2 Formation of the Heishankou Basin and its tectonic implications 30
2.5 Conclusions 33

2.6 References 34
2.7 Figures and captions 37
Chapter 3 Evolving Permian magmatism associated with arc migration in the southern Beishan Orogenic Collage, Central Asian orogenic belt, NW China 50
3.1 Abstract 50
3.2 Introduction 50
3.3 Geological background 52
3.3.1 Central Asian Orogenic Belt and Beishan orogen 52
3.3.2 Geological nomenclature and regional geological context 53
3.4 Results of petrography, field relationships, and geochronology 56
3.4.1 Volcano-plutonic lithodeme 57
3.4.2 Red bed lithodeme 58
3.4.3 Volcano-sedimentary lithodeme 59
3.5 Results of whole-rock geochemistry 60
3.5.1 Major and trace elements 61
3.5.2 Tectonic discriminations 63
3.6 Results of Hf-O isotope systematics 65
3.7 Discussion 67
3.7.1 Arc-like geochemistry of the Ganquan Complex 67
3.7.2 Tectonic transitions from the lower to upper sequence 70
3.7.3 Regional tectonic implications 72
3.8 Conclusions 75
3.9 References 76
3.10 Figures and captions 84
Chapter 4 A Permian transpressional continental arc and arc-arc collision recorded in the Baidunzi Complex, southern Central Asian orogenic belt, NW China 98
4.1 Abstract 98
4.2 Introduction 99
4.3 Regional geological context 100
4.3.1 Dunhuang Terrane 100
4.3.2 Terranes in southern Beishan Orogen 101

4.4 Results of lithology, field relations, and geochronology 103
4.4.1 Old basement rock units 104
4.4.2 Younger meta-sedimentary strata 105
4.4.3 Baidunzi Intrusive Suite 107
4.4.4 Late Intrusive Suite 113
4.5 Geochemistry 114
4.5.1 Major and trace element compositions 114
4.5.2 Geochemical classification and tectonic discrimination 117
4.5.3 Zircon Hf isotopes 118
4.6 Discussion 120
4.6.1 Evolution and tectonic nature of the Baidunzi basement rocks 120
4.6.2 Late Carboniferous to Early Permian geology of Baidunzi Complex 123
4.6.3 Regional geological model and tectonic implications 124
4.6.4 Proterozoic to Paleozoic paleogeographic constraints 128
4.7 Conclusion 131
4.8 References 132
4.9 Figures and captions 141
Chapter 5 : Summary of Conclusions 158
5.1 Summary 158
5.1.1 Geology and tectonics of the Ganquan Complex 158
5.1.2 Geology and tectonics of the Baidunzi Complex 159
5.1.3 Structural amalgamation and syn-tectonic formation of Heishankou Basin 161
5.2 Future work 162
References 166
Appendix 170

List of Figures

Figure 1-1: Satellite image and corresponding generalized map of the Central Asian Orogenic Belt. 10
Figure 1-2: Tectonic overview and division of the Central Asian Orogenic Belt and adjacent cratons.. 11
Figure 1-3: Tectonostratigraphic terrane map of the Beishan orogenic collage. 12
Figure 2-1: Tectonic frameworks showing location of the Liuyuan BOC.....37
Figure 2-2: Simplified geological map and related cross sections of the Baidunzi area. 38
Figure 2-3: Simplified geological map of central part of the Liuyuan Complex and adjacent rocks of Huaniushan-Shibanshan terrane. 41
Figure 2-4: Reconstruction of regional stratigraphy in the Liuyuan BOC.....42
Figure 2-5: Stereonet plots of foliation and lineation data in shear zones with related fault planes.....43
Figure 2-6: Field photos from Baidunzi Complex showing D1 deformation. 45
Figure 2-7: Field photos along fault zones bounded by Panel 1, 2 and 3. 46
Figure 2-8: Field photos of outcrops in the Heishankou Basin. 47
Figure 2-9: Structures in the Heishankou Basin. 48
Figure 2-10: Fold-and-thrust style deformation in the Heishankou Basin.....49
Figure 3-1: Tectonic elements of the Central Asian Orogenic Belt, Beishan Orogen and adjacent areas.....84
Figure 3-2: Geological map of the Ganquan Complex and surrounding area. 85
Figure 3-3: Field relations and lithology of Ganquan Complex and surrounding tectonic constituents.....86
Figure 3-4: Thin section photos of volcano-plutonic lithodeme rocks. 87
Figure 3-5: Thin section photos of red bed lithodeme and volcano-sedimentary lithodeme. 88
Figure 3-6: Concordia diagrams for samples from volcano-plutonic lithodeme. 89
Figure 3-7: Concordia diagrams for samples from red bed and volcano-sedimentary lithodeme. 90
Figure 3-8: Major element classification diagrams of igneous rocks from Ganquan Complex.....91
Figure 3-9: Trace element plots of igneous rocks from Ganquan Complex. 92
Figure 3-10: REE and trace element pattern diagrams. 93
Figure 3-11: Histograms and probability density plots of δ18O (zircon) and zircon εHf(t) results from the hornblende gabbro unit.....94
Figure 3-12: Summary of zircon εHf(t) values plotted against 206Pb/238U sample ages. 95
Figure 3-13: Plot of εHf(t) zircon values vs δ18O (zircon) ratios. 96
Figure 3-14: Proposed tectonic model.....97
Figure 4-1: Tectonic context maps of Central Asia Orogenic Belt, Beishan Orogen and Liuyuan Complex. ...141
Figure 4-2: Geological map of Baidunzi Complex and surronding area. 142
Figure 4-3: Field photos of Baidunzi Complex rocks.....143

Figure 4-4: Field and petrographic photos of meta-sedimentary rocks. 144
Figure 4-5: Precambrian U-Pb zircon detrital geochronology histograms with KDE plots. 145
Figure 4-6: Paleozoic U-Pb zircon detrital geochronology histograms. 146
Figure 4-7: Field photos showing meta-plutonic units and cross-cutting relations in the Baidunzi Complex. ..147
Figure 4-8: Concordia plots showing age results of orthogneiss and Baidunzi Intrusive Suite rocks. 148
Figure 4-9: Major element geochemical plots of rock units from the Orthogneiss, Baidunzi Intrusive Suite and Late Intrusive Suite.....150
Figure 4-10: Chondrite normalized REE trace element patterns of rocks in the Orthogneiss, Baidunzi Intrusive Suite and Late Intrusion Suite. 151
Figure 4-11: Tectonic discrimination plots of rocks in the Orthogneiss, Baidunzi Intrusive Suite and Late Intrusion Suite. 152
Figure 4-12: Hf isotope analytical results of igneous rocks from Baidunzi Intrusive Suite. 153
Figure 4-13: Cross section sketch for the proposed tectonic model of the coeval doubly vergent subduction scenario.....154
Figure 4-14: Block diagram sketch for the proposed tectonic model of the along-strike north-dipping subduction scenario in Late Carboniferous to Early Permian (ca. 294-289 Ma). 155
Figure 4-15: Epsilon Hf(t) versus age plots for crystalline, captured or inherited zircons of Archean to Triassic igneous rocks, from northern and southern Tarim Craton. 156
Figure 4-16: Sketch showing Gondwana breakup in Ordovician to Early Devonian. 157

Chapter 1 Introduction

1.1 Introduction

The unique architecture of the wide mountain belt covering large parts of central Asia, was first distinguished from classical Alpine-type orogenic belts by Suess (1901, 1908). Suess stated that this mountain belt is fundamentally different, having broad and non-linear geometry, being ubiquitous in steep bedding and schistosity, and presenting low-grade Palaeozoic rocks at a considerable volume. After a century after Suess' findings, Şengör et al. (1993) synthesized most of the geological data obtained up to 1990 and integrated them into a Paleozoic tectonic model of central Asia. While this pioneering model has become incompatible with more recent data, it sparked numerous discussions and prompted detailed research into the orogenic belts of Central Asia. These belts encompass the Siberian portion of Russia, Kazakhstan, the Uzbek, and Kyrgyzstani regions of western Tianshan, Mongolia, and Northwest China (Figure 1-1a), collectively known as the Central Asian Orogenic Belt (CAOB). The increased addition of recent data based on the application of modern methods in field geology, petrology, geochemistry, geochronology, and palaeobiological observations has yielded abundant evidence for constructing the geological history and tectonic synthesis of the CAOB. The diverse constraints from tectonic models also facilitate a better understanding of the broader tectonic framework of Central Asia and the reconstruction of the paleogeographic evolution of this significant center of crustal growth during the Phanerozoic.

The Chinese segment of the southern Central Asian Orogenic Belt, encompassing the Tianshan and Beishan Orogens, plays a crucial role in its Paleozoic evolutionary narrative. This contribution is visually depicted in a readily accessible 1:1,000,000 scale map (Anonymous, 1997). There also exist maps of the Beishan from 1966, produced at a scale of 1:200,000, which are accessible to Chinese researchers. More recent regional maps at a scale of 1:50,000 (e.g., Niu et al.,

2020) have been generated by the Gansu Bureau of Geology and Mineral Exploration and Development. However, most of these newer maps lack intricate details in tectonically complex areas and do not fully integrate newly discovered data and findings from the available literature.

The area investigated in this thesis covers a portion of the Beishan Orogen, located in the southern part of the Central Asian Orogenic Belt (CAOB). This specific region was chosen due to its excellent outcrop and structural relationships, and its critical location, which holds the potential to investigate the Late Paleozoic evolutionary history of the Central Asian Orogenic Belt. Through detailed mapping at a 1:25,000 scale (Appendix 1), this thesis provides new field observations, combined with geochronological and geochemical studies, to better constrain the tectonic evolutionary history, and contribute to a broader understanding of the global paleogeographic changes during Paleozoic time.

1.2 The Central Asian Orogenic Belt (CAOB)

The Central Asian Orogenic Belt (CAOB), historically known as the Altaids of Central Asia (Suess, 1901, 1908), is the world's largest accretionary orogenic belt. It has also been called the Ural-Amurian and Ural-Mongolian with the major difference being that the CAOB is believed to have a longer evolution history, beginning ca. 1 Ga as documented by its oldest ophiolitic sequence in southern Siberia (Khain et al., 2002; Rytsk et al., 2011) and terminating ca. 250 Ma as documented by the late Permian Solonker Suture (Windley et al., 2007; Xiao et al., 2003). It was also noted by Kröner and Rojas-Agramonte (2014) that use of the term Altaids can be misleading and may give rise to misinterpretation of the ages, structures, and geological history of the high-grade metamorphic complexes, thus the non-model-oriented term - the Central Asian Orogenic Belt (CAOB) is favoured instead. However, names such as the Altaids, Altaid collage, Central Asian Fold Belt, Central Asian Orogenic System and CAOB are now becoming synonymous amongst research papers and reviews.

They all generally represent the same orogen which extends from the Baltic craton in the northwest to the Siberian craton in the northeast and is constrained by the Tarim craton in the southwest and the North China craton in the southeast, exhibiting an east-west trending interrelated orogen between the four cratons (Figure 1-1b).

The tectonic evolutionary model of the Central Asian Orogenic Belt (CAOB) has undergone changes and evolution over the years as new evidence and research emerged. The original tectonic model suggesting that the Central Asian Orogenic Belt (CAOB) originated from a single giant arc complex (Şengör et al., 1993) has been widely rejected due to conflicting evidence, such as paleontological data and paleogeographic interpretations indicating significant distances between the involved cratons (McKerrow et al., 1992; Fedorova et al., 2013; Meert & Lieberman, 2008; Windley et al., 2007). Additionally, recent findings suggest that the presumed large contribution of juvenile continental material from Mesozoic granitoid plutons to CAOB evolution (Jahn et al., 2000a; Jahn et al., 2000b; Jahn, 2004) may have been overestimated (Kröner et al., 2014), highlighting the presence of pre-existing basement rocks and reworked signatures in arc complexes.

The modern island archipelago model, or multiple subduction zone model, is most compatible with current evidence, which was developed from work in the Tianshan Orogen, indicating subduction zones under both its north and south margins (Windley et al., 1990; Allen et al., 1992; Gao et al., 1998; Chen et al., 1999; Laurent-Charvet et al., 2002; Xiao et al., 2004). The earliest recorded evolution of the CAOB is believed to start from the accretion and collision of multiple island arcs toward the southern margin of the Siberia craton (present coordinates), which generated the Baikal collisional belt (Figure 1-1b). The ophiolitic complexes and associated island arcs in East Sayan dated at ca. 1020 to 1035 Ma and ca. 1034 to 1048 Ma, respectively (Kuzmichev & Larionov, 2013; Khain et al., 2002), are strong evidence for Late Mesoproterozoic opening of the Paleo-Asian

Ocean (PAO) between northern Mongolia and East Sayan in Russian Siberia. Successive accretion was also corroborated by the discovery of a well-developed accretionary prism dated at 775 to 819 Ma, which through detailed mapping shows an association with the island arcs (Kuzmichev & Larionov, 2013). This early active margin displays great similarity to the present SW Pacific, showing complex collisions that amalgamated components of the Neoproterozoic island arc assemblages, ophiolitic complexes, and microcontinental fragments and produced high-grade metamorphic terranes in the Early Cambrian (Gladkochub et al., 2010).

Since the Late Neoproterozoic to Cambrian, several independent and short-lived arc systems have been welded together by a process of consecutive collisions, closing the Paleo-Asian Ocean progressively and dividing it into several interconnected oceans among cratons and microcontinents. The tectonic evolution of the CAOB since this point can be generally discussed in terms of three subdivided accretionary collages: the Kazakhstan collage system in the west connected to the Baltic craton, the Tuva-Mongolian collage system in the north connected to the Siberian craton, and the Tarim-North China collage system in the south connected to the Tarim and North China cratons (Figure 1-2).

The Kazakhstan collage system, originating from subduction beneath the Kazakhstan continent in the Ordovician, evolved through arc migrations and collisions, eventually forming a composite arc complex by the Devonian (Filippova et al., 2001). Subsequent oroclinal bending led to the development of Alaska Arc-type forearc accretion systems (Levashova et al., 2003; Windley et al., 2007). Meanwhile, in the western South Tien Shan, accretionary wedges formed, during convergence which led to collision between the Tarim craton and Kazakhstan (Kröner et al., 2007). In contrast, the Tuva-Mongolia collage formed from the subduction of the Mongol-Okhotsk Ocean, producing a single ribbon-like arc chain (Windley et al., 2007). Oroclinal bending of the Tuva-

Mongolia arc magmatic axis occurred due to slab retreat and the convergence of the Tarim-North China collage system from the south (Xiao et al., 2009). The Tarim-North China collage system marked the Paleo-Asian Ocean's closure, leading to the accretion and collision of multiple blocks now preserved in the Beishan Orogen, South Tianshan, and Solonker sutures. The terminal orogenesis involved collision of the Tarim Craton with the Tianshan orogen southeastern margin in the west and collision with North China Craton along the Solonker suture in the east during the Late Carboniferous-Permian and Permian to Triassic, respectively (Xiao et al., 2003; Xiao et al., 2015).

1.3 The Beishan Orogen

The Beishan Orogen, situated in the central-southern region of the Tarim-North China collage within the Central Asian Orogenic Belt (CAOB), serves as a crucial link between the two primary terminal sutures, the South Tien Shan and Solonker sutures (Figure 1-2). This region hosts some of the youngest ophiolitic complexes, arc terranes, and sedimentary basins of the CAOB, making the Beishan Orogen a pivotal location for correlating geological elements on both sides and allowing better reconstruction of the tectonic history responsible for the closure of the Paleo-Asian Ocean.

The tectonic evolution of the Beishan Orogen predominantly comprises the development of several Early to Mid-Paleozoic arcs in parts of the southern Paleo-Asian Ocean and their collisions between the arcs and/or Precambrian cratonic slivers of multiple different sources, which include the Baltic (He et al., 2018) and the Tarim cratons (Zhang et al., 2015; Kröner et al., 2013; Zuo et al., 2003) as determined by provenance studies. The common nomenclature used by researchers in the Beishan region is defined and summarized in a review paper by Xiao et al. (2010), which provided a framework for tectonic classification of the various terranes in the Beishan region including the major bordering shear zones and ophiolite-bearing mélange zones. From north to south, the framework (Figure 1-3) includes the Queershan composite arc unit, the Gongpoquan accretionary complex, the

Dundunshan terrane and the Shibanshan arc unit. The Queershan composite arc unit is composed of multiple arc packages with ages ranging from the Ordovician to Permian, representing a long-term evolving north-verging subduction system associated with continuous accretion and continental growth. The Gongpoquan accretionary complex, also called the Mazongshan terrane (Cleven et al., 2018), was developed from the amalgamation of the Cambrian to Silurian Mazongshan arc with the Ordovician Hanshan arc complex before the Devonian and the subsequent accretion to the Heiyinshan arc complex by the Late Carboniferous (Xiao et al., 2010).

The southernmost and youngest Shibanshan terrane is connected to a Permian ophiolitic complex, with controversial tectonic histories regarding its juxtaposition with the northern Huaniushan-Dundunshan terrane. The Shibanshan terrane, initially mapped as Ordovician to Silurian gneissic rocks (BGMRGS, 1997), was believed to share a similar history with the Ordovician to Devonian Huaniushan-Dundunshan terrane (Chen et al., 2016; BGMRG, 2005). The southern boundary of the Huaniushan-Dundunshan terrane is defined by a thrust fault, with the structurally underlying mafic-ultramafic belt of the Liuyuan Complex. The Liuyuan Complex, which geographically separates the two terranes to the north and south, has been interpreted as a product of an incipient rift (Wang et al., 2017), while other researchers consider these units as two independent tectonic entities (Guo et al., 2012; Tian et al., 2014, 2020; Mao et al., 2012). Detrital zircon analyses comparing sedimentary basin rocks in both the northern and southern areas adjacent to the Liuyuan Complex suggest a similar provenance (Song et al, 2013; Cleven et al., 2018), adding complexity to the debate. This thesis provides evidence that the Shibanshan terrane differs from the Ordovician to Devonian Huaniushan-Dundunshan terrane. It is neither a Carboniferous to Permian composite arc; instead, it consists of two distinct Permian arc complexes: the Ganquan Complex and the Baidunzi Complex.

The tectono-stratigraphic classification of the region has seen inconsistencies due to varying tectonic models, with some relying more on geochemical and geochronological analyses rather than stratigraphic and structural evidence. This thesis adopts stratigraphic nomenclatures from the BGMRG (1997, 2005) incorporating recent biostratigraphy and radiometric dating results (Jin, 1974; Niu et al., 2018).

1.4 Thesis objectives

The research objectives of this thesis are to address regional and local tectonic questions regarding the phases and processes responsible for the evidence of accretionary orogenesis preserved in the Beishan Orogen. The Beishan Orogen is significant since it connects two major suture zones within the Central Asian Orogenic Belt (CAOB), hence representing a key segment to understand the Paleozoic tectonic evolution. However, the regional context and the arrangement of various tectonic components within the Beishan Orogen have been a subject of contention. To construct up-to-date tectonic models for the Beishan Orogen and understand the final stages of the CAOB's tectonic evolution, this thesis has three main objectives:

1. Establish a detailed description of the tectono-stratigraphic packages that constitute the southern Beishan Orogen through detailed field-based studies mainly focusing on the stratigraphic make-up-of and structural relationships between the various tectonic units. Analyse the structural and deformation history regarding the kinematic evolution and timing of the major shear zones that were involved in the tectonic amalgamation of the units.
2. Examine the Ganquan Complex by analyzing the lithology, stratigraphy, geochemistry of its individual lithodemes, with the aim of understanding the nature, tectonic setting and duration of its magmatism.

3. Study the lithologies, stratigraphy, geochemical properties, and geochronology of the rock units comprising the Baidunzi Complex, aiming:

    a. Understand the tectono-stratigraphy and provenance of the meta-sedimentary sequences mainly through using geochronology, and to test potential geochronological and isotopic linkages between preserved basement and any known cratons.

    b. Compare the settings and characteristics of magmatic features between the Ganquan and Baidunzi Complexes within the Shibanshan terrane, utilizing the constraints provided by the stratigraphy, timing, deformation, and tectonic context of distinct tectono-stratigraphic units to further refine the Late Paleozoic tectonic model for the Shibanshan terrane and southern Central Asian Orogenic Belt.

To achieve these objectives in the southern Beishan area, a multidisciplinary approach involving structural analysis, petrographic studies, U-Pb zircon geochronology (including both LA-ICP-MS and SHRIMP analyses of igneous and clastic sedimentary rocks), as well as whole-rock and isotope geochemistry, was used. Data and observations from the available literature are also included and have been cited.

1.5 Organization of the thesis

This thesis consists of three journal articles, each addressing distinct but related topics and intended to be standalone papers. Hence there is some necessary repetition in maps, regional geology, and tectonic descriptions. The chapters are arranged in a logical sequence to build a cohesive understanding of key conclusions. References are included at the end of each chapter, and all appendices are consolidated at the end of the thesis.

This thesis is based on geological investigations and mapping work conducted in southern Beishan, which led to publication of a new geological map by the China Geological Survey in 2021 (Appendix 1). Chapter 2 summarizes the results covering regional lithology, stratigraphy, deformation history, and the division of tectono-stratigraphic units based on the findings amassed during field work. These newly recognised units from north to south include the Liuyuan Complex, Ganquan Complex, Baidunzi Complex, and Shiyaozi Complex. This chapter has been revised based on a short perspective paper published by Hong et al. (2022), featuring updated interpretations and conclusions from subsequent chapters (Chapter 3 and Chapter 4). It also includes additional structural data and more detailed field observations for each tectono-stratigraphic unit obtained during the field-based investigations.

The third chapter delves into the Ganquan Complex, focusing on two distinct sequences separated by unconformities and/or thrusts. This chapter presents detailed stratigraphic analysis, along with geochronological and geochemical data, to explore the tectonic context and magmatic evolution of the Ganquan Complex volcanism. It establishes a temporal and spatial link between the Ganquan and Liuyuan complexes, revealing an arc migration process corresponding to the opening of the Liuyuan back-arc basin.

The fourth chapter comprehensively explores lithology and stratigraphy of the Baidunzi Complex. Assisted by geochemistry and U-Pb igneous and detrital zircon geochronology data, it characterizes the Baidunzi Complex as an exotic Permian continental arc with a possible Proterozoic basement. The ca. 281 Ma emplacements of the stitching gabbro and the coeval metamorphism in arc plutonic rocks are linked with the conclusions presented in Chapter Three, expanding the interpretation of a shutdown of the Ganquan arc due to sinistral oblique convergence during arc-arc collision. The fifth chapter synthesizes the main conclusions of the thesis.

1.6 Figures and captions

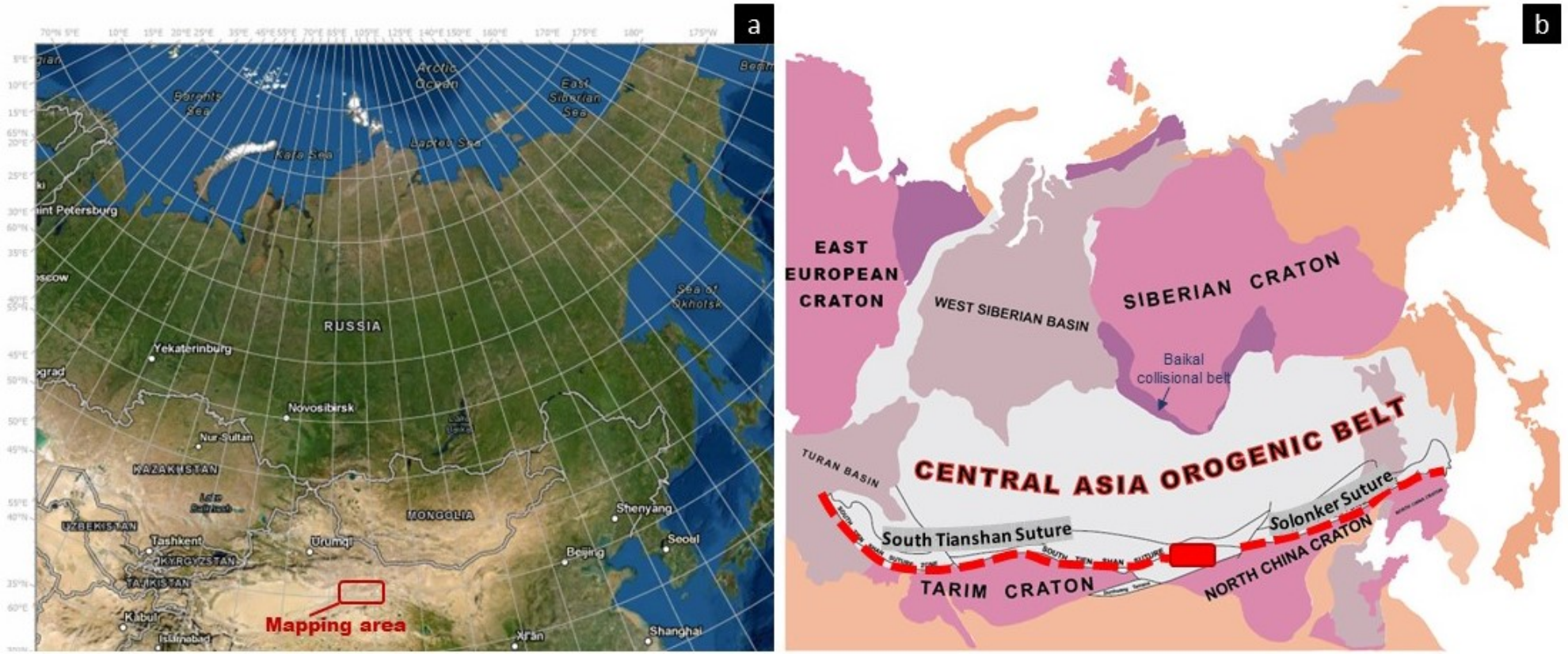


Figure 1-1: Satellite image (a) and corresponding generalized map of the Central Asian Orogenic Belt (b). Modified from Kröner et al. (2014).

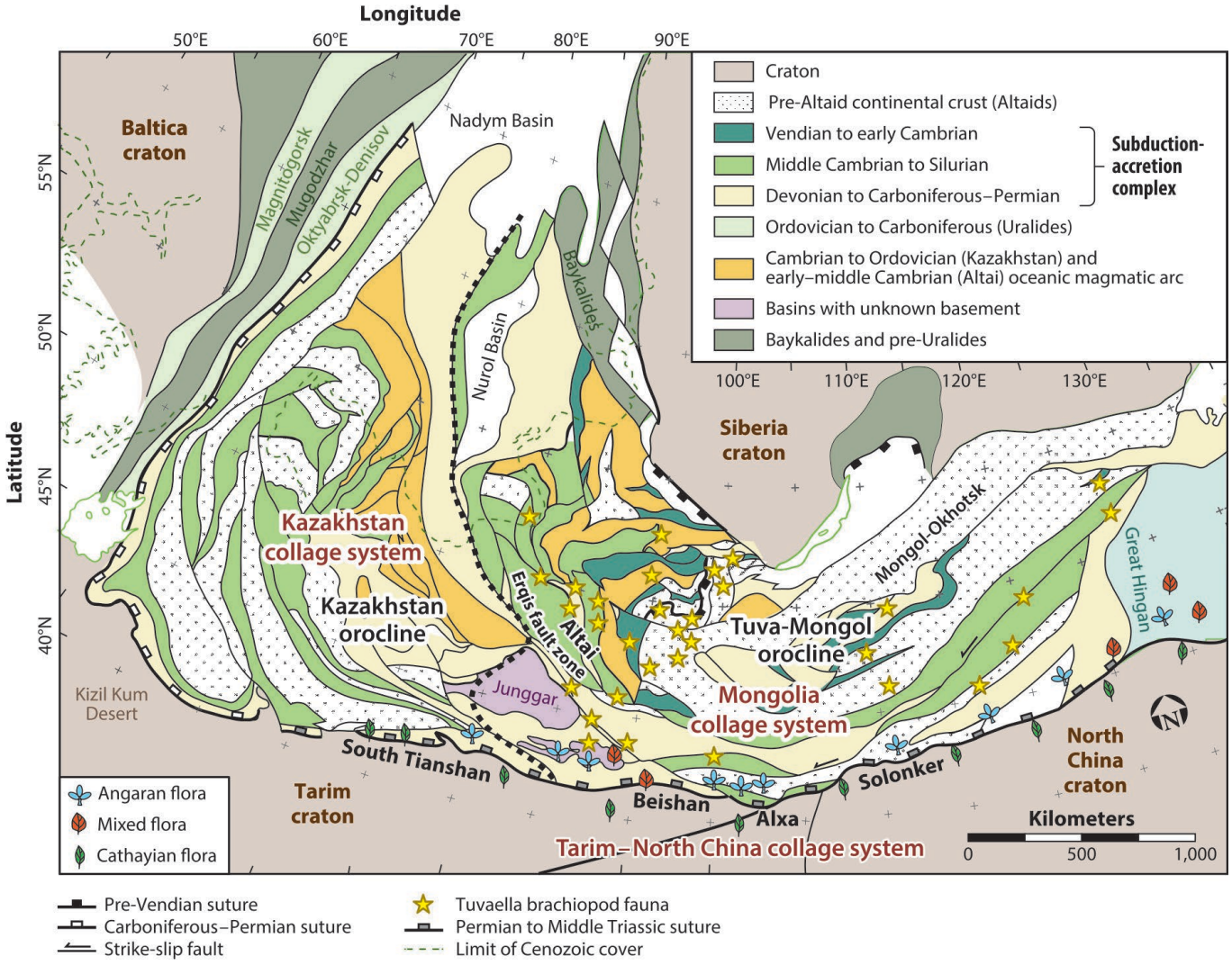


Figure 1-2: Tectonic overview and division of the Central Asian Orogenic Belt and adjacent cratons. Source from Xiao et al., 2018 and Han and Zhao, 2018.

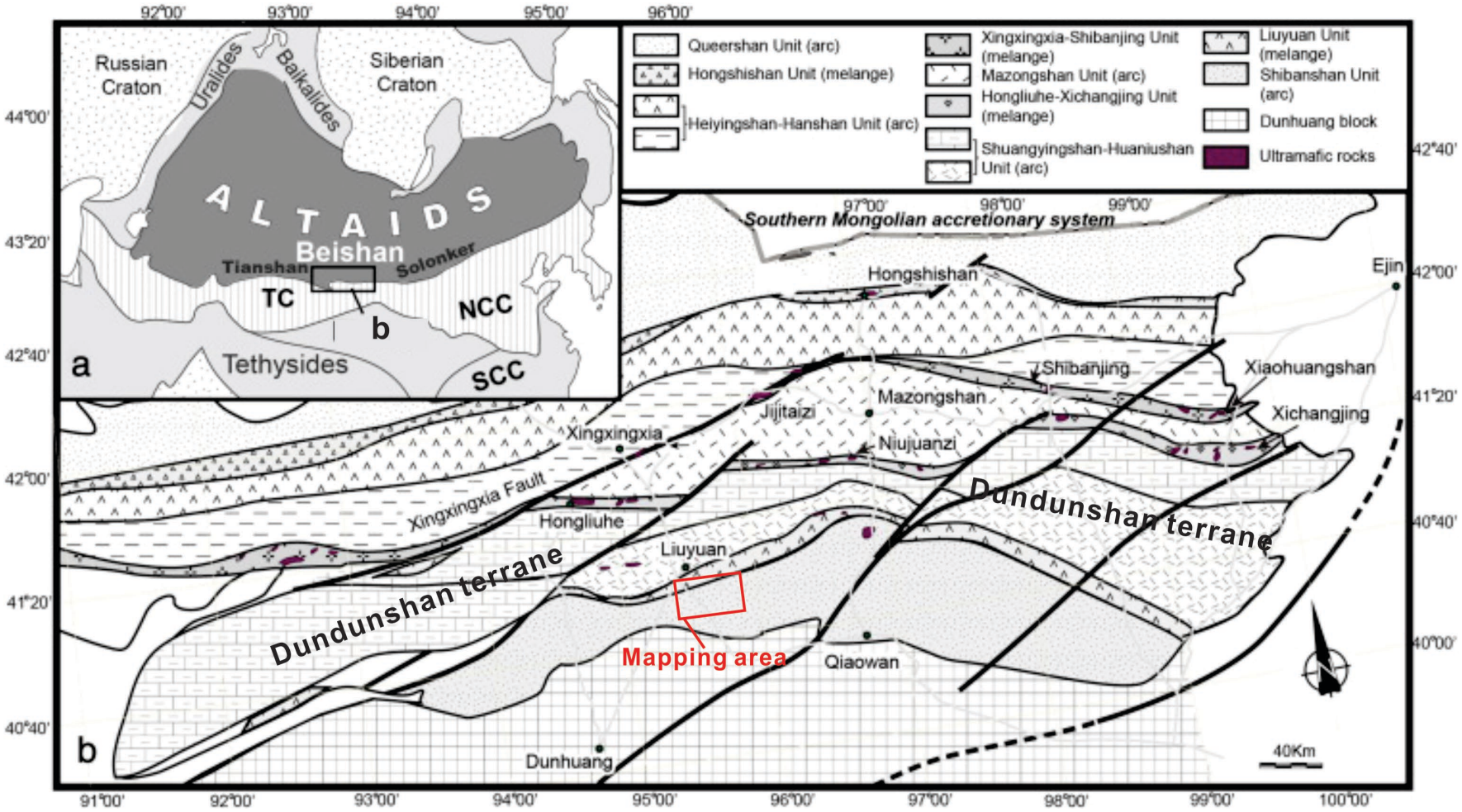


Figure 1-3: Tectonostratigraphic terrane map of the Beishan orogenic collage. Modified from Mao et al., 2012. (TC-Tarim Craton; NCC- North China Craton; SCC-South China Craton).

Chapter 2 Detailed geological mapping uncovered complex arc-arc accretions and progressive tectonic stacking during Permian to Triassic in the southern Beishan Orogen, southern Central Asian Orogenic Belt

2.1 Introduction

The Central Asian Orogenic Belt (CAOB), surrounded by the Baltic and Siberia cratons to the north, and the Tarim and North China cratons to the south, preserves a record of successive tectonic cycles involving subductions and accretions from the Neoproterozoic to the Paleozoic eras. These processes led to the consumption and eventual closure of the Paleo-Asian Ocean (Windley et al., 2007).

Tectonic models concerning the terminal phase of this orogenesis remain contentious, with discussions spanning topics such as the timing and location of the final closure of the Paleo-Asian Ocean, as well as the regional context and configuration of its various tectonic components. The results of detailed mapping in the southern Beishan Orogen, located within the southern Central Asian Orogenic Belt, were obtained through a collaborative effort involving the China Geological Survey, the University of Waterloo (Canada), and the Geological Survey of Canada. These findings suggest that certain portions of the Paleo-Asian Ocean remained open until the Permian period and indicate that its ultimate closure involved the accretion of several distinct terranes. This included the amalgamation of multiple Permian arc and arc-backarc systems, a process of greater complexity than previously proposed.

The Beishan Orogen is an east-west trending collage of accreted terranes situated between two southern suture zones of the CAOB: the Tianshan suture in the west and the Solonker suture in the east (Figure 2-1a). This region contains some of the youngest Permian ophiolitic and arc

complexes, as well as sedimentary basins within the CAOB (Xiao et al., 2010), making it a crucial area for investigating the contentious terminal collision history of this orogen.

Through detailed mapping at a 1:25,000 scale (van Staal et al., 2021, Appendix 1), we have delineated five distinct tectono-stratigraphic packages in our mapping area near the town of Liuyuan, in southern Beishan, referred to as Liuyuan Beishan Orogenic Collage (Liuyuan BOC). These units exhibit individual stratigraphic characteristics and have been juxtaposed during three prominent phases of deformation. The identified packages include the Shiyaozi Complex, Baidunzi Complex, Ganquan Complex, Liuyuan Complex, and the Heishankou sedimentary sequences (Figure 2-2).

2.2 Geological background

The Liuyuan BOC provides a well exposed cross-section through the various tectono-stratigraphic units that occur adjacent to the mafic Liuyuan Complex, and the cratonic terranes to the north attached to composite Siberia, and south to the Dunhuang terrane. The Dunhuang terrane is known for its extensive Archean and Paleozoic high-grade metamorphosed basement rocks, dating back to 3.3-3.0 Ga, 2.7-2.5 Ga, and 2.0-1.6 Ga (Zhao et al., 2015). It is recently interpreted as a Paleozoic tectonic belt with major crustal formation event in the Cambrian (ca. 520-470 Ma), Silurian (ca. 440-400 Ma) and Carboniferous (ca. 335-315 Ma) (Soldner et al., 2022, 2023; Feng et al., 2020; Zhao et al., 2016, 2017).

In the Liuyuan BOC, there are various terranes located between composite Siberia and the Dunhuang terrane and bounded by interconnecting E-W trending major structural lineaments, yet the evolutionary histories of their development and amalgamation against the northern margin of the Dunhuang terrane are contentious. Recent studies by Xiao et al. (2010) and associated researchers propose the presence of at least two distinct tectonic units within these terranes: the Huaniushan-Dundunshan arc terrane and the Shibanshan arc terrane. These units are situated in tectonic contact

with the Liuyuan Complex to its north and south, respectively (Figure 2-1b). The Huaniushan-Dundunshan arc terrane consists of predominantly Ordovician to Silurian high-grade metamorphic tectonite (de Vries, 2021), volcanic complexes predominantly related to the Late Ordovician-Silurian Huaniushan arc magmatism and Devonian Dundunshan arc magmatism (Guo et al., 2014; Tian et al., 2015), as well as their Carboniferous to Permian sedimentary cover (Santos, 2021; Li, 2019).

The Shibanshan terrane, originally mapped as predominantly Ordovician to Silurian gneissic rocks (BGMRGS, 1997 and 2005), was later reinterpreted as a Carboniferous to Permian continental arc by Xiao et al. (2010). Recent research conducted as part of our studies suggests that the Shibanshan terrane actually comprises at least two distinct Permian arcs: the Ganquan Complex and the Baidunzi Complex (van Staal et al., 2021; Santos et al., 2022; Hong et al., 2022).

The Ganquan Complex consists of felsic volcanic and volcaniclastic sedimentary rocks with arc-like geochemical signatures and contains magmatic zircon with juvenile and mantle-like isotope characteristics (see Chapter 3 or Hong et al., 2024). A temporal and spatial linkage was established between the Ganquan and Liuyuan Complexes (Santos et al., 2023 and Hong et al., 2024), suggesting they represent an extensional intra-oceanic arc-backarc system in the Early Permian. On the other hand, the Baidunzi Complex represents a continental magmatic arc complex, characterized by variably sheared and isoclinally folded continental-derived metasedimentary and syn-kinematic intrusive rocks with continental arc-like geochemistry (van Staal et al., 2021; see Chapter 4). Notably, a Permian sedimentary cover sequence has been found to structurally overlie these complexes. However, these sedimentary sequences were previously classified as part of the Carboniferous Hongliuyuan Formation and the Early Permian Zhesi Group, which were interpreted as being conformably overlain by the Liuyuan Complex (BGMRGS, 1997). The regional stratigraphy

originally relied on outdated interpretations of Shibanshan terrane correlation with regional Ordovician to Silurian geology.

Recent stratigraphic studies and nomenclature in the Liuyuan BOC have largely followed the mapping work conducted by the Bureau of Geology and Mineral Resources of Gansu Province (BGMRGS, 1967, 1989, 1997, and 2005). However, different researchers have divided and named the updated Paleozoic stratigraphy inconsistently to align with their proposed tectonic models (e.g., Cleven et al., 2018 vs. Guo et al., 2014). Additionally, some interpretations have primarily relied on geochemical and geochronological analyses of magmatic and meta-sedimentary rocks, lacking sufficient stratigraphic and structural evidence.

In this chapter, we predominantly adopt the stratigraphic nomenclature of BGMRGS (2005) and integrate the most recent biostratigraphy and radiometric dating results outlined in Niu et al. (2018, 2021). However, we emphasize significant revisions and changes in the Upper Paleozoic strata based on our mapping results and associated structural studies.

2.3 Tectono-stratigraphic divisions uncovered by bedrock mapping

2.3.1 Structural panel division and deformation history

The deformation history of the Liuyuan BOC is polyphase and complex. It involved at least three generations of ductile and locally brittle structures (D1-3), although not all generations are everywhere present, and deformation is highly heterogeneous on the scale of the Liuyuan BOC area. Separation of structures is based on overprinting relationships and was further aided by unconformities, and syn-tectonic magmatism and sedimentation, whereas kinematic analyses of the major shear zones helped to interpret the complex movement histories. The tectonostratigraphic units recognised in the Liuyuan BOC to the south of the Liuyuan Complex, have been divided into several distinct D3 structural panels (Figure 2-2) which created a north-verging imbricate stack of previously

imbricated and folded (D1-2) rocks. In structural descendancy the D3-related tectono-stratigraphic units are: (1) the Shiyaozi Complex; (2) the Baidunzi Complex; (3 and 4) two distinct structural panels involving both sequences in the Ganquan Complex; (5) clastic sedimentary rocks of a Permian cover, including the Heishankou formation and the Liuyuan conglomerate synthem. The Permian cover is structurally overlain by (6) the Liuyuan Complex and cut by Late Permian and/or Triassic late syn- to post-tectonic felsic to mafic dykes.

The oldest phase of structures (D1) has only been observed in rocks of the Baidunzi Complex and possibly also in the Ganquan Complex. However, it is absent in the Permian cover, and not recognised in the Liuyuan Complex, suggesting it predates deposition of the former. In the Baidunzi Complex, D1 structures comprise a gneissic layering and compositional layering-parallel foliation that locally exhibit isoclinal intrafolial folds (S1 and F1, Figure 2-6A-C). Thrust-related shear zones predominantly accommodated sinistral oblique reverse transcurrent motion based on east-plunging stretching lineations on shear plane and shear sense indicators (Figure 2-5N and Figure 2-6F). Dikes of the 294-289 Ma Baidunzi Intrusive Suite rocks locally cut across S1 foliations but were also folded and sheared by the same D1 deformation (Figure 2-6D-E), which indicates that D1 and Baidunzi Complex magmatism overlapped. Tectonic foliations (S1) are locally axial planar to isoclinal folds (F1) in veins and intrusive sheets (Figure 2-6A). Hence, the emplacement of D1 structures in the Baidunzi Complex, is interpreted to have occurred during a progressive, non-coaxial deformation between 294 and 289 Ma.

It is possible that the S1 foliations in Baidunzi Complex in part formed during unrelated phases of deformation because both D1 and D2 structures were associated with similar kinematics in the Baidunzi Complex, hence folding of S1 could equally have formed during increments of a progressive D1 deformation instead of by overprinting during D2 (Figure 2-7A). However, the

extensional setting of the Ganquan Complex compared to the compressional Baidunzi Complex suggests they were likely distal to each other during D1 (see Chapter 3 and 4). The south-verging deformation observed in the Ganquan Complex is grouped into D2. Tight to isoclinal recumbent or overturned folds (F2) associated with south-directed thrusting related mylonitic shear zones represent D2. Folded thrust contacts suggest this deformation is complex and progressive as well (Figure 2-2 cross section B-B'). F2 folds are commonly accompanied by a crenulation cleavage (S2), which is generally only preserved in the hinges and large ductile-brittle shear zones. The main foliation along the limbs of the F2 folds is generally a composite foliation of S1 and S2 (Figure 2-7A-B).

The south-directed D2 thrusts are folded by F3 which occur also in the Liuyuan Complex and rocks of the Permian Cover in the Heishankou basin, and probably caused some structurally interleaving of the Ganquan and Baidunzi Complexes in structural panels 3 and 5. D3 is represented by north-directed reverse shear zones, which locally grade from ductile south-dipping phyllonite zones into ductile-brittle faults, and upright to northerly overturned folds. D3 folds and thrusts are coeval since they locally overprint each other (Figure 2-7C). D3 structures are largely responsible for the present structural architecture of the Liuyuan BOC and divided the various unrelated tectonostratigraphic units into moderately to shallowly south-dipping structural panels (Figure 2-2). D3 folding and thrusting are commonly weak and locally are even absent in the Liuyuan Complex, hence earlier structures are locally well preserved. Age constraints (see below) of D3 indicate it postdates the south-verging thrusting in the Heishankou Basin.

2.3.2 The Shiyaozi Complex

The Shiyaozi Complex (panel 1) occurs in the southernmost part of the Liuyuan BOC. These rocks are either connected to the Dunhuang terrane or form an independent terrane between the Dunhuang terrane and the other units described herein. Desert with little or no outcrop separates the

Liuyuan BOC from bona fide rocks of the Dunhuang terrane further to the south. Panel 1 contains various phases of amphibolite and orthogneiss with protolith ages from 336 to 324 Ma (van Staal et al., 2021). They were intruded by megacrystic granite and hornblende diorite, and dykes of grey granodiorite that yielded ages from ca. 273 to 261 Ma, the magmatism of which is interpreted to be arc-related (Worthington, 2022). Multiple pre- to syn-kinematic granitic dykes intruded along the fault zone with the Baidunzi Complex in panel 2 (Figure 2-7D). The Shiyaozi Complex was only subjected to the latest north-verging D3 thrusting and associated deformation but lacks evidence of the preceding phases of south-directed thrusting (D2) present in the structurally lower panels. Hence, the moderately south-dipping shear zone with shear sense indicators of oblique reverse dextral shear (Figure 2-5F, G and 2-7D), serves as the boundary between the Shiyaozi Complex to the south and the Baidunzi Complex to the north, dividing the area into two distinct tectonic panels, each characterized by its unique geological features.

2.3.3 The Baidunzi Complex

The Baidunzi Complex (panel 2) comprises a mixture of variably sheared and isoclinally folded metasedimentary and syn-kinematic meta-plutonic rocks. Deformation (D1-D2) commonly transformed the rocks into well-layered upper greenschist to amphibolite facies tectonites with moderate to steep southerly dips. The oldest known rocks in the Baidunzi Complex are thick-bedded orthoquartzite and minor argillaceous chlorite-muscovite schist. The orthoquartzite rock unit comprises metamorphosed and deformed sandstone that is made of exclusively quartz sand (Figure 4-4A and C1). Detrital zircon analyses of the quartzite show no age peaks younger than ca. 1060 Ma. The structurally overlying metasedimentary rocks include a regionally extensive unit of marble and marl associated and interlayered with quartz-rich meta-psammite and schist, indicating a shallow

shelf environment. The calcareous rocks are older than ca. 294 Ma, based on the emplacement ages of the meta-plutonic rocks, which cut the marble (see Chapter 4).

The extensive meta-plutonic rocks are smeared out into narrow sheets giving the rocks a well-developed banded geometry on map-scale (Figure 2-2 and 2-6C, F). These rocks are categorized into two distinct suites: the Baidunzi Intrusive Suite and the Late Intrusive Suite (see Chapter 4). The Baidunzi Intrusive Suite is comprised of extensive sheets of sheared hornblende quartz diorite, tonalite, granodiorite, granite, and minor trondhjemite. The D1 shear zones are confined to the Baidunzi Complex, and the duration of progressive deformation is constrained by the crystalline ages of the syn-tectonic plutons within the Baidunzi Intrusive Suite (294 to 289 Ma). Since these plutons were emplaced syn-tectonically with D1, they display various phases that intersect and overlap with the earliest foliation (S1). The D1 shear zones are characterized by sinistral oblique reverse and, less commonly, normal kinematics (Figures 2-5N and 2-6E, F), suggesting that the magmatism of the Baidunzi Intrusive Suite developed within an overall transpressional environment, occasionally intersected by extensional jogs.

The Late Intrusive Suite comprises numerous hornblende gabbro sills and white leuco-granodiorite bodies with compositions ranging from granite to tonalite, locally including trondhjemite. The gabbro sills are localized along the shear zone that separates the Baidunzi and Ganquan Complexes and stitch all rocks of the Baidunzi Complex and the contact with the volcano-sedimentary unit of the Ganquan Complex. Geochronological investigations on the recrystallized zircon rims from the diorite and tonalite units within the Baidunzi Intrusive Suite have revealed a metamorphic event around 280 Ma, which is absent in the volcanic zircons of the Ganquan Complex. The metamorphic zircon rims align closely with the intrusion of the syn-tectonic suite of hornblende gabbro around 281 Ma, suggesting that the amalgamation of the Baidunzi and Ganquan complexes

took place approximately 281 Ma. The south directed D2 thrusting and folding within the Ganquan Complex are considered to be unrelated to the kinematics responsible for the D1 folding observed in the Baidunzi Complex. However, the late stages of D1 in the Baidunzi Complex may have been continuous with the initial stages of D2 during the amalgamation of these two complexes and if so, making an abrupt change in the kinematic regimes. The white leuco-granodiorite bodies intrude all igneous units of the Baidunzi Intrusive Suite and the hornblende gabbro sills, typically forming subparallel intrusive sills, most likely were late syn- or post tectonic with respect to the D2 event.

2.3.4 The Ganquan Complex

The Ganquan Complex is separated from the Baidunzi Complex by a significant shear zone between panel 2 and 3. It primarily consists of felsic volcanic and volcaniclastic sedimentary rocks, divided into lower and upper sequences by an unconformity. The inferred genetic connection between these two sequences is confirmed by U-Pb ages and εHf values of detrital zircons (see Chapter 3). The lower sequence ranges approximately 295-286 Ma, while the upper sequence ranges about 283-281 Ma.

The older unit of the Ganquan Complex (panel 4) mainly comprises rhyolitic lithic and quartz and feldspar-phyric tuff, locally interbedded with green basalt and minor volcanoclastic rocks. These likely represent pyroclastic flows on a large regional extent. The upper sequence contains the red bed unit and volcano-sedimentary unit, both featuring distinctive polyphase deformed volcaniclastic meta-sedimentary rocks and interlayers of dacitic to rhyolitic tuff. Although the volcanic rocks of the lower sequence partially overlap in age with the Baidunzi Intrusive Suite rocks in the Baidunzi Complex, several lines of evidence indicate they are distinct entities. This evidence include (1) the complete absence of the distinct metasedimentary and plutonic rocks seen in the Baidunzi Complex in both sequences of Ganquan Complex, (2) significant differences in zircon inheritance and isotope content

(as discussed in Chapters 3 and 4), and (3) noticeable variances in structural and metamorphic characteristics, regarding the D1 and syn-kinematic magmatism which are exclusively restricted to the Baidunzi Complex, and absent in panel 3 and 4 of the Ganquan Complex. The main macroscopic structure displayed by the Ganquan Complex in the wester part of the study area exhibits a dome-shape geometry. The hanging wall comprises rocks from the younger volcano-sedimentary unit, which were intruded by gabbro. In contrast, the footwall is characterized by rhyolite from the older volcano-plutonic unit, which, notably, remained unintruded by gabbro sills. The fault contact between them was deformed into a recumbent or overturned fold, as shown in Figure 2-2, cross section B-B'. In this fold, the stretching lineations exhibit shallow plunging directions that vary from the W to NW and from the E to SE. We interpret this as evidence of a south-verging thrust and fold associated with D2 and the original NW-trending lineation. This structure has been subsequently overprinted by NW-directed D3 deformation.

Both sequences of Ganquan Complex exhibit geochemical signatures indicative of an arc-like environment. Additionally, their magmatic zircons display mantle-like $\delta^{18}O$ values and increasing radioactive εHf values up-section, implying a progressively more juvenile magma source from the mantle over time (as detailed in Chapter 3). According to recent findings by Santos et al. (2022) and Hong et al. (2024), it is suggested that the Ganquan and Liuyuan Complexes together represent components of an extensional arc-back arc system. This extensional environment culminated in backarc opening, possibly associated with slab steepening and/or rollback, resulting in elevated juvenile geochemical signatures. This setting contrasts with the compressional magmatic environment observed in the Baidunzi Complex.

2.3.5 Liuyuan Complex

The spatially closely associated Liuyuan Complex in panel 5, records active magmatism between ca. 290-282 Ma, and corresponds in age, geochemistry, and tectonic setting with the Ganquan Complex. Detailed mapping and petrological studies by Santos (2022) allow the Liuyuan Complex to be subdivided into a troctolite, melatroctolite, and varitextured olivine gabbro, separated from overlying pillow basalt and chert beds by a newly discovered laterally continuous sheeted dyke complex (Santos, 2022). The basalts exhibit characteristic supra-subduction zone signatures, featuring positive Th and negative Nb anomalies. The low V/Ti ratios, along with La/Sm and La/Nb values akin to those of basalts from Tonga, Izu Bonin, and Mariana back-arc basins, provide compelling evidence that the Liuyuan Complex originated within a back-arc setting. This aligns with the concurrent occurrence of arc rocks in the neighboring Ganquan Complex, collectively constituting an oceanic back-arc basin situated north of the south-facing Ganquan arc (Hong et al., 2023; Santos et al., 2023).

The mapping area within the Liuyuan BOC encompasses segments of igneous and sedimentary rock from the Liuyuan Complex, juxtaposed with the unconformably overlying conglomerate, sandstone, and siltstone of the Cover Sequence (panel 6). They together were thrust southwards over the older units of the Cover Sequence that form part of panel 5 (Figure 2-2 cross section A-A'). The structural core of panel 6 is characterized by shallowly doubly plunging F3 antiforms (Figure 2-5H to K), which may also affect the underlying ductile-brittle thrust. The initial D2 thrusts are preserved along the northern and southern boundaries of the primary body of Liuyuan Complex, as noted by Santos (2022). These thrusts are typically characterized by the presence of phyllonite, fault gouge, and laterally extensive, locally brecciated quartz veins that cut across and repeated sequences of volcanic rocks within the Ganquan and Liuyuan Complexes. This suggests that

these thrusts occurred during late stage and/or after the cessation of Ganquan arc-Liuyuan back-arc volcanism around ca. 281 Ma.

2.3.6 The Heishankou Basin

The Permian sedimentary cover in the basin south of the Liuyuan Complex was previously grouped into the Shuangbutang, Jushitan and/or Fangshankou formations (Cleven et al., 2018; Guo et al., 2014; Niu et al., 2018). In this thesis, the rocks are recognized as two individual unconformity-bounded units and named after the local geographical locations: the Heishankou formation and the Liuyuan conglomerate synthem. The Heishankou formation contains three members, in ascending order, consisting of (1) a dark grey to black shale interbedded with micaceous sandstone and occasional conglomerate, which occasionally are structurally interleaved with a limestone unit; (2) a polymictic conglomerate bed containing numerous pebbles of deformed and metamorphosed granitoids, gabbro and clasts of felsic volcanics and epiclastic rock fragments, possibly originating from the Baidunzi and Ganquan complexes; (3) a massive light green to brown sandstone beds exhibiting well-developed cross-bedding (Figure 2-7A to E). The Heishankou formation is separated by a disconformity from the overlying Liuyuan conglomerate synthem. The Liuyuan synthem differs from the underlying lower formations by the presence of pebbles and boulders of gabbro and basalt derived from the Liuyuan Complex, and lithic fragments of the underlying formations (Figure 2-7F, G). It is characterized by a dark green conglomerate unit containing clasts of basalt, chert, and lithic fragments of siltstone and shale from underlying members of Heishankou formation. The conglomerate commonly alternates with thin beds and interlayers of bluish to purplish siltstone and sandstone of turbidite sequences, with flaser laminations and debris of fossils present locally (Figures 2-8J and K). The Liuyuan conglomerate synthem generally unconformably overlies the southwards transported sheet of Liuyuan Complex rocks and part of the Ganquan Group, whereas the lower

Heishankou formation unconformably overlies the volcano-sedimentary member of the Ganquan Group and received detritus from denuded Baidunzi Complex (panel 2).

The sedimentary rocks of the two units act as a separator between the Ganquan Complex of panel 4 and the mafic rocks of the Liuyuan Complex, which were thrust from the north during the D2 deformation. Bedding is now typically sub-parallel to S2 cleavages and imbricate D2 thrusts, which are locally overprinted by D3 structures, such as presented by the F3 re-folding of F2 folded quartz veins and other F2 folds (Figure 2-9). The stretching lineation (L2) is commonly represented by elongated clasts, which are parallel to the F2 fold axes, plunging shallowly either to the east or west (see Figure 2-5 A to C and H to K).

2.4 Discussion

2.4.1 Reconstructions of regional Upper Paleozoic stratigraphy

The regional literature based on the 1:20,000 regional map (BGMRGS, 1967) has historically documented the presence of abundant Ordovician to Silurian schist, marble, and high-grade gneiss in the southern Shibanshan district. These rocks were previously inferred to be correlatives of the Ordovician-Silurian Huaniushan Group situated to the north of the Liuyuan Complex, which in turn was used as evidence supporting a rifting model to account for the mafic rocks of the Liuyuan Complex as described by Chen et al. (2016) and Wang et al. (2017). However, our detailed mapping results necessitate a new interpretation because these rocks constitute part of at least three distinct Early Permian tectono-stratigraphic complexes, which from south to north comprise the Shiyaozi, Baidunzi, and Ganquan Complexes. Consequently, a major revision of the Upper Paleozoic strata was necessary.

2.4.1.1 Shibanshan formation

The stratigraphy of the meta-sedimentary host rocks within the Baidunzi Complex is significantly hampered by the intense transposition and the presence of interleaved plutonic sheets. Nevertheless, detrital zircon analysis (see Chapter 4) has helped to establish a tentative stratigraphy. As described above, this sequence comprises possible Precambrian basement fragments and Upper Paleozoic meta-sedimentary strata. The Upper Paleozoic strata comprises volcaniclastic sedimentary rocks, marble, marl, interlayered psammite, and shale, with a maximum depositional age range from the Kasimovian to the Asselian (306 – 295 Ma). The strata are inferred to comprise massive carbonate at the base and interlayered limestone and siltstone higher up in the sequence and interpreted to represent a transition from a reef-shelf environment to a tidal-flat depositional environment (Niu et al., 2018; 2021).

At the southern boundary of the Baidunzi Complex, a fault zone delineates a separation between the aforementioned rocks and different phases of amphibolite and orthogneiss of the Shiyaozi Complex. The amphibolite and orthogneiss were intruded by plutons of mega-crystic granite and hornblende diorite to granodiorite. These rocks are situated in the southernmost part of the Liuyuan BOC, and their affiliation is either linked to the Dunhuang terrane (Tian et al., 2015, 2020, 2023 and Soldner et al., 2022) or interpreted as forming an independent terrane situated between the Dunhuang terrane and the other units described herein (Worthington, 2022). However, these rocks are poorly understood and the presence of a desert area with limited outcrops hinders direct observation of the Liuyuan BOC's connection to the bona fide rocks of the Dunhuang terrane located further south.

2.4.1.2 Ganquan group

At the northern boundary, a shear zone separates Baidunzi Complex from sequences of variably tectonised felsic volcanic and volcaniclastic rocks of the Ganquan Complex. However, it should be noted that the Ganquan Complex discussed herein may not necessarily correlate with the coeval felsic volcanic rocks of the Kasimovian to Sakmarian Ganquan Formation (BGMRGS, 1997; Niu et al., 2018). This is due to previous stratigraphic interpretations of the Ganquan Formation in the area neglecting internal unconformities and structural complexities that are presented in this paper.

The previously defined Ganquan Formation was characterized by basal poorly stratified clastic rocks and upper bimodal volcanic rocks composed of basalt and rhyolite (BGMRGS, 1997). Niu et al. (2018) later modified the regional distribution and stratigraphy of Ganquan Formation and provided evidence from a selection of marine fossils in the massive limestone to demonstrate a shallow marine environment, constraining its ages to Kasimovian to Asselian or Sakmarian with additional radiometric data. Our mapping results have identified unconformities and thrust faults within the Ganquan Group, leading to the subdivision of the Ganquan Complex into lower and upper sequences that comprise three lithodemes (see Chapter 3). The lower sequence primarily consists of pyroclastic volcanics dated at 295-292 Ma, with occasional occurrences of green basaltic tuff and a lack of continental derived clastic rocks, suggesting a marine volcanic setting. The upper sequence comprises (1) a red bed unit that unconformably overlies the volcanic rocks of the lower sequence and (2) a coeval subaerial siliciclastic to calcareous epiclastic sedimentary unit that is consistently separated from the structurally underlying lower sequence by thrust faults. Radiometric dating of volcanic tuff interbeds indicates a depositional age range of approximately 283 to 281 Ma.

The large volume of pillow basalt in the Liuyuan Complex were previously classified within the Permian Jinta Formation or as part of the Zhesi Group (BGMRGS, 1967; Chen et al., 2016; Niu et

al., 2018). However, fossiliferous sandstone underlying the pillow basalt contains Pseudogastrioceras, Spiriferella rajah, and Phricodothyris asiatica fossils, which are indicative of Capitanian time. This age is considerably younger than the radiometric ages of the overlying pillow lava in the Liuyuan Complex demanding a tectonic relationship between the basalt and overlying sedimentary rocks. Additionally, the igneous rocks of the oceanic Liuyuan Complex are deformed and lack layering yet are interpreted to be intercalated with shallow-marine strata. Here it is proposed that the sandstone and associated younger subaqueous clastic sedimentary strata of the Jinta Formation were deposited unconformably over the Liuyuan Complex, possibly part of the Shuangbutang and Jushitan Formations (see below). These sediments are now structurally overlain by the pillow basalt due to D2 folding and/or thrusting (Figure 2-2 cross section A-A'). Since a temporal and tectonic connection between the Liuyuan Complex and the contemporaneous Ganquan Complex has been established (Santos et al., 2022; Hong et al., 2023; Santos, 2022), it is suggested to correlate the shallow marine sedimentary rocks that were previously assigned to the Jinta Formation, with the upper sequence of Ganquan Complex.

2.4.1.3 Heishankou formation and Liuyuan conglomerate synthem

These Permian sedimentary cover units structurally and/or unconformably overlie the Ganquan Complex. However, these units were previously mapped and grouped into the Carboniferous Hongliuyuan Formation and/or the Early Permian Zhesi Group, interpreted as conformably overlain by the Liuyuan Complex (BGMRGS, 1997; Niu et al., 2018). In our map, the Heishankou formation and Liuyuan conglomerate synthem of Heishankou Basin situated between the Liuyuan and Ganquan complexes to the north serves as a distinct demarcation between these two complexes. However, its regional correlation has remained a subject of debate. Guo et al. (2014, 2022) have distinguished it from the turbidite strata (Li, 2019) to the north, associating it instead with

the southern portion of the Heishankou Basin. In contrast, Cleven et al. (2018) and Niu et al. (2018) have the rocks correlated with the northern turbidite strata, grouping them together under the Shuangbutang Formation and/or Jushitan Formation, respectively.

In the previous regional literature and stratigraphic interpretations, the Shuangbutang Formation has been described as having several coarsening-upward successions predominantly composed of limestone and felsic volcanic rocks. Conversely, the Jushitan Formation is characterized as a fining-upward sequence that occasionally intersects with the Shuangbutang Formation in certain areas. It was commonly believed that both formations were stratigraphically overlain by the basaltic lava of the Liuyuan Complex (Niu et al., 2018). However, our investigations suggest the sedimentary cover sequence rocks of Heishankou Basin unconformably overlie rocks of the Baidunzi, Ganquan and Liuyuan complexes. This is supported by conglomerate beds within the Heishankou Formation and Liuyuan conglomerate synthem, containing lithic clasts of granitoids, felsic tuff, basaltic rocks, and gabbro, lithologies of which are typical of the aforementioned underlying complexes. Importantly, the Heishankou formation and Liuyuan conglomerate synthem both unconformably overlie the Ganquan Complex and Baidunzi Complex and they do not intersect each other. Instead, they are separated by internal unconformities and tectonic contacts, indicating the absence of an equivalent correlation or facies change between the Shuangbutang and Jushitan formations. Instead, these two units are separated by unconformities and thrusts.

Zhesi formation or group is another commonly used stratigraphic name to represent the Cisuralian and Guadalupian strata in the Beishan Region (Zhu, 1983), the stratigraphy of which include the Shuangbutang, Jushitan and Jinta formations in an ascending order. This study shows evidence that most of the previously recognized unconformable contacts outlined by Zhu (1983) and Niu et al. (2018) are better interpreted as fault contacts that emplaced older sections above younger

rocks (Figure 2-2, 2-3 and 2-4). These findings consideration raise questions about the applicability of the existing nomenclature, necessitating their redefinition in light of new structural and stratigraphic insights.

2.4.2 Formation of the Heishankou Basin and its tectonic implications

As previously mentioned, the Heishankou Formation primarily consists of a flysch-like sequence with three members exhibiting an overall fining-upward trend. The basal conglomerate is predominantly composed of clasts of granitoids and felsic volcanics. Part of the lower Heishankou Formation unconformably overlies the volcano-sedimentary lithodeme, and we interpret the clast sources to be derived from the Baidunzi and Ganquan Complexes.

In contrast, the Liuyuan conglomerate synthem predominantly contains clasts of mafic volcanic and gabbroic rocks. It unconformably overlies the southward-transported sheet of Liuyuan Complex rocks and the Heishankou Formation. We interpret the deposition of the Liuyuan conglomerate synthem as primarily receiving detritus eroded from the denuded Liuyuan Complex and the underlying Heishankou Formation. Notably, the Liuyuan conglomerate synthem was also locally overthrust by the Liuyuan Complex and members of Heishankou Formation, suggesting a syn-tectonic deposition. Bedding is commonly parallel to the F2 fold axial planes and thrust faults.

The polyphase deformation history of the Heishankou basin sediments is partly shared (D2 & D3) with the Liuyuan, Ganquan and the Baidunzi complexes; however, it lacks the oldest structures observed in the Ganquan and Baidunzi complexes. The three lower members of the Heishankou formation contains clasts from the rocks in panels 2 and 4 and hence were likely deposited syn-tectonically during their uplift and exhumation and represents an intramontane basin that locally overstepped the amalgamated panels 3 and 4. The basin probably formed as a foredeep associated with the late D2, southward thrusting of the Liuyuan Complex over panels 3 and 4, previously

structurally assembled during D1 and/or D2 (Figure 2-9). The Liuyuan conglomerate synthem started deposition after the Liuyuan Complex breached sea level, following progressive southward transport over the already imbricated Ganquan Complex and Heishankou formation. Notably, here the name Liuyuan conglomerate synthem is preferred as it represents a particular syn-kinematic depositional phase formed during uplift of the underlying source rocks. The D2 structures observed in the Heishankou Basin sedimentary rocks resembles a fold-and-thrust belt style of deformation (Polet and Lisle, 2011). Cross section A-A' and Figures 2-10 show a set of imbricate thrusts and antiformal stacks, with local hanging wall ramps over the disrupted footwall.

The D2 deformation present further south is related to the amalgamation of the Ganquan and the Baidunzi Complexes. Shutdown of the Ganquan Arc magmatism at ca. 281 Ma coincides with uplift and erosion of at least part of the Ganquan arc recorded by deposition of the unconformable red beds lithodeme, D2 deformation and metamorphism in the Baidunzi Complex and the approximately onset of inversion of the Liuyuan backarc basin. We infer that D2 deformation associated with south-directed tectonic transport in the Ganquan Complex was coeval with deformation and metamorphism in the Baidunzi Complex, because panels 2,3 and 4 had amalgamated at ca. 281 Ma, based on the stitching hornblende gabbro of this age, and supported by the metamorphic rim ages of zircon sampled from the Baidunzi intrusive suite (see Chapter 4). Therefore, we relate D2 to collision between the Ganquan and the Baidunzi complexes, and the Baidunzi Complex was arriving from the south and structurally situated on the lower plate during thrusting.

In addition, accretion of the Baidunzi Complex forced the previously-existing north-dipping subduction zone that created the arc volcanism in the Ganquan Complex to step into the trailing backarc basin, which led to renewed, short-lived andesite-dacite-rhyolite arc magmatism (282-276 Ma), first built upon the Huaniushan terrane (e.g., 282-279 Ma), but later (279-276 Ma) migrating

onto part of the Liuyuan Complex (Santos et al., 2023; Mao et al., 2012a), which at this time was transferred into a forearc to arc setting during closure of the backarc basin it was formed in. Closure of the backarc basin led to late D2 southward transport of the Liuyuan Complex and deposition of the Heishankou Basin in a narrow foredeep and terminated with accretion of the previously assembled tectonostratigraphic units in panels 2, 3 and 4 with the Liuyuan Complex and Huaniushan terrane.

The D3-related north-directed thrusting and folding, are coeval with the juxtaposition and accretion of Shiyaozi Complex with the Baidunzi Complex, synchronous with or postdating the ca. 273 to 261 Ma intrusion of hornblende diorite pluton and multiple granodiorite dykes (Worthington, 2022). D1-2 is absent in the Shiyaozi Complex, and an upper plate setting with respect to the tectonostratigraphic units to its north is probably the cause for the north-directed tectonic transport. The post 270 Ma arc-like magmatism in Shiyaozi Complex suggests that the tectonostratigraphic units of panels north of the fault zone were transferred to a lower plate setting, possibly as a result of a subduction polarity reversal following termination of backarc closure. If this is correct, it implies that the seaway separating the Shiyaozi Complex from the northern Baidunzi-Ganquan composite arcs was relatively narrow with initiation of renewed subduction immediately north of the Shiyaozi Complex. Any potential oceanic remnants of such a seaway other than the intervening metasedimentary rocks (northern margin of Panel 1, Figure 2-2) have not been preserved. Alternatively, significant strike-slip movements, although not obvious from field relationships and structure, may have been involved. Regardless the lower plate the Shiyaozi Complex was situated further to the south and may have a relationship to the Dunhuang terrane. The north-directed D3 tectonic transport emplaced panel 4 over the Heishankou formation sediments and folded and steepened the previously formed D2 thrust contacts. Accretion of the Shiyaozi Complex may have marked closure of the last remnants of the Paleo-Asian Ocean if it were part of the Dunhuang terrane.

However, the relationships between the Shiyaozi Complex, the Dunhuang terrane, and the Tarim craton remain poorly understood and require further investigation.

2.5 Conclusions

The small cross-section across only a couple dozens of kilometers in the study area involves a complex tectonic evolution over a period of 30 Ma: the syn-D1 arc magmatism of the Baidunzi Intrusive Suite was emplaced within a transpressional tectonic setting, as the start of the tectonic evolution since ca. 295 Ma. This phase was succeeded by the stepwise accretion of multiple segments of the Ganquan Arc with the Baidunzi Complex, marking the onset of south-verging D2 deformation initiated ca. 281 Ma. Subsequently, the Liuyuan back-arc basin was closed during subduction of most of its oceanic lithosphere, which led to accretion of the Liuyuan Complex and associated arc from the north, leading to the establishment of a foreland basin (Heishankou Basin) above the Ganquan Complex late during D2. Ultimately, this geological evolution culminated in the amalgamation and collision with the Shiyaozi Complex from the south, resulting in the north-verging D3 deformation, postdating the 273-261 Ma magmatism recorded in the Shiyaozi Complex.

Modern arc accretionary systems, like those present in the island archipelagos of the Southwest Pacific Ocean, serve as valuable analogs to illustrate how the successive evolutionary cycles of subduction can be initiated and terminated through multi-phased arc accretion and collision events. Studies of their geometries and kinematics involving tectonic processes such as slab rollback (Martinez et al., 2006; Boutelier and Cruden, 2013), subduction polarity reversal, and doubly vergent subduction zones, highlight the potential complexities that can accompany the arc-continent collisions in ancient orogens. These complexities will not be easily recognised without detailed field work and associated multi disciplinary investigations such as those done in the Liuyuan BOC. Contrary to previous research, which largely depended on interpretations drawn from geochemical data,

complementary tectonostratigraphic and structural investigations refined and drastically changed the regional tectonic framework of the southern Beishan area. The multi disciplinary approach as documented herein led to a more comprehensive understanding of the Late Paleozoic terminal collisional history of Central Asian Orogenic Belt.

2.6 References

BGMRGS (Bureau of Geology and Mineral Resources of Gansu Province), 1967. 1/200 000 Geological map and guidebook of the Hongliuyuan district, 67 pp. (in Chinese).

BGMRGS (Bureau of Geology and Mineral Resources of Gansu Province), 1989. Regional Geology of Gansu Province: Beijing, Geological Publishing House, People's Republic of China, Ministry of Geology and Mineral Resources Geological Memoirs, Series 1, No. 19 (in Chinese).

BGMRGS (Bureau of Geology and Mineral Resources of Gansu Province), 1997. Stratigraphy (Lithostratic) of Gansu Province. China University of Geosciences Press, Wuhan, 314 pp. (in Chinese).

BGMRGS (Bureau of Geology and Mineral Resources of Gansu Province), 2005. Report of 1: 250,000 Regional Geological Survey of Anxi (K46C004001) (in Chinese).

Boutelier, D., & Cruden, A. (2013). Slab rollback rate and trench curvature controlled by arc deformation. Geology, 41(8), 911-914.

Chen, S., Guo, Z., Qi, J., Zhang, Y., Pe-Piper, G., & Piper, D. J. (2016). Early Permian volcano-sedimentary successions, Beishan, NW China: Peperites demonstrate an evolving rift basin. Journal of Volcanology and Geothermal Research, 309, 31-44.

Cleven, N. R., Lin, S., Xiao, W., Davis, D. W., & Davis, B. (2018). Successive arc accretion in the southern Central Asian orogenic belt, NW China: Evidence from two Paleozoic arcs with offset magmatic periods. GSA Bulletin, 130(3-4), 537-557.

de Vries, J. (2021). A structural-metamorphic approach to deciphering the exhumation of the Gubaoquan eclogite in the Beishan Orogenic Collage, NW China. Master thesis, University of Waterloo.

Feng, L., Lin, S., Li, L., Davis, D. W., Song, C., Li, J., ... & Lu, K. (2020). Constraints on the tectonic evolution of the southern central Asian orogenic belt from early Permian–middle Triassic granitoids from the central Dunhuang orogenic belt, NW China. Journal of Asian Earth Sciences, 194, 104283.

Guo, Q., Xiao, W., Hou, Q., Windley, B. F., Han, C., Tian, Z., & Song, D. (2014). Construction of Late Devonian Dundunshan arc in the Beishan orogen and its implication for tectonics of southern Central Asian Orogenic Belt. Lithos, 184, 361-378.

Guo, Q. Q., Chung, S. L., Lee, H. Y., Xiao, W. J., & Hou, Q. L. (2022). Termination of the Paleo-Asian Ocean in the Beishan orogen, NW China: Constraints from detrital zircon U-Pb age and Hf isotope analysis of turbidites. Geological Society of America Bulletin.

Hong, T., Santos, G. S., van Staal, C. R., Ji, W., & Lin, S. (2022). Mapping uncovered a multi-phase arc—back-arc system in southern Beishan during the Permian. National Science Review. .org/10.1093/nsr/nwac204

Hong, T., van Staal, C., Lin, S., Santos, G. S., & Wang, K. (2024). Evolving Permian magmatism associated with arc migration in the southern Beishan Orogenic Collage, Central Asian orogenic belt, NW China. Geological Society, London, Special Publications, 542(1), SP542-2022.

Li, J. (2019). A structural and stratigraphic study in Liuyuan area, Southern Beishan orogenic collage, Northwest China. Master thesis, University of Waterloo.

Mao, Q., Xiao, W., Windley, B. F., Han, C., Qu, J., Ao, S., ... & Guo, Q. (2012a). The Liuyuan complex in the Beishan, NW China: a Carboniferous–Permian ophiolitic fore-arc sliver in the southern Altaids. Geological Magazine, 149(3), 483-506.

Mao, Q., Xiao, W., Fang, T., Wang, J., Han, C., Sun, M., & Yuan, C. (2012b). Late Ordovician to early Devonian adakites and Nb-enriched basalts in the Liuyuan area, Beishan, NW China: implications for early Paleozoic slab-melting and crustal growth in the southern Altaids. Gondwana Research, 22(2), 534-553.

Martinez, F., Taylor, B., Baker, E. T., Resing, J. A., & Walker, S. L. (2006). Opposing trends in crustal thickness and spreading rate along the back-arc Eastern Lau Spreading Center: Implications for controls on ridge morphology, faulting, and hydrothermal activity. Earth and Planetary Science Letters, 245(3-4), 655-672.

Niu, Y., Liu, C., Shi, G. R., Lu, J., Xu, W., & Shi, J. (2018). Unconformity-bounded Upper Paleozoic megasequences in the Beishan Region (NW China) and implications for the timing of the Paleo-Asian Ocean closure. Journal of Asian Earth Sciences, 167, 11-32.

Niu, Y., Shi, G. R., Wang, J., Liu, C., Zhou, J., Lu, J., ... & Xu, W. (2021). The closing of the southern branch of the Paleo-Asian Ocean: Constraints from sedimentary records in the southern Beishan Region of the Central Asian Orogenic Belt, NW China. Marine and Petroleum Geology, 124, 104791.

Poblet, J. and R. J. Lisle, 2011: Kinematic evolution and structural styles of fold-and-thrust belts. Geological Society, London, Special Publications, 349, 1-24.

Santos, G. S., Hong, T., van Staal, C. R., Bedard, J., Lin, S., & Wang, K. (2022). Permian back‐arc basin formation and arc migration in the southern Central Asian Orogenic Belt, Northwest China. Geological Journal. https://doi.org/10.1002/gj.4609

Santos, G.S., (2022). Petrology, tectonic setting, and regional implications of the ophiolitic Liuyuan Complex, NW China. PhD thesis, University of Waterloo.

Santos, G.S., Bedard, J., van Staal, C., Lin S., Hong, T., and Wang, K. (2023). Geology of the Liuyuan Complex, NW China: a Permian back-arc basin ophiolite at the southern edge of the Central Asian Orogenic Belt. GSA bulletin, https://doi.org/10.1130/B36736.1

Soldner, J. (2023). Two distinct Paleozoic metamorphic events in the Tarim-North China Collage. National Science Review, 10(2), nwac133.

Soldner, J., Yuan, C., Schulmann, K., Jiang, Y., Štípská, P., Zhang, Y., ... & Wang, X. (2022). Early Paleozoic Cascadia-type active-margin evolution of the Dunhuang block (NW China): Geochemical and geochronological constraints. Bulletin, 134(9-10), 2503-2530.

Tian, J., Xin, H. T., Teng, X. J., Li, M., Liao, Q. A., Zhang, Y., & Ren, B. F. (2023). Petrogenesis and Tectonic Implications of the Late Silurian–Early Devonian Bimodal Intrusive Rocks in the Central Beishan Orogenic Belt, NW China: Constraints by Petrology, Geochemistry and Hf Isotope. Journal of Earth Science, 34(2), 431-443.

Tian, Z., & Xiao, W. (2020). An Andean‐type arc transferred into a Japanese‐type arc at final closure stage of the Palaeo‐Asian Ocean in the southernmost of Altaïds. Geological Journal, 55(3), 2023-2043.

Tian, Z., Xiao, W., Sun, J., Windley, B. F., Glen, R., Han, C., ... & Song, D. (2015). Triassic deformation of Permian Early Triassic arc-related sediments in the Beishan (NW China): Last pulse of the accretionary orogenesis in the southernmost Altaids. Tectonophysics, 662, 363-384.

van S taal, C.R., Hong, T., L in, S., Ji, W .H, 2021. Bedrock Geological Map of the Baidunzi-Heishankou Area, Guazhou, Gansu, China, scale 1:25,000: China Geological Survey, DOI: 10.35080/data.C.2021.P01.

Wang, Y., Luo, Z., Santosh, M., Wang, S., & Wang, N. (2017). The Liuyuan Volcanic Belt in NW China revisited: Evidence for Permian rifting associated with the assembly of continental blocks in the Central Asian Orogenic Belt. Geological Magazine, 154-2, 265–285.

Windley, B. F., Alexeiev, D., Xiao, W., Kroner, A., & Badarch, G. (2007). Tectonic models for accretion of the Central Asian Orogenic Belt. Journal of the Geological Society, 164(1), 31–47.

Worthington, Q. (2022). A ca. 273-261 Ma multi-component arc pluton in the southern area of the Beishan Orogenic Collage, NW China: a geochronological, geochemical, and petrogenetic analysis. Master thesis, University of Waterloo.

Xiao, W. J., Mao, Q. G., Windley, B. F., Han, C. M., Qu, J. F., Zhang, J. E., Ao, S. J., Guo, Q. Q., Cleven, N. R., Lin, S. F., Shan, Y. H., & Li, J. L. (2010). Paleozoic multiple accretionary and collisional processes of the Beishan orogenic collage. American Journal of Science, 310(10), 1553–1594.

Zhao, Y., Sun, Y., Diwu, C., Guo, A. L., Ao, W. H., & Zhu, T. (2016). The Dunhuang block is a Paleozoic orogenic belt and part of the Central Asian Orogenic Belt (CAOB), NW China. Gondwana Research, 30, 207-223.

Zhao, Y., Sun, Y., Diwu, C., Zhu, T., Ao, W., Zhang, H., & Yan, J. (2017). Paleozoic intrusive rocks from the Dunhuang tectonic belt, NW China: Constraints on the tectonic evolution of the southernmost Central Asian Orogenic Belt. Journal of Asian Earth Sciences, 138, 562-587.

Zhao, Y., Sun, Y., Yan, J., & Diwu, C. (2015). The Archean-Paleoproterozoic crustal evolution in the Dunhuang region, NW China: Constraints from zircon U–Pb geochronology and in situ Hf isotopes. Precambrian Research, 271, 83-97.

Zhu, W.Y., 1983. On the Permian marine stratigraphy and the fundamental characteristics of the fauna in Beishan, Gansu Province. Gansu Geol. 121–140 (in Chinese with English abstract).

Zuo, G.C., He, G.Q., 1990. Plate Tectonics and Metallogenic Regularities in Beishan Region. Peking University Publishing House Beijing.

2.7 Figures and captions

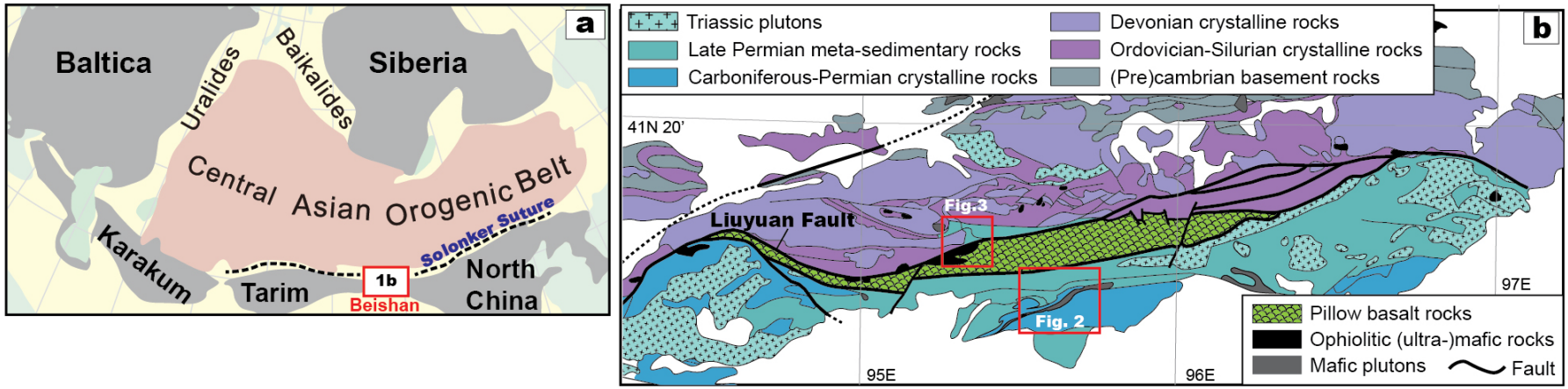


Figure 2-1: Tectonic frameworks showing location of Liuyuan BOC.

a) Sketch of the Central Asian orogenic belt showing the locations of sutures and the southern Beishan orogen; b) Simplified tectonic map of the southern Beishan orogen (modified from Mao et al., 2012).

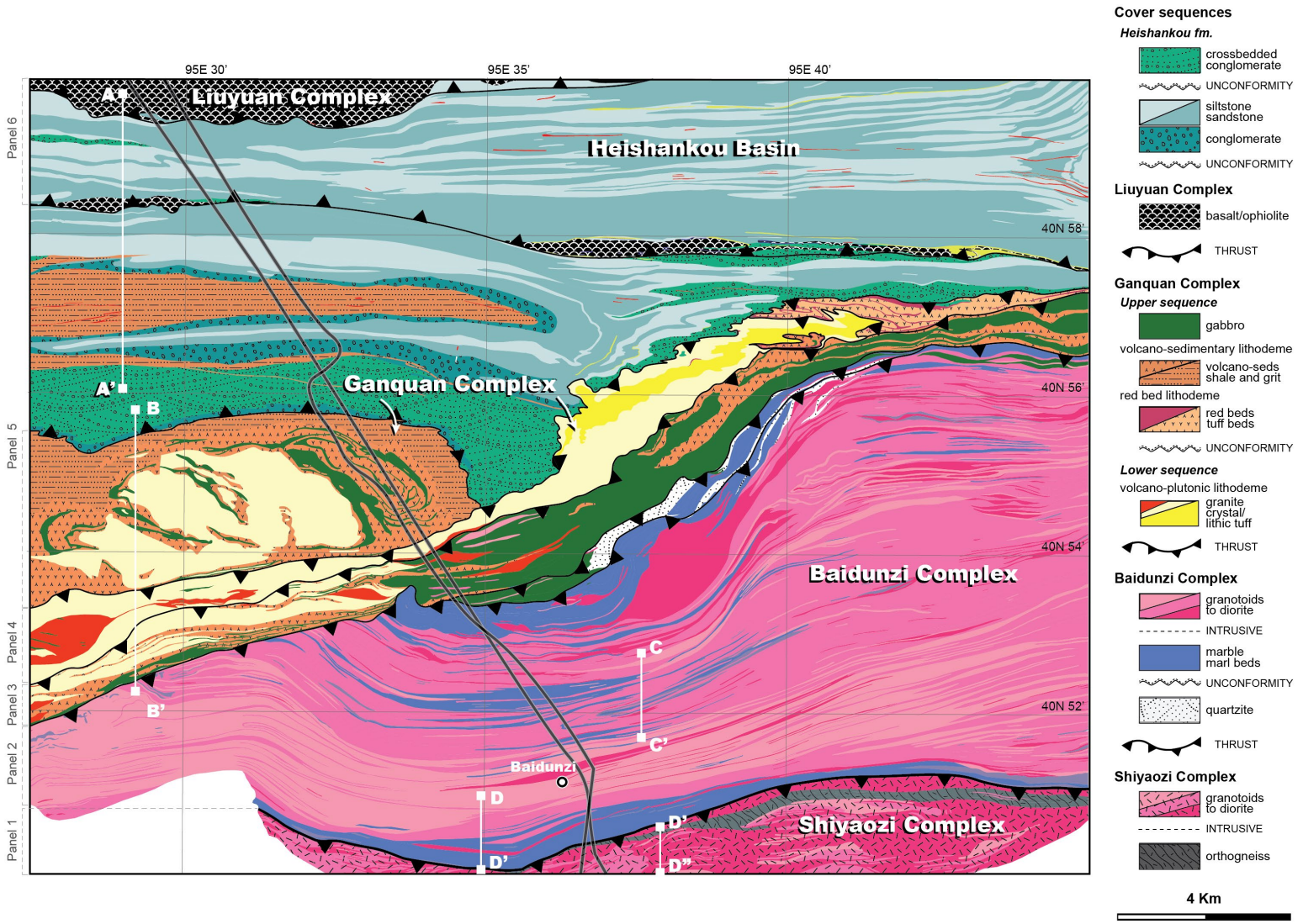
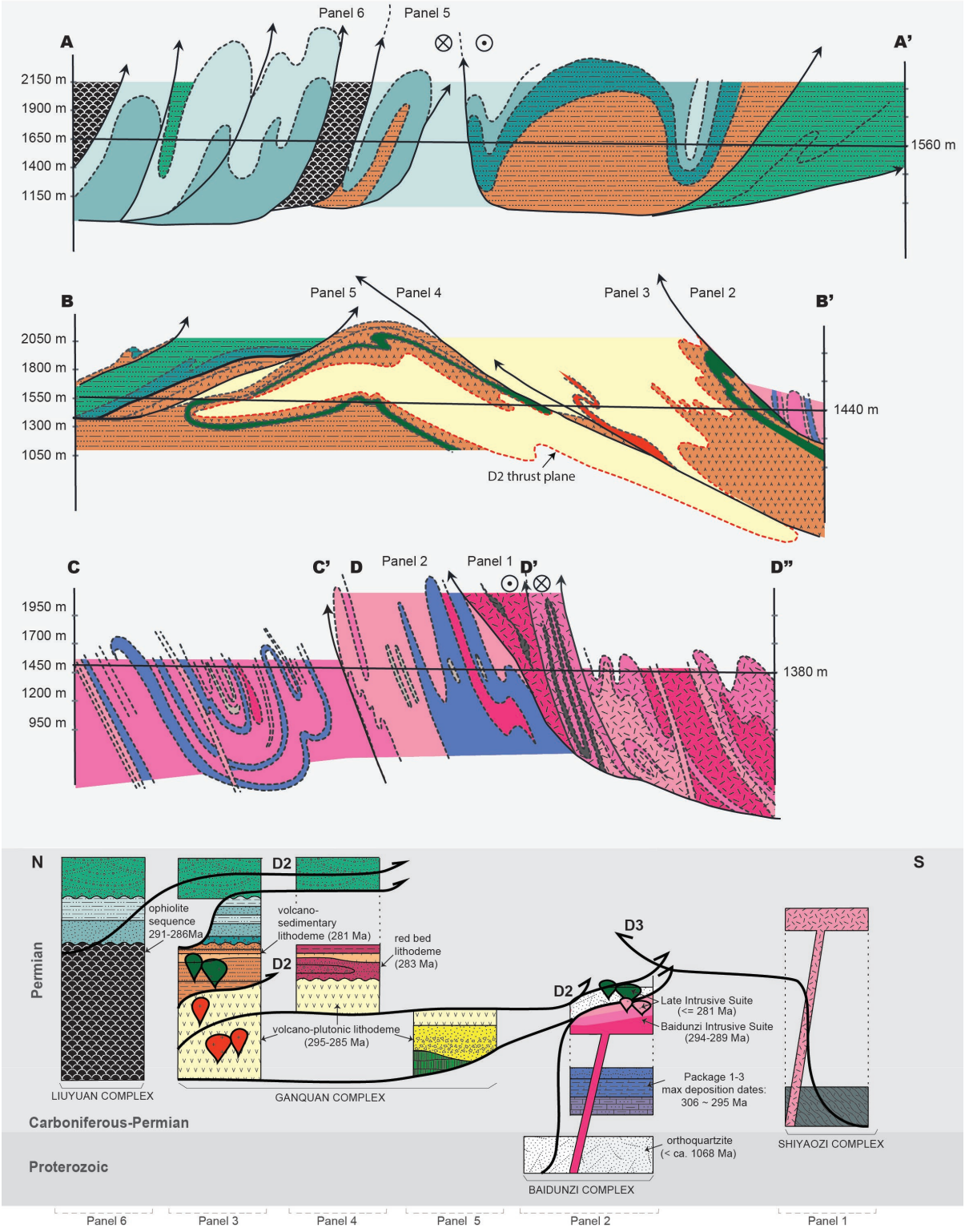
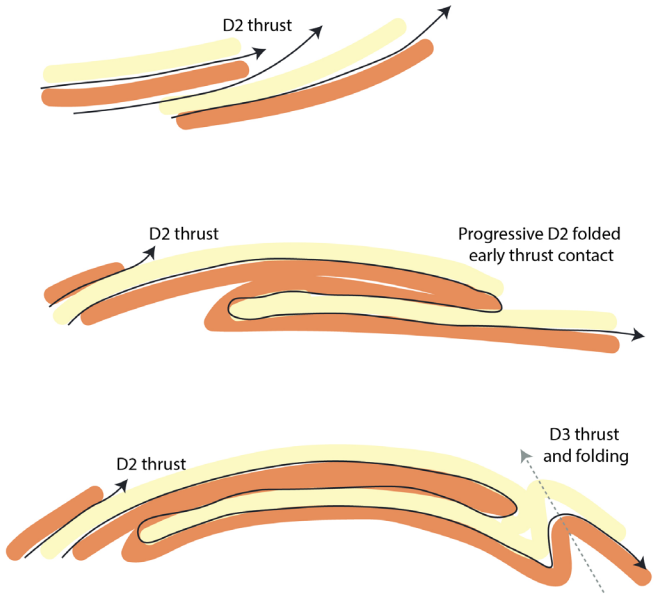


Figure 2-2: (a) Simplified geological map (van Staal et al., 2021) and (b) cross sections of the Baidunzi area (this study). (c) Structural evolutionary model of the dome-shape geometry in the Ganquan Complex shown in cross section B-B'.

(continued)


Panel 6
Panel 5
A
A'
2150 m
1900 m
1650 m
1400 m
1150 m
1560 m
B
B'
Panel 5
Panel 4
Panel 3
Panel 2
2050 m
1800 m
1550 m
1300 m
1050 m
1440 m
D2 thrust plane
C
C'
D
D'
D"
Panel 2
Panel 1
1950 m
1700 m
1450 m
1200 m
950 m
1380 m
N
S
Permian
ophiolite sequence 291-286Ma
D2
volcano-sedimentary lithodeme (281 Ma)
red bed lithodeme (283 Ma)
D2
volcano-plutonic lithodeme (295-285 Ma)
D3
D2
Late Intrusive Suite (<= 281 Ma)
Baidunzi Intrusive Suite (294-289 Ma)
Package 1-3 max deposition dates: 306 ~ 295 Ma
orthoquartzite (< ca. 1068 Ma)
LIUYUAN COMPLEX
GANQUAN COMPLEX
BAIDUNZI COMPLEX
SHIYAOZI COMPLEX
Carboniferous-Permian
Proterozoic
Panel 6
Panel 3
Panel 4
Panel 5
Panel 2
Panel 1

(continued)


D2 thrust
D2 thrust
Progressive D2 folded
early thrust contact
D2 thrust
D3 thrust
and folding

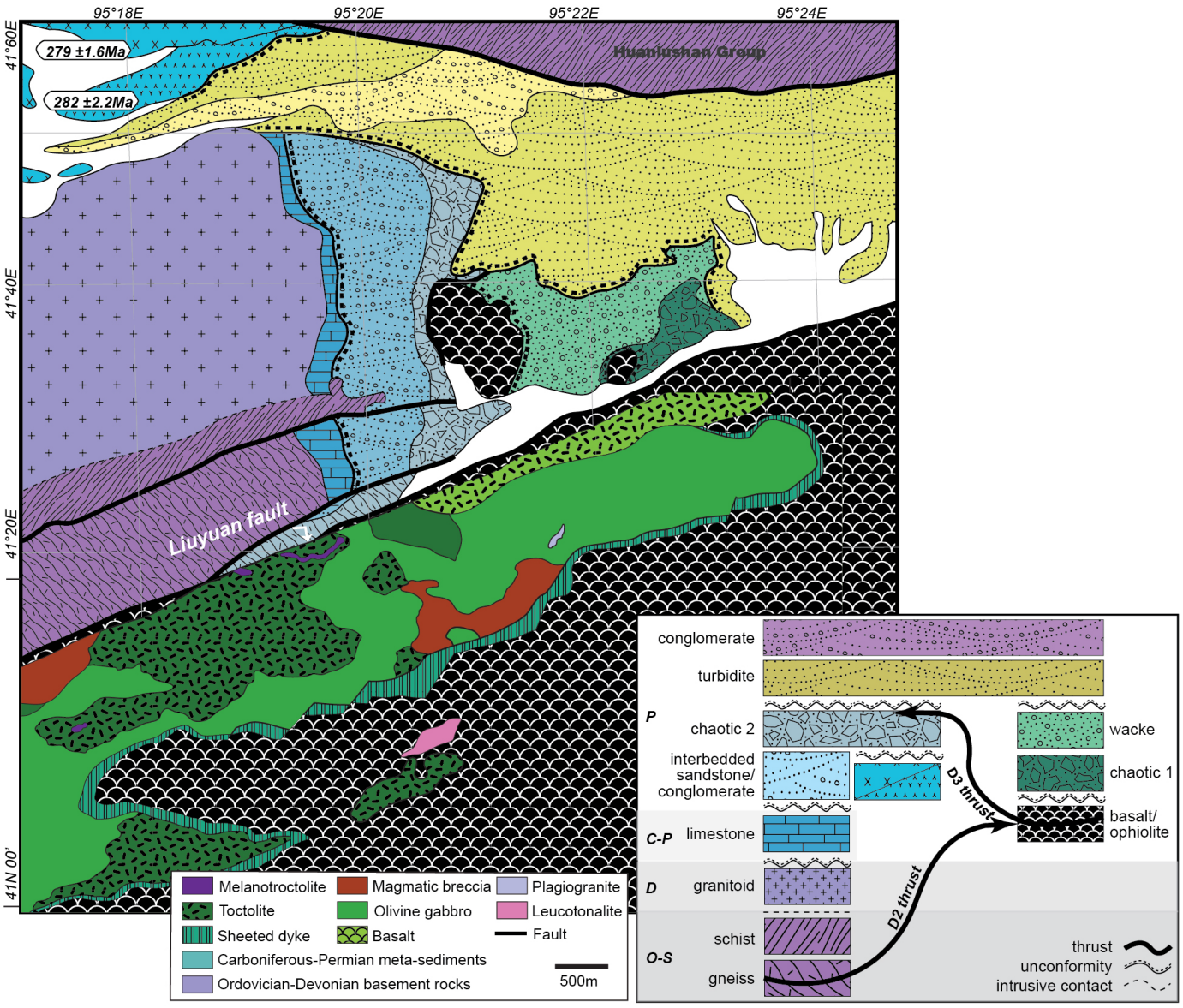


Figure 2-3: Simplified geological map of central part of the Liuyuan Complex and adjacent rocks of Huaniushan-Shibanshan terrane. Simplified from unpublished 1:25,000 geological maps that are modified from Li (2018) and Santos (2022).

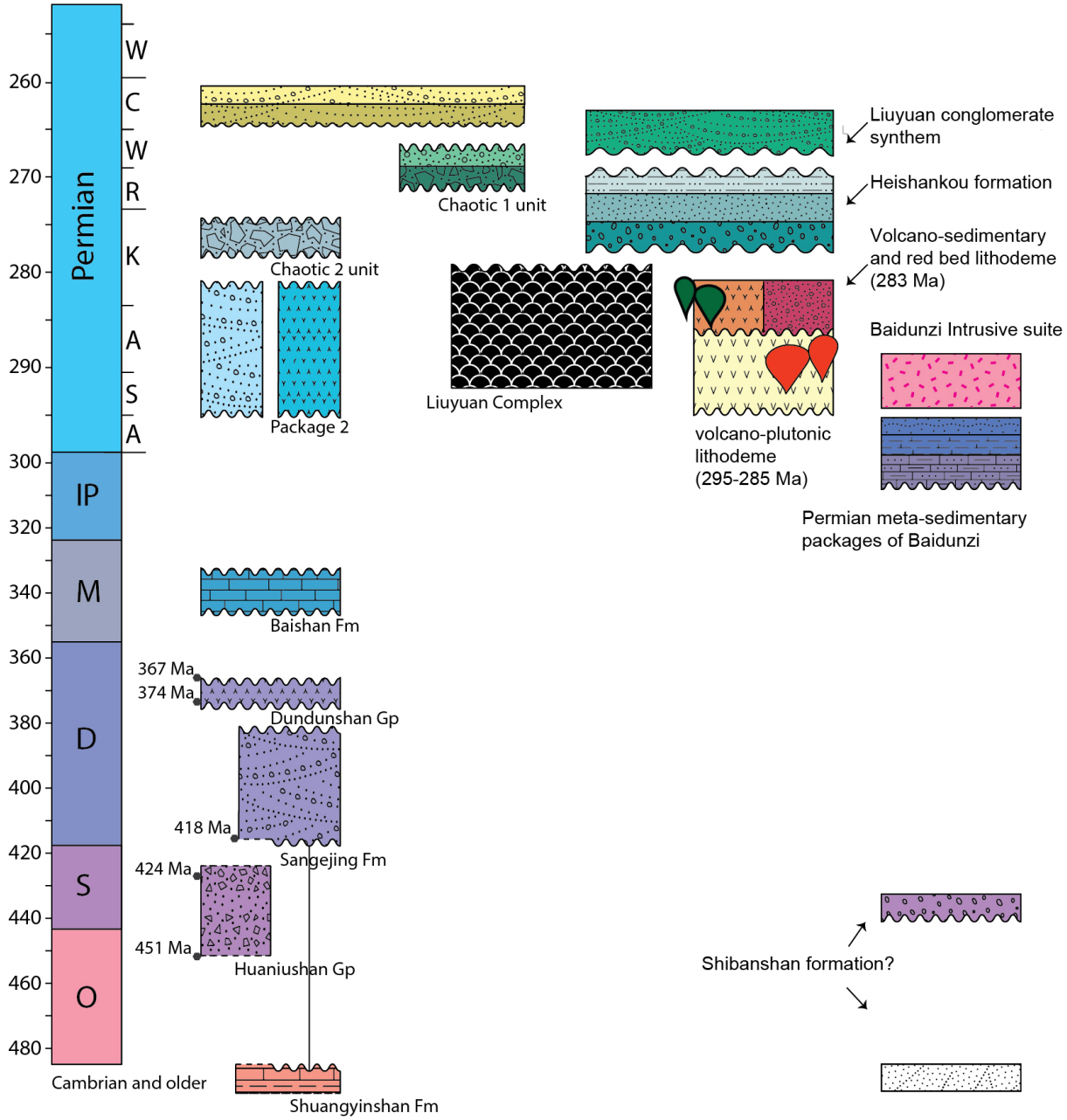


Figure 2-4: Reconstruction and comparism of regional stratigraphy in the north (left) and south (right) of the Liuyuan Complex. Interpretation and revision of Permian stratigraphy of the left session are based on Li (2018). Remaining stratigraphy of the left session from Shuangyinshan Fm. to Baishan Fm. of the Huaniushan-Dundunshan terrane is constructed from Niu et al. (2018, 2021), and BGMRGS (1967, 1989, 1997, 2005). The right session is constructed in this study.

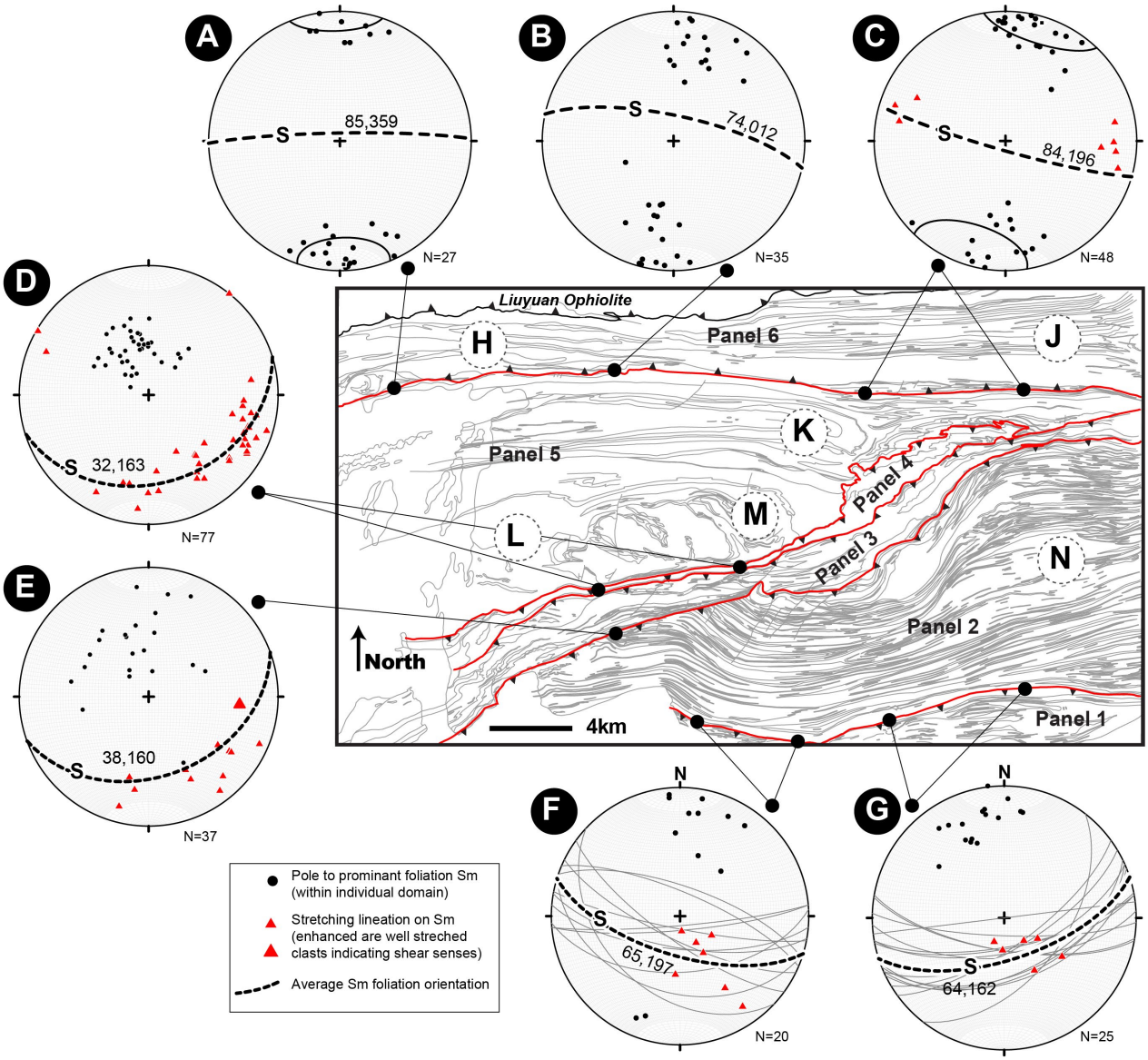
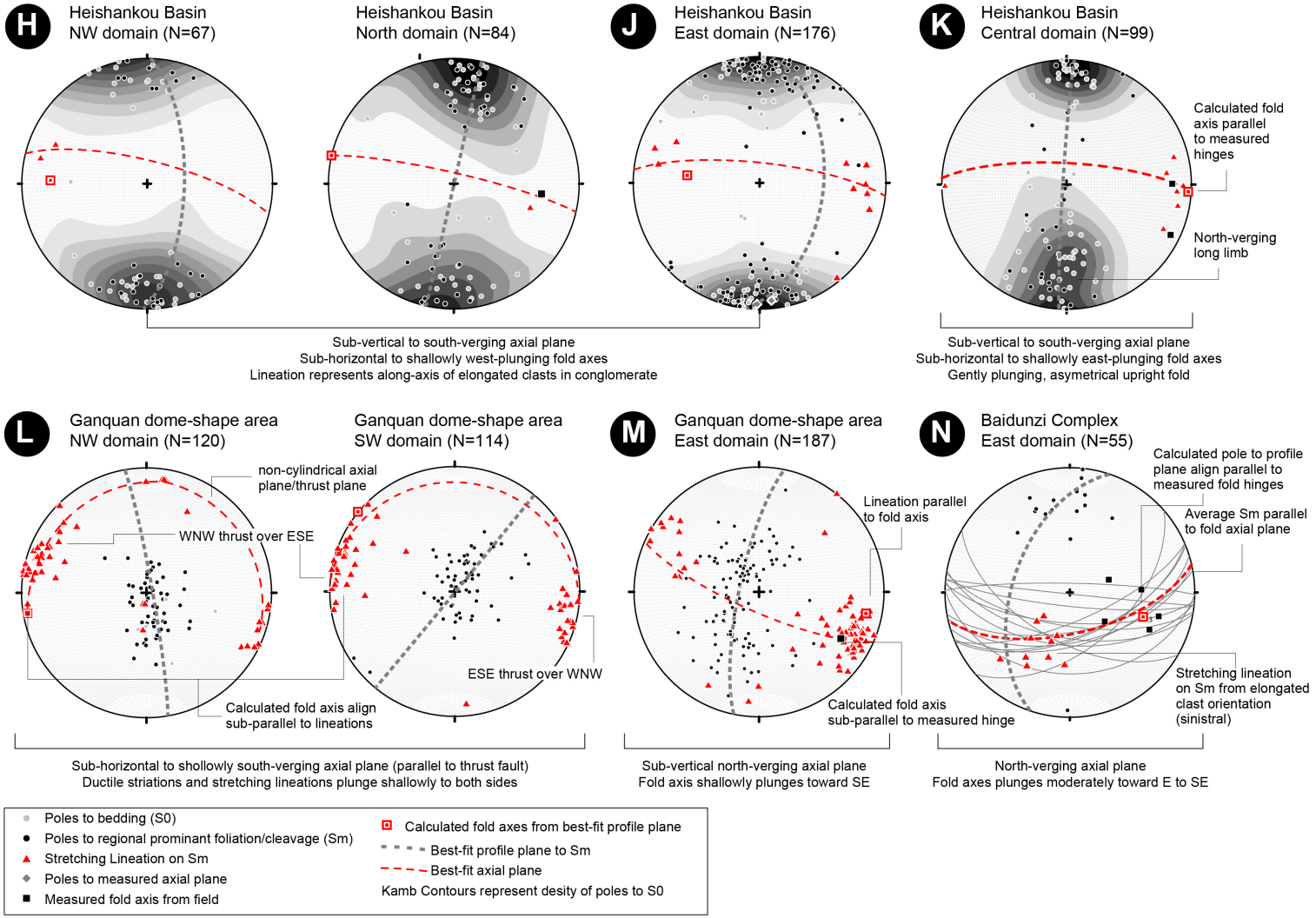


Figure 2-5: Stereonet plots of foliation and lineation data in shear zones with related fault planes (A) The western NE-striking segments of the thrust between Panel 6 and Panel 5. (B) The central E-W striking segments of the thrust between Panel 6 and Panel 5. (C) The eastern E-W striking segments of the thrust with stretching lineation data collected from elongated clasts in sandstone and conglomerate. (D) A compilation of all data over thrusts bounded by Panel 5, 4 and 3. (E) The western NE-striking segments of the shear zone between the Ganquan and Baidunzi Complex (Panel 2 over Panel 3). (F and G) The western and eastern segments of the thrust plane between Panel 1 and 2. (H-K) Data from folded structural domains in northwestern, north, east and central parts of the Heishankou Basin, respectively. (L-M) The weatern and eastern segments of the dome-shaped geometry in Ganquan Complex. (N) Data from folded structural domain in the NE side of the Baidunzi Complex.

(continued)


H
Heishankou Basin
NW domain (N=67)
Heishankou Basin
North domain (N=84)
J
Heishankou Basin
East domain (N=176)
K
Heishankou Basin
Central domain (N=99)
Calculated fold axis parallel to measured hinges
North-verging long limb
Sub-vertical to south-verging axial plane
Sub-horizontal to shallowly west-plunging fold axes
Lineation represents along-axis of elongated clasts in conglomerate
Sub-vertical to south-verging axial plane
Sub-horizontal to shallowly east-plunging fold axes
Gently plunging, asymetrical upright fold
L
Ganquan dome-shape area
NW domain (N=120)
Ganquan dome-shape area
SW domain (N=114)
M
Ganquan dome-shape area
East domain (N=187)
N
Baidunzi Complex
East domain (N=55)
non-cylindrical axial plane/thrust plane
WNW thrust over ESE
ESE thrust over WNW
Calculated fold axis align sub-parallel to lineations
Lineation parallel to fold axis
Calculated fold axis sub-parallel to measured hinge
Calculated pole to profile plane align parallel to measured fold hinges
Average Sm parallel to fold axial plane
Stretching lineation on Sm from elongated clast orientation (sinistral)
Sub-horizontal to shollowly south-verging axial plane (parallel to thrust fault)
Ductile striations and stretching lineations plunge shallowly to both sides
Sub-vertical north-verging axial plane
Fold axis shallowly plunges toward SE
North-verging axial plane
Fold axes plunges moderately toward E to SE
Poles to bedding (S0)
Poles to regional prominant foliation/cleavage (Sm)
Stretching Lineation on Sm
Poles to measured axial plane
Measured fold axis from field
Calculated fold axes from best-fit profile plane
Best-fit profile plane to Sm
Best-fit axial plane
Kamb Contours represent desity of poles to S0

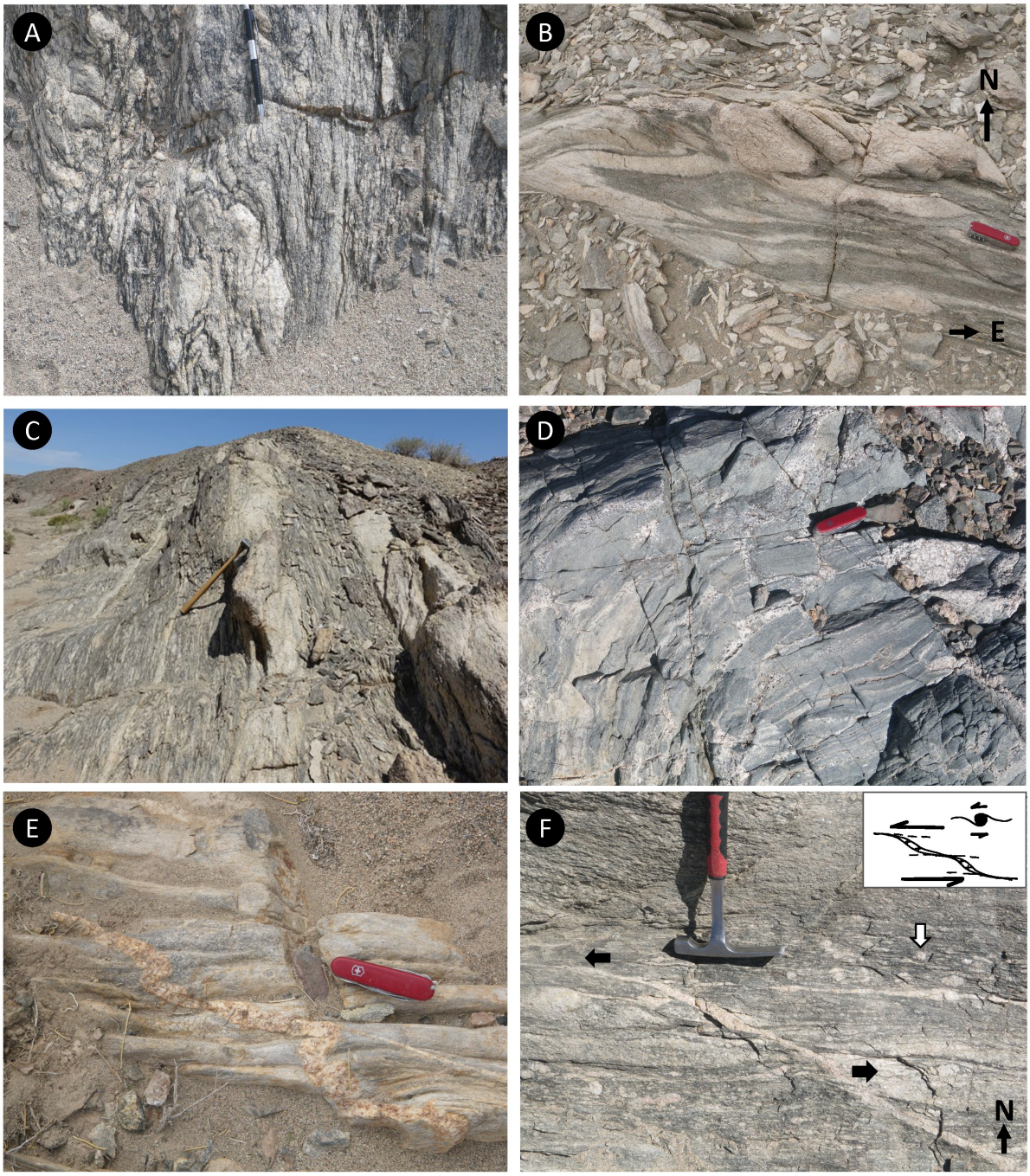


Figure 2-6: Field photos from Baidunzi Complex showing D1 deformation.
(A and B) Folded meta-sedimentary rocks and Baidunzi Intrusive Suite rocks, showing isoclinal recumbent fold with hinge steeply plunging toward east. (C and D) Syn-tectonic intrusions of granodiorite and tonalite from Baidunzi Intrusive Suite, showing dykes cut across the S1 foliations and also were folded by F1. (E and F) The same syn-tectonic intrusive veins and dykes showing sinistral kinematics.

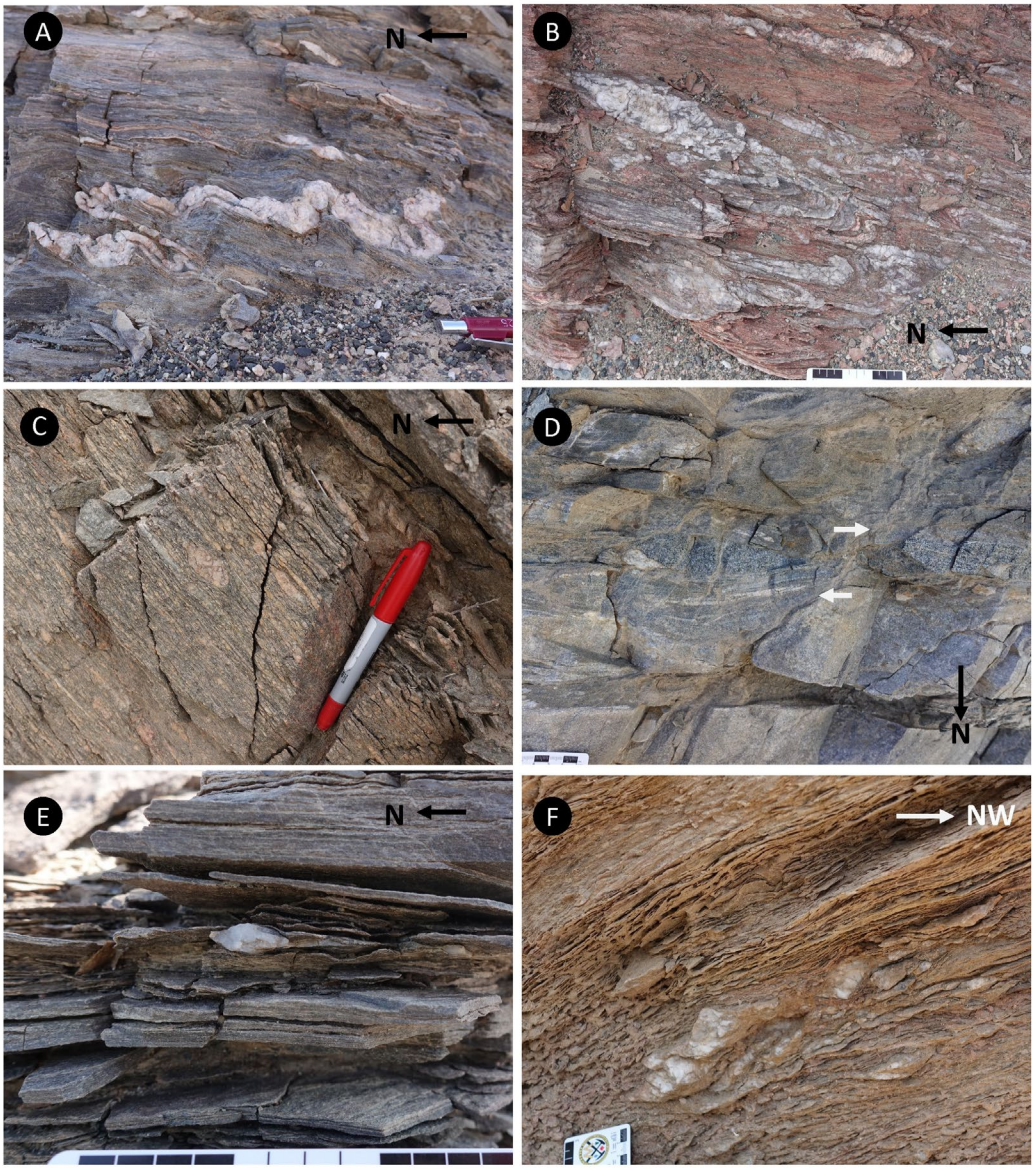


Figure 2-7: Field photos along fault zones bounded by Panel 1, 2 and 3.
(A-B) Shear zone between Panel 2 and 3, showing an ealier cleavage and phase of folding (S2, F2) were overprinted and refolded by D3, which is dominanted by N-verging reversal movement and produces shallowly S-dipping thrust planes at boundary between Panel 2 and 3. In (B) the main foliation along the limbs of the F2 folds is generally composite foliation of S1 and S2. (C-D) Strong reversal shearing shown by sigma-shaped porphyroclasts and S-C fabrics, indicating Panel 1 thrust over Panel 2 along a sub-vertical S-dipping plane (C) and dextral strike-slip movement on the planar view in (D). (E-F) Kinematics from Panel 2 and 3 fault zone. Assymetrical Z-fold and stretched sigma pyroclastic quartz vein boundins both show N to NW-directed thrusting of southern Baidunzi Complex over the Ganquan Complex along a shallowly to moderately SE-dipping fault plane.

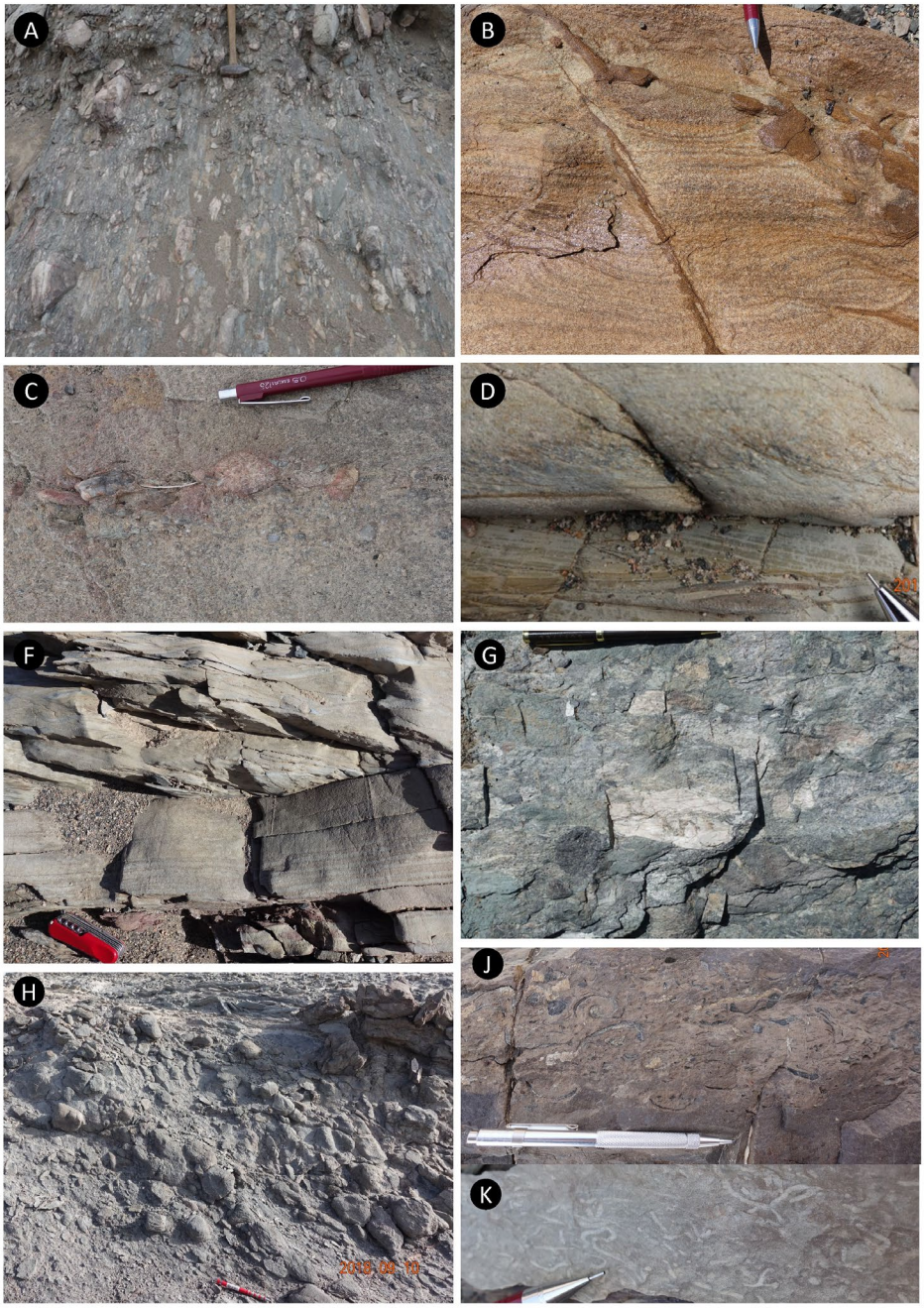


Figure 2-8: Field photos of outcrops in the Heishankou Basin.

(A) The basal conglomerate of Heishankou Formation, show clasts dominanted by felsic volcanic rocks and granitoid rocks. (B) Cross bedding in the sandstone member of the Heishankou Formation. (A and C) Elongated granitoid clasts that represent stretching lineation orientation, which is parallel to the central domain fold aixs, shallowly plunging toward west. (D-E) grit, sandstone and siltstone interbeds showing cross beddings. (G-H) The conglomerate member of the Liuyuan conglomerate synthem showing lithc clasts of basalt, gabbro, and siltstone and sandstone. (J-K) Debrics of trace fossils in the Liuyuan conglomerate synthem.

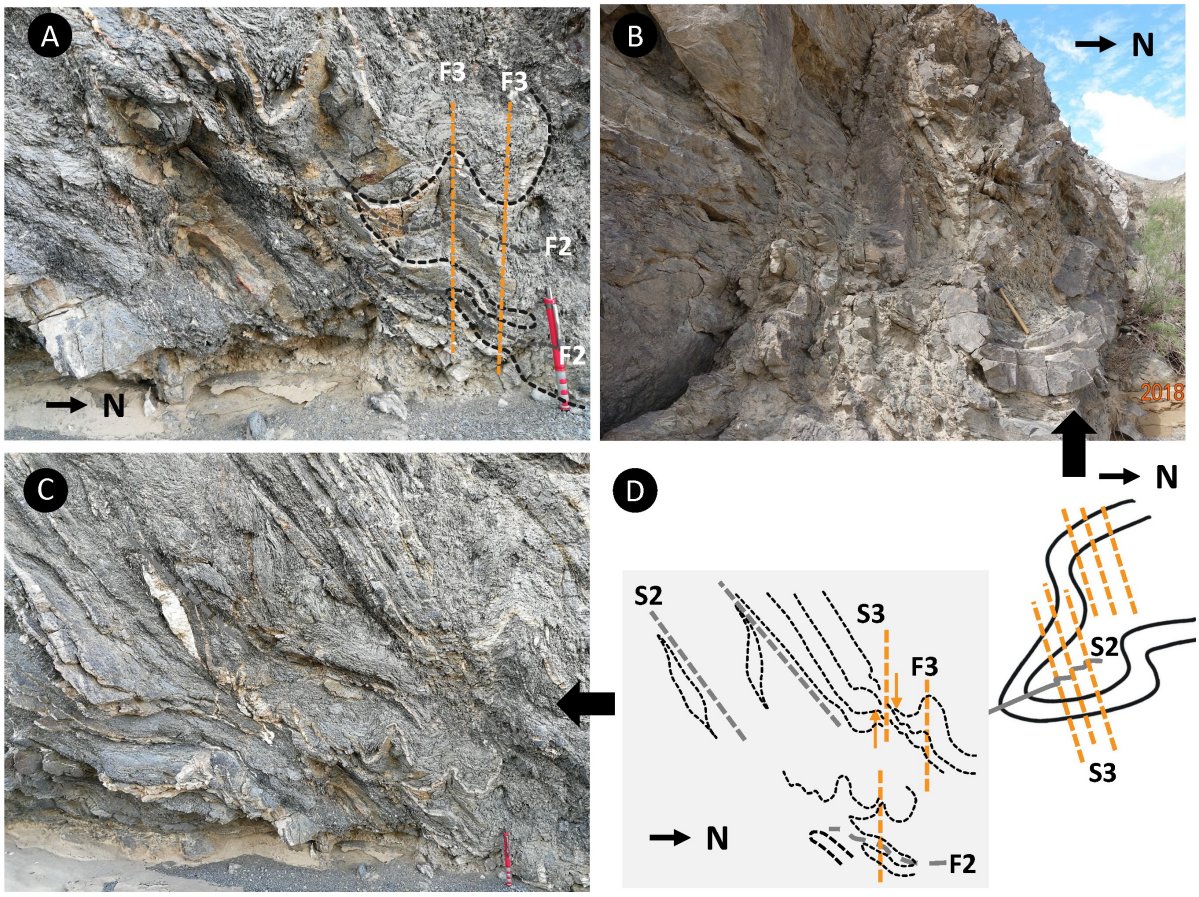


Figure 2-9: Structures in the Heishankou Basin.
Beddings and quartz veins were thrusted and folded by the south-verging D2, producing south-verging S2 and F2. A later north-verging D3 overprinted S2 and re-folded F2, forming a sub-vertical S3 with locally normal movement and F3 folds with sub-vertical fold axis.

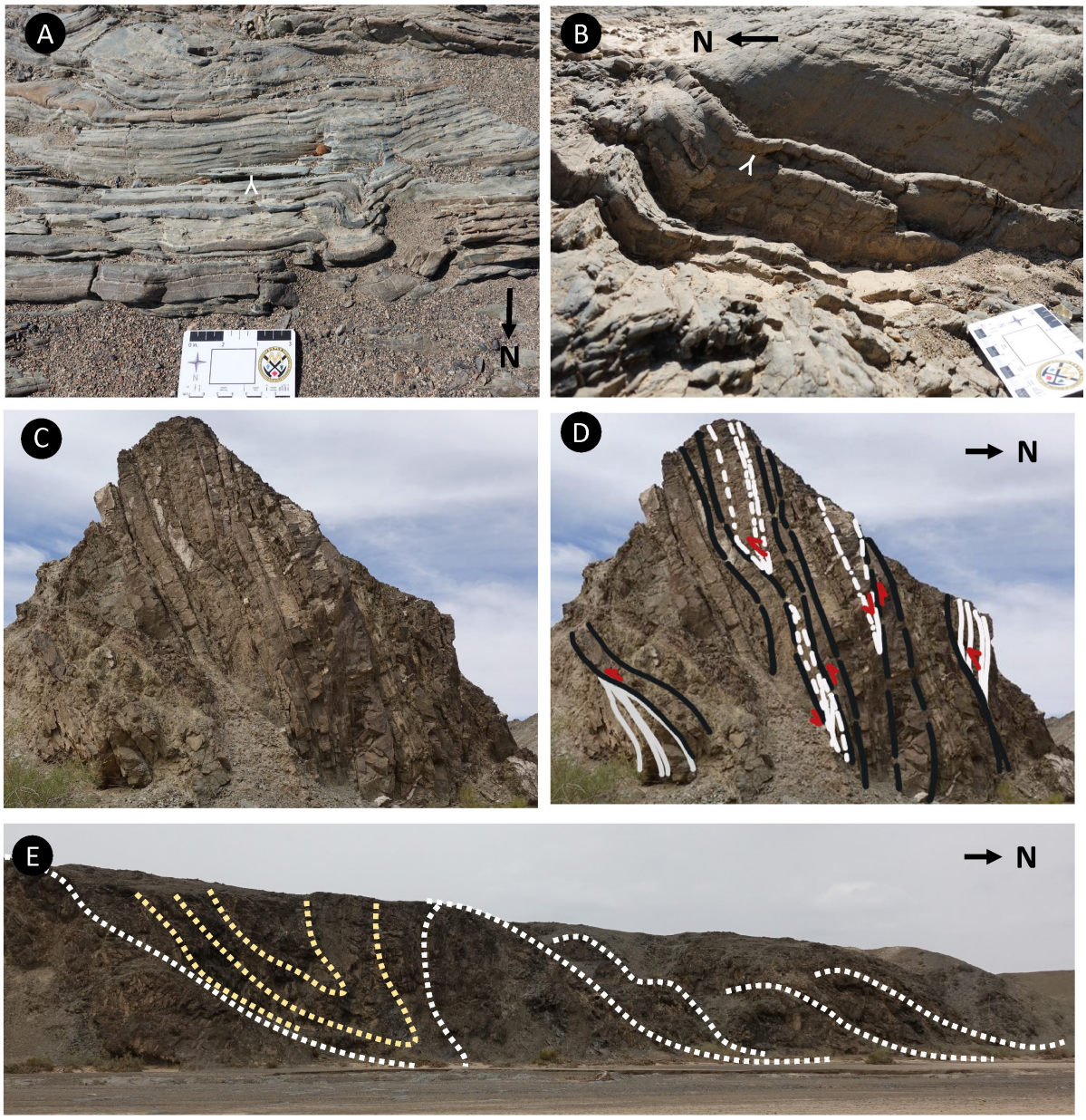


Figure 2-10: Fold-and-thrust style deformation in the Heishankou Basin.

Chapter 3 Evolving Permian magmatism associated with arc migration in the southern Beishan Orogenic Collage, Central Asian orogenic belt, NW China

3.1 Abstract

The Beishan Orogen contains the youngest suture in the Central Asian orogenic belt and is vital understanding its terminal collision history and closure of the last vestiges of the Paleo-Asian Ocean. Multidisciplinary evidence is provided for a close temporal and spatial linkage between the Liuyuan Complex backarc ophiolite, and the Ganquan Complex arc rocks. The Ganquan Complex mainly comprises felsic volcanic and volcaniclastic rocks and is divided into a lower and upper sequence, which both exhibit arc-like geochemical signatures, and have magmatic zircons characterized by mantle-like $\delta^{18}O$ values. Their U-Pb zircon ages range between 295 and 286 Ma and between 283 and 281 Ma, with corresponding εHf values varying from -4.2 to +1.9 and from +1.3 to +7.6, respectively, indicating a more juvenile magma source overtime. The increase of juvenile isotopic signatures in the Ganquan Complex rocks is attributed to arc-trench migration exhibits, which progressively removed the arc from influences of an old arc basement contaminant and led to backarc spreading and formation of the Liuyuan ophiolite. Cessation of the multi-phase Ganquan arc system at ca. 280 Ma coincided with the accretion of the continental Baidunzi Complex in the south; the latter constrained by the emplacement of a stitching gabbro.

3.2 Introduction

Suture zones that separate disparate accreted terranes are commonly key elements to guide studies in ancient orogens and reconstruct regional tectonic evolution. As with other orogens worldwide, most of the laterally distributed ophiolites and ophiolitic mélanges within the Central Asian orogenic belt (CAOB) are interpreted to be remnants of oceanic lithosphere. These remnants of

oceanic rocks are marked as suture zones that separate continental and/or buoyant intra-oceanic terranes with dissimilar pre-collisional histories (Windley et al., 2007; Xiao et al., 2009, 2010, 2015). The terrane that records arc magmatism is generally considered to represent the overriding plate and determines the subduction polarity. However, this method can easily neglect important surrounding tectonic constituents and actual closures preserved within terranes, especially in cases of multi-phase arc accretion and collision events.

A good example is the Early Permian Liuyuan Complex, a 9-km-thick, 130-km-long mafic-ultramafic belt located along the southern rim of the Beishan Orogenic Collage, in northwestern China, which forms part of a much larger accretionary orogen: the Late Mesoproterozoic (Khain et al., 2002; Kuzmichev & Larionov, 2013) to Early Mesozoic (Xiao et al., 2003) CAOB (Fig. 1a-b). The Liuyuan Complex, is interpreted as one of the youngest ophiolites that outline a Carboniferous to Permian suture (Xiao et al., 2010; Mao et al., 2012a) and if so, is pivotal for understanding the Permian evolution of the Paleo-Asian Ocean and the termination of orogenesis in the CAOB. In contrast, Wang et al. (2017) and He et al. (2018) proposed that the Liuyuan Complex formed in an intracontinental rift setting (Zuo et al., 1991; Su et al., 2011; Chen et al., 2016). Recent detailed mapping results revealed the preservation of a nearly complete oceanic crustal section, including sheeted dikes, in the Liuyuan Complex (Santos et al., 2023). However, ignoring the nature of associated tectonic elements of the Liuyuan Complex has led to intense debate, with the discussions ranging from how and when the remnant of Paleo-Asian Ocean was consumed (Zheng et al., 2020, 2021b), to interpretations of the regional context and setting of the associated tectonic elements (e.g., Guo et al., 2012 vs. Cleven et al., 2018). In general, the field relationships and tectonostratigraphic correlations between rocks of the Liuyuan Complex and the surrounding terranes, the Huaniushan-Dundunshan terrane to the north and the Shibanshan terrane to the south, remain poorly understood.

In this study, we present results of detailed new investigations of the rocks adjacent to the Liuyuan Complex, which revealed the presence of a newly identified volcanic sequence to the south – the Ganquan Complex. Our new geochronological, geochemical, and isotopic data are consistent with the proposed backarc setting of the Liuyuan Complex (Tian & Xiao, 2020; Santos et al., 2022, Santos, 2022). We propose an evolving and migrating Permian island-arc system (Ganquan arc) as a result of slab rollback and slab steepening in the southern CAOB. Our new results necessitate modification of current tectonic models of the Beishan orogenic belt and the Late Paleozoic evolution of the southern CAOB in general.

3.3 Geological background

3.3.1 Central Asian Orogenic Belt and Beishan orogen

The Central Asian orogenic belt (CAOB) is one of the largest accretionary orogens on Earth and has been the focus of numerous studies in recent decades. It is an east-west trending, overall southward-younging accretionary orogen, with the terminal collision creating sutures which from west to east respectively joined the Tarim craton, the Dunhuang terrane, and the North China craton along its southern border with the northern composite Siberia (Fig. 1a; Windley et al., 2007; Xiao et al., 2009, 2010, 2013, 2015; Zhao et al., 2019). Composite Siberia herein refers to the northern continental landmass, which progressively grew southwards as a result of multiple terrane accretion (Xiao et al., 2010). The southern E-W trending collage of accreted terranes in the CAOB comprises the Beishan orogen (Fig. 1b), which contains the youngest known (Permian) ophiolitic, arc complexes, and associated sedimentary basins in the CAOB (Zheng et al., 2018). Therefore, the Beishan Orogenic Collage is a key segment to assess and study the latest phases of terrane accretion and terminal collision in the CAOB. The part of the Beishan orogen discussed herein is bounded to the south by the Dunhuang terrane - a tectonic belt that comprises Precambrian complexes and Early

Silurian to Late Carboniferous rocks associated with ca. 440-400 Ma and ca. 370-310 Ma magmatic events (Zhao et al., 2016, 2017, 2019).

3.3.2 Geological nomenclature and regional geological context

The Liuyuan Complex. The mafic igneous rocks of the Liuyuan Complex comprise pillow basalts, with subordinate sheeted dikes, gabbro, trondhjemite, and cherts (Zuo and He, 1990; Mao et al., 2012a; Santos et al., 2022). The mafic rocks in the Liuyuan Complex were previously grouped into the Permian Jinta Formation or Zhesi Group (Chen et al., 2016; Niu et al., 2018), mainly based on the large volume of basalt. However, a lithodemic nomenclature of Liuyuan Complex is preferred since recent detailed mapping of the Liuyuan Complex shows that the unit is deformed and mainly made up of mafic igneous rocks lacking layering. The mapping results, together with detailed petrological and structural studies (Santos et al., 2022, Santos, 2022), confirm that the Liuyuan Complex represents an ophiolitic fragment, with nearly all constituent parts (Dilek, 2003) present: from bottom to top it includes basal troctolite cumulates, vari-textured gabbro, a newly discovered sheeted dyke complex and pillowed basalt with interlayered chert. One trondhjemite forming a magmatic breccia at the base of the sheeted dyke yielded a 206Pb/238U age of 290.4 ± 1.4 Ma, providing the oldest age constraint for the formation of the ophiolite, which remained magmatically active until at least 286.3 ± 1 Ma (Santos et al., 2022). The geochemistry of the ophiolite is characterized by a progressively diminishing supra-subduction zone (SSZ) signature up-section, which suggests the Liuyuan Complex formed as a relatively fast-spreading backarc basin (Santos et al., 2023). The backarc setting of the Liuyuan Complex is consistent with the close spatial association and geochemical linkage of felsic volcanic rocks in its unconformable cover with a coeval arc system, the Ganquan Complex (see below), discussed in this paper.

The Liuyuan Complex is tectonically bounded by the Huaniushan-Dundunshan terrane and Shibanshan terrane (Fig. 1b and 1c) to north and south, respectively. The Huaniushan-Dundunshan terrane is interpreted as a composite arc terrane and predominantly consists of an Ordovician to Silurian tectonite belt of high-grade metamorphic rocks, intrusions of the Silurian to Devonian granitoids with arc-like geochemical signatures (Guo et al., 2014; Tian et al., 2014a; Saktura et al., 2017; Soldner et al., 2020), and Carboniferous to Triassic meta-sedimentary cover sequences (Guo et al., 2012). Some have interpreted the suprasubduction nature of the Liuyuan Complex to indicate a tectonic boundary delineating the Huaniushan-Dundunshan and Shibanshan terranes (Xiao et al., 2010; Guo et al., 2012; Mao et al., 2012a; Tian et al., 2014b, 2021), while others consider the two terranes as one long-lived forearc accretionary complex to the Dunhuang terrane (Zheng et al., 2021a).

The Shibanshan terrane was interpreted as a Carboniferous to Permian continental arc (Xiao et al., 2010; Guo et al., 2012; Mao et al., 2012a), proximal along the northern margin of the Dunhuang terrane. Recent work by Tian and Xiao (2020) suggested that the final closure of the Paleo-Asian Ocean took place in Permian when the Shibanshan arc, interpreted as a continental arc attached to the Dunhuang terrane, collided with the Huaniushan-Dundunshan terrane to the north. However, our detailed field-base studies (van Staal et al., 2021; Hong et al., 2022) revealed that the Shibanshan terrane contains at least two different arc complexes separated by a major tectonic contact, each with individual magmatic and tectonic histories before ca. 281 Ma: (1) the Baidunzi Complex, characterized by sheared and transposed Carboniferous-Permian sedimentary rocks interlayered with a syn-kinematic meta-diorite to granite plutonic suite; and (2) The Ganquan Complex, mainly comprising Permian volcanic and volcaniclastic sedimentary rocks as well as subvolcanic intrusions.

The Baidunzi Complex is a geographic name, describing the local mixture of variably sheared and isoclinally folded metasedimentary and syn-kinematic meta-plutonic rocks in the Baidunzi area. The oldest known rocks in the Baidunzi Complex (Fig. 2) are thick-bedded orthoquartzite and minor argillaceous chlorite-muscovite schist with a maximum Stenian depositional age (van Staal et al., 2021; Hong et al., 2022). The structurally overlying metasedimentary rocks include a regionally extensive unit of marble and marl associated and interlayered with quartz-rich meta-psammite and schist, as well as meta-epiclastic sedimentary beds with detrital zircon age spectra yielding maximum depositional date from Asselian to Sakmarian ages. The meta-plutonic granitoid intrusive suite cuts the marble and psammite beds, which were previously mapped as Ordovician-Silurian gneiss (BGMRGS, 1967). However, our field mapping studies (van Staal et al., 2021) updated the U-Pb zircon crystallization ages of the intrusive suite, which yielded ca. 294-289 Ma ages, with metamorphic rims yielding ages of ca. 281-280 Ma. The metamorphic zircon rims are broadly coeval with intrusion of a syn-tectonic suite of ca. 281 Ma hornblende gabbro (Hong et al., 2022 and see below) that was localized along and stitched the shear zone between the Baidunzi and the Ganquan complexes.

The Ganquan Complex is a name modified from the Ganquan Formation. The Ganquan Formation in the Beishan region was first mapped and reported in the 1: 200,000 geological map by BGMRGS (1967) and was later correlated and grouped into regional stratigraphic nomenclatures in BGMRGS (1997). Niu et al. (2018) made significant modifications and revisions to the regional stratigraphy and summarized the Ganquan Formation as a Kasimovian to Sakmarian formation predominantly consists of felsic volcanic rocks and beds of limestone and sandstone, occurring in the southern Beishan region, which includes our mapping area shown in Fig. 1c and Fig. 2. Regional correlation of the existing paleontological data suggests that deposition of lower Ganquan Formation

initiated during Kasimovian to Asselian time, also supported by a Gzhelian age (302 Ma) from radiometric dating of a rhyolitic tuff (Niu et al., 2018). However, it also concluded that the felsic volcanic rocks are consistently separated from the calcareous sedimentary strata by tectonic contacts and contain dissimilar tectonic histories. Our mapping shows that the bedded calcareous sedimentary strata form part of the Baidunzi Complex, whereas the felsic volcanics and associated epiclastic sedimentary rocks are grouped into the Ganquan Complex. The previous stratigraphic interpretations of the Ganquan Formation also neglected internal unconformities and structural complexities in the area investigated by us. The Ganquan Complex contains internal unconformities, and high strain transformed most rocks into greenschist facies phyllonites such that contacts were strongly tectonised during imbrication. Hence, the Ganquan Complex discussed herein may also not necessarily correlate with the synchronous felsic volcanic rocks of the Ganquan Formation, with which it is regionally widely correlated by other researchers.

This study is mainly concerned with the Ganquan Complex. For all the geochronological, geochemical and isotope data reported below, detailed data, including the analytical methods, are presented in the Supplementary Materials.

3.4 Results of petrography, field relationships, and geochronology

The Ganquan Complex comprises three lithologically and structurally distinct, but tectonically related units characterised by tectonised felsic volcanic rocks: (1) the volcano-plutonic lithodeme, forming the older lower sequence; (2) the younger red bed strata and (3) the interlayered volcano-sedimentary rocks. The latter two units together represent the upper sequence. The three recognised lithodeme are distinguished from each other mainly on basis of their distinctive lithological features. The threefold division is also supported by their geochronological, geochemical and isotope characteristics as reported in the following sections.

3.4.1 Volcano-plutonic lithodeme

The oldest and stratigraphically/structurally lowest unit is the volcano-plutonic lithodeme, which dominantly comprises pyroclastic volcanic rocks and minor sub-volcanic granitic intrusions. The pyroclastic rocks comprise mostly yellow rhyolitic crystal and lithic tuffs, and rare green basaltic tuff. They are predominantly metamorphosed to greenschist facies, containing quartz, plagioclase (albite), white mica, biotite, chlorite, and Fe-Ti oxides (Fig. 3a-c and Fig. 4a-d). Most rocks are strongly foliated and/or lineated, displaying well-developed shear bands around tectonically modified phenocrysts, spaced cleavages or differentiated metamorphic layering defined by phyllosilicate- and fine-grained recrystallized quartz-feldspar-rich layers. Primary volcanic structures include phenocrysts of embayed quartz crystals and glomerocrysts of plagioclase (Fig. 4c), which are interpreted as results of magmatic corrosion in high-level intrusive/eruptive environment and crystal growth during the fractionation processes, respectively. Reworked, non-volcanogenic clastic sediments are absent in this unit, and most rounded phenoclasts of quartz in tuffites are due to strain-induced modification and recrystallization during deformation. One rhyolite (S-85) and one phyric tuff (H-3090A) sample were collected for radiometric dating, yielding concordia ages of 294.8 ± 3.7 Ma and 292.4 ± 2.2 Ma respectively (Fig. 6a-b). These are the best estimates of the age of felsic volcanism, suggesting volcanism of the lower unit started no later than 295 Ma.

Reddish-coloured biotite granite bodies are interpreted as sub-volcanic intrusions. They are commonly characterised by a mineral assemblage of quartz, K-feldspar, oligoclase, ±albite, biotite, and accessory Fe-Ti oxides and titanite. The recrystallised quartz, albite, ±biotite, ±muscovite and ±calcite commonly define a spaced, differentiated foliations (Fig. 4e-f). In general, the large-scale mylonization of the volcanic rocks into phyllonites obscured most primary features and transformed most rocks into greenschist facies tectonites. Two granite samples (V-1106 and V-1082) yield a weighted mean $^{206}Pb/^{238}U$ age of 286.1 ± 2.7 Ma and a concordia age of 284.8 ± 2.1 Ma, respectively

(Fig. 6c-d). These are the best estimate ages for granite emplacement, implying the magmatism of the lower unit continued at least until 285 Ma.

The overall absence of diagnostic primary sedimentary features does not allow a reliable evaluation of the environment of deposition, i.e., whether the volcanic rocks were predominantly deposited subaqueously or subaerially. The presence of an unconformity beneath the overlying red beds and the absence of continent-derived clastic sediments as well as heavily reworked volcanic rocks, likely indicate an overall marine volcanic setting lacking significant weathering and distal from continents during 295-292 Ma volcanism.

3.4.2 Red bed lithodeme

The red bed unit, located in the eastern part of the study area, unconformably overlies the volcanic rocks of the volcano-plutonic lithodeme (Fig. 3c). It contains red to purple, occasionally light green shale, gritty sandstone, and conglomerate, which generally show less strain than the underlying volcano-plutonic unit rocks (Fig. 3d). Figure 5a shows that the sandstone in the red beds predominantly contains subangular to subrounded felsic lithic/crystal fragments of red to dark grey rhyolite and individual broken phenocrysts of quartz and feldspar. The red color of this sedimentary package is mainly from the red rhyolite clasts, whereas the matrix of clastic rocks and finer shales are also moderately reddened due to weathering of these rhyolites and hematite pigmentation developed during early diagenesis in a semi-arid, non-marine depositional environment.

Detrital zircon age population of an epiclastic red shale bed (V-233, n=14) displays bimodal distributions, with the younger and older age spectra yielding weighted mean $^{206}Pb/^{238}U$ ages of 282.1 ± 5 Ma (n=7) and 303.4 ± 3.9 Ma (n=7), respectively (Fig. 7d). The younger peak represents a maximum depositional age of the red bed strata, while the older peak consisting of ages ranging from 312 to 295 Ma indicates a slightly older volcanic provenance, likely the underlying volcano-plutonic

unit. An interlayered andesitic tuff (V-176) yielded a $^{206}Pb/^{238}U$ zircon crystallization age of 283.1 ±2.4 Ma (Fig. 7a), within error consistent with the detrital zircon results. Hence, the deposition of red beds is interpreted as coeval with the volcanism during ca. 283 Ma. Considering the unconformity and evidence for erosion of the underlying volcano-plutonic unit, it suggests that the older Ganquan volcanic phase was uplifted and eroded above the sea level at ca. 283 Ma, which is consistent with the associated depositional transition from overall marine to semi-arid, non-marine environment.

3.4.3 Volcano-sedimentary lithodeme

The volcano-sedimentary lithodeme mostly occurs in the western part of the study area and is separated structurally from the volcano-plutonic unit by thrusts (Fig. 3e). Rocks occurring along the tectonic contact between the Baidunzi and Ganquan complexes, are also lithologically correlated to this lithodeme, and were also intruded by numerous hornblende gabbro sills (Fig. 2 and 3f).

Unlike the volcano-plutonic lithodeme, the volcano-sedimentary lithodeme is typically characterized by tuffaceous and epiclastic sedimentary rocks, including light grey, brown or black tuffaceous or volcaniclastic shale, sandstone, and conglomerate. The high strain and metamorphism accommodated by the tuffaceous sedimentary rocks locally transformed shale and siltstone into greenschist phyllonites and locally lower amphibolite facies schist. Porphyroclasts of tuffaceous rocks are predominantly represented by deformed phenocrysts of feldspar and quartz, which are commonly surrounded by strain shadows (Fig. 5c-e). The epiclastic sandstone contains fine to medium-size white felsic volcanic clasts and calcareous lithic clasts (Fig. 3g-h). Combined with preserved crossbedding and graded bedding in sandstone and siltstone beds, it suggests the siliciclastic to calcareous sediments were likely deposited in shallow water exposed to wave currents.

The depositional timing of this unit is constrained by the eruptive age dated from an interlayered ash tuff (H-3009), which yielded a $^{206}Pb/^{238}U$ age of 280.8 ±2.6 Ma (Fig. 7b). The

tuffaceous sedimentary rocks are commonly intruded by hornblende gabbro sills. Because the sills are absent in the older rocks of the volcano-plutonic lithodeme, they must predate the structural amalgamation. A hornblende gabbro yielded an imprecise 238U/206Pb age of 285.4 ±5.7 Ma from a small cluster of four youngest data (H-3345, Fig. 7e), while another sheared gabbro of the same unit collected from the shear zone between the Ganquan and Baidunzi complexes yielded a precise 238U/206Pb zircon crystallization age of 281.1 ± 2.3 Ma (V-163, Fig. 7c). Both are within error coeval with the volcanism and depositional age of the volcano-sedimentary lithodeme. Considering that the gabbro sills intrude and must postdate the lithodeme, we estimate that the depositional age of this lithodeme within analytical error is between 283 and 281 Ma, and the subsequent intrusions of gabbro took place shortly after during 281 to 279 Ma, suggesting that the rocks were likely deposited rapidly coeval with bimodal magmatism.

The volcano-sedimentary lithodeme is invariably separated from the underlying volcano-plutonic rocks by thrusts and the gabbro intrusions exclusively exist in the hanging wall rocks. This indicates that the volcano-sedimentary unit rocks of the hanging wall were not deposited above the lower volcano-plutonic unit, but at a location proximal to a subaerial siliciclastic and calcareous source terrane and distal from the ca. 295-285 Ma volcanic rocks before the 281 Ma structural amalgamation.

3.5 Results of whole-rock geochemistry

Whole-rock major and trace element compositions were determined for Ganquan Complex volcanic and intrusive rocks to quantify the chemical variation of these rocks and, together with literature data, to evaluate their possible tectonic settings. However, as seen in the field, large-scale mylonization and associated alteration transformed most rocks into greenschist facies phyllonites. This could increase the mobility of low-field-strength elements (e.g., K, Rb, Cs, U, Pb) and certain

major elements (e.g., Fe, Na, P, Ti) (Ague, 1991; Kalita et al., 2022; Oliot et al., 2010), which obscures analytical results and lithogeochemical characteristics of samples, i.e., the anomalous high content of silica (71-81 wt.%) for felsic samples (Aitchison, 1982). Therefore, in the following results, parameters employing mobile elements are of limited use to classify rocks and assign important chemical trends/series.

Major oxide, trace element and rare earth element (REE) data of analysed rocks are reported in the supplementary material (Table SM2). These data are compared with published data for rocks from modern arcs as references, which include oceanic arc rocks of Izu Bonin (compiled from Heywood et al., 2020 and Gill et al., 2018) and Fiji (Todd et al., 2021 and Marien et al., 2022) and continental island arc rocks of Taupo Volcanic Zone, New Zealand (Millet et al.,2014; Allan et al., 2008 and 2017). The combined data are shown as variation and discrimination diagrams of major and trace elements in Fig. 8 and 9, and as chondrite- normalized rare earth element (REE) patterns and primitive mantle (PRIMA) or mid-ocean ridge basalt (MORB)-normalized multi-element patterns in Fig. 10. The analytical techniques conducted to acquire whole-rock geochemical data and the associated references are reported in the supplementary materials.

3.5.1 Major and trace elements

Samples of volcano-plutonic lithodeme (n=23 volcanic rocks; n=4 granite) range in composition from basalt to rhyodacite/dacite and rhyolite, with the latter being the most common (Fig. 8c, from Winchester and Floyd, 1977) and the mafic ones rarely exposed (n=1). The felsic volcanic and granite rocks overall show no distinguishable geochemical difference, supporting their cogenetic relationship, consistent with the field interpretation. They both have high silica content, ranging from 71.5 to 80.6 wt. % SiO_2; they are mostly peraluminous (aluminum saturation index (ASI)=1.03-1.65). With increasing SiO_2, K_2O and Na_2O display dispersed scatters, whereas Al_2O_3,

MgO, Fe2O3, CaO and TiO2 all decrease. The variation diagrams of trace elements (ratios) do not show consistent correlation with increasing SiO2 yet display an overall overlap within the data field of Taupo Volcanic Zone rocks.

Volcanic rocks of the red bed unit (n=10) predominantly consist of rhyolite and dacite, with SiO2 content ranging from 66.7 to 81.5 wt. %. They are metaluminous to slightly peraluminous (ASI=1.01-1.31). Most major element oxides of this unit show a linear negative correlation with SiO2, except for Al2O3, Na2O and K2O, which scatters between 11.6 to 13.9 wt.%, 4.2 to 5.5 wt.% and 0.3 to 3 wt.%, respectively. The volcanic-sedimentary unit includes 8 tuff samples, which have silica content ranging from 54.9 to 77.7 wt.%, with compositions vary from andesite to rhyolite, with the felsic ones being more common. Patterns of rock samples in Harker and trace element variation diagrams show great similarity with the red bed rocks. Both units of the upper sequence show distinct trace element concentrations and ratios compared to the volcano-plutonic unit; they commonly plot in the transitional field between continental island and oceanic arc rocks (Fig. 8g-i).

The general chemical characteristics of major elements of all felsic volcanic samples appear dominantly magnesian, calc-alkaline and metaluminous to slightly peraluminous (Fig. 8a-b and Fig. 9a), and display affinities with those of magnesian calc-alkalic and/or magnesian calcic types of granite and rhyolite of the silica-rich rock classification of Frost et al. (2016). Such felsic rocks are commonly associated with continental arc batholiths and volcanoes and/or are constituent of oceanic arc and ophiolite rock assemblages, agreeing with the results comparing to modern arc references.

Rocks of the hornblende gabbro unit have SiO2 content of 42.1-57.1 wt% with compositions ranging from gabbro to diorite. Major oxides of CaO and TiO2+MgO+FeOt are generally negatively correlated with SiO2, whereas major and trace elements show no clear trend. They generally plot in the transitional field between tholeiite and calc-alkaline rocks on the Th/Yb vs. Zr/Y plot (Fig. 9a) of

Ross and Bédard (2009), with MgO/FeOt varying from 0.17 to 0.84 (Mg#=0.24-0.6). The three samples of Liuyuan Complex basalt and one mafic sample of volcano-plutonic lithodeme generally match the compositional range of the hornblende gabbro unit and fall within the gabbro's range.

3.5.2 Tectonic discriminations

A variety of discrimination diagrams employed to fingerprint magma type and tectonic settings show that the volcanic rocks of the Ganquan Complex overall have geochemical characteristics typical of calc-alkaline arc-related rocks. The rocks display large-ion-lithophile element (LILE) enrichment with negative high-field strength element (HFSE) (Nb) anomalies, and high LILE/HFSE ratios (e.g., Nb/Zr and Th/Zr), indicative of a melt source from metasomatized mantle wedge (Mišković & Francis, 2006) or a source underwent depleted fractionation of Nb. As shown in Fig. 9b, the felsic volcanic rocks of the Ganquan Complex display strong Rb and Th enrichment, typified by high Rb/Y and Th/Zr ratios at systematically low ratios of Nb/Y and Nb/Zr. This suggests increasing hydrous fluid involvement in their mantle source (Kepezhinskas et al., 1997; Pearce & Norry, 1979), which also resemble felsic rock data of the Taupo Volcanic Zone. The felsic samples are also characterized by relatively low concentrations of Y+Nb and Ta+Yb, which are readily separated from A-type granites (e.g., within-plate granite and oceanic ridge granite); they also lack 'slab failure-like' signatures for relatively low ratios of La/Yb, Gd/Yb, Sm/Yb and Nb/Y and hence plot mostly in the arc fields on the discrimination diagrams of Pearce et al. (1984) and Whalen and Hildebrand (2019) for felsic rocks (Fig. 9c-d). They also combine increase in Th/Yb with generally low Ta/Yb, plotted within the same data field of the felsic Taupo Volcanic Zone rocks, which represents a modern analog of continental margin island arc setting. However, the mafic samples mostly overlap with the oceanic arc basalt samples (Izu Bonin and Fiji) with a few straddling between NMORB and arc fields (Fig. 9e-g).

Trace element compositions of the magmatic rocks of the three lithodeme units overall share similar envelope profile patterns, all resembling that of subduction-related magmatic arcs. All of them show enrichment in large ion lithophile elements (LILEs), and negative anomalies in Nb, Ta, Sr and Eu when normalized to CI-chondrite and primitive mantle (PRIMA). CI-chondrite-normalized REE patterns (Fig. 10a) for the volcano-plutonic unit and red bed unit rocks mostly overlap and are generally parallel, both displaying LREE-enrichments and flat HREE characteristics in concave-upward shapes. The red bed unit displays slightly shallower slopes, with smaller primitive mantle normalized LaN/SmN ratios (1.99-2.53) compared to the volcano-plutonic unit (2.16-3.73). The volcanic-sedimentary unit rocks are characterized by relatively lower concentrations in trace elements, especially HREE, compared to the above two units. They have comparatively large LaN/SmN ratios (2.81-4.59), and slightly lower Dy/Dy* ratios (0.47-0.68).

The PRIMA-normalized trace elements (Fig. 10c) of the three units are prominently featured by negative anomalies of Ba, Sr and Eu, positive anomalies of Th, U and Pb, and pronounced Nb-Ta troughs, except for the samples from volcano-plutonic unit and red bed unit, which are overall more enriched in MREEs and HREEs. The variations in LILEs (Cs, Rb and Ba) are most likely due to secondary alteration and metamorphism as mentioned above. The large negative Sr and Eu anomalies (most <100ppm) are associated with fractionation of plagioclase phenocrysts in silica-rich eruptions. The positive anomalies in Th and U are commonly associated with accessory minerals like monazite and zircon and/or siliceous melts derived from melting continent materials. The Pb spikes could indicate mixing with continental components in the magma source, and the significant depletion in Nb and Ta suggests a subduction-related setting. Except for the wide ranges in enrichment of Cs, Rb and Ba, PRIMA-normalized trace element concentrations and patterns of the three units all closely resemble rhyolites from the Taupo Volcanic Zone (TVZ). The profiles also lack strong depletion of

Y, Yb and Lu, hence precluding source regions that underwent melting of thick continental or arc crust. In contrast, the volcano-sedimentary unit has relatively low concentrations of HSFEs and shows slight depletion in MREE and HREE, which resemble those of middle crust average and enriched tonalite suite of Fiji. This could possibly be related to relatively dehydrated melting and/or amphibole fractionation during magma crystallization.

The chondrite normalised REE patters of hornblende gabbro unit rocks are straight and smooth, with slight enrichment of LREEs and slightly negative to no Eu anomalies, which resemble patterns of E-MORB and enriched MORB-like back arc basalt (Fig. 10e). The N-MORB-normalized multi-element diagram reveals large negative Nb-Ta anomalies yet lacks prominent negative Zr, Hf and Ti anomalies. This suggests the melt was derived from the subduction-related metasomatized mantle wedge but lacked fractionation and crystallization of biotite and amphibole typical of differentiated arc lava (Murphy 2007).

3.6 Results of Hf-O isotope systematics

The Hf and O isotope compositions of the analysed zircons are summarized in Fig.11-13 and Table SM3. The results are presented by rock type or unit and characterize the intra- and inter-sample variations of Hf ratios and Oxygen compositions in the zircons, including single-grain data of detrital and inherited zircons.

All oxygen isotopic data are presented as the $\delta^{18}O$ notation, expressed as deviations from Vienna standard mean ocean water (VSMOW, $^{18}O/16O = 0.0020052$, Baertschi, 1976) in parts of per thousand. The present-day chondritic parameters reported by Bouvier et al. (2008) were used to calculate εHf(t). The εHf(t) range for arc mantle reported by Iizuka et al. (2013) (Fig. 12) and the $\delta^{18}O$ range of mantle-like zircon reported by Valley et al. (2005) are plotted as reference. Other data

plotted for comparison purpose include εHf(t) zircon values of Liuyuan Complex rocks from Yu et al. (2022) and Santos (2022) in Fig. 12a.

The Lu-Hf and O isotopic analyses reveal that zircons from the ca. 295-292 Ma volcanic rocks of the volcano-plutonic unit display a limited range of εHf(t) values from -4.2 to +1.9 and have mantle-like to slightly elevated zircon $\delta^{18}O$ values (4.5–7.25‰), with most ranging between 4.8‰ and 6.4‰ (sample S-85 and H-3090A). The subvolcanic granite samples yielded a more heterogenous distribution of εHf(t) values ranging from -5.8 to +3.9, with most falling between -1.8 to +1.4 (samples V-1106 and V-1082). Magmatic zircons from sample V-1106 display mantle-like zircon $\delta^{18}O$ values ranging from 4.9‰ to 5.9‰. Samples from the lower sequence rocks of Ganquan Complex are overall characterized by negative to slightly radiogenic of εHf(t) values, mantle-like zircon $\delta^{18}O$ signatures, and Proterozoic Lu-Hf depleted mantle model ages. The similar isotopic characteristics provide additional evidence supporting the case that the granite bodies are subvolcanic intrusions and were derived from the same magma that produced the Lower Ganquan volcanic rocks, although the younger subvolcanic intrusions have relatively more radiogenic εHf(t) values.

The volcanic rocks of the upper sequence show comparatively radiogenic εHf signatures and a larger spread in $\delta^{18}O$ values that lie between 3.7 ‰ and 5.9‰, with most in the mantle-like zircon $\delta^{18}O$ range or lower. Volcanic samples from both the red bed and the volcano-sedimentary units yielded restricted ranges of radiogenic εHf(t) values from +0.5 to +4.7 and +3.6 to +7.6, respectively. The ash tuff of the volcano-sedimentary lithodeme also has a comparatively restricted $\delta^{18}O$ range between 4‰ and 5.9‰. The heterogeneous and relatively low $\delta^{18}O$ values are from the red bed unit, ranging from 3.7‰ to 7.9‰ with most between 3.7‰ and 5.2‰. Zircons with slightly lower $\delta^{18}O$ values in the red bed unit are likely caused by remelting and/or assimilation of hydrothermally altered sea floor basalt and/or low $\delta^{18}O$ wall rock through fracture systems during shallow magmatism

(Valley, 2003). However, their εHf(t) values are more radiogenic and arc-mantle like than those of the lower sequence rocks, suggesting a juvenile contribution from the magmatic source. Detrital zircons from an epiclastic red shale sample (V-233) exhibit εHf(t) values that range between those of the lower and upper sequences of the Ganquan Complex (Fig. 12b), indicating provenances from both lower and upper sequences of the Ganquan Complex. The result is consistent with field and petrological evidence, confirming a genetic relationship between the two sequences.

The hornblende gabbro sills that intruded the volcano-sedimentary lithodeme display overall radiogenic εHf(t) values ranging from -0.7 to +8.6 and slightly elevated $\delta^{18}O$ values ranging from 4.8‰ to 6.3‰. An older group of zircon inheritance (Carboniferous to Precambrian ages from sample H-3345) show a wide variation of non-radiogenic εHf(t) values, suggesting a variable contamination from a crust-like source rocks with Precambrian provenance. The two anomalous values of -17.5 and +30 are most likely associated with systematic error, based on the fact that LA-ICP-MS collects its material from a greater sample depth compared to SHRIMP, which makes it likely that it may have mixed isotope compositions of the zircon's core and rim. Nonetheless the analysed rocks overall are characterized by low $\delta^{18}O$ signatures and show a trend towards radiogenic εHf(t) values with decreasing crystallization age.

3.7 Discussion

3.7.1 Arc-like geochemistry of the Ganquan Complex

The detailed mapping results, combined with petrographical and U-Pb zircon age data reported above, provide new insights into the Ganquan Complex, which has been divided into lower and upper sequences separated by an unconformity and/or intervening thrust. The three recognised distinctive lithodemes record two pulses of volcanism at 295-285 Ma and 283-281 Ma, respectively. Both sequences show a lack of mafic volcanic rocks but instead are dominated by voluminous high-

SiO2 pyroclastic rocks. As discussed above, the geochemical data of the Ganquan Complex resemble that of subduction-related magmatic arcs, especially the recent continental island arc Taupo Volcanic Zone in New Zealand. The felsic samples exhibit limited variations in source heterogeneity proxies such as Nb/Y and Nb/Zr in plots of Rb/Y versus Nb/Y and Nb/Zr versus Th/Zr. However, they display significant variations in proxies indicative of fluid transfer/involvement, such as Rb/Y and Th/Zr. This is inconsistent with simple fractionation of arc liquids, as elements such as La, Zr, and Nb are generally equally incompatible and should remain relatively constant in relation to compatible elements like Y and Yb (Pearce et al., 2005). Therefore, the large variations in their ratios are likely attributed to processes such as magma mixing from heterogeneous sources, crustal assimilation, and/or deeper melting. On the other hand, Th and Rb are incompatible elements and readily partitions into siliceous melts and fluids, respectively, hence a wide range in ratios of these elements with respect to compatible elements are indicative of fractionation and/or fluid involvement. Similar results are shown in spider diagrams, displaying high LILEs/HFSEs ratios and prominent negative Nb, Ta anomalies normalized to primitive mantle. The origin of felsic magma showing arc-related geochemical signatures, however, is contentious and can arise by several means: 1) fractionation of a more mafic parent not necessarily subduction-related; 2) differentiation from mafic magma derived from metasomatized mantle; and 3) partial melting of continental crust that was mostly formed by earlier arc magmatism (Murphy, 2007).

Hf and Oxygen isotopes in zircon have been systematically used to characterize the putative source of granites (Kemp et al., 2007, 2008), hence they are employed herein as tracers to better yield information about their original magmatic source. The analysed felsic volcanics and granite of the Ganquan Complex overall show great homogeneity within sample groups. The zircons from the ca. 295-285 Ma felsic rocks of the volcano-plutonic lithodeme are however, characterized by slightly

negative εHf(t) values yet display mantle-like zircon $\delta^{18}O$ signatures, which suggests a magmatic source that incorporated older igneous rocks which were never exposed to the Earth's surface where they likely would have undergone large oxygen isotopic fractionation (Iizuke et al., 2013). A few outliers display slightly larger $\delta^{18}O$ values (6-7.25‰), albeit not with strongly negative εHf(t) values (Fig. 13). This is possibly due to the duration and large extent of magmatic crystallization and differentiation, which culminated in silica-rich magmas with higher $\delta^{18}O$ ratios as the heavy ^{18}O preferably partitions into quartz and feldspar instead of other coexisting mafic phases during crystallization (Valley et al., 1994; Bindeman, 2008). Despite that magma formed by reworking of continental rocks can also cause non-radiogenic εHf and elevated $\delta^{18}O$ values in zircon, melting of supracrustal sedimentary rocks would produce much more elevated $\delta^{18}O$ zircon signatures (commonly > 8‰; Valley et al., 2005). Additionally, the volcano-plutonic unit lacks reworked, volcano- or continental derived sedimentary rocks and zircon inheritance, precluding anatexis of mature crustal rocks during melting but indicating an infracrustal source. Combined with the evidence for an overall marine depositional environment, we interpret that the lower sequence of the Ganquan Complex as an early arc (295-285 Ma) erupted in an intra-oceanic island arc setting below sea level and distal from a continent. The arc was likely built upon a slightly older and enriched andesitic arc or seamount basement, and the slightly evolved Hf signatures are attributed to limited partial melting and/or assimilation of a slightly older arc crust.

The red bed lithodeme that lies unconformably above the volcano-plutonic lithodeme, is a correlative of the volcano-sedimentary lithodeme, which ties the two coeval lithodemes together into one related arc complex, despite the fact that they occur in different structural panels. They both contain clastic sedimentary rocks with voluminous epiclastic materials deposited between ca. 283-281 Ma and are characterized by relatively radiogenic εHf values as well as low $\delta^{18}O$ ratios with most

representing a mantle-like zircon $\delta^{18}O$ range. Zircons from the volcano-sedimentary unit particularly have moderately high εHf values, giving almost zero crustal residence time with assumption of an arc mantle source of Iizuka et al. (2013), suggesting derivation from a source with more juvenile components. The two units overall share similar isotopic characteristics yet display some differences in ranges of εHf values and $\delta^{18}O$ ratios, possibly due to spatial variations of arc magma composition. This interpretation is consistent with their distinctive stratigraphy: the red bed unit suggests a semi-arid non-marine setting, whereas the volcano-sedimentary lithodeme contains shale and volcanogenic turbidites indicative of a proximal marine environment. Based on the above lines of geochemical evidence, we interpret the younger volcanic rocks to be co-magmatic and derived from a relatively juvenile mantle source. Such a transition from the earlier phase volcanism also explains the change of depositional environment and heterogeneities in geochemical and isotopic compositions, suggesting differences in the locations where the Ganquan arc magmas were erupted.

In summary, we conclude the volcanic rocks of the Ganquan Complex to be the result of an evolving island arc, with increasing input from a juvenile magma source and decreasing influence from a slightly older arc-basement contaminant evident from the transition from the lower to upper sequence. Furthermore, the Ganquan arc is distinct from the previously defined Shibanshan arc terrane or the Baidunzi Complex, as it lacks a continental-like stratigraphy and shows no evidence of incorporating older sediments or involving anatexis of continental crust rocks during magmatism.

3.7.2 Tectonic transitions from the lower to upper sequence

As mentioned above, the recorded 295-285 Ma and 283-281 Ma phases of magmatism belong to one evolving arc system and were related to the same subduction event. The small age gap (~ 2my) between 285 and 283 Ma falls within error of the age determinations and likely has no tectonic significance. There is no evidence suggesting a temporary shutdown of the former arc due to tectonic

processes such as a collision or a flattening slab. Rather, the geochemistry and stratigraphy of the adjacent backarc Liuyuan Complex requires a relatively steep slab that facilitated opening of an oceanic backarc basin by spreading by ca. 292 Ma (Santos et al., 2023). The zircon εHf values of trondhjemite in the Liuyuan ophiolite (Santos et al., 2022) and consanguineous felsic volcanic tuff that unconformably overlie the Liuyuan Complex indicate a genetic relationship with the Ganquan volcanic rocks (Fig. 12a). Accordingly, the observed progressive increase in juvenile components may be attributed to an arc migration process that was temporally associated with backarc spreading. This would have resulted in an increased influx of mantle-derived magma, gradually removing the magma source of the Ganquan arc from the influence of an older mafic to intermediate precursor that is inferred to have been present in the substrate of the older phase (Fig. 14). An alternative explanation for the unconformity and/or intervening thrusts that separate the older and younger lithodemes would require a collision and a subsequent restarting of subduction immediately thereafter. Such a collision could have ceased arc magmatism of the lower sequence, whereas volcanism recorded in the upper sequence requires initiation of a new subduction zone. However, in such a scenario the zircon εHf values recorded in the red bed and volcano-sedimentary lithodemes would be expected to have been more evolved and show a wider range of geochemical compositions due to anatexis of the older volcano-plutonic rocks, instead of being more juvenile and homogeneous. The U-Pb ages and εHf values of detrital zircons in the red bed lithodeme also support the ca. 295-285 Ma volcanic rocks of the lower sequence as being a major source, such that erosion and weathering of the breached former arc produced epiclastic materials which was deposited in the unconformably overlying red bed lithodeme. Additionally, the mantle-like $\delta^{18}O$ zircon values and elevated εHf(t) ratios of the upper sequence rocks suggest the influence of an old arc-basement contaminant was removed.

Such distinctions between felsic lavas derived from an evolved oceanic arc and island arc built on continental crust such as the Taupo, Sumatra and Northeastern Japan arcs (Garrison et al., 2011; Zulkarnain, 2011; Ayalew and Ishiwatari, 2011; Smith and Price, 2006) are not easy to address solely through geochemistry, especially where the arc crust progressively thickens following multiple episodes of magmatism or where the arc forms near a continental margin on the lower plate. For example, the similarities are apparent when comparing geochemical profiles of the Izu-Bonin intra-oceanic arc and the Taupo Volcanic Zone continental island arc. A clearer tectonic picture emerges when field relationships, and the Hf and Oxygen systematics are incorporated in the interpretations. This suggests that the observed oceanic island arc system, characterized predominantly by felsic volcanic rocks, does not necessarily conform to an Andean-type continental arc nor indicate increasing arc crustal thickness (Miyashiro,1974; Murphy, 2006). Instead, the evidence presented here supports the notion of a progressively migrated and evolved oceanic island arc system, highlighting the complex and dynamic nature of island arc processes.

3.7.3 Regional tectonic implications

The evidence of arc-backarc magmatism between ca. 295 and 281 Ma in the Ganquan Complex and Liuyuan Complex, requires that the Paleo-Asian Ocean, or a local related trapped oceanic basin had not completely closed yet, and its oceanic lithosphere continued subducting in this segment until at least 281 Ma. This is in contrast with the models of Wang et al. (2017) and Niu et al. (2018) in which the ocean closed by Silurian (Fig. 14a). These models interpret the Liuyuan Complex as a layered intrusion with an extrusive cap that formed in an intracontinental rift setting, either caused by post-collisional extension (Chen et al., 2016; Wang et al., 2017), or mantle upwelling resulting from subduction along the continental margins (He et al., 2018). However, recent investigations presented by Santos et al. (2022 and 2023) challenge these interpretations and support

the Liuyuan Complex as an ophiolite. The presence of a continuous sheeted dike complex between the lower gabbroic rocks and the upper pillow basalts, especially indicates that magmatic supply kept pace with oceanic spreading, a characteristic feature of relatively fast-spreading ridges. Furthermore, the presence of chert, which typically forms in deep oceanic basins, and the absence of coarse to fine continentally derived clastic sedimentary rocks, argues against an intracontinental rift setting for the formation of the Liuyuan Complex.

The alternative models proposed by Xiao et al. (2009) and associated workers also suggest a late Permian final closure of the Paleo-Asian Ocean in the southern CAOB. These models however, either suggest that the Liuyuan Complex represents a forearc ophiolite associated with Huaniushan arc above a north-dipping subduction system to its south (Xiao et al. 2010, Guo et al. 2012, and Mao et al., 2012a), or a backarc ophiolite associated with Huaniushan arc above a south-dipping subduction zone to the north of Huaniushan-Dundunshan terrane (Tian & Xiao 2020). Both interpretations link the Liuyuan Complex with the Huaniushan arc to the north (Fig. 14a). However, the radiometric dates obtained for the Liuyuan ophiolite, ranging from 290.4 ± 1.4 Ma (Santos et al., 2022) to 280 ± 6 Ma (Wang et al., 2017), are not consistent with the ages of arc magmatism in the Huaniushan-Dundunshan terrane. This composite arc terrane predominantly comprises a Late Ordovician-Silurian Huaniushan continental arc (Li et al., 2015; Mao et al., 2012b), an Early Devonian Gongpoquan Island arc (Wang et al., 2018), and a Late Devonian Dundunshan arc (Guo et al., 2017), but lacks Late Carboniferous to Early Permian arc magmatism. Therefore, the Ganquan arc is a better candidate, consistent with the spatial and volcanic linkages.

Hence, based on the spatial association of the Ganquan and Liuyuan Complexes, the subduction polarity was towards the north. The Ordovician-Silurian Huaniushan-Dundunshan terrane to the north of Liuyuan Complex was only minimally, if any, involved during the Ganquan arc-

Liuyuan backarc system. Opening of Liuyuan oceanic backarc basin to the north of the south facing Ganquan arc was either due to slab steepening and/or rollback (Fig. 14c). Southward migration of the arc towards the trench (present coordinates) onto another oceanic substrate, produced the stratigraphic, geochemical, and isotopic differences between the lower and upper sequences of the Ganquan Complex. The upper plate most likely was a piece of the Paleo-Asian Ocean attached to the southern boundary of the Huaniushan-Dundunshan terrane, which was probably modified and thickened by oceanic arc magmatism immediately preceding development of the Ganquan arc. The extensional and juvenile nature of the Ganquan Arc–Liuyuan backarc system contradicts models that propose it as a component of the long-lived forearc accretionary complex, which was previously interpreted as part of the north-facing Dunhuang continental arc (Cleven et al., 2018; Zheng et al., 2021a).

Termination of the Ganquan arc magmatism at ca. 281 Ma is interpreted to be due to accretion of the Baidunzi Complex, which was exotic to the Ganquan arc before 281 Ma due to its distinctive tectono-stratigraphy and geological history. It possibly is the remnant of a (micro)continent, located further to the south and related to the converging continent along the southern margin of the Paleo-Asian Ocean. Accretion of Baidunzi Complex is constrained by an extensive ca. 281 Ma suite of syn-tectonic hornblende gabbro, which is spatially localised and injected into the shear zone that separates the Baidunzi and Ganquan complexes and stitches the two different complexes together (Fig. 2). The mixed signatures of both juvenile and inheritance of less-radiogenic materials in zircons (Fig. 11 and 12a) also support the syn-collisional characteristics of the stitching gabbro. The juvenile signatures may reflect the same source from attenuation of the lithospheric mantle during the opening of the Liuyuan backarc basin, while the non-radiogenic signatures were derived from significant continental contamination (e.g., the Baidunzi Complex).

This relationship suggests a causal linkage between arc termination and accretion of the Baidunzi Complex. Additional support for such a scenario is provided by metamorphic zircon rims from the Baidunzi Complex rocks (lower plate during accretion), which overlap in error with the ca. 281-280 Ma ages of arc termination and emplacement of the hornblende gabbro sills (Hong et al., 2022). Hence these relationships also discount potential alternative colliders, now removed by strike-slip movements (Cleven, 2016; Tian et al., 2021). The observed early phase of south-directed tectonic transport (van Staal et al., 2021) is also consistent with a collision between the Ganquan arc and the Baidunzi Complex on the lower plate.

3.8 Conclusions

A combination of detailed field work and geochemical and geochronological studies led to recognition of multiple dissimilar terranes with dissimilar tectono-stratigraphies, some of which are spatially closely associated and contain synchronous magmatic histories. The coeval Liuyuan and Ganquan complexes represent part of a related arc-backarc system, which initiated between 295 Ma and 292 Ma. Southward-directed arc-trench migration led to opening of a backarc basin and continuing arc magmatism until ca. 281 Ma. Cessation of the multi-phase Ganquan arc system occurred at ca. 281-280 Ma and coincided with accretion of the Baidunzi Complex, which is constrained by the emplacement of the syn-tectonic stitching gabbro. The evolutionary process developed in this study suggests that the geology of the Shibanshan terrane and its relationships with adjacent tectonic constituents are more complex than previously thought. The multi-phase arc magmatism and evidence for accretion also shed new light on the existing arc-continent collision models proposed for the closure of the Paleo-Asian Ocean. This study provides an example where tectonic processes such as trench rollback and arc migration in ancient orogens can be reconstructed from a combination of detailed field work and analytical investigations.

3.9 References

Ague, J. (1991). Evidence for major mass transfer and volume strain during regional metamorphism of pelites. Geology: 19 (8): 855–858. doi: https://doi.org/10.1130/0091-7613(1991)019<0855:EFMMTA>2.3.CO;2

Aitchison, J. (1982). The Statistical Analysis of Compositional Data. Journal of the Royal Statistical Society. Series B (Methodological), 44(2), 139–177. http://www.jstor.org/stable/2345821

Allan, A. S. R., Baker, J. A., Carter, L., & Wysoczanksi, R. J. (2008). Reconstructing the Quaternary evolution of the world's most active silicic volcanic system: insights from an ~1.65 Ma deep ocean tephra record sourced from Taupo Volcanic Zone, New Zealand. Quaternary Science Reviews, 27(25–26), 2341–2360. https://doi.org/10.1016/J.QUASCIREV.2008.09.003

Allan, A. S. R., Barker, S. J., Millet, M. A., Morgan, D. J., Rooyakkers, S. M., Schipper, C. I., & Wilson, C. J. N. (2017). A cascade of magmatic events during the assembly and eruption of a super-sized magma body. Contributions to Mineralogy and Petrology, 172(7). https://doi.org/10.1007/S00410-017-1367-8

Ayalew, D., & Ishiwatari, A. (2011). Comparison of rhyolites from continental rift, continental arc and oceanic island arc: Implication for the mechanism of silicic magma generation. Island Arc, 20(1), 78–93. https://doi.org/10.1111/J.1440-1738.2010.00746.X

Baertschi, P. (1976). Absolute 18O content of standard mean ocean water. Earth and Planetary Science Letters, 31(3), 341–344. https://doi.org/10.1016/0012-821X(76)90115-1

Bindeman, I. (2008). Oxygen isotopes in mantle and crustal magmas as revealed by single crystal analysis. Reviews in Mineralogy and Geochemistry, 69, 445–478. https://doi.org/10.2138/rmg.2008.69.12

Bouvier, A., Vervoort, J. D., & Patchett, P. J. (2008). The Lu–Hf and Sm–Nd isotopic composition of CHUR: Constraints from unequilibrated chondrites and implications for the bulk composition of terrestrial planets. Earth and Planetary Science Letters, 273(1–2), 48–57. https://doi.org/10.1016/J.EPSL.2008.06.010

Cabanis, B., & Lecolle, M. (1989). Le diagramme La/10-Y/15-Nb/8; un outil pour la discrimination des series volcaniques et la mise en evidence des processus de melange et/ou de contamination crustale. The La/10-Y/15-Nb/8 diagram; a tool for distinguishing volcanic series and discovering crustal mixing and/or contamination. Comptes Rendus de l'Academie des Sciences, Serie 2, Mecanique, Physique, Chimie, Sciences de l'Univers. Sciences de la Terre, 309(20): 2023–2029.

Chen, S., Guo, Z., Qi, J., Zhang, Y., Pe-Piper, G., & Piper, D. J. W. (2016). Early Permian volcano-sedimentary successions, Beishan, NW China: Peperites demonstrate an evolving rift basin. Journal of Volcanology and Geothermal Research, 309, 31–44. https://doi.org/10.1016/J.JVOLGEORES.2015.11.004

Cleven, N. R. (2016). Paleozoic transpressional tectonics in the Beishan orogenic collage, Northwest China: Evolution of the Hongliuhe suture zone. PhD thesis. UWSpace. http://hdl.handle.net/10012/10190

Cleven, N. R., Lin, S., Xiao, W.J., Davis, D. W., & Davis, B. (2018). Successive arc accretion in the southern Central Asian orogenic belt, NW China: Evidence from two Paleozoic arcs with offset magmatic periods. Bulletin of the Geological Society of America, 130(3–4), 537–557. https://doi.org/10.1130/B31434.1

DeBari, S. M., Heywood, L. J., & Gill, J. B. (2020). Izu Bonin Across Arc Geochemical Dataset between latitudes 32°40' to 30°20', Version 1.0. Interdisciplinary Earth Data Alliance (IEDA). https://doi.org/10.1594/IEDA/111493

Dilek, Y. (2003). Ophiolite concept and its evolution. Special Paper of the Geological Society of America, 373, 1–16. https://doi.org/10.1130/0-8137-2373-6.1

Frost, C. D., Frost, B. R., & Beard, J. S. (2016). On silica-rich granitoids and their eruptive equivalents. American Mineralogist, 101(6), 1268–1284. DOI: http://dx.doi.org/10.2138/am-2016-5307

Gansu Bureau of Geology and Mineral Resources (BGMRGS), 1967. 1:200,000 Regional Geological Map Sheet of the Hongliuyuan Area (in Chinese).

Gansu Bureau of Geology and Mineral Resources (BGMRGS), 1997. Stratigraphy (Lithostratic) of Gansu Province. China University of Geosciences Press, Wuhan, 314 pp. (in Chinese).

Garrison, J. M., Davidson, J. P., Hall, M., & Mothes, P. (2011). Geochemistry and Petrology of the Most Recent Deposits from Cotopaxi Volcano, Northern Volcanic Zone, Ecuador. Journal of Petrology, 52(9), 1641–1678. https://doi.org/10.1093/PETROLOGY/EGR023

Gill, J. B., Bongiolo, E. M., Miyazaki, T., Hamelin, C., Jutzeler, M., Debari, S., Jonas, A. S., Vaglarov, B. S., Nascimento, L. S., & Yakavonis, M. (2018). Tuffaceous Mud is a Volumetrically Important Volcaniclastic Facies of Submarine Arc Volcanism and Record of Climate Change. Geochemistry, Geophysics, Geosystems, 19(4), 1217–1243. https://doi.org/10.1002/2017GC007300

Guo, Q., Xiao, W.J., Hou, Q., Windley, B. F., Han, C., Tian, Z., & Song, D. (2014). Construction of late Devonian Dundunshan arc in the Beishan orogen and its implication for tectonics of southern Central Asian orogenic belt. Lithos, 184–187, 361–378. https://doi.org/10.1016/j.lithos.2013.11.007

Guo, Q., Xiao, W.J., Windley, B. F., Mao, Q., Han, C., Qu, J., Ao, S., Li, J., Song, D., & Yong, Y. (2012). Provenance and tectonic settings of Permian turbidites from the Beishan Mountains, NW China: Implications for the Late Paleozoic accretionary tectonics of the southern Altaids. Journal of Asian Earth Sciences, 49, 54–68. https://doi.org/10.1016/j.jseaes.2011.03.013

Guo, Q. Q., Chung, S. L., Xiao, W.J. J., Hou, Q. L., & Li, S. (2017). Petrogenesis and tectonic implications of Late Devonian arc volcanic rocks in southern Beishan orogen, NW China: Geochemical and Nd–Sr–Hf isotopic constraints. Lithos, 278, 84-96.

He, Z. Y., Klend, R., Yan, L. L., & Zhang, Z. M. (2018). The origin and crustal evolution of microcontinents in the Beishan orogen of the southern Central Asian Orogenic Belt. Earth-Science Reviews, 185, 1–14.

Heywood, L.J., DeBari, S.M., Gill, J.B., Straub, S.M., Schindlbeck-Belo, J.C., Escobar-Burciaga, R.D. and Woodhead, J. 2020. Across-arc diversity in rhyolites from an intra-oceanic arc: evidence from IODP site U1437, Izu-Bonin Rear Arc, and surrounding area. Geochemistry, Geophysics, Geosystems, 21, e2019G C008353, https://doi.org/10.1029/2019GC008353

Hollocher, K., Robinson, P., Walsh, E., & Roberts, D. (2012). Geochemistry of amphibolite-facies volcanics and gabbros of the Storen Nappe in extensions west and southwest of Trondheim, western gneiss region, Norway: A key to correlations and paleotectonic settings. American Journal of Science, 312(4), 357–416. https://doi.org/10.2475/04.2012.01

Hong, T., Santos, G. S., van Staal, C. R., Ji, W., & Lin, S. (2022). Mapping uncovered a multi-phase arc—back-arc system in the southern Beishan during the Permian. National Science Review. .org/10.1093/nsr/nwac204

Iizuka, T., Campbell, I. H., Allen, C. M., Gill, J. B., Maruyama, S., & Makoka, F. (2013). Evolution of the African continental crust as recorded by U–Pb, Lu–Hf and O isotopes in detrital zircons from modern rivers. Geochimica et Cosmochimica Acta, 107, 96–120. .org/10.1016/J.GCA.2012.12.028

Kalita, P., Phukon, P., Goswami, T. K., Imayama, T., & Srivastava, H. B. (2022). Chemical mass transport during deformation and metamorphism: Insights from the Main Central Thrust and its footwall of Western Arunachal Himalaya, NE India. Lithos, 416–417, 106641. .org/10.1016/J.LITHOS.2022.106641

Kemp, A. I. S., Hawkesworth, C. J., Foster, G. L., Paterson, B. A., Woodhead, J. D., Hergt, J. M., Gray, C. M., & Whitehouse, M. J. (2007). Magmatic and crustal differentiation history of granitic rocks from Hf-O isotopes in zircon. Science, 315(5814), 980–983. https://doi.org/10.1126/SCIENCE.1136154/SUPPL_FILE/KEMP.SOM.PDF

Kemp, A. I. S., Hawkesworth, C. J., Paterson, B. A., Foster, G. L., Kinny, P. D., Whitehouse, M. J., Maas, R., & Eimf. (2008). Exploring the plutonic-volcanic link: a zircon U-Pb, Lu-Hf and O isotope study of paired volcanic and granitic units from southeastern Australia. Earth and Environmental Science Transactions of The Royal Society of Edinburgh, 97(4), 337–355. https://doi.org/10.1017/S0263593300001498

Kepezhinskas, P., McDermott, F., Defant, M. J., Hochstaedter, A., Drummond, M. S., Hawkesworth, C. J., Koloskov, A., Maury, R. C., & Bellon, H. (1997). Trace element and Sr-Nd-Pb isotopic constraints on a three-component model of Kamchatka Arc petrogenesis. Geochimica et Cosmochimica Acta, 61(3), 577–600. https://doi.org/10.1016/S0016-7037(96)00349-3

Khain, E. v., Bibikova, E. v., Kröner, A., Zhuravlev, D. Z., Sklyarov, E. v., Fedotova, A. A., & Kravchenko-Berezhnoy, I. R. (2002). The most ancient ophiolite of the Central Asian fold belt: U-Pb and Pb-Pb zircon ages for the Dunzhugur Complex, Eastern Sayan, Siberia, and geodynamic implications. Earth and Planetary Science Letters, 199(3–4), 311–325. https://doi.org/10.1016/S0012-821X(02)00587-3

Khain, E. v., Bibikova, E. v., Kröner, A., Zhuravlev, D. Z., Sklyarov, E. v., Fedotova, A. A., & Kravchenko-Berezhnoy, I. R. (2002). The most ancient ophiolite of the Central Asian fold belt: U-Pb and Pb-Pb zircon ages for the Dunzhugur Complex, Eastern Sayan, Siberia, and geodynamic implications. Earth and Planetary Science Letters, 199(3–4), 311–325. https://doi.org/10.1016/S0012-821X(02)00587-3

Kuzmichev, A. B., & Larionov, A. N. (2013). Neoproterozoic island arcs in East Sayan: Duration of magmatism (from U-Pb zircon dating of volcanic clastics). Russian Geology and Geophysics, 54(1), 34–43. https://doi.org/10.1016/j.rgg.2012.12.003

Kuzmichev, A. B., & Larionov, A. N. (2013). Neoproterozoic island arcs in East Sayan: Duration of magmatism (from U-Pb zircon dating of volcanic clastics). Russian Geology and Geophysics, 54(1), 34–43. https://doi.org/10.1016/j.rgg.2012.12.003

Li X-F, Zhang C-L, Li L, Bao Z-A, Zhang B-L, Wei Q. (2015). Formation age, geochemical characteristics of the Mingshujing pluton in Beishan area of Gansu Province and its geological significance. Acta Petrologica Sinica, 31(9), 2521-2538 (in Chinese).

Mao, Q., Xiao, W.J., Windley, B. F., Han, C., Qu, J., Ao, S., Zhang, J., & Guo, Q. (2012a). The Liuyuan complex in the Beishan, NW China: a Carboniferous–Permian ophiolitic fore-arc sliver in the southern Altaids. Geological Magazine, 149(3), 483–506. https://doi.org/10.1017/S0016756811000811

Mao, Q., Xiao, W.J., Fang, T., Wang, J., Han, C., Sun, M., & Yuan, C. (2012b). Late Ordovician to early Devonian adakites and Nb-enriched basalts in the Liuyuan area, Beishan, NW China: implications for early Paleozoic slab-melting and crustal growth in the southern Altaids. Gondwana Research, 22(2), 534-553.

Marien, C. S., Drewes-Todd, E. K., Stork, A., Todd, E., Gill, J. B., Hoffmann, J. E., ... & Münker, C. (2022). Juvenile continental crust evolution in a modern oceanic arc setting: Petrogenesis of Cenozoic felsic plutons in Fiji, SW Pacific. Geochimica et Cosmochimica Acta, 320, 339-365. https://doi.org/10.1016/j.gca.2021.11.033

Millet, M.-A., Tutt, C. M., Handler, M. R., & Baker, J. A. (2014). Processes and time scales of dacite magma assembly and eruption at Tauhara volcano, Taupo Volcanic Zone, New Zealand. Geochemistry, Geophysics, Geosystems, 15(1), 213–237. https://doi.org/10.1002/2013gc005016

Mišković, A., & Francis, D. (2006). Interaction between mantle-derived and crustal calc-alkaline magmas in the petrogenesis of the Paleocene Sifton Range volcanic complex, Yukon, Canada. Lithos, 87(1–2), 104–134. https://doi.org/10.1016/J.LITHOS.2005.05.007

Miyashiro, A. (1974). Volcanic rock series in island arcs and active continental margins. American Journal of Science, 274(4), 321–355. https://doi.org/10.2475/AJS.274.4.321

Murphy, J. (2006). Igneous Rock Associations 7. Arc Magmatism I: Relationship Between Subduction and Magma Genesis. Geoscience Canada, 33(4), 145–168. https://id.erudit.org/iderudit/geocan33_4ser01

Murphy, J. (2007). Igneous Rock Associations 8. Arc magmatism II: Geochemical and isotopic constraints on petrogenesis. Geoscience Canada, 34(1), 1-29. https://journals.lib.unb.ca/index.php/GC/article/view/10230

Niu, Y., Liu, C., Shi, G. R., Lu, J., Xu, W., & Shi, J. (2018). Unconformity-bounded Upper Paleozoic megasequences in the Beishan Region (NW China) and implications for the timing of the Paleo-Asian Ocean closure. Journal of Asian Earth Sciences, 167, 11-32. https://doi.org/10.1016/j.jseaes.2018.06.019

Oliot, E., Goncalves, P., & Marquer, D. (2010). Role of plagioclase and reaction softening in a metagranite shear zone at mid-crustal conditions (Gotthard Massif, Swiss Central Alps). Journal of Metamorphic Geology, 28(8), 849–871. https://doi.org/10.1111/J.1525-1314.2010.00897.X

Pearce, J. A., & Norry, M. J. (1979). Petrogenetic implications of Ti, Zr, Y, and Nb variations in volcanic rocks. Contributions to Mineralogy and Petrology 1979 69:1, 69(1), 33–47. https://doi.org/10.1007/BF00375192

Pearce, J. A., Harris, N. B., & Tindle, A. G. (1984). Trace element discrimination diagrams for the tectonic interpretation of granitic rocks. Journal of petrology, 25(4), 956-983. Pearce, J. A., Stern, R. J., Bloomer, S. H., & Fryer, P. (2005). Geochemical mapping of the Mariana arc-basin system: Implications for the nature and distribution of subduction components. Geochemistry, geophysics, geosystems, 6(7).

Pearce, J. (1996). Sources and settings of granitic rocks. Episodes, 19(4), 120–125. https://doi.org/10.18814/EPIIUGS/1996/V19I4/005

Pearce, J. A., Stern, R. J., Bloomer, S. H., & Fryer, P. (2005). Geochemical mapping of the Mariana arc-basin system: Implications for the nature and distribution of subduction components. Geochemistry, Geophysics, Geosystems, 6(7). https://doi.org/10.1029/2004GC000895

Ross, P. S., & Bédard, J. H. (2009). Magmatic affinity of modern and ancient subalkaline volcanic rocks determined from trace-element discriminant diagrams. Canadian Journal of Earth Sciences, 46(11), 823–839. https://doi.org/10.1139/E09-054

Rudnick, R.L. and Gao, S. (2003) The Composition of the Continental Crust. In: Holland, H.D. and Turekian, K.K., Eds., Treatise on Geochemistry, Vol. 3, The Crust, Elsevier-Pergamon, Oxford, 1-64. http://dx.doi.org/10.1016/b0-08-043751-6/03016-4

Saktura, W. M., Buckman, S., Nutman, A. P., Belousova, E. A., Yan, Z., & Aitchison, J. C. (2017). Continental origin of the Gubaoquan eclogite and implications for evolution of the Beishan Orogen, Central Asian Orogenic Belt, NW China. Lithos, 294–295, 20–38. https://doi.org/10.1016/J.LITHOS.2017.10.004

Santos, G. S., Hong, T., van Staal, C. R., Bedard, J., Lin, S., & Wang, K. (2022). Permian back-arc basin formation and arc migration in the southern Central Asian Orogenic Belt, Northwest China. Geological Journal. https://doi.org/10.1002/gj.4609

Santos, G.S., Bedard, J., van Staal, C., Lin S., Hong, T., and Wang, K. (2023). Geology of the Liuyuan Complex, NW China: a Permian back-arc basin ophiolite at the southern edge of the Central Asian Orogenic Belt. GSA bulletin, https://doi.org/10.1130/B36736.1

Santos, G.S., (2022). Petrology, tectonic setting, and regional implications of the ophiolitic Liuyuan Complex, NW China. PhD thesis, University of Waterloo.

Smith, I. E. M., & Price, R. C. (2006). The Tonga–Kermadec arc and Havre–Lau back-arc system: Their role in the development of tectonic and magmatic models for the western Pacific. Journal of Volcanology and Geothermal Research, 156(3–4), 315–331. https://doi.org/10.1016/J.JVOLGEORES.2006.03.006

Soldner, J., Štípská, P., Schulmann, K., Yuan, C., Anczkiewicz, R., Sala, D., Jiang, Y., Zhang, Y., & Wang, X. (2020). Coupling of P–T–t–D histories of eclogite and metagreywacke—Insights to late Ordovician–Silurian crustal folding events recorded in the Beishan Orogen (NW China). Journal of Metamorphic Geology, 38(6), 555–591. https://doi.org/10.1111/JMG.12531

Su, B. X., Qin, K. Z., Sun, H., Tang, D. M., Sakyi, P. A., Chu, Z. Y., ... & Xiao, Q. H. (2012). Subduction-induced mantle heterogeneity beneath Eastern Tianshan and Beishan: insights from Nd–Sr–Hf–O isotopic mapping of Late Paleozoic mafic–ultramafic complexes. Lithos, 134, 41-51. https://doi.org/10.1016/j.lithos.2011.12.011

Sun, S.S. and McDonough, W.F. (1989) Chemical and Isotopic Systematics of Oceanic Basalts: Implications for Mantle Composition and Processes. In: Saunders, A.D., Norry, M.J., Eds., Magmatism in the Ocean Basins, Geological Society, London, Special Publications, 42, 313-345. https://doi.org/10.1144/GSL.SP.1989.042.01.19

Tian, Z., Xiao, W.J., Windley, B. F., Lin, L., Han, C., Zhang, J., Wan, B., Ao, S., Song, D., & Feng, J. (2014a). Structure, age, and tectonic development of the Huoshishan-Niujuanzi ophiolitic mélange, Beishan, southernmost Altaids. Gondwana Research, 25(2), 820–841.

Tian, Z., Xiao, W.J., Sun, J., Windley, B. F., Glen, R., Han, C., Zhang, Z., Zhang, J., Wan, B., Ao, S., & Song, D. (2014b). Triassic deformation of Permian Early Triassic arc-related sediments in the Beishan (NW China): Last pulse of the accretionary orogenesis in the southernmost Altaids. Tectonophysics, 662, 363–384. https://doi.org/10.1016/J.TECTO.2015.01.009

Tian, Z., & Xiao, W.J. (2020). An Andean-type arc transferred into a Japanese-type arc at final closure stage of the Palaeo-Asian Ocean in the southernmost of Altaïds. Geological Journal, 55(3), 2023–2043. https://doi.org/10.1002/GJ.3700

Tian, Z., Xiao, W.J., Windley, B. F., Huang, P., Zhang, J., Ao, S., Zhang, Z., Song, D., & Liu, F. (2021). Two key switches in regional stress field during multi-stage deformation in the Carboniferous–Triassic

southernmost Altaids (Beishan, NW China): Response to orocline-related roll-back processes. GSA Bulletin, 133(11–12), 2591–2611. https://doi.org/10.1130/B35898.1

Todd E., Stork A., Drewes-Todd E.K., Tani K., Allen C.M. and Gill J.B. (2021). Geochemistry and geochronology of Cenozoic plutons of Viti Levu, Fiji, Version 1.0, Interdiscip. Earth Data Alliance. doi:10.26022/IEDA/111854

Valley, J. W., Chiarenzelli, J. R., & McLelland, J. M. (1994). Oxygen isotope geochemistry of zircon. Earth and Planetary Science Letters, 126(4), 187–206. https://doi.org/10.1016/0012-821X(94)90106-6

Valley, J. W. (2003). Oxygen isotopes in zircon. Reviews in Mineralogy and Geochemistry, 53. https://doi.org/10.2113/0530343

Valley, J. W., Lackey, J. S., Cavosie, A. J., Clechenko, C. C., Spicuzza, M. J., Basei, M. A. S., Bindeman, I. N., Ferreira, V. P., Sial, A. N., King, E. M., Peck, W. H., Sinha, A. K., & Wei, C. S. (2005). 4.4 billion years of crustal maturation: Oxygen isotope ratios of magmatic zircon. Contributions to Mineralogy and Petrology, 150(6), 561–580. https://doi.org/10.1007/S00410-005-0025-8/FIGURES/12

van S taal, C.R., Hong, T., L in, S., Ji, W .H, 2021. Bedrock Geological Map of the Baidunzi-Heishankou Area, Guazhou, Gansu, China, scale 1:25,000: China Geological Survey, DOI: 10.35080/data.C.2021.P01.

Wang, Y., Luo, Z., Santosh, M., Wang, S., & Wang, N. (2017). The Liuyuan Volcanic Belt in NW China revisited: Evidence for Permian rifting associated with the assembly of continental blocks in the Central Asian Orogenic Belt. Geological Magazine, 154-2, 265–285.

Wang, X., Yuan, C., Zhang, Y., Long, X., Sun, M., Wang, L., Soldner, J., & Lin, Z. (2018). S-type granite from the Gongpoquan arc in the Beishan Orogenic Collage, southern Altaids: Implications for the tectonic transition. Journal of Asian Earth Sciences, 153, 206–222.

Whalen, J. B., & Hildebrand, R. S. (2019). Trace element discrimination of arc, slab failure, and A-type granitic rocks. Lithos, 348–349, 105179. https://doi.org/10.1016/j.lithos.2019.105179

Winchester, J. A., & Floyd, P. A. (1977). Geochemical discrimination of different magma series and their differentiation products using immobile elements. Chemical Geology, 20(C), 325–343. https://doi.org/10.1016/0009-2541(77)90057-2

Windley, B. F., Alexeiev, D., Xiao, W.J., Kroner, A., & Badarch, G. (2007). Tectonic models for accretion of the Central Asian Orogenic Belt. Journal of the Geological Society, 164(1), 31–47. https://doi.org/10.1144/0016-76492006-022

Xiao, W.J., Windley, B. F., Hao, J., & Zhai, M. (2003). Accretion leading to collision and the Permian Solonker suture, Inner Mongolia, China: Termination of the central Asian orogenic belt. Tectonics, 22(6). https://doi.org/10.1029/2002tc001484

Xiao, W.J., Windley, B. F., Yuan, C., Sun, M., Han, C. M., Lin, S. F., Chen, H. L., Yan, Q. R., Liu, D. Y., Qin, K. Z., Li, J. L., & Sun, S. (2009). Paleozoic multiple subduction-accretion processes of the southern Altaids. American Journal of Science, 309(3), 221–270. https://doi.org/10.2475/03.2009.02

Xiao, W.J., Mao, Q. G., Windley, B. F., Han, C. M., Qu, J. F., Zhang, J. E., Ao, S. J., Guo, Q. Q., Cleven, N. R., Lin, S. F., Shan, Y. H., & Li, J. L. (2010). Paleozoic multiple accretionary and collisional processes of the Beishan orogenic collage. American Journal of Science, 310(10), 1553–1594. https://doi.org/10.2475/10.2010.12

Xiao, W.J., Windley, B. F., Allen, M. B., & Han, C. (2013). Paleozoic multiple accretionary and collisional tectonics of the Chinese Tianshan orogenic collage. Gondwana Research, 23(4), 1316–1341. https://doi.org/10.1016/j.gr.2012.01.012

Xiao, W.J., Windley, B. F., Sun, S., Li, J., Huang, B., Han, C., Yuan, C., Sun, M., & Chen, H. (2015). A Tale of Amalgamation of Three Permo-Triassic Collage Systems in Central Asia: Oroclines, Sutures, and Terminal Accretion. Annual Review of Earth and Planetary Sciences, 43(1), 477–507. https://doi.org/10.1146/annurev-earth-060614-105254

Yu, Y., Zong, K., Yuan, Y. et al. Crustal Contamination of the Mantle-Derived Liuyuan Basalts: Implications for the Permian Evolution of the Southern Central Asian Orogenic Belt. J. Earth Sci. 33, 1081–1094 (2022). https://doi.org/10.1007/s12583-022-1706-1

Zhao, Y., Sun, Y., Diwu, C., Guo, A. L., Ao, W. H., & Zhu, T. (2016). The Dunhuang block is a Paleozoic orogenic belt and part of the Central Asian Orogenic Belt (CAOB), NW China. Gondwana Research, 30, 207–223. https://doi.org/10.1016/J.GR.2015.08.012

Zhao, Y., Ao, W., Yan, J., Zhai, M., Zhang, H., Wang, Q., Sun, Y., Zhao, Y., Ao, W., Yan, J., Zhai, M., Zhang, H., Wang, Q., & Sun, Y. (2019). Paleozoic tectonothermal event in Mt. Dongbatu, Dunhuang terrane, southernmost Central Asian Orogenic Belt (CAOB): Implications for petrogenesis and geological evolution. Litho, 326, 491–512. https://doi.org/10.1016/J.LITHOS.2018.12.037

Zhao, Y., Sun, Y., Diwu, C., Zhu, T., Ao, W., Zhang, H., & Yan, J. (2017). Paleozoic intrusive rocks from the Dunhuang tectonic belt, NW China: Constraints on the tectonic evolution of the southernmost Central Asian Orogenic Belt. Journal of Asian Earth Sciences, 138, 562–587. https://doi.org/10.1016/J.JSEAES.2017.02.037

Zheng, R., Li, J., Xiao, W.J., & Zhang, J. (2018). Nature and provenance of the Beishan Complex, southernmost Central Asian Orogenic Belt. International Journal of Earth Sciences, 107(2), 729–755. https://doi.org/10.1007/s00531-017-1525-2

Zheng, R., Li, J., Zhang, J., Xiao, W.J., & Wang, Q. (2020). Permian oceanic slab subduction in the southmost of Central Asian Orogenic Belt: Evidence from adakite and high-Mg diorite in the southern Beishan. Lithos, 358–359, 105406. https://doi.org/10.1016/J.LITHOS.2020.105406

Zheng, R., Li, J., Zhang, J., & Xiao, W.J. (2021a). A prolonged subduction-accretion in the southern Central Asian Orogenic Belt: Insights from anatomy and tectonic affinity for the Beishan complex. Gondwana Research, 95, 88–112. https://doi.org/10.1016/J.GR.2021.02.022

Zheng, R., Li, J., Zhang, J., Xiao, W.J., & Wang, Q. (2021b). Permian oceanic slab subduction in the southern Beishan: Reply to comment by Liu et al. on “Permian oceanic slab subduction in the southernmost Central Asian Orogenic Belt: Evidence from adakite and high-Mg diorite in the southern Beishan.” Lithos, 396–397, 106244. https://doi.org/10.1016/j.lithos.2021.106244

Zulkarnain, I. (2011). Geochemical Evidence of Island-Arc Origin for Sumatra Island; a New Perspective Based on Volcanic Rocks in Lampung Province, Indonesia. Indonesian Journal on Geoscience, 6(4), 213–225. https://doi.org/10.17014/IJOG.6.4.213-225

Zuo, G.C., He, G.Q., (1990). Plate Tectonics and Metallogenesis Regularities in Beishan Region. Peking University Press, Beijing (in Chinese).

Zuo, G., Zhang, S., He, G., & Zhang, Y. (1991). Plate tectonic characteristics during the early Paleozoic in Beishan near the Sino-Mongolian border region, China. Tectonophysics, 188(3-4), 385-392. https://doi.org/10.1016/0040-1951(91)90466-6

3.10 Figures and captions

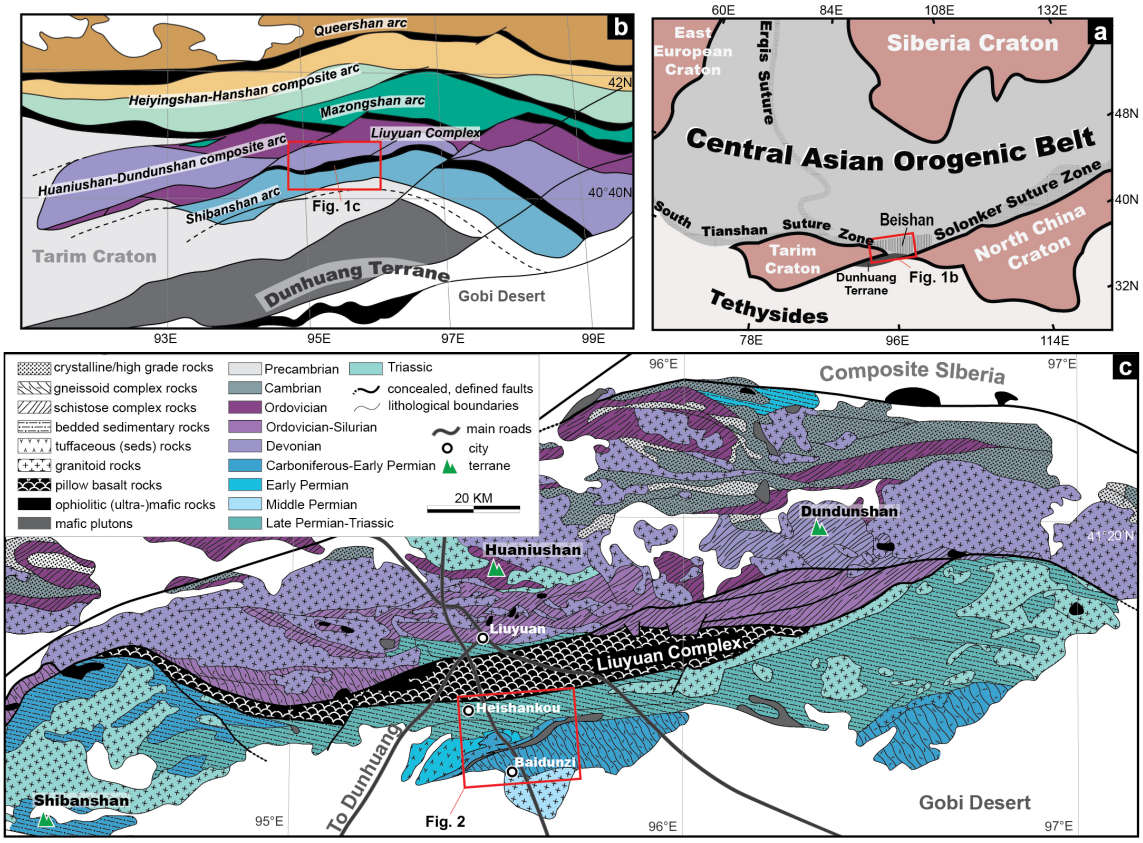


Figure 3-1: (a) Tectonic elements of the Central Asian Orogenic Belt. The shaded area shows the Beishan Orogen, and the dark grey area shows the Dunhuang Terrane. (b) Schematic tectonic map of the Beishan Orogen and adjacent areas showing arc terranes and intervening ophiolite complexes (black). (c) Tectonic setting of the Liuyuan Complex between the Huaniushan–Dundunshan and Shibanshan terranes. Source: (a) modified from Xiao et al. 2010; (b) modified from Xiao et al. (2010); (c) modified from Mao et al. 2012a

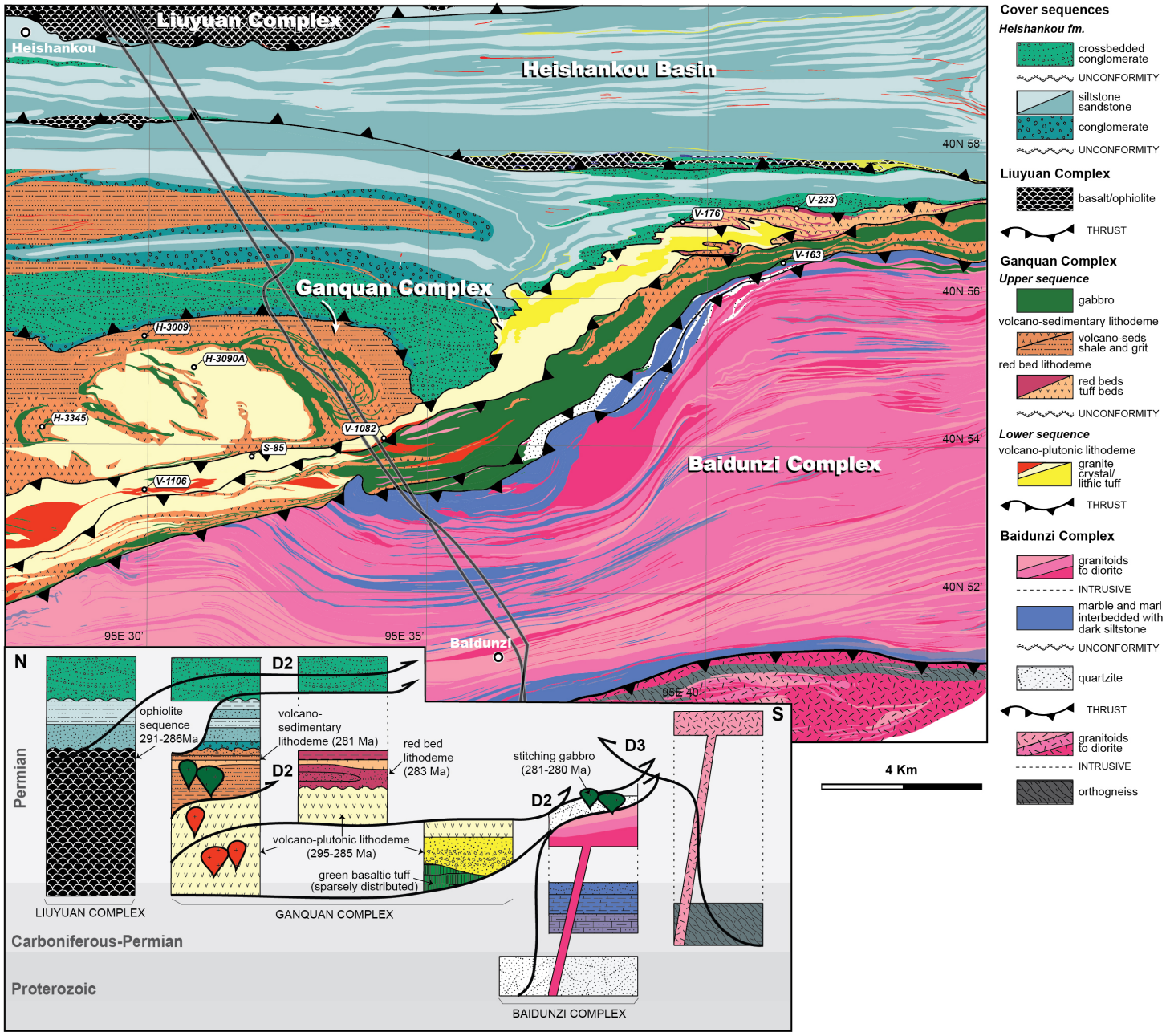


Figure 3-2: Geological map of the Ganquan Complex and surrounding area.

The tectono-stratigraphic columns show comparative geology of structural panels bounded by major thrusts, which comprise an early southwards-directed phase of tectonic transport, followed by a late phase of northwards-directed movement. Source: modified from van Staal et al. (2021).

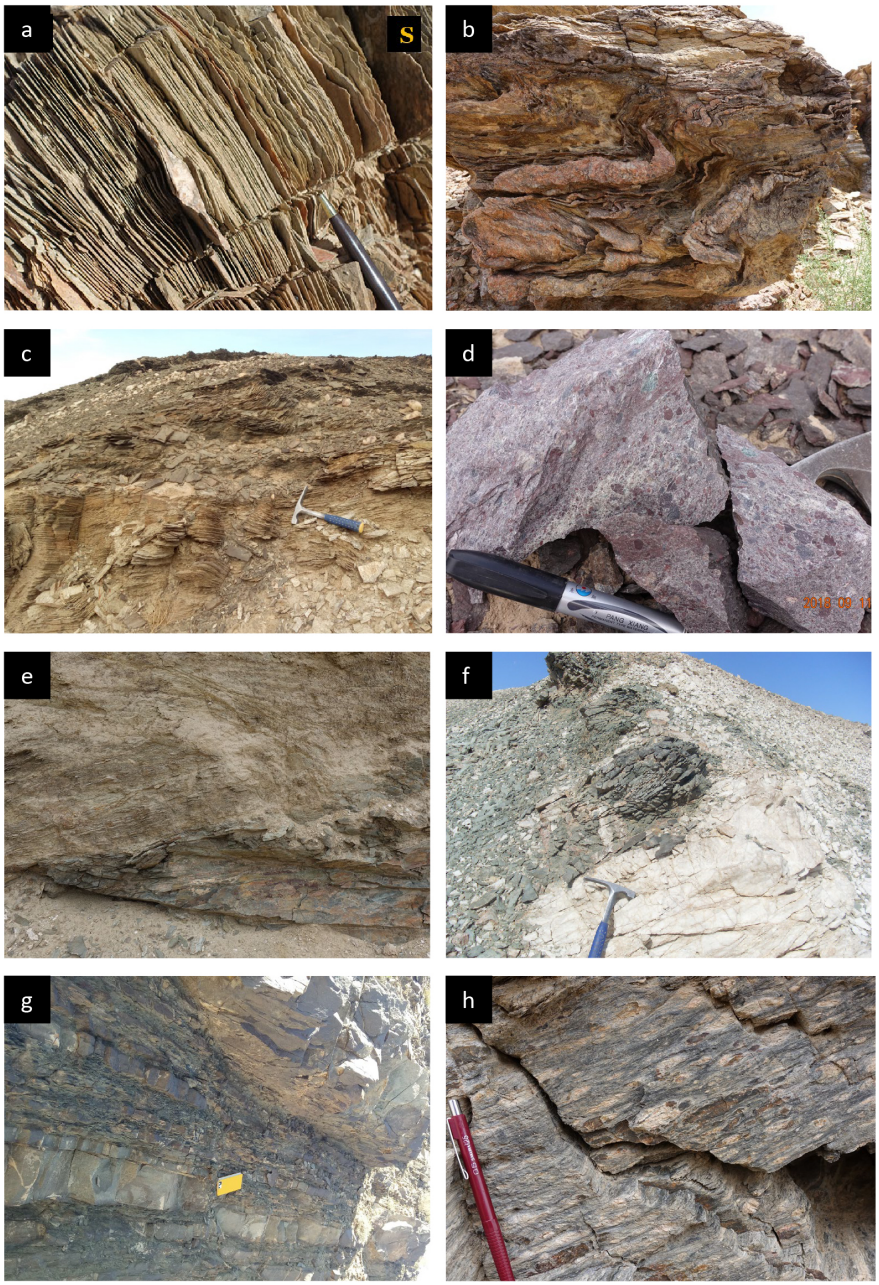


Figure 3-3: Field relations and lithology of Ganquan Complex and surrounding tectonic constituents. (a) Yellow pyroclastic volcanic rock of volcano-plutonic unit. Rocks are deformed into mylonite with a σ-type porphyroclastic quartz vein showing late thrust up toward north. (b) White to yellow crystal tuff (top) and associated pyroclastic volcanic rocks (center) are intruded by red granite, in the volcano-plutonic unit. (c) Unconformity contact between yellow phyric tuff of the lower volcano-plutonic unit and green epiclastic sandstone of the upper red bed unit. (d) Red gritty sandstone of the red bed unit. (e) Thrust contact between the yellow lithic tuff of the volcano-plutonic unit (top) and the grey siltstone of volcano-sedimentary unit (bottom). (f) Hornblende gabbro at the shear zone intruded quartzite unit of the Baidunzi Complex and deformed into greenschist facies mylonite. (g) and (h) Grey to black bedded shale, siltstone, and bottom conglomerate of volcano-sedimentary unit.

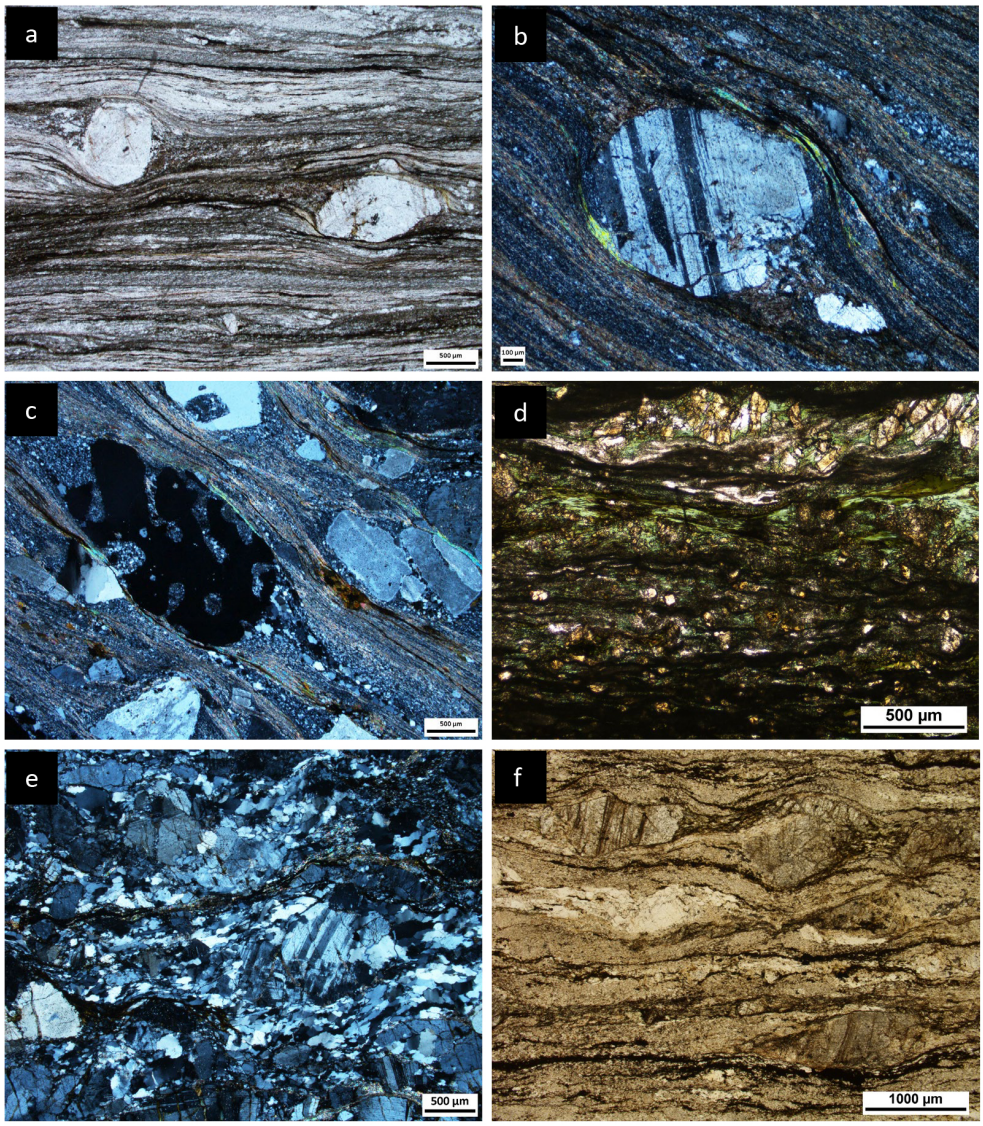


Figure 3-4: Thin Section photos of volcano-plutonic lithodeme rocks.
(a) and (b) Examples of δ- and σ-type porphyroclasts of quartz and plagioclase phenocrysts in strongly foliated pyroclastic rocks of volcano-plutonic unit. (c) An example of embayed quartz crystal and other phenocrysts in the surroundings. (d) An example of the green tuff preserved in the volcano-plutonic unit that are strongly deformed and completely metamorphosed into greenschist facies, with mafic minerals mostly replaced by epidote and biotite. (e) and (f) XPL and PPL petrographic photos of deformed sub-volcanic granite characterized by spaced and differentiated foliations with broken plagioclase clast and recrystallized quartz in the matrix.

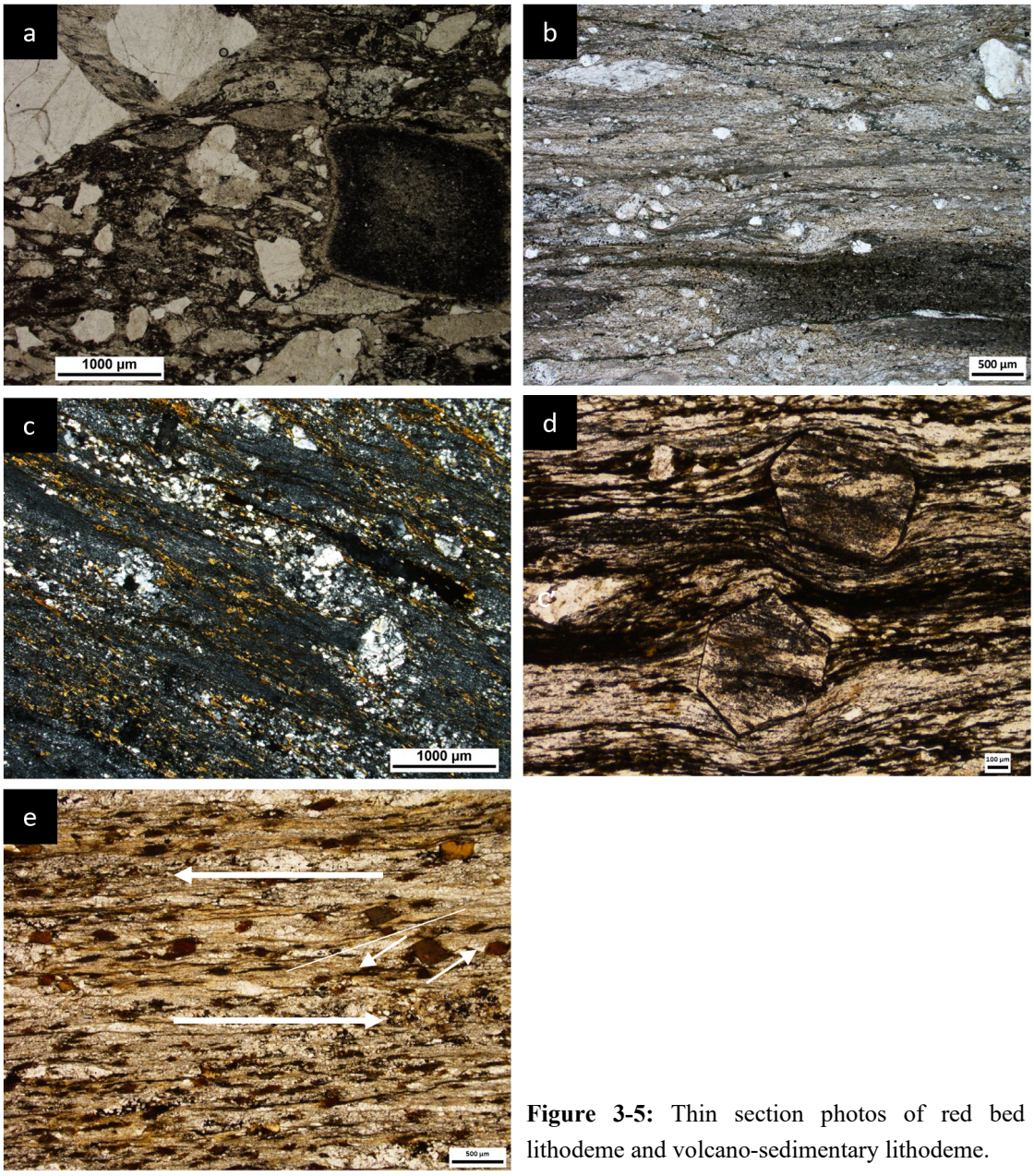


Figure 3-5: Thin section photos of red bed lithodeme and volcano-sedimentary lithodeme.

(a) An example of red sandstone showing the pigmentation in the matrix and clasts of rhyolite. (b) Lithic tuff of red bed unit. (c) Strongly foliated volcaniclastic siltstone showing micro-isoclinal folding from volcano-sedimentary unit. (d) An epiclastic siltstone of volcano-sedimentary unit showing strong foliation and porphyroclasts of garnet that may indicate an earlier burial event. (e) An epiclastic shale showing porphyroblasts of biotite fish in discontinuous foliations, suggesting sinistral kinematics (toward south).

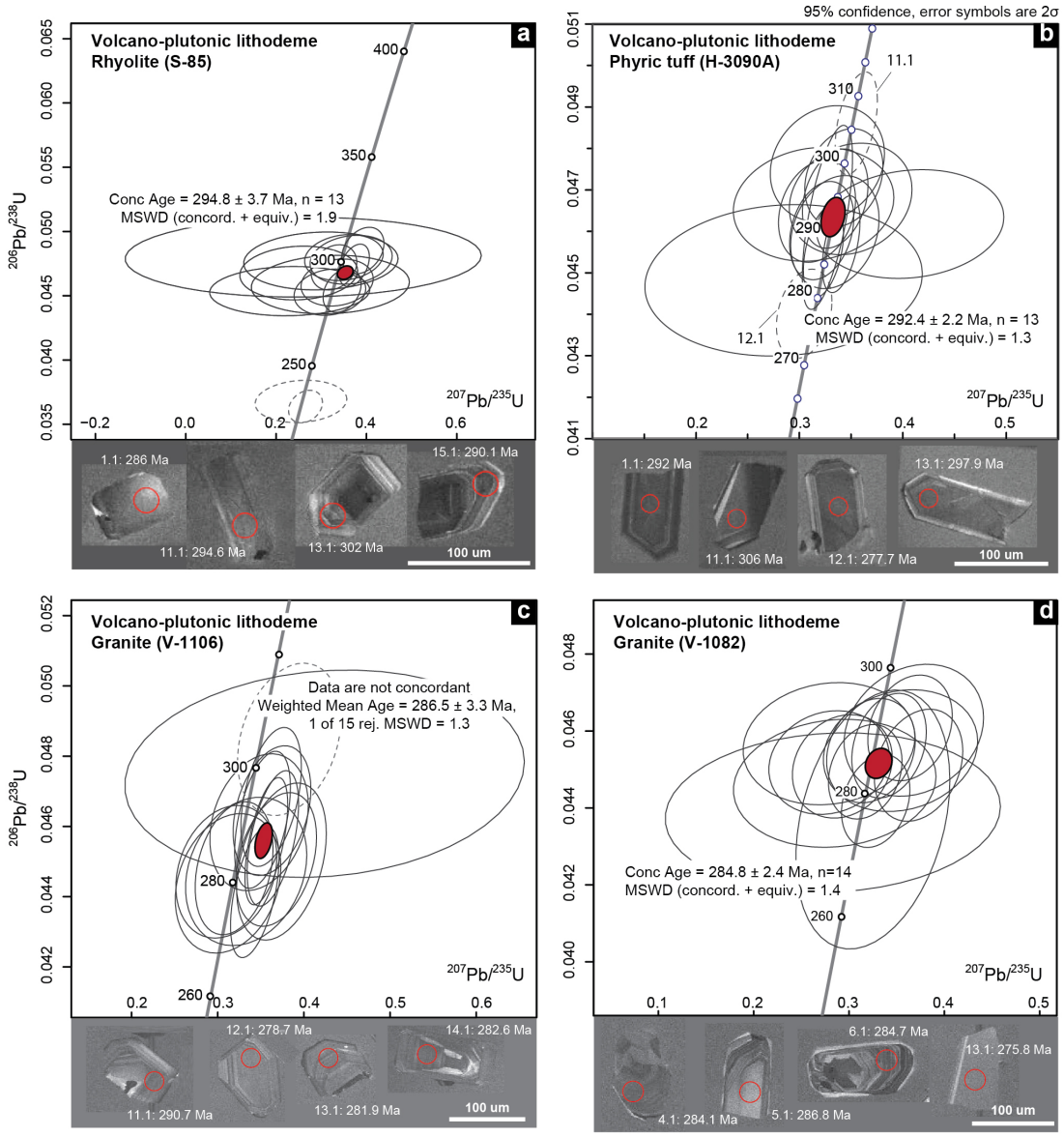


Figure 3-6: Concordia diagrams for samples from volcano-plutonic lithodeme.

(a) S-85, (b) H-3090A, (c)V-1106, (d) V-1082. CL (Cathodoluminescence) images of representative zircon populations and age for individual grains are attached below. Data points in dash line are excluded when calculating the crystallization ages. MSWD, mean square weighted deviation. Detailed data are reported in Table SM1.

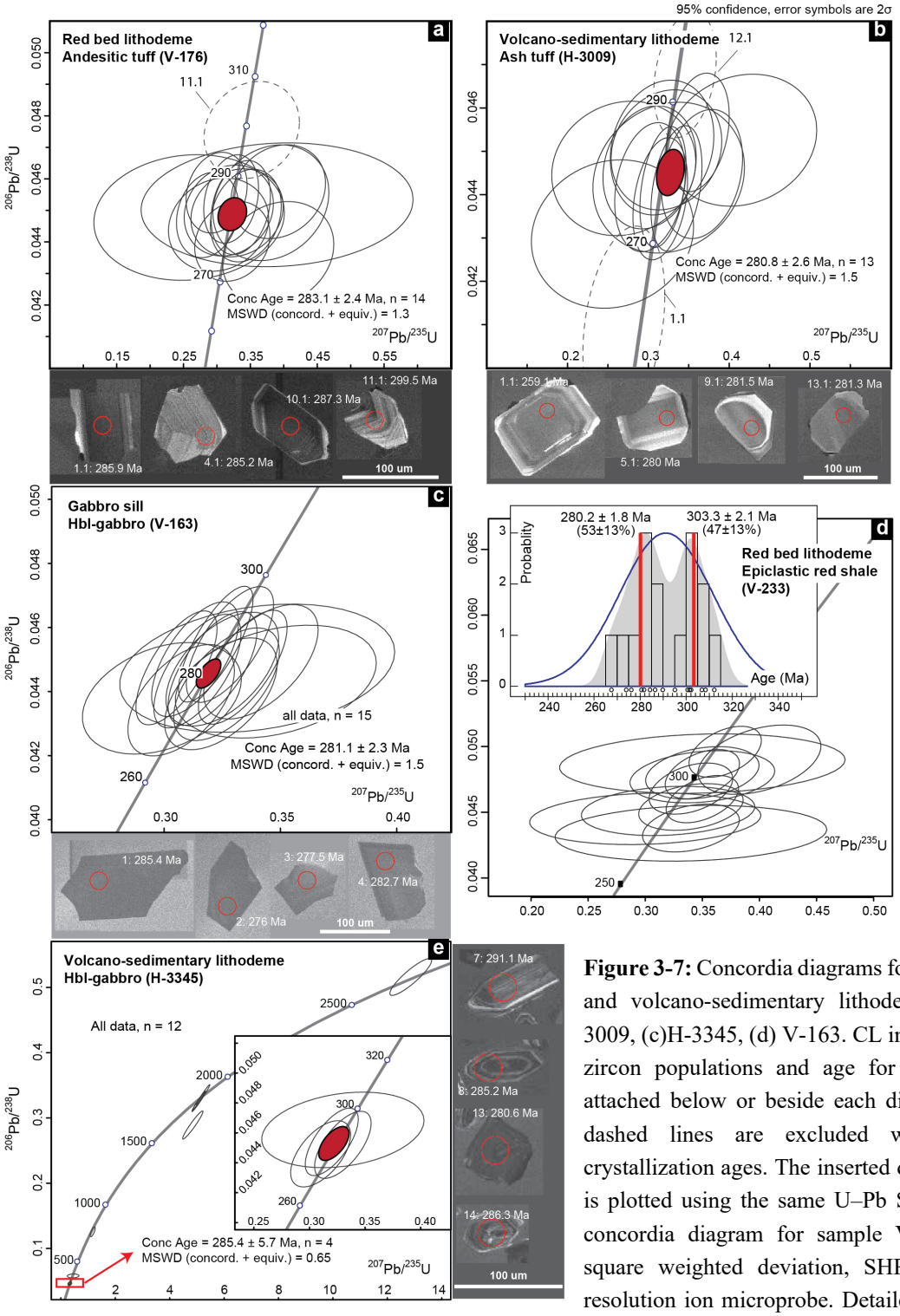


Figure 3-7: Concordia diagrams for samples from red bed and volcano-sedimentary lithodeme (a) V-176, (b)H-3009, (c)H-3345, (d) V-163. CL images of representative zircon populations and age for individual grains are attached below or beside each diagram. Data points in dashed lines are excluded when calculating the crystallization ages. The inserted detrital age distribution is plotted using the same U–Pb SHRIMP age from the concordia diagram for sample V-233. MSWD, mean square weighted deviation, SHRIMP, sensitive high-resolution ion microprobe. Detailed data are reported in Table SM1.

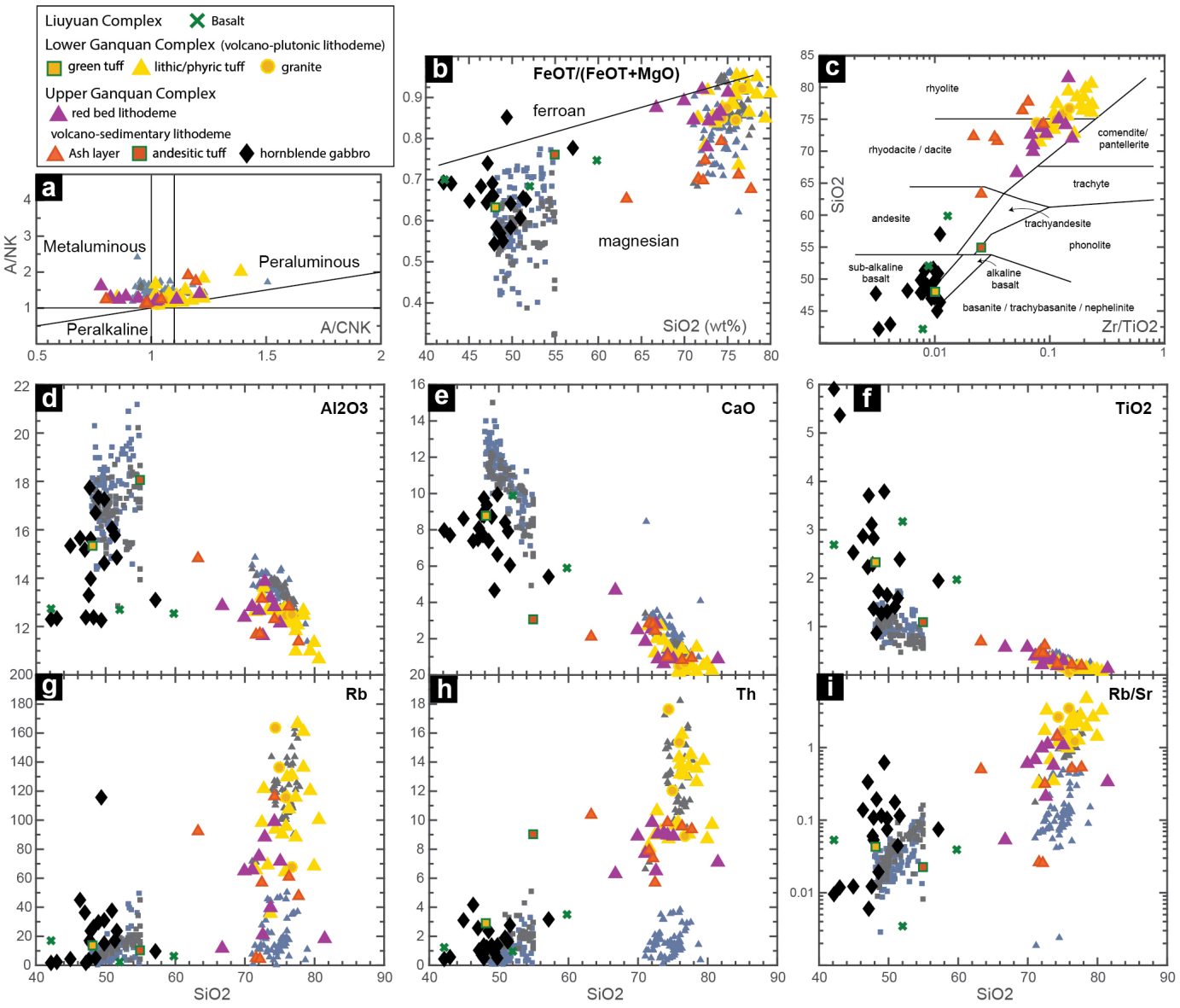


Figure 3-8: Major element classification diagrams of igneous rocks from Ganquan Complex. (a) and (b) Major element classification diagrams of A/NK vs. A/CNK and FeOT/(FeOT+MgO) plots. (c) Classification diagrams for altered volcanic rocks (Winchester and Floyed, 1977). (d-f) Selected Harker diagrams plotting Al2O3, CaO and TiO2 against SiO2. (g-i) Selected trace elements of Rb, Th and Rb/Sr ratios plots against SiO2. Triangle and square represent felsic and mafic volcanic rock samples, respectively. Blue and grey colored data points represent oceanic arc of Izu Bonin and Fiji and continental island arc of Taupo Volcanic Zone, respectively. Source: (c) from Winchester and Floyd 1977.

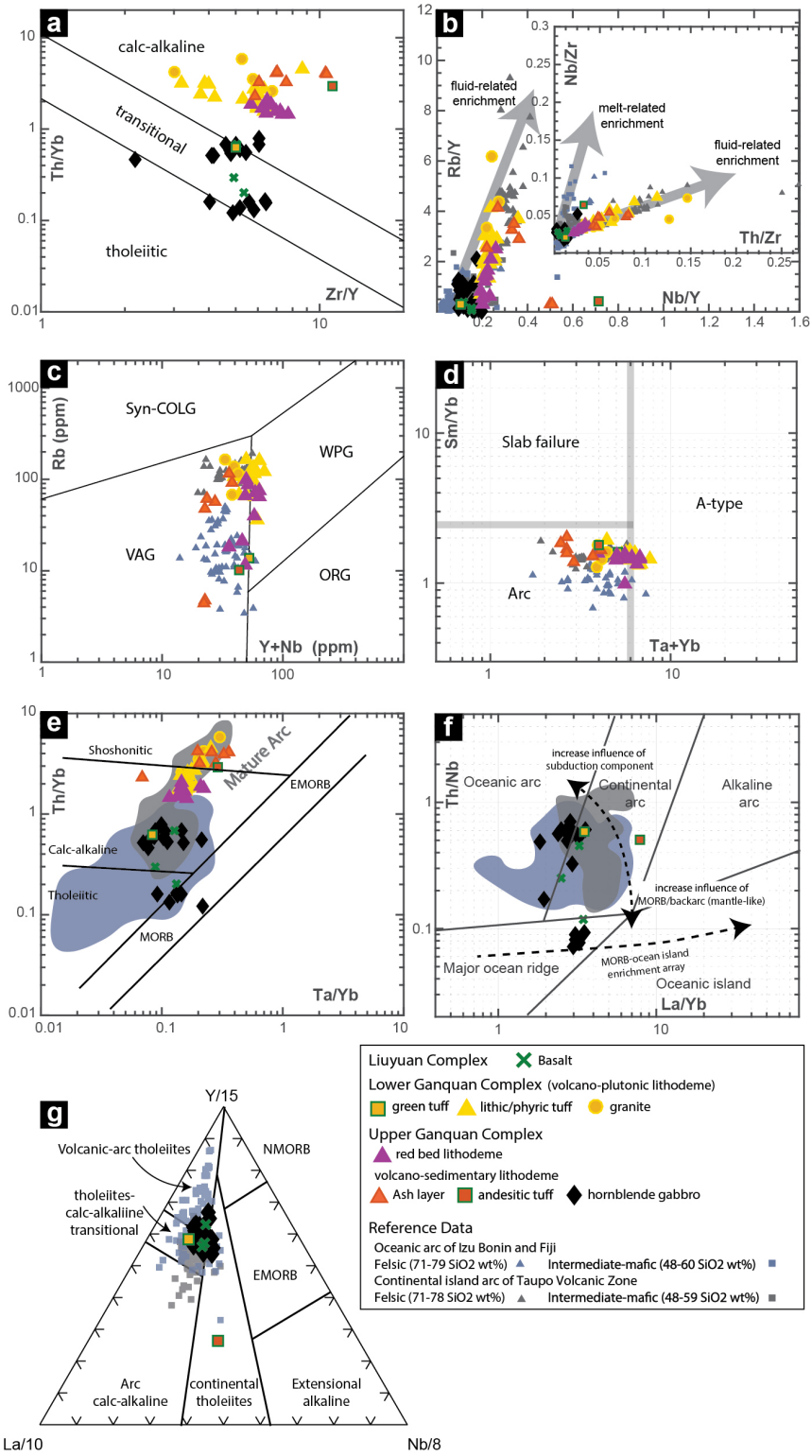


Figure 3-9: Trace element plots of igneous rocks from Ganquan Complex. (a) Magma series diagram. (b) Plots of Rb/Y v. Nb/Y with an inset plot of Nb/Zr v. Th/Zr. (c) Selected tectonic discrimination diagrams for felsic rocks. Log–log plot of Rb v. (Y + Nb). Other plots from the same sources gave similar results, plotting in the volcanic arc granite (VAG) field. (d) Selected tectonic discrimination diagrams. Log–log plot of Sm/Yb v. (Ta + Yb). Other plots from the same source gave similar results, plotting in the arc field. (e) Log–log plot of Th/Yb v. Ta/Yb. (f) Log–log plot of Th/Nb v. La/Yb that shows mafic samples. (g) La/10 v. Y/15 v. Nb/8 ternary discrimination diagram that shows mafic samples and reference data. The blue and grey shadow area represents combined data from oceanic arc of Izu Bonin and Fiji, and continental island arc of the Taupo Volcanic Zone, respectively. Source: (a) Ross and Bédard (2009); (c) Pearce et al. (1984) and Pearce (1996); (d) Whalen and Hildebrand (2019); (e) after Pearce et al. (1984, 2005); (f) after Hollocher et al. 2012; (g) Cabanis and Lecolle 1989.

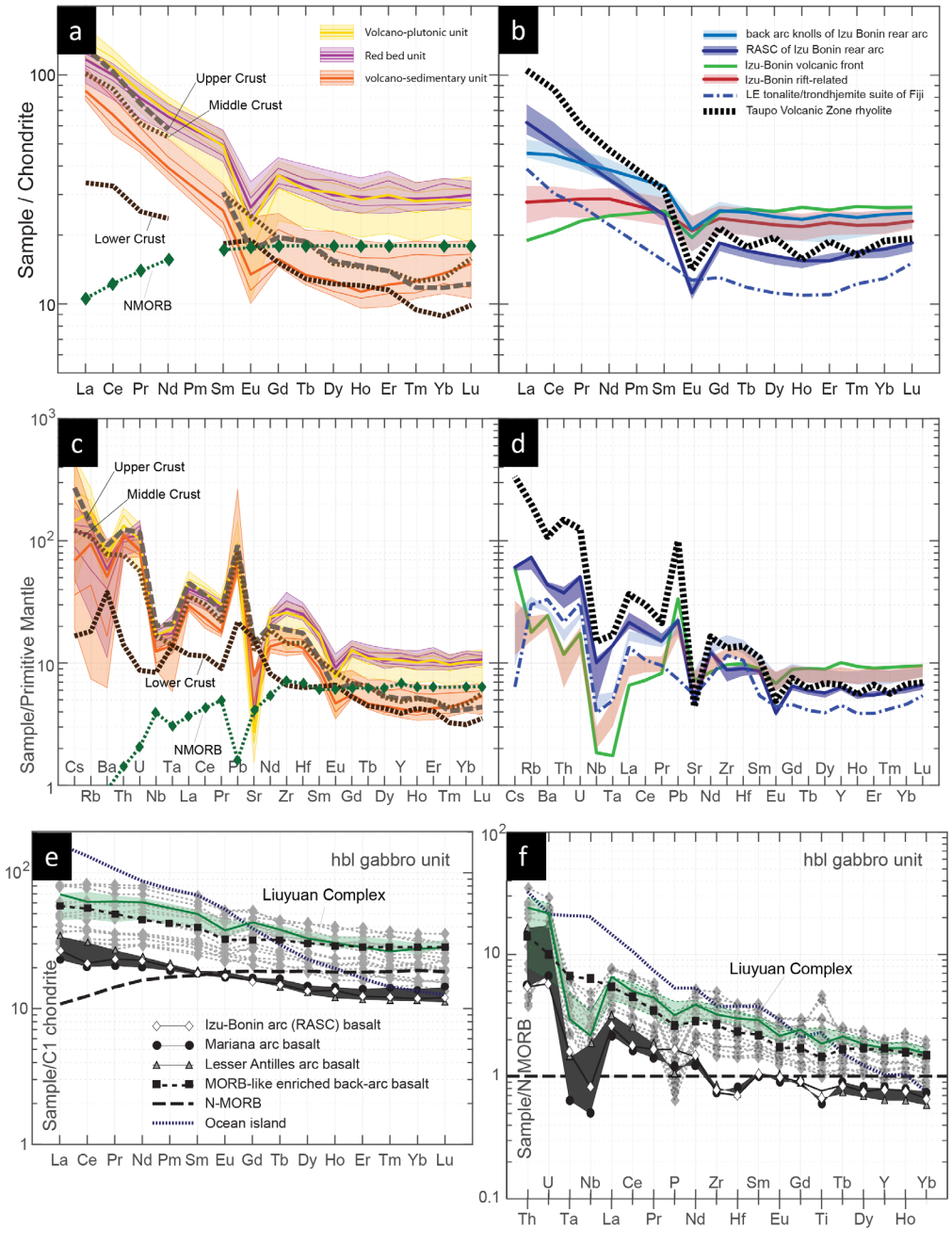


Figure 3-10: REE and trace element pattern diagrams. (a–d) Felsic rock REE diagrams and multi-element diagrams (normalized to primitive mantle) for Ganquan Complex and reference compositions for lower, middle, and upper crust, N-MORB, high-silica volcanic rocks with SiO2 window .70 wt% from Izu-Bonin intra-oceanic arc, Fiji intra-oceanic arc and the Taupo Volcanic Zone continental island arc. (e) and (f) Mafic rock REE diagrams and multi-element diagrams (normalized to N-MORB) for hornblende gabbro unit and reference compositions for Liuyuan Complex, ocean island, E-MORB and MORB basalt reference lines and Izu-Bonin, Mariana and Lesser Antilles arc basalt. E-MORB, incompatible element-enriched MORB; LE, light rare earth element enriched; MORB, mid-ocean ridge basalt; N-MORB, normal-type MORB; RASC, rear arc seamount chain. Source: (a–d) lower, middle and upper crust, Rudnick and Gao (2003); N-MORB, Sun and McDonough (1989); Izu-Bonin intra-oceanic arc, DeBari et al. (2020), Heywood et al. (2020); Fiji intra-oceanic arc, Marien et al. (2022); Taupo Volcanic Zone continental island arc, Millet et al. (2014), Allan et al. (2017); (e) and (f) Liuyuan Complex, Santos et al. (2022); ocean island, E-MORB and MORB, Sun and McDonough (1989); Izu-Bonin, Mariana and Lesser Antilles arc, Hollocher et al. (2012).

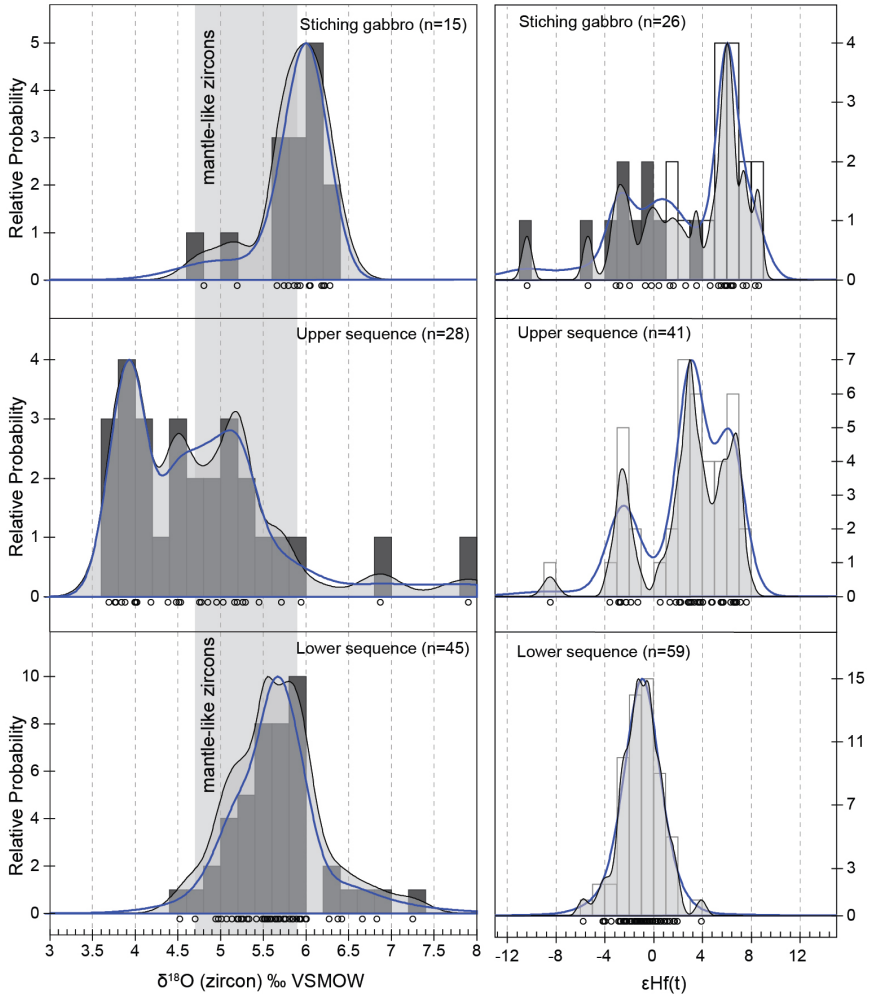


Figure 3-11: Histograms and probability density plots of δ18O (zircon) and zircon εHf(t) results from the hornblende gabbro unit.

(a, d), the upper (b, e) and lower (c, f) sequences of Ganquan Complex. Plot (a) only includes data of V-163 and the shadowed and white bands in plot (d) represent data from H-3345 and V-163 samples respectively.

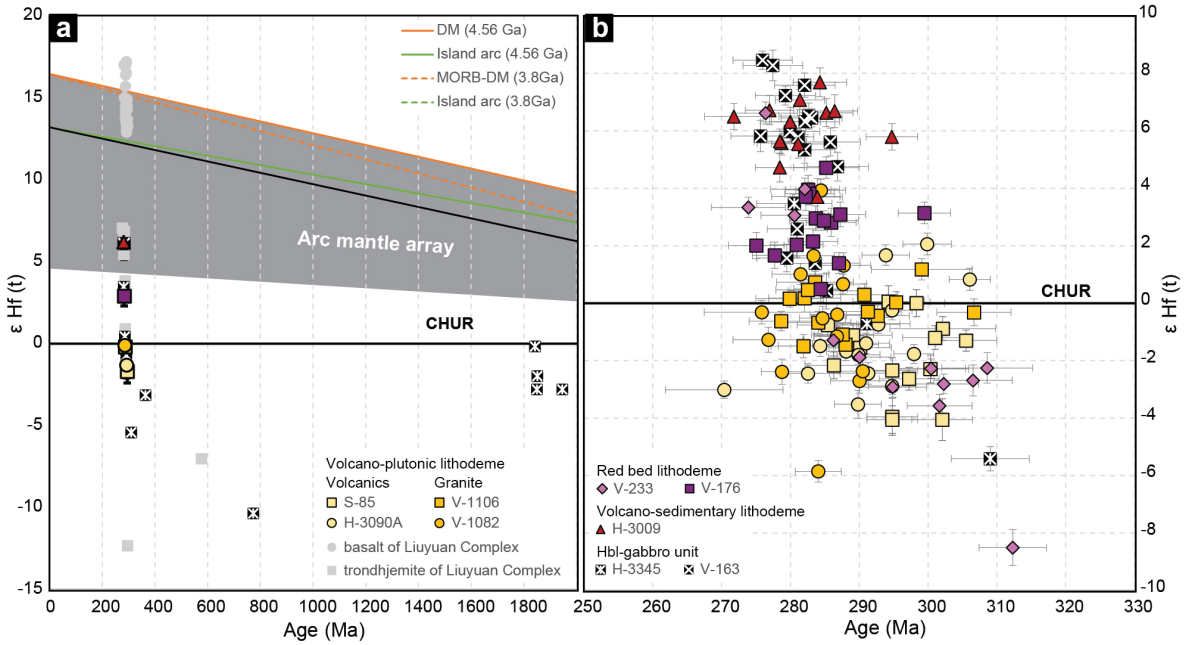


Figure 3-12: Summary of zircon εHf(t) values plotted against 206Pb/238U sample ages. (a) and 206Pb/238U individual grain ages (b) for zircon from Ganquan Complex, hornblende gabbro unit, and reference data from basalt and trondhjemite of Liuyuan Complex (Yu et al., 2022 and Santos 2022c).

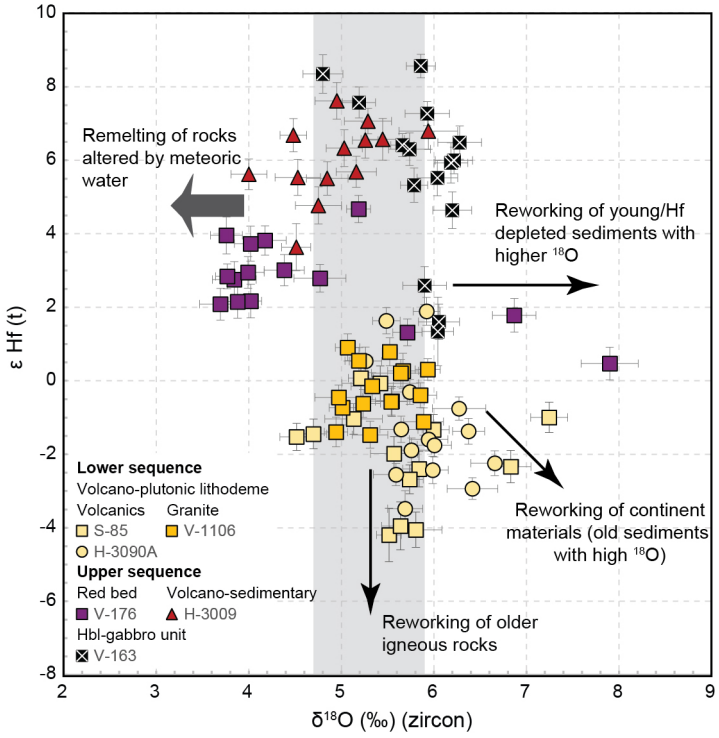


Figure 3-13: Plot of εHf(t) zircon values vs δ18O (zircon) ratios. Interpretation of data trends are modified after Iizuka et al. (2013).

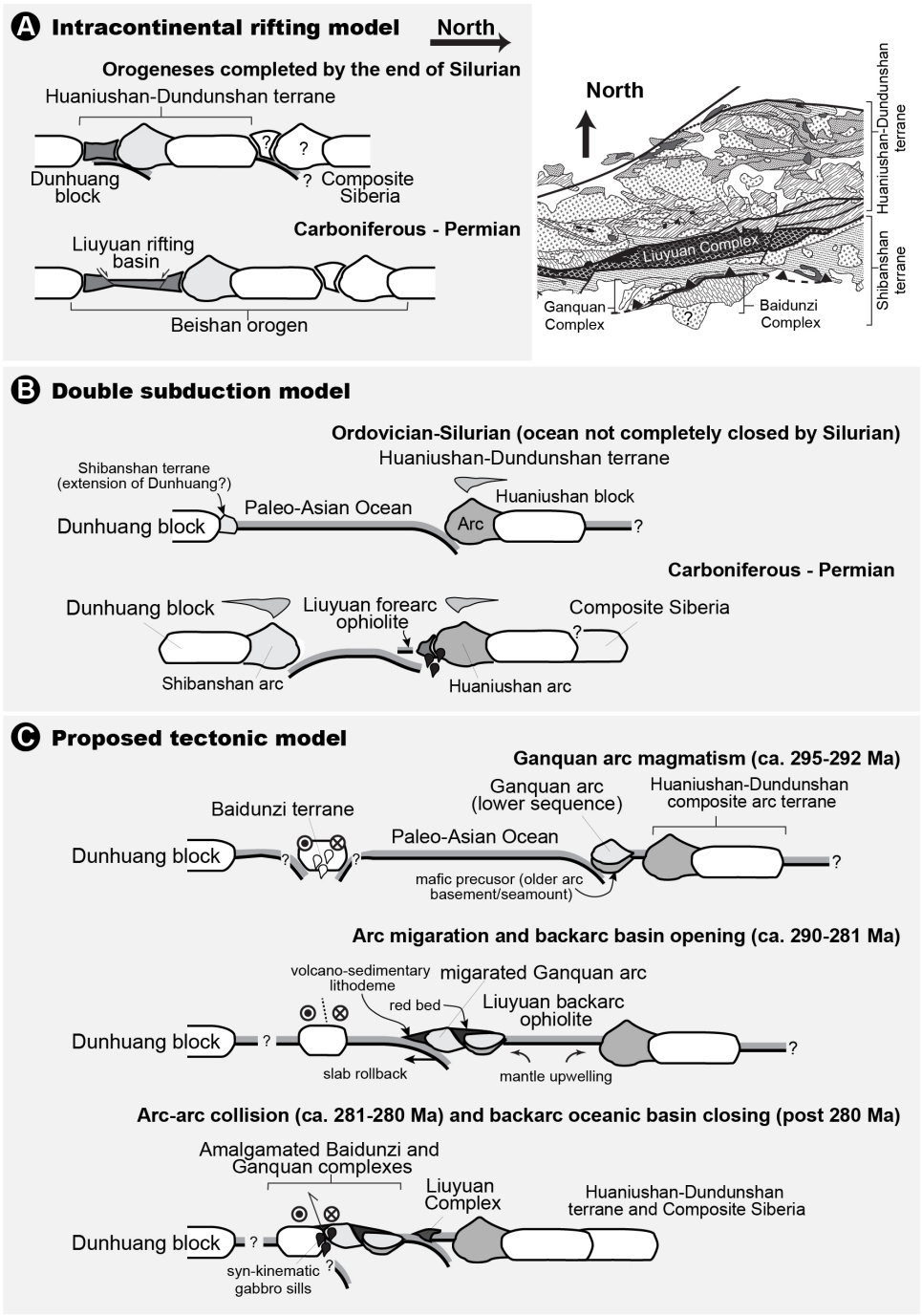


Figure 3-14: Proposed tectonic model.

Modified after Santos et al. (2023). (a) The initiation of Ganquan arc magmatism. (b) Slab roll back beneath the Ganquan arc induces arc migration and back-arc basin spreading. The inserted map is modified from Fig. 1c.

Chapter 4 A Permian transpressional continental arc and arc-arc collision recorded in the Baidunzi Complex, southern Central Asian orogenic belt, NW China

4.1 Abstract

The southern Beishan orogen in NW China, between the Tienshan and Solonker suture zones, is crucial to understanding the closure of the Paleo-Asian Ocean and termination of orogeneses in the Central Asian Orogenic Belt. Our multidisciplinary study combines field data with geochronological, geochemical, and isotopic data to identify an exotic Permian transpressional continental arc terrane, known as the Baidunzi Complex. The complex consists of variably sheared and isoclinally folded metasedimentary and syn-kinematic plutonic rocks, transformed into upper greenschist to amphibolite tectonites. The complex includes (1) thick-bedded orthoquartzite, which represents the oldest known rocks with no age peaks younger than 1.0 Ga; (2) younger meta-sedimentary strata consisting of volcaniclastic sedimentary rocks, marble, marl interlayered psammite, and schist, with young detrital zircon contents yielding Kasimovian to Asselian maximum depositional time (306–295 Ma); (3) The Baidunzi Intrusive Suite comprising 294–289 Ma hornblende diorite, tonalite, granodiorite and granite, with the petrology, pervasive zircon inheritance, trace element signatures and wide ranges of εHf(t) values (-3 to +7), all indicative of a continental arc tectonic setting; and (4) late intrusive rocks including dykes and sills of leuco-granite to trondhjemite and a stitching gabbro unit, giving an amalgamation age of 281–280 Ma between the Baidunzi arc and the previously defined Ganquan arc. The spatial and temporal linkage between the Baidunzi continental arc and the Liuyuan backarc-Ganquan arc suggest they were either built on a coeval doubly vergent subduction system or from the same north-vergent subduction system and structurally juxtaposed by sinistral convergence. The combined geochronological and Hf isotope evidence in conjunction with the overall continental

affinity of the rocks suggest a close association between the Baidunzi Complex and the northern margin of the Tarim Craton during the breakup of Gondwana and assembly of Pangea.

4.2 Introduction

The Central Asian orogenic belt (CAOB) represents the largest Phanerozoic accretionary orogen, welding the Baltica, Siberia, Karakum, Tarim and North China cratons together. The CAOB preserves a long tectonic history from the Late Mesoproterozoic (Khain et al., 2002; Kuzmichev & Larionov, 2013) until its termination in the Early Mesozoic (Xiao et al., 2003, 2009), witnessing histories of Gondwana dispersal and Pangea assembly (Han et al., 2016; Stampfli et al., 2013; Wilhem et al., 2012; Zhao et al., 2018). Recent studies suggest that the CAOB mainly formed during two main cycles of collision–accretion: one is the Early Paleozoic evolution that largely involved shrinking of the Proto-Tethys Ocean (Metcalfe, 2021), associated with the North Indo-Australia subduction system in northeast Gondwana (Cawood et al., 2021); and the other is related to Late Paleozoic subduction of the Paleo-Asian Ocean, leading to the docking of Gondwana-derived microcontinents (e.g., Altay, Central Tienshan, and Tuva-Mongolia) toward southern Siberia as part of peri-Pangea (Khukhuudei et al., 2020; Wang et al., 2022; Wang et al., 2018a; Wilhem et al., 2012). The terminal orogeneses occurred in Permian to Triassic time when three southerly Gondwana-derived cratons, the Karakorum, Tarim and North China, successively collided from west to east against composite Siberia (present coordinates), along the South Tienshan and Solonker suture zones (Xiao et al., 2003, 2013). However, uncertainties remain regarding their peri-Gondwana paleographic positions and the timing of their separation from northeastern Gondwana, resulting in various geodynamic scenarios and different models on the time and style of subduction and accretion to Siberia. (Buslov et al., 2001; Domeier, 2018; Li et al., 2019; Merdith et al., 2021).

The southern Beishan orogen and the Dunhuang Terrane both consist of an E-W trending collage of accreted terranes, occupying a significant position bridging the Southern Tianshan Suture to the west and the Solonker Suture to the east (Fig 4- 1B). They are spatially associated with both the Early Paleozoic closure of the Proto-Tethys Ocean and the Late Paleozoic closure of the Paleo-Asian Ocean (Fig 4- 1A; Zhao et al., 2018; Metcalfe et al., 2021). Our study area (Fig 4- 1C) forms part of the southernmost Beishan orogen, situated immediately north of the Dunhuang Terrane, providing an ideal location to study the final episodes of terrane accretion and terminal collision in the CAOB and investigate its role in the history of supercontinent cycles. This study combines detailed regional field-based studies in the southern Beishan orogen, with stratigraphic, geochemical, and geochronological analyses of associated rocks in the Baidunzi area to test current tectonic models of the southern Beishan orogen and the Paleozoic tectonic evolution of the southern CAOB in general. We discovered an exotic tectonic constituent – the Baidunzi Complex, which comprises fragments of Precambrian basement and the Carboniferous to Permian meta-sedimentary strata that are largely reworked by the Permian syn-transpressional arc magmatism. The geological relationships of the Baidunzi Complex with the adjacent constituents reveal complex tectonic processes of arc development and arc–arc collision in the Permian.

4.3 Regional geological context

4.3.1 Dunhuang Terrane

The southernmost CAOB is bounded by the Dunhuang Terrane (Fig 4- 1B). The Dunhuang Terrane was previously referred to as the Dunhuang block due to ample exposure of Precambrian basement rocks (Zhao et al., 2016). These include Archean (3.3–3.0 Ga and 2.7–2.5 Ga) grey gneisses and Paleoproterozoic (2.0–1.6 Ga) high-grade metamorphosed basement rocks (He et al., 2013; Zhao et al., 2015). Recent studies of the Dunhuang Terrane (Zhao et al., 2016; Soldner, 2022) considered it

an extension of the southern CAOB due to similar Paleozoic crustal evolutionary histories, compared to terranes elsewhere along the suture zones (e.g., the Central-South Tienshan terranes and southern Beishan terranes). The crystalline basement remained thermo-tectonically stable from the Mesoproterozoic until the Cambrian crustal growth event due to mantle upwelling (520–445 Ma; Soldner et al., 2022), followed by subduction-related tectonism that included two major periods of arc magmatism at ca. 440–400 Ma and ca. 370–360 Ma, and a collisional or post-collisional thermal-tectonic event at ca. 335–315 Ma (Zhao et al., 2016, 2017). The late Permian to middle Triassic granitoid rocks located in the southern Dunhuang Terrane were interpreted to be either arc-related (ca. 284–275 Ma) and/or formed during post-collision processes (ca. 255–238 Ma) (Feng et al., 2020).

4.3.2 Terranes in southern Beishan Orogen

The Huaniushan-Dundunshan and Shibanshan terranes represent the southmost terranes of the Beishan orogen. They are separated by the Liuyuan Complex and directly bounded by the northern border of the Dunhuang Terrane along strike (Fig 4- 1C). The Huaniushan-Dundunshan terrane in the north is a tectonite belt predominantly comprising amphibolite- to granulite- facies metamorphic rocks and is interpreted as a composite arc terrane. The three major arcs reported are the Late Ordovician to Silurian rocks of Huaniushan continental arcs, the Early Devonian Gongpoquan Island arc (Wang et al., 2018b) and the Late Devonian Dundunshan arc (Guo et al., 2017). Large Silurian to Devonian meta granitoid plutons are characterized by arc-like geochemical signatures (Guo et al., 2014; Tian et al., 2014a, 2020; Saktura et al., 2017; Soldner et al., 2020). Cover sequences predominantly comprise terrestrial to shallow marine Carboniferous to Triassic meta-sedimentary rocks (Guo et al., 2012; Tian et al., 2014b, 2021).

The Liuyuan Complex in the center of the field area was previously interpreted by some workers as an ophiolitic fragment representing a suture zone between terranes to the south and north

(Xiao et al., 2010; Guo et al., 2012; Zheng et al., 2020). Recognition of a nearly complete oceanic crustal section with basal troctolite cumulates, vari-textured gabbro affected by intense sub-seafloor hydrothermal circulation and a laterally continuous sheeted dyke complex capped by pillow basalt lava by Santos et al. (2022, 2023) confirmed it represents an ophiolite. The geochemical signatures of the lava reveal a diminishing supra-subduction zone (SSZ) signature up-section in an oceanic back-arc basin setting (Santos et al., 2023). One trondhjemite forming a magmatic breccia at the base of the sheeted dyke of the Liuyuan Complex yielded a 238U/206Pb age of 290.4 ± 1.4 Ma, and the magmatism remained active at least until 286.3 ± 1 Ma (Santos et al., 2023).

The Shibanshan terrane is located south of the Liuyuan Complex (Fig 4- 1C) and predominantly comprises Precambrian orthogneiss and Paleozoic intrusive rocks and sedimentary strata. The inherited and detrital zircon ages of these rocks display populations with age peaks at ca. 1400, 890, 420 and 290 Ma (Yuan et al., 2015; He et al., 2018a; Zheng et al., 2018). Lower Paleozoic strata have not been identified in this terrane (BGMRG, 1997). The investigated intrusive rocks and associated volcano-sedimentary strata are mostly Carboniferous to Permian (Niu et al., 2018). Their nature and linkages with the surrounding tectonic constituents are poorly understood. The area discussed in this paper is mainly located in the central part of the Shibanshan terrane, directly bounded by the Liuyuan Complex to the north, and contains at least two distinct arc complexes with overlapping temporal evolutionary histories: the Ganquan Complex and the Baidunzi Complex.

The fast-spreading back-arc setting of the Artinskian (ca. 290 to 286 Ma) Liuyuan Complex is spatially linked with the adjacent, coeval arc rocks of the Ganquan Complex (Santos et al., 2023; Hong et al., 2023). The Ganquan Complex mainly comprises felsic volcanic and volcaniclastic rocks, which can be divided into a lower and upper sequence separated by an unconformity. Volcanic rocks of both sequences have arc-like compositions, zircons with mantle-like δ18O values and radiogenic

εHf values resembling those of the Liuyuan Complex (Hong et al., 2023), compatible with an island arc-like setting, which is temporally and tectonically linked with the adjacent back-arc ophiolitic rocks in the Liuyuan Complex. Detailed mapping of the Carboniferous-Permian strata (van Staal et al., 2021), revealed that the rocks are strongly deformed into an imbricate stack juxtaposing panels with tectono-stratigraphic sequences of similar ages, but with different lithological compositions and associations. Some of the imbricate panels share analogous tectonic characteristics as revealed by trace element tectonic discriminant analysis yet are strikingly different in their lithological make-up and tectonic evolutions. A prominent example is the Baidunzi Complex, which was previously either grouped together with Ganquan Complex into the Permian Shibanshan arc that collided with the Dunhuang Terrane (Guo et al., 2012; Mao et al., 2012); or interpreted to form part of the Huaniushan-Dundunshan arc complexes with continuous arc magmatism from Devonian to Permian (Zheng et al., 2021; Cleven et al., 2018). However, our investigation has revealed distinct continental features for the Baidunzi Complex, setting it apart from the Ganquan Complex with island arc characteristics. At its southern border, the Baidunzi Complex is delimited by a significant shear zone, separating it from the Shiyaozi Complex (Fig 4- 2), which is a poorly studied tectono-stratigraphic package known for distinct tectono-thermal events that occurred at approximately 336-326 Ma, 273-269 Ma, and 261 Ma (van Staal et al., 2021; Worthington, 2022). These findings shed new light on the complexities and intricate geological history of the study area, providing valuable insights into the tectonic history and evolution of the region.

4.4 Results of lithology, field relations, and geochronology

Detailed mapping combined with petrographic and geochronological studies assisted by U-Pb zircon geochronology (Laser Ablation Inductively Coupled Plasma Mass Spectrometry and Sensitive High-Resolution Ion Microprobe–LAICPMS and SHRIMP), help to delineate rock units and group

assemblages below. A tectono-stratigraphic framework for the metasedimentary and meta-plutonic units of the Baidunzi Complex is well established. Detailed geochronology analytical procedures and data repository of samples are reported in the supplementary materials.

The Baidunzi Complex comprises intensely deformed metasedimentary rocks interleaved with a large volume of syn-tectonic mafic to felsic plutonic sheets, now resembling a large, banded, and foliated sill complex, namely the Baidunzi Intrusive Suite (Fig 4- 2). The Baidunzi Intrusive Suite is separated by screens of polyphase deformed metasedimentary rocks (Fig 4- 3A), locally outlining large isoclinal folds, parallel to the foliation in the adjacent igneous sheets, which also display gneissic layering. The few observed shear sense indicators (Fig 4- 3B-C) are associated with a moderately plunging stretching lineation and indicate sinistral oblique convergence during emplacement of the plutonic rocks. Several shear zones dissect the complex. This style of deformation and associated greenschist to amphibolite facies metamorphism is absent in the adjacent tectono-stratigraphic packages (e.g., the Ganquan and Liuyuan complexes). The deformed rocks of the Baidunzi Complex were intruded and cut by gabbro and leuco-granodiorite of a Late Intrusive Suite, which themselves are locally also deformed and foliated due to a younger phase of deformation (D3, see Chapter 2, Fig 4- 3D-F). The relationships between the various metasedimentary units in the Baidunzi Complex are poorly understood due to the overall high strain, intense transposition, and the presence of voluminous interleaved plutonic sheets. Hence primary depositional relationships between the sedimentary units generally cannot be determined, except possibly where different units are closely interlayered.

4.4.1 Old basement rock units

The potentially oldest known metasedimentary rocks in the Baidunzi Complex form a unit of massive bedded white orthoquartzite and minor interbedded chlorite-muscovite schist, which is solely

exposed near the tectonic contact with the adjacent Ganquan Complex but separated by mylonite and phyllonite, or sheets of plutonic rocks, from adjacent metasedimentary units. Primary sedimentary layering is locally well preserved on outcrop scale. The orthoquartzite is dominated by granoblastic quartz (Fig 4- 4A-B). Detrital zircon analyses of the orthoquartzite rock sample reveal age peaks at ca. 1.41, 1.24 and 1.09 Ga, and yield a maximum depositional limit of 1068 ± 10 Ma (sample H18, Table SM1, Fig 4- 5A).

The orthoquartzite is spatially associated and locally structurally juxtaposed with small slivers of a monomict conglomerate unit, which comprises pebble to cobble-sized rounded clasts of predominantly quartz-rich felsic volcanic- and sub-volcanic intrusive rocks. They lack lithic quartzite fragments, but instead predominantly contain volcanogenic clasts (Fig 4- 4C), with dominant age peaks at ca. 906 Ma and 440 Ma sampled from matrix, yielding a maximum Middle Devonian depositional age of 417 ± 6 Ma (Fig 4- 5B and 6A).

4.4.2 Younger meta-sedimentary strata

The primary relationships between the other metasedimentary units and the conglomerate and quartzite units are unknown because they are structurally juxtaposed. The plutonic rocks of the Baidunzi Intrusive Suite commonly segregate the various units of sedimentary rocks into narrow isolated lenses or lenticular xenoliths or screens enveloped and cut by sills and dykes (Fig 4- 3 and 4).

The metasedimentary rocks are divided into several spatially closely associated units, referred to as packages 1, 2 and 3 (Fig 4- 2). Package 1 comprises interlayered epiclastic psammite and arkose, and dark, biotite-rich schist, all containing abundant plagioclase phenoclasts suggestive of a volcanogenic origin. This is also supported by their characteristic unimodal detrital zircon age distribution (Fig 4- 6A). The detrital zircon from an epiclastic schist (V1052) and a volcanogenic conglomerate sample (V161) from this package yield concordant U–Pb data within a relatively

narrow age window between the Late Carboniferous to Early Permian, with single peak ages at ca. 304 Ma and ca. 297 Ma, respectively. The two samples combined yield a maximum depositional age of 300 ± 7 Ma (Table SM1, Fig 4- 6B).

Package 2 comprises bedded marble intricately interlayered with calcite and quartz-rich non-volcanogenic psammite (Fig 4- 4E). The analyzed calcareous psammite sample (V361) contains a small number of detrital zircons, and the majority that lie on concordia yielded ages with a similar Late Carboniferous to Early Permian range as the volcanogenic units of package 1, and a maximum depositional age at 295 ± 2 Ma (Table SM1, Fig 4- 6C). There are also a few older Paleozoic ages ranging from 460 to 330 Ma, but critically there are no Precambrian ages as found in the orthoquartzite unit.

Package 3 comprises the sedimentary units in the southernmost part of the Baidunzi Complex, immediately north of the contact with Shiyaozi Complex (Fig 4- 4F), which comprises another association of interlayered, highly tectonised marble, meta-psammite and phyllite to schist. A schist with late porphyroblasts of green clinoamphibole (S5041) yielded zircon dates ranging between 322 and 289 Ma with a peak at 308 Ma, overlapping in range with the marble-psammite of package 2 in the center of the Baidunzi Complex. It also has older ages between 483 to 385 Ma with a peak at 433 Ma, and one Precambrian age at 1194 Ma. Another analyzed epidote-rich schist (sample V1110) is spatially associated with marble and has two dominant zircon age peaks at ca. 896 Ma and 305 Ma. Their combined distinct Late Paleozoic age spectra yielded a Late Carboniferous maximum depositional age at 306 ± 1 Ma (Table SM1, Fig 4- 5C and 6D).

In summary, the detrital zircon age spectra of the three sedimentary packages are characterized by detrital zircon with Kasimovian to Asselian ages (306 to 295 Ma). Package 3 has the oldest maximum depositional age and the epiclastic rocks of package 1 are characterized by a single

prominent distribution due to late Carboniferous to early Permian, syn-volcanic sedimentation. This age probably reflects their time of deposition. Precambrian and Ordovician-Silurian detrital zircons preserved in packages 3 and 2 suggest that potential basement rocks with these ages were likely proximally exposed at the time of deposition and were distal from those in package 1.

4.4.3 Baidunzi Intrusive Suite

Sheared sheets of fine to coarse-grained hornblende quartz diorite, tonalite, granite, gabbro and leuco-granodiorite intruded syn-tectonically into the metasedimentary packages and the inferred basement rocks. Geochronological and geochemical results indicate that rock units of diorite, tonalite and granite form the older Baidunzi Intrusive Suite, with magmatism starting at ca. 294 Ma and continuing intermittently until ca. 289 Ma. The units of hornblende gabbro and leuco-granodiorite form the younger Late Intrusive Suite, emplaced at ca. 281 Ma or later.

The meta-plutonic rocks of Baidunzi Intrusive Suite are products of syn-tectonic magmatism, as they cut through structures in wall rocks and also exhibit deformation caused by the same structures (Fig 4- 3A). The protolith compositions of these rocks range from gabbro, hornblende diorite to tonalite, granodiorite and granite, with granite being the most abundant and widespread type. The following rock units are grouped on the basis of distinctive field lithologies and ordered based on crosscutting relationships, assisted by zircon U-Pb geochronology data analyzed by SHRIMP to determine their crystallization ages (see details in the Table SM2.1, 2.2, and Data Repository).

4.4.3.1 Orthogneiss

The orthogneiss is locally preserved as screens of wall rocks or as host rocks to the granitic sill-like bands of the Baidunzi Intrusive Suite and post-tectonic intrusions. It comprises two varieties separated on the basis of composition. The red to grey granodioritic orthogneiss unit comprises

quartz, plagioclase, K-feldspar, brown biotite, muscovite, and minor brown hornblende with a well-developed gneissic or schistose foliation, commonly with an augen texture (Fig 4- 7A-B, 7D). The grey to white tonalitic orthogneiss is rarer and contains green hornblende, plagioclase, biotite and zoisite in melanocratic layers with accessary titanite and hematite, and quartz and muscovite in leucocratic layers with relatively coarse grains particularly in pegmatitic patches (Fig 4- 7C). The above rock units are all strongly deformed and injected by syn-tectonic plutons and dykes of the Baidunzi Intrusive Suite, hence creating a stromatic gneissic appearance (Fig 4- 7D).

A mesocratic layer of the granodioritic gneiss, free of veins and intrusive structures, yielded a concordia crystallization age of 879.9 ± 7.5 Ma from a relatively small spread of 206Pb/238U ages (915 Ma to 840 Ma), with uniformly low Th/U ratios from 0.06 to 0.12 (sample S5143, Fig 8A). A red granite sample from injected dykes in the leucocratic layers of granodioritic orthogneiss (sample S5136, Fig 4- 8B), contains one zircon core also yielding a Tonian age of 840.6 ± 13.3 Ma. The remaining 11 zircon grains are characterized by lighter cores and darker rims which as yet show no distinguishable age difference, and the whole population of zircons gives a relatively coherent 206Pb/238U age group (306 Ma to 281.5 Ma), yielding an early Permian concordia age of 293.7 ± 3.9 Ma. The age dichotomy within the bimodal-age zircons is likely related to younger crystal growth on earlier crystallized cores.

Similar younger crystal growths have also been observed in a tonalitic orthogneiss (Sample V1109), except mostly as thin rims on inherited zircons of Ordovician instead of Tonian ages. Thirty-five analyses show two populations of zircon. The major population of oscillatory and sector zoned magmatic zircon (n=20) overlaps within error, yielding a weighted mean age of 456.2 ± 6 Ma, while the other population (n=15) gives younger late Paleozoic ages with a wider range from 395.3 ± 8.2 Ma to 287.4 ± 7.3 Ma (Fig 4- 8C, Table SM2.1). The younger data are generally from thin featureless

or zoned bright overgrowths and have relatively low concentrations in both U and Th, compared to the Ordovician population. Their Th/U ratios are variable and mostly are greater than 0.1, suggesting they likely represent magmatic rims (Williams and Claesson, 1987). A good example is spot 12.2, which has a 206Pb/238U age of 295.3 ± 5.6 Ma with magmatic-type Th/U ratio of 0.31 and shows oscillatory zonation. A subset of 6 overlapping data from this population yielded a concordia age of 297.9 ± 7.8 Ma (MSWD = 1.9), interpreted as the crystallization age of the tonalite. Thus, we suspect that the zircon inheritance is retained from a relatively homogeneous melt source of Ordovician age.

A titanite data set from the same tonalite orthogneiss shows a wide range of Th/U ratios (0.16-7.09) but gives a uniform U-Pb age of 291.4 ± 1.4 Ma (Sample V1109, MSWD = 1.5; Fig 4-8D, Table SM2.2), which is in reasonable agreement with the above younger generation of zircon. Because U/Pb signatures of magmatic titanite could survive an overprint during mid- to upper amphibolite facies conditions (Stearns et al., 2015 and Schwartz et al., 2016) and occurrence of older titanite inheritance in igneous rocks is relatively uncommon (Corfu, 1996), we suggest that all titanite are magmatic and the well constrained age population dates a single cooling event. The wide range of Th/U ratios (see Table SM2.2) is possibly due to titanite grains having crystallized late from small residual melt pockets with variable Th/U ratios during relatively slow cooling. This could also apply to the late zircon, which supports the hypothesis that an Ordovician source rock from deeper crust was partial melted and the produced melt together with entrapped pieces of the original rock was emplaced syn-kinematically during the late Carboniferous to early Permian period. A similar process might have occurred in the granodioritic orthogneiss unit, except that the melt source is likely attributed to a Tonian pluton instead. Notably, the Tonian melt source appears to be abundant and widely distributed within the Baidunzi Complex, evident from the pervasive presence of Tonian zircon inheritance observed in the plutons of the Baidunzi Intrusive Suite.

An alternative interpretation is that the younger Permian growths of zircon and titanite were a result of contact metamorphism associated with the 294–289 Ma syn-tectonic intrusions of the Baidunzi Intrusive Suite (see below) and the Tonian and Ordovician age populations would represent protolith ages of the two orthogneiss units. However, this interpretation is less favored due to the presence of magmatic zonation and the uniform titanite population (Fig 4- 8D). The presence of syn-tectonic granite and tonalite dykes cutting through but also parallel to the gneissose foliations, also is inconsistent with the contact metamorphic explanation.

4.4.3.2 Red granite unit

The most voluminous phase of the Baidunzi Complex is a red granite unit which forms sub-concordant tabular sills locally intruding in the host granitic augen orthogneiss discussed above (Fig 4- 7B), forming an injection gneiss complex. They are most common in the southern part of the study area. The rocks commonly contain both metamorphic white mica and biotite along the foliation plane, and igneous plagioclase and K-feldspar phenocrysts (up to 3mm) that are pseudomorphed by albite and microcline. Brown or green hornblende is rare or absent. Accessory garnet, zircon, titanite and apatite occur as inclusions or along grain boundaries. The gneiss
complex underwent high strain during and after crystallization, which attenuated and boudinaged the host orthogneiss (Fig 4- 7A). Some granitoid veins were rotated into near-parallelism where others are folded and may have gradational biotite-rich selvedges, possibly caused by reaction between the host and the injected veins. A K-feldspar megacrystic granite dyke sample from this unit yielded a U-Pb zircon crystallization age of 291.8 ± 5.3 Ma (sample S5137, Fig 4- 8E), within error consistent with the age of a more leucocratic granite layer mentioned above (293.7± 3.9 Ma, sample S5136, Fig 4- 8B).

4.4.3.3 Hornblende diorite unit

Hornblende diorite to gabbro occurs mainly in the northern part of the Baidunzi Complex. The hornblende diorite shows a banded gneissic foliation defined by lenticular leucocratic and melanocratic bands or layers (Fig 4- 7E). Rocks of this unit primarily comprise plagioclase and brownish-green hornblende with or without quartz. Melanocratic bodies typically contain interstitial amphibole and accumulated plagioclase, while leucocratic layers comprise plagioclase and recrystallized quartz and minor K-feldspar (Fig 4- 3D). Accessory apatite, zircon, and titanite occur as inclusions in the above minerals or along grain boundaries. Combined U-Pb zircon analyses from two hornblende gabbro and one diorite yielded a magmatic core of 288.9 ± 2.8 Ma with a metamorphic rim age of 281.3 ± 3.5 Ma (Sample V1385, V266, S5145; Fig 4- 8G-H) for the diorite unit. Significant lower U content is consistently detected in the metamorphic overgrowths compared to the internal magmatic-zoned cores, reflecting contrasting crystallizing environments. We interpret that the magmatic core ages record the magmatism and crystallization of the diorite unit, and the subsequent overgrowth may be related to a burial or contact metamorphism event. The Neoproterozoic ages (ca. 900 - 800 Ma) of relict ancient zircon cores may indicate entrained xenolithic fragments or inheritance from the melting source, similar to the source of granodioritic orthogneiss.

4.4.3.4 Tonalite unit

The hornblende diorite unit is spatially closely associated with or locally grades into a coeval tonalite unit (Fig 4- 7E and 7F). The tonalite predominantly comprises tabular plagioclase with sizes ranging from 1 to 5mm and a matrix of recrystallized quartz, biotite, white mica and clinozoisite or epidote, with compositions ranging from tonalite to leuco-diorite. Green clinoamphibole is locally present as well. The grey to white tonalite and dark diorite are locally highly strained and transformed

into layered gneissic rocks. They are locally intruded by leucocratic veins and dykes (Fig 4- 7F-G). A combined tonalite and a leuco-diorite of this unit yielded a magmatic core age of 289.5± 3.4 Ma. Similar low-U overgrowths as seen in the diorite unit are also present on zircon in the tonalite and yielded a metamorphic rim age of 280.4 ± 4.4 Ma (sample V1384, V1096, Figs. 8I-J). Both ages are in good agreement with what is measured in the hornblende diorite. The magmatic and metamorphic ages as well as the inherited core age distributions in the tonalite unit are indistinguishable from those of the hornblende diorite, which suggests these two associated igneous rock units are coeval.

4.4.3.5 Quartz-rich granitoid unit

White to pink quartz-rich granitoid bodies intruded the above granite, diorite and tonalite bodies. They commonly form red, pink, or white aplite to pegmatite with compositions varying from monzogranite to quartz-rich granite (Fig 4- 7F), and locally form discordant veins or have diffuse boundaries with respect to the other intrusive bodies. They locally contain xenoliths of diorite, tonalite and orthogneiss. The granite contains euhedral K-feldspars and plagioclase surrounded by an extensively recrystallized quartz matrix displaying microstructures typical of grain boundary migration. They are sometimes muscovite-bearing and locally contain garnet and monazite. The diffuse bodies and veins may represent pockets of late melt, emplaced during the final stages of deformation. A granite dyke sample from this unit yielded a crystallization age of 292 ± 3.2 Ma (sample S5146, Fig 4- 8F), which is indistinguishable from the associated units it intruded into (e.g., granite, diorite and tonalite units). Based on the interpretation that the obtained coeval crystallization ages do not represent entrained zircon xenocrysts from the wall rocks, this implies that crystallization of the various igneous units was synchronous within error. The high degree of recrystallization present in all units suggests that the deformation outlasted magmatism, indicative of rapid ascent

relative to the duration of the strain regime. Hence, the progressive non-coaxial deformation had started before or at ca. 294 Ma and continued intermittently until after ca. 289 Ma.

4.4.4 Late Intrusive Suite

Numerous hornblende gabbro sills are localized along the shear zone that separates the Baidunzi and Ganquan complexes (Figs. 2 and 4B). The gabbro stitches all rocks of the Baidunzi Complex and the contact with the volcano-sedimentary unit of the Ganquan Complex. The spatially associated feldspar-phyric diorite to gabbro sills in the adjacent Ganquan Complex are also included in this unit. The gabbroic rocks are typically heterogeneously deformed. Deformation is characteristically concentrated near shear zones, and the mafic intrusive bodies were generally strongly altered at amphibolite or greenschist-facies conditions. Most metagabbro samples contain green to greenish blue clino-amphibole, optically determined as hornblende, albite, epidote, chlorite, and magnetite. Relicts of clinopyroxene are rare. The radiometric dating of this unit by Hong et al. (2023) suggests the gabbro sills were emplaced at ca. 281 Ma, indicating that the Ganquan and Baidunzi complexes were assembled by 281 Ma. Notably, the U-Pb age results of the metamorphic zircon rims/overgrowths observed in the diorite and tonalite of the Baidunzi Intrusive Suite are coeval with the emplacement date of the gabbro, suggesting the two events are genetically related.

Another late intrusive unit is represented by white leuco-granodiorite bodies with compositions ranging from granite to tonalite, locally trondhjemitic, which intrude all the above igneous units, including the hornblende gabbro, and generally form subparallel intrusive sills. They commonly have sharp and straight boundaries and are hard to separate in the field from the older leucocratic bodies of the granitoid unit of Baidunzi Intrusive Suite (Fig 4- 3F, 4F, 7G-J). The leuco-granodiorite bodies typically comprise very coarse blocky feldspar phenocrysts (up to 2cm), dynamically recrystallized quartz, muscovite, biotite, and rare garnet. Analyzed zircon of leucogranite

and leuco-tonalite bodies of this unit does not give coherent ages (see V385 and V1097 in Table SM2) displaying a wide spread of inherited U-Pb zircon ages ranging from 1556 to 294 Ma. The youngest zircon from the two samples does not postdate the above Baidunzi Intrusive Suite and gabbro, inconsistent with the intrusive relationships, and is interpreted as inheritance.

4.5 Geochemistry

4.5.1 Major and trace element compositions

Thirty-seven fresh samples were analyzed for major, trace and rare earth elements (REEs) to investigate the origin and nature of various units that make up the Baidunzi Intrusive Suite and its associated rock units. These data are combined with other existing data (Hong et al., 2023) and presented in variation diagrams for major oxides and trace elements in Fig 4- 9 and 11, and as chondrite normalized REE patterns in Fig 4- 10. Methods employed for the analyses are described in the Data Repository, and the complete data set is presented in Table SM3.

4.5.1.1 Tonalitic and granitic orthogneiss

Two samples collected from each type of orthogneiss interpreted to predate emplacement of the bulk of the Baidunzi Intrusive Suite, have dissimilar characteristics. The tonalitic orthogneiss rocks have SiO2 contents of 63-64 wt.% and represent distinctive outliers compared to most trends of the Baidunzi Intrusive Suite rocks in rock classification and discriminant plots (Fig 4- 9A-F). They display a smooth chondrite-normalized REE patterns (Fig 4- 10A), with enriched Light Rare Earth Element (LREE: La-Sm) and relatively flat heavy REE (HREE; Ho-Lu). The granitic orthogneiss is more enriched in SiO2 (72.5-73.3 wt.%) and has similar concentrations of major and trace elements as the felsic plutons of the Baidunzi Intrusive Suite (Fig 4- 9A-E), especially with rocks of the quartz-rich granitoid unit. However, their chondrite-normalized REE profiles (Fig 4- 10A) are moderately steeper and more depleted in HREE than those of the felsic plutons in Baidunzi Intrusive Suite. The

sample displays greater depletion in HREEs than middle or lower crust averages (Rudnick & Gao, 2003), suggesting derivation from a source depleted in HREEs, or removal of HREEs from garnet fractionation.

4.5.1.2 Baidunzi Intrusive Suite

Samples of the Baidunzi Intrusive Suite (n = 26) include mafic to intermediate samples having SiO2 contents between 47 and 61 wt.% (n = 10) and felsic samples with SiO2 contents from 67 to 78 wt.% (n = 17). Samples of diorite and associated tonalite are mainly grouped into the mafic to intermediate assemblage, except three porphyritic tonalite dykes with high SiO2 contents, which are grouped with the granite and quartz-rich granitoid into a felsic assemblage. The Baidunzi Intrusive Suite rocks are mainly metaluminous to slightly peraluminous, with ASI (aluminum saturation index) varying from 1.1 to 1.4. The contents of Al2O3, FeOT+MgO+TiO2 and CaO generally decrease with increasing SiO2, whereas K2O, Rb, Ba, Th and La remain nearly constant within mafic to intermediate rocks. No systematic patterns have been observed in the rocks of the high SiO2 range.

The mafic diorite and tonalite rocks exhibit a wide range of REE abundances and smooth chondrite normalized REE patterns (Fig 4- 10C) that generally are slightly convex for the enriched LREE, with LaN/LuN of 3-5 and slightly negative to moderately positive Eu anomalies (EuN/EuN* = 0.8-1.4). Except for one leucodiorite sample (V1384) of the tonalite unit that displays greater enrichment in LREEs with LaN/LuN of 9, NMORB-normalized multi-element diagrams of these mafic rocks closely resemble the arc reference patterns (Fig 4- S5). Most samples display similar concentrations of HREEs, and their profile patterns exhibit negative P anomalies, invariably large negative Nb-Ta, and moderate negative Ti anomalies, closely resembling those of oceanic to

continental arcs. The variable Zr-Hf anomalies are possibly controlled by variable behaviors of accessory zircon in the source.

In contrast, felsic samples show variable chondrite-normalized REE patterns. The red granite unit rocks (Fig 4- 10B) display generally parallel chondrite normalized REE profiles with enriched-LREE, flat-HREE concave-up shape (LaN/SmN: 2.3-3.4; DyN/YbN: 1.2-1.7), and negative Eu anomalies (EuN/EuN* = 0.4-0.6, with one exception S5143 of 1.1). Felsic rocks of the tonalite unit (Fig 4- 10D) show a relatively narrow range of REE concentrations and only positive Eu anomalies (EuN/EuN* = 1.9-2.4), suggestive of plagioclase accumulation. The quartz-rich granitoid unit exhibits the most variable chondrite-normalized REE patterns (Fig 4- 10E), which appear concave-up with steep enriched LREEs, and variable depletions in HREEs. Their Eu anomalies (EuN/EuN*) vary from negative (0.2-0.6) to positive (1.1-4.1), and the positive ones show concave HREEs with depletion of Dy to Yb.

4.5.1.3 Late Intrusive Suite

Rocks from the stitching hornblende gabbro to diorite unit show SiO2 content of 42-57 wt%. They are mainly tholeiitic and less commonly plot in the transitional to calc-alkaline field, with MgO/FeOt varying from 0.2 to 0.8. CaO and TiO2+MgO+FeOt are generally negatively correlated with increasing SiO2 (Fig 4- 9A, 9E-F, 11D-E). Major and trace elements generally show no clear trends. All samples show a parallel and moderately wide range of REE concentrations (Fig 4- S5). The chondrite-normalized REE patters are straight to concave upward, with slight enrichment of LREEs and slightly negative to no Eu anomalies, which resemble patterns of E-MORB and enriched MORB-like back arc basin basalt; while the MORB-normalized multi-element diagram reveals large negative Nb-Ta anomalies, whose profiles closely resemble patterns of intra-oceanic arcs yet are overall more enriched in LILEs, likely due to crustal contamination (Hong et al., 2023).

The leuco-granodiorite unit (n = 10) has a limited range of silica contents (74.4-77.4 wt.%). The contents of major and trace elements mostly overlap with felsic rocks of the Baidunzi Intrusive Suite, with the exception of the relatively lower concentrations of P2O5, Zr, Sr, Ba, Th and La (Fig 4-9 and 11). The leuco-granodiorites (Fig 4- 10F) have variable flat to concave-up normalized REE patterns (LaN/LuN of 1.2-4.2) with a depletion maximum at MREE (Sm-Tb). All except one show typical moderate to large negative Eu anomalies (EuN/EuN* = 0.2-0.99; exception = 1.4) that are unrelated to SiO2 content.

4.5.2 Geochemical classification and tectonic discrimination

The rocks of the Baidunzi Intrusive Suite are in general magnesian, calc-alkalic to calcic, metaluminous to weakly peraluminous, and comparable to the Cordilleran granitoids in the classification of Frost et al. (2001). In general, the Baidunzi Intrusive Suite rocks do not show a trend of Fe-Ti enrichment with increase of silica. On the Th/Yb vs. Zr/Y plot (Fig 4- 9E) of Ross and Bedard (2009), rocks of granodioritic to granitic composition mostly display calc-alkaline characteristics, while the mafic compositions vary from tholeiitic to calc-alkaline. The development of ‘transitional’ and ‘tholeiitic’ signatures in certain mafic samples most likely results from fractionation of titanite.

Both the Baidunzi Intrusive Suite granitoid rocks and leuco-granodiorite rocks of the Late Intrusive Suite have high LILE/HFS elemental ratios and Nb/Th values <7 (Table SM3). Both datasets display arc tectonic affinities on the trace elemental ratio discrimination plots of Whalen and Hildebrand (2019, Fig 4- 11C) and are generally characterized by lower concentrations of Nb+Y and Ta+Yb compared to A-type compositions, and smaller ratios of Nb/Y, La/Yb, Gd/Yb and Sm/Yb compared to ‘slab failure-like’ compositions. Except for two samples of quartz-rich granitoid unit (S5146 and H3531), and granitic orthogneiss samples (H3564 and H3535), the rocks exhibit

relatively elevated ‘slab failure-like’ features based on La/Yb, Gd/Yb and Sm/Yb, but not on Sr/Y, which is relatively low. On the discrimination diagrams for granitic rocks (Peace et al., 1984; Fig 4-11B), datasets of orthogneiss units, Baidunzi Intrusive Suite granitoids and leuco-granodiorite unit all fall within the volcanic arc granitoid field, with a few straddling boundaries to syn-collisional granite and within-plate granite fields. Tectonic discrimination diagrams (Pearce et al., 1983; Cabanis and Leocolle, 1989; Fig 4- 11D-E) for mafic to intermediate rocks of Baidunzi Intrusive Suite also exhibit arc-like tectonic affinities.

4.5.3 Zircon Hf isotopes

Zircon Hf isotopic data were obtained by laser ablation using ICPMS directly on top of the SHRIMP U-Pb analyses. Analytical results are summarized and reported in Supplementary Table SM4. The results are presented by rock unit and characterize the intra- and inter-sample variations of Hf ratios in the zircons, including core-rim relationships from individual samples.

Results of εHf(t) values for the co-genetic Baidunzi Intrusive Suite magmatic zircons of each sample from red granite, diorite and tonalite units are plotted in a box-violin diagram (Fig 4-12A) for comparison purposes. The red granite magmatic zircons (S5136) show a bimodal distribution with two ranges of εHf(t) values from +6.7 to +9.5 and from -0.7 to +1.8, yielding Ediacaran and Tonian Lu-Hf depleted mantle model ages, respectively. The inherited zircon that crystallized at ca. 841 Ma has a εHf(t) value of +5.3. A majority of the magmatic zircons from the diorite unit (V266 and S5145) have comparatively radiogenic εHf(t) values ranging from +1.8 to +4.7 to +4.5 to +7.5, respectively. Sample V266 displays a wider spread due to two distinct outlying values of -2.2 and +7.1, whereas its inherited zircon dated at ca. 443 Ma gives a less radiogenic εHf(t) value of -6.0. Two samples of the tonalite unit (V1384 and V1096) yielded distinctive εHf(t) spreads from -5.7 to -0.5 and +2.3 to +5.2 (excluding an outlier at +11.7), respectively. The non-radiogenic sample V1384

has inherited cores with ages varying from ca. 855 to 388 Ma and εHf(t) values ranging from +6 to -14.5. Notably, magmatic zircons from samples with evidence for inheritance commonly yield a wider range of εHf(t) values. Even if their non-inherited magmatic zircons crystallized co-genetically, a significant portion could still retain less radiogenic or non-radiogenic εHf(t) values, producing a bimodal pattern of εHf(t) straddling the lower limit of the arc mantle array. This compositional variance is likely caused by incomplete magma mixing (Griffin et al., 2002; Shaw and Flood, 2009) or source heterogeneity (Spencer et al., 2019). Additionally, no distinguishable difference was observed in individual samples of the diorite and tonalite unit between zircon εHf(t) values of the metamorphic overgrowths and those of the magmatic cores.

Zircons from granitic orthogneiss samples 18LYS5143 are characterized by a wide range of non-radiogenic εHf(t) values from –21 to –4.3 and yielded Archean to Paleoproterozoic Hf depleted mantle model ages (Fig 4- 12B). However, the Ordovician inherited zircons from the tonalitic orthogneiss unit yielded the most radiogenic εHf(t) values, which display a narrow range from +7.2 to +9.4 and yielded Neoproterozoic Hf depleted mantle model ages. Lu-Hf data could not be obtained from their thin Carboniferous-Permian magmatic overgrowths. Precambrian inherited zircons of the leuco-granodiorite sample of the Late Intrusion Suite (V385) yielded mainly radiogenic εHf(t) values of +2.7 to +13.8 (with one exception of -7.1), whereas its Late Paleozoic inherited zircons yielded variable εHf(t) values ranging from -4.4 to +1.1.

In summary, the new Hf and U-Pb zircon ages for the Baidunzi Complex rocks reported here represent three pulses of magmatism. (1) The analyzed zircons of Tonian age define two distinct populations. The non-radiogenic population, with a wide range of negative εHf(t) values, is predominantly from the granite orthogneiss sample, suggesting a crustal-derived source. The other radiogenic population of Tonian age contains inherited zircons from the granitoid rocks of the

Baidunzi Intrusive Suite and Late Intrusive Suite, indicating a relatively depleted source. (2) The Ordovician inherited zircon ages of the tonalite orthogneiss unit exhibit a restricted range of strongly depleted εHf(t) values, suggesting derivation from a uniform juvenile Ordovician melt source. (3) The Late Carboniferous to Early Permian Baidunzi Intrusive Suite and Late Intrusion Suite rocks display overall radiogenic characteristics with a large spread of εHf(t) values. The non-radiogenic εHf(t) values are restricted to certain isotopically distinct samples (e.g., V1384) or samples with anatexis characteristics (e.g., S5136, H3345). These features suggest that both the Baidunzi Intrusive Suite and Late Intrusion Suite were derived from more than one isotopically distinct source, possibly due to partial melting of mantle-derived mafic underplate with a crustal contribution.

4.6 Discussion

4.6.1 Evolution and tectonic nature of the Baidunzi basement rocks

Several workers reported the presence of Precambrian basement fragments in the Beishan Orogen and Central Asia Orogenic Belt (e.g., Kröner et al., 2007, 2014; Rojas-Agramonte et al., 2014). However, this interpretation is mainly based on the juvenile isotopic signatures of inherited Precambrian zircons extracted from Paleozoic rocks (He et al., 2018). The nature of the Precambrian basement is thus poorly known and difficult to correlate between different segments of the orogen. The orthoquartzite and associated argillaceous beds may represent the first known exposures of Precambrian strata in our mapping area, although its relationships to other metasedimentary rocks in the Baidunzi Complex are obscure. The quartzite has a mature composition with over 95% quartz yet produced no detrital zircon age younger than 1.0 Ga and does not record evidence for more recent tectono-thermal events, occurring in the Tonian (ca. 950-800 Ma), Ordovician-Silurian (ca. 460 - 430 Ma) and Carboniferous-Permian (ca. 320 – 280 Ma), which are generally preserved in other rocks of the Baidunzi Complex. Neither do they contain zircon representative of distinct magmatic events that

affected surrounding tectonic terranes, such as Tonian magmatism documented in the Tarim craton to the southwest (Wen et al., 2018) and Ordovician-Devonian arc magmatism in Huaniushan-Dundunshan terrane to the north and the Dunhuang Terrane to the south (Guo et al., 2014; Saktura et al., 2017; Soldner et al., 2020; Zhao et al., 2016, 2019). In addition, there is no evidence for an unconformable depositional relationship with the structurally overlying metasedimentary rocks of the Baidunzi Complex. Hence, we infer that the quartzite was probably deposited during the early Tonian and remained buried until after 290 Ma. It may have formed part of the basement to the Baidunzi Intrusive Suite, but this is unclear based on a lack of unambiguous intrusive field relationships.

A similar ambiguous relationship applies to the volcanogenic monomict conglomerate unit. Its detrital zircon age spectra mainly define Tonian and Ordovician-Silurian tectono-magmatic events that peaked around 990 Ma and 450 Ma but do not contain Carboniferous to Permian ages, typical of the associated metasedimentary units of packages 1-3 (see above). On the basis of its volcanogenic nature, the conglomerate was probably deposited syn-volcanically in the Devonian. If both the quartzite and monomict conglomerate indeed prove to represent basement to the Baidunzi Complex, they were likely not exposed until the Permian. Alternatively, considering their position along the tectonic boundary of Baidunzi and Ganquan complexes, these rocks could alternatively represent exotic tectonic sliver(s) of unknown provenance assembled with the other rocks after 289 Ma but before 281 Ma.

Other Precambrian basement rocks may include the ca. 880 Ma source of granite orthogneiss, which was subjected to extensive reworking by the Permian Baidunzi Intrusive Suite. The orthogneiss preserves evidence of multiple crustal sources that formed between 916 and 843 Ma, producing a wide range of crust-derived εHf(t) values from -21.0 to -4.3 that are characteristic of old continental realms. This is also supported by its steeper and highly depleted chondrite normalized HREE profiles

that are also suggestive of a deep crustal source. The Tonian ages of the preserved gneiss enclaves in the Baidunzi Intrusive Suite are typical of the orogenic rocks of the Tarim craton (ca. 900-720 Ma) that formed through amalgamation of the North and South Tarim blocks during the final assembly of Rodinia from 900 to 720 Ma (Wen et al., 2018). An association with the Dunhuang block is negated due to a lack of Mesoproterozoic tectono-magmatic events in this block (Zhao et al., 2016). Hence, the tectonic models of Zheng et al. (2020 and 2021) suggesting that the Shibanshan continental arc terrane developed on the northern margin of the Dunhuang block by south-directed subduction is not supported by our data. Instead, we prefer a Tarim provenance based on the new data.

Rocks with Cambrian to Devonian ages are rare in the investigated area yet late Ordovician to Devonian ages are common in detrital zircon spectra and zircon inheritance. They are particularly present in the discontinuous monomict conglomerate unit and the inherited zircons of the tonalitic orthogneiss. The former has a poorly constrained depositional age between ca. 390 and 294 Ma and may have been deposited syn-volcanically (see above) around 390 Ma. The latter was likely derived from the melting of a juvenile mafic underplate during the Permian. The source of this underplate could have been separated from the mantle around 456 Ma and is characterized by a narrow range of depleted εHf(t) values between +7.2 and 9.4. However, the tonalitic orthogneiss is a discontinuous unit, sparsely distributed and in general very rarely recognized in outcrop. Considering the rare occurrences of Ordovician rocks and the extensive plutonic bodies of the Permian Baidunzi Intrusive Suite in the Shibanshan terrane, which are largely distinguished from the extensive Late Ordovician to Devonian arc magmatism recorded in the Huaniushan-Dundunshan terrane, the Baidunzi Complex (or the Shibanshan terrane) was likely allochthonous to the Huaniushan-Dundunshan terrane, at least from the Late Ordovician to Devonian. Hence, correlation with the Ordovician to Silurian Huaniushan-Dundunshan strata on regional geological maps is inappropriate (Tian & Xiao, 2020;

Cleven et al., 2018). Nevertheless, the Late Ordovician to Early Devonian inherited- and detrital zircons in the Baidunzi Complex permit a possible relationship with the Huaniushan-Dundunshan terrane during the Carboniferous to Permian.

4.6.2 Late Carboniferous to Early Permian geology of Baidunzi Complex

Deposition of the metasedimentary packages that are interleaved with the Baidunzi Intrusive Suite, is constrained to a short time interval between the youngest detrital zircon age peaks at 295 Ma and 307 Ma (Fig 4- 6) and the 293.7 ± 3.9 Ma age of the oldest known intrusive rock. Hence, the maximum depositional age of 295 Ma of packages 1 and 2 also constrains the onset of syn-tectonic magmatism, which must postdate deposition of the sedimentary rocks. The carbonate rocks of this package were previously correlated with the older, Serpukhovian to Moscovian limestone beds of the Shibanshan Formation (Niu et al., 2021), which were interpreted based in part on the presence of Fusulinella-Fusulina as part of a carbonate ramp associated with high-energy turbidite flows, but subsequently transitioned to a tidal channel environment with abundant influx of bioclasts, debris of reef materials as well as limestone breccia. The detrital zircon spectrum suggests the marble and associated calcareous sandstone were deposited either shortly before or during the onset of arc magmatism. The absence of any volcanic detritus in the psammite, typical for the sedimentary rocks of package 1 argues against the latter interpretation. More likely, the sedimentary rocks of packages 2 and 3 represent the remnants of a short-lived continental margin of Asselian age, which possibly formed in a magmatic lull between the various stages in the evolution of a continental arc(s).

The arc-like calc-alkaline geochemistry of the Baidunzi Intrusive Suite and its close association with the epiclastic metasedimentary rocks of package 1 suggest a continental arc-like setting during the Early Permian. Both the trace elements characteristics and REE/multi-element patterns closely resemble those of other documented continental arcs (Hollocher et al., 2012).

However, the period of active magmatism recorded in the Baidunzi Intrusive Suite (ca. 294 to 289 Ma) is relatively short for a continental arc. Slightly older volcanic rocks of late Carboniferous to early Permian ages may possibly exist as an earlier phase of the same arc based on the youngest detrital zircon age spectra of the epiclastic metasedimentary rocks of package 1, although these igneous rocks have not been detected yet in the studied area.

The short phase (294–289 Ma) of arc-like plutonism in the Baidunzi area took place during shortening as evidenced by isoclinal folds in the metasedimentary rocks (Fig 4- 3). The linearity of the intrusive sheets with large aspect ratios (width to thickness), shallow plunging stretching lineations, and shear sense indicators suggests that emplacement of the intrusions was localized in a wide transpressive shear zone with sinistral kinematics. The intrusive sheets resemble the large, elongate sills found in parts of the Andes and North American Cordillera, which were generated by continuously rising arc magmas and mixed with crustal melts above subduction zones in relatively high-standing regions that represent increased crustal thickness during compression (e.g., Bateman 1992, Ducea, 2002; Ducea et al., 2015). The paradox of voluminous granitoid emplacement in an overall compressional magmatic arc has been explained by the suggestion of pluton emplacement in tension cracks and dilatational jogs within arc-parallel, strike-slip fault systems (e.g., Klepeis et al., 2022); or alternatively en-echelon P-shear arrays which may provide batholith-scale zones of dilation along the trend of active magmatism during transpressional tectonics (Tikoff 1992).

4.6.3 Regional geological model and tectonic implications

The geology of Baidunzi Complex reveals a distinct evolutionary history, which lacks extensive igneous rocks of Ordovician to Devonian ages compared to the surrounding tectonic blocks (e.g., Dunhuang and Huaniushan-Dundunshan terranes). It is also dissimilar to the adjacent juvenile Ganquan arc complex and associated oceanic Liuyuan back-arc system, despite the fact that they

overlap in age. The intermediate to felsic volcanic rocks of the extensional Ganquan arc complex (295-281 Ma) were linked to the associated 290-286 Ma oceanic Liuyuan back-arc basin, above a northward-dipping subduction zone (present coordinates) with backarc opening being due to slab rollback (Fig 4- 13A, 14; Hong et al., 2022, 2023; Santos et al., 2022). The structurally juxtaposed Baidunzi Complex contains arc magmatic rocks that overlap with the older arc phases in the Ganquan Complex between 294 and 289 Ma but is characterized by distinctive continental-derived clastic strata that are absent in the Ganquan Complex. It represents a compressional rather than an extensional arc regime such as preserved in the Ganquan Complex (Hong et al., 2022). Hence, the two different arc complexes either formed above a coeval doubly vergent subduction system with both north- and south-dipping subduction zone or they formed in distal locations above the same northward subduction zone, which changed from extension to compression along strike (Fig 4- 13 vs. Fig 4- 14).

The former model provides a simple solution to explain the two coeval arc systems between 294 and 281 Ma. In such a scenario, the compressional, short-lived Baidunzi continental arc formed above a southward-dipping subduction zone, whereas the longer-lived extensional oceanic Ganquan arc and associated Liuyuan backarc system were built above a retreating northward-dipping subduction zone. Regardless of which of the two models is correct, arc magmatism in the Ganquan Complex terminated around 281 Ma, which either coincided with or was shortly preceded by accretion of the Baidunzi Complex along its southern boundary. The time of accretion is constrained by: (1) ca. 281 Ma hornblende gabbro sills in the Ganquan Complex (Hong et al., 2023), which are spatially localized along the shear zone that separates the two arc complexes, and locally also intrude rocks (orthoquartzite unit) inferred to form part of the Baidunzi Complex; and (2) regional metamorphism in the Baidunzi Complex, evident from the metamorphic zircon rim ages analyzed in

the diorite and tonalite units of the Baidunzi Intrusive Suite, occurring simultaneously at 281-280 Ma. In addition, accretion probably led to an early phase of under-thrusting of the Baidunzi Complex beneath the Ganquan and Liuyuan Complexes because the latter rocks contain a prominent early phase of south-direct tectonic transport (van Staal et al., 2021; Hong et al. 2023), which is consistent with the postulated tectonic burial of Baidunzi Complex during accretion (Fig 4- 13C).

At first glance, the first model seems the simplest solution to explain the two coeval arc systems during 294 to 281 Ma. However, it requires (1) that subduction was initiated more or less coevally on both sides of the oceanic basin that separated the two arc complexes, which requires a causal mechanism; and (2) it needs a tectonic mechanism capable of explaining why the Baidunzi continental arc shut off at ca. 289 Ma, 8 to 9 m.y. before its accretion with the Ganquan Complex, while volcanism in the latter and the Liuyuan backarc remained ongoing. Potential processes that could explain cessation of continental arc magmatism in the Baidunzi Complex prior to its accretion include (1) significant shallowing of the south-dipping subducting slab; (2) arrival of a buoyant oceanic plateau or a microcontinent; or (3) ridge subduction. Evidence for a collider such as a microcontinental sliver or ridge is meagre or lacking. The only potential candidate is the orthoquartzite unit, which lies structurally beneath the remainder of the Baidunzi Complex and whose contacts with all other Baidunzi Complex rocks are consistently tectonic. The exposed areal extent of this unit, however, is small, which makes the inferred accretion of this potentially exotic unit an unattractive candidate to have caused cessation of Baidunzi arc magmatism. Ridge subduction is another possibility but is expected to have created a slab-window beneath the Baidunzi Complex, for which no evidence is preserved in the magmatic rocks of the Baidunzi Intrusive Suite. Instead, the radiogenic Hf isotope ratios of the felsic to intermediate members of the Baidunzi Intrusive Suite suggest a dominant input of arc mantle derived juvenile rather than contaminated components.

The evidence supporting an along strike origin of the Baidunzi Complex, where its arc rocks formed above the same north-dipping subduction zone as the Ganquan Complex, is neither strong nor convincing and demands an explanation why arc magmatism ceased significantly earlier in the Baidunzi Complex. There is ample evidence for sinistral convergence during formation of the Baidunzi Intrusive Suite (e.g., Fig 4- 3B-C) consistent with translation of the Baidunzi Complex from a position further west. However, the sinistral movements necessary to explain juxtaposition of a compressional continental arc segment with an extensional oceanic arc segment of the same convergence system between 294 and 281 Ma must have been substantial, but little field evidence is present or preserved other than the linearity and banded nature of the voluminous southern foliated granite belt. Hence, it is conceivable that syn-tectonic intrusion largely obscured and/or destroyed most of the evidence, such as extensive mylonites, for a major ductile shear zone(s) that accommodated such movements. Sinistral ductile shearing must have finished before 281 Ma, which is the age of the gabbro suite that stitches large parts of the boundary between Baidunzi and Ganquan complexes (see map and Fig 4- 13C). The stitching relationship is only valid if the orthoquartzite unit formed part of the Baidunzi Complex prior to its amalgamation with the Ganquan complex. The structural boundary between the Baidunzi and Ganquan complexes is now marked by a young north-directed, ductile to brittle reverse fault zone, which locally also deforms the gabbro into narrow mylonite zones (van Staal et al., 2021).

Regardless of which of the two tectonic scenarios is correct, several lines of evidence suggest that the initial structural juxtaposition of Ganquan and Baidunzi Complexes between 289 and 281 Ma was mainly accommodated by sinistral-oblique, south-directed tectonic transport. Older Ganquan Complex volcanic rocks in the north were emplaced over younger volcanic rocks of the southern Ganquan Complex, consistent with north-dipping subduction, and upper greenschist to amphibolite

facies metamorphism of the Baidunzi Complex, characterized by hornblende, biotite, albite and rare garnet. This phase of metamorphism was dated by metamorphic zircon rims at ca. 281 Ma, which suggests these rocks were probably subjected to enhanced tectonic burial compared to the Ganquan Complex, which is characterized by lower greenschist facies conditions characterized by white mica, chlorite, and rare biotite. This structural assembly was responsible for termination of arc magmatism at ca. 281 Ma in the Ganquan Complex, suggesting that the ocean immediately faced to its south had closed.

4.6.4 Proterozoic to Paleozoic paleogeographic constraints

Zircon Hf isotope ratios exhibit a strong genetic link with magmatic source, revealing past isotopic fractionation events and potential reworking of pre-existing crust or incorporating new addition from the depleted mantle. Theoretically, variations or evolutionary patterns in the Hf isotopic systematics of detrital and igneous rock-hosted zircons can serve as a powerful tool to trace magmatic source characteristics of orogenic system, spanning both spatial and temporal dimensions (Spencer et al., 2019; Gardiner et al., 2016; Collins et al., 2011). Through synthesis of previously published data, we present a comparison of zircon Hf isotopic signatures hosted within igneous rocks from the spatially neighboring tectonic components adjacent to the Baidunzi Complex, to establish genetic linkages and elucidate potential paleogeographic attributes.

Recent paleogeographic models of Central Asia suggest that the Tarim and North China cratons together with their peri-cratonic fragments (e.g., the Alxa, Altyn, Dunhuang, Central Tienshan blocks) formed parts of the northeastern destructive margin of Gondwana in the Cambrian to Early Ordovician (e.g., Metcalfe, 2021; Zhao et al., 2018; Li et al., 2018). The North China and Tarim cratons both predominantly comprise Archean TTG basement rocks that formed at 2.8-2.7 Ga and 2.6-2.45 Ga (Lu et al., 2008a; Zhao and Zhai, 2013; Diwu et al., 2011; Xu et al., 2013). The Greater

Tarim mainly formed during the 900-720 Ma interval as part of the final assembly of Rodinia, suturing the northern and southern continental blocks together (Wen et al., 2017, 2018). The Grenvillian aged crystalline basement associated with the Rodinia assembly event is largely preserved within Tarim Craton and its peri-cratonic fragments and neighboring terranes (e.g., the Central-South Tienshan, the Altyn terranes and certain microcontinents in Beishan – Wang et al., 2021; He et al., 2018b).

The Neoproterozoic (ca. 970–800 Ma) continental arc system in the southern CAOB and Central-South Tienshan is interpreted to have been situated on the periphery of Rodinia, as part of a late-formed exterior orogen (Zong et al., 2017). Notably, these ages are absent in the basement rocks of the North China Craton and the Dunhuang Terrane, consistent with the Paleoproterozoic geographic model of Evans et al. (2016), which also emphasized that the North China Craton was isolated and distal from Rodinia. The Baidunzi microcontinent, as previously discussed, is characterized by a Neoproterozoic crustal evolutionary history distinct from the Dunhuang Terrane. However, it closely resembles the northern Tarim Craton and the Central-South Tienshan Terrane, which have ca. 1000–800 Ma crystalline ages and display a wide range of non-radiogenic to weakly radiogenic εHf(t) signatures. The range is also constrained between the Hf evolutionary lines of ca. 2.4 and 1.4 Ga (Fig 4- 12 and 15).

Radiogenic εHf(t) signatures, reflecting a major input of juvenile materials during the Late Cambrian to Ordovician, are characteristic of the southern Tarim Craton, the Central-South Tienshan and Dunhuang Terrane, yet are rarely observed in the northern Tarim Craton. At the southern Tarim margin, studies found that the Rodinia-forming-related Tonian basement rocks (ca. 950–750 Ma) spatially overlap with the Gondwana-related orogenic belts (ca. 550-450 Ma), which were correlated with Neoproterozoic to Ordovician strata in northern India (Wang et al., 2022), suggesting a closely

related position along the periphery of northeastern Gondwana (Fig 4- 16). The southern Tarim block, together with its peri-cratonic terranes, is characterized by radiogenic Hf signatures in the Early Cambrian, followed by the wide range of εHf(t) values in younger rocks reflecting a mixture of evolved and juvenile magmatism from the Middle to Late Ordovician to Early Silurian (Fig 4- 15). We suggest that the Cambrian juvenile input was related to the subduction and Late Cambrian collision that closed the Proto-Tethys Ocean between the southern margin of the Tarim Craton and northern India during the assembly of Gondwana. The subsequent separation of southern Tarim Craton from northern India ca. 50 Ma later initiated the opening of the Paleo-Tethys Ocean, followed by increasing crustal reworking and growth that is recorded in the southern Tarim and Kunlun terranes.

Notably, juvenile εHf(t) signatures are observed in the Central-South Tienshan, Dunhuang and the Huaniushan-Dundunshan terranes, but not in the northern Tarim block. On the basis of their spatial relationships, we suggest that during the breakup of Gondwana, the southern Siberian composite acted as a tectonic active margin with accretions of peripheral microcontinents and arcs, which are now largely preserved in the Kygyz, Central-South Tienshan and Dunhuang Terranes. In contrast, the northern margin of the Tarim was not actively involved in this tectonic activity. It may have been a passive margin on the other side of the Paleo-Asian Ocean. The juvenile εHf(t) signatures, which become increasingly more radiogenic from the Late Ordovician to Silurian in the Central-South Tienshan and Dunhuang Terranes, could also suggest significant breakup and rifting processes, related to the opening of backarc basins and the expansion of the Paleo-Asian Ocean, which occurred simultaneously with its north-directed subduction.

Another major episode of juvenile magmatism is evident from the Carboniferous to Early Permian, as shown by the increase of radiogenic Hf values in the southern CAOB (Central-South

Tienshan terranes and most of the southern Beishan Orogen) and the southern Tarim block. The terranes in the southern CAOB exhibit slightly offset juvenile magmatic peaks, indicating successive arc accretions, and closing of the Paleo-Asian Ocean along the respective suture zones (Cleven et al., 2018). The deposition of the Baidunzi sedimentary strata during the Late Carboniferous to Early Permian (packages 1-3) suggests that the terranes accreted in the Late Ordovician to Silurian (ca. 460-430 Ma; e.g., the Dundunshan-Huaniushan terrane or equivalents) were proximal to the Shibanshan terrane. However, the Shibanshan terrane was not affected by active magmatism during the Early to Middle Paleozoic but predominantly formed during the Late Carboniferous to Permian. We infer that the Shibanshan terrane, particularly the Baidunzi microcontinent, was closely associated with the northern margin of the Tarim Craton and had limited involvement in the Ordovician-Silurian tectonic event.

Additionally, the Huaniushan-Dundunshan terrane lacks a Grenvillian tectonic evolutionary history, except in the Gongpoquan area where it is spatially associated with the Liuyuan Complex. This suggests that the two terranes may have been exotic to each other before the Permian amalgamation. Similarly, unlike the Baidunzi microcontinent and the surrounding tectonic elements, the Dunhuang block was exotic to the Tarim Craton from the Mesoproterozoic until the formation of CAOB. The Late Permian formation of the southern CAOB involved the amalgamation of multiple unrelated terranes, and their strike-slip movements may have been largely underestimated.

4.7 Conclusion

To summarize, we propose alternative tectonic models for the Baidunzi continental arc and the Liuyuan backarc-Ganquan arc. We believe they were constructed either through a concurrent doubly convergent subduction system or by the same north-vergent subduction system and structurally juxtaposed by sinistral convergence. Both of these models deviate from current

perspectives, which suggest that the Shibanshan terrane, encompassing the Baidunzi and Ganquan Complexes, represents a Carboniferous to Permian composite continental arc terrane or may be an extension of the Dunhuang Terrane. The Baidunzi Complex is inferred to represent an individual microcontinent with basement rocks sharing a similar Tonian history with peri-cratonic fragments of the Tarim Craton but lacking any affinity with the Dunhuang Terrane. In comparison to the surrounding tectonic constituents (e.g., Huaniushan-Dundunshan and Dunhuang terranes), the Shibanshan terrane, particularly the Ganquan and Baidunzi Complexes, shows a paucity or lack of Cambrian to Devonian tectono-thermal events typical of these terranes and hence they likely were exotic to one another until the Late Carboniferous to Permian. Even though both the Ganquan and the Baidunzi complexes of the Shibanshan terrane share Early Permian arc magmatism that partially overlaps in age, they represent distinctive contrasting tectonic regimes. Hence these two tectonic arc complexes may be unrelated and exotic as well. The amalgamation of the two arc complexes, accomplished by sinistral oblique arc-arc accretion at 281-280 Ma, is constrained by the emplacement of the stitching gabbro unit and the time of tectonic burial metamorphism of the Baidunzi Intrusive Suite. According to our tectonic model, the closure of the Paleo-Asian Ocean took place in stages and mainly occurred during two main orogenic phases in the Ordovician to Silurian and the Carboniferous to Permian respectively. Significant oblique displacements may have assembled peripheral fragments derived from the Tarim craton situated further west. Regardless of what exactly happened tectonically, the evolutionary history of subduction and collision between the Beishan Orogen and Dunhuang Terrane appears exceptionally complex, and our evidence is incongruent with existing models.

4.8 References

Attia, S., Cottle, J. M., & Paterson, S. R. (2020). Erupted zircon record of continental crust formation during mantle driven arc flare-ups. Geology, 48(5), 446-451.

Bateman, P. C. (1992). Plutonism in the central part of the Sierra Nevada batholith, California (No. 1483). US Government Printing Office.

BGMRG, 1997. Stratigraphy (Lithostratic) of Gansu Province. China University of Geosciences Press, Wuhan, 314 pp. (in Chinese).

Bouvier, A., Vervoort, J. D., & Patchett, P. J. (2008). The Lu–Hf and Sm–Nd isotopic composition of CHUR: constraints from unequilibrated chondrites and implications for the bulk composition of terrestrial planets. Earth and Planetary Science Letters, 273(1-2), 48-57.

Buslov, M.M., Saphonova, I., Watanabe, T., Obut, O., Fujiwara, Y., Iwata, K., Semakov, N., Sugai, Y., Smirnova, L., and Kazansky, A., 2001, Evolution of the Paleo-Asian Ocean (Altai-Sayan region, Central Asia) and collision of possible Gondwana-derived terranes with the southern marginal part of the Siberian continent: Geosciences Journal , v. 5, no. 3, p. 203–224, https://doi.org/10.1007/BF02910304.

Cabanis, B., & Lecolle, M. (1989). The La/10-Y/15-Nb/8 diagram: A tool for distinguishing volcanic series and discovering crustal mixing and/or contamination: Comptes Rendus de l'Academie des Sciences, serie 2. Science de la Terre, 309, 20.

Cawood, P. A., Martin, E. L., Murphy, J. B., & Pisarevsky, S. A. (2021). Gondwana's interlinked peripheral orogens. Earth and Planetary Science Letters, 568, 117057. https://doi.org/10.1016/J.EPSL.2021.117057

Cleven, N. R., Lin, S., Xiao, W.J., Davis, D. W., & Davis, B. (2018). Successive arc accretion in the southern Central Asian orogenic belt, NW China: Evidence from two Paleozoic arcs with offset magmatic periods. Bulletin of the Geological Society of America, 130(3–4), 537–557. https://doi.org/10.1130/B31434.1

Collins, W. J., Belousova, E. A., Kemp, A. I., & Murphy, J. B. (2011). Two contrasting Phanerozoic orogenic systems revealed by hafnium isotope data. Nature Geoscience, 4(5), 333-337.

Corfu, F. (1996). Multistage zircon and titanite growth and inheritance in an Archean gneiss complex, Winnipeg River Subprovince, Ontario. Earth and Planetary Science Letters, 141(1-4), 175-186.

Dhuime, B., Hawkesworth, C. J., Cawood, P. A., & Storey, C. D. (2012). A change in the geodynamics of continental growth 3 billion years ago. Science, 335(6074), 1334-1336.

Dhuime, B., Hawkesworth, C., & Cawood, P. (2011). When continents formed. Science, 331(6014), 154-155.

Diwu, C., Sun, Y., Guo, A., Wang, H., & Liu, X. (2011). Crustal growth in the North China Craton at~ 2.5 Ga: Evidence from in situ zircon U–Pb ages, Hf isotopes and whole-rock geochemistry of the Dengfeng complex. Gondwana Research, 20(1), 149-170.

Domeier, M., 2018, Early Paleozoic tectonics of Asia: Towards a full-plate model: Geoscience Frontiers, v. 9, no. 3, p. 789–862, doi.org/10.1016/j.gsf.2017.11.012.

Ducea, M. N. (2002). Constraints on the bulk composition and root foundering rates of continental arcs: A California arc perspective. Journal of Geophysical Research: Solid Earth, 107(B11), ECV-15.

Ducea, M. N., Saleeby, J. B., & Bergantz, G. (2015). The architecture, chemistry, and evolution of continental magmatic arcs. Annual Review of Earth and Planetary Sciences, 43, 299-331.

Evans, D.A.D., Li, Z.X., Murphy, J.B. (2016). Four-dimensional context of Earth's supercontinents. Geological Society, London, Special Publications Volume 424 p.1 – 14, doi.org/10.1144/SP424.12

Feng, L., Lin, S., Li, L., Davis, D. W., Song, C., Li, J., Ren, S., Han, X., Ge, Y., & Lu, K. (2020). Constraints on the tectonic evolution of the southern central Asian orogenic belt from early Permian–middle Triassic granitoids from the central Dunhuang orogenic belt, NW China. Journal of Asian Earth Sciences, 194, 104283. doi.org/10.1016/J.JSEAES.2020.104283

Frost, B. R., Barnes, C. G., Collins, W. J., Arculus, R. J., Ellis, D. J., & Frost, C. D. (2001). A geochemical classification for granitic rocks. Journal of petrology, 42(11), 2033-2048.

Frost, C. D., Frost, B. R., & Beard, J. S. (2016). On silica-rich granitoids and their eruptive equivalents. American Mineralogist, 101(6), 1268–1284. DOI: http://dx.doi.org/10.2138/am-2016-5307

Gardiner, N. J., Kirkland, C. L., & Van Kranendonk, M. J. (2016). The juvenile hafnium isotope signal as a record of supercontinent cycles. Scientific reports, 6(1), 38503.

Glorie et al., 2011. Tectonic history of the Kyrgyz South Tien Shan (Atbashi-Inylchek) suture zone: The role of inherited structures during deformation-propagation.

Griffin, W. L., Pearson, N. J., Belousova, E., Jackson, S. V., Van Achterbergh, E., O'Reilly, S. Y., & Shee, S. R. (2000). The Hf isotope composition of cratonic mantle: LAM-MC-ICPMS analysis of zircon megacrysts in kimberlites. Geochimica et cosmochimica acta, 64(1), 133-147.

Griffin, W.L., Wang, X., Jackson, S.E., Pearson, N.J., O'Reilly, S.Y., Xu, X., Zhou, X., 2002. Zircon chemistry and magma mixing, SE China: In-Situ analysis of Hf isotopes, Tonglu and Pingtan Igneous Complexes, 61. Lithos, pp. 237–269.

Guo, Q. Q., Chung, S. L., Xiao, W. J., Hou, Q. L., & Li, S. (2017). Petrogenesis and tectonic implications of Late Devonian arc volcanic rocks in southern Beishan orogen, NW China: Geochemical and Nd–Sr–Hf isotopic constraints. Lithos, 278, 84-96.

Guo, Q., Xiao, W.J., Hou, Q., Windley, B. F., Han, C., Tian, Z., & Song, D. (2014). Construction of late Devonian Dundunshan arc in the Beishan orogen and its implication for tectonics of southern Central Asian orogenic belt. Lithos, 184–187, 361–378. https://doi.org/10.1016/j.lithos.2013.11.007

Guo, Q., Xiao, W.J., Windley, B. F., Mao, Q., Han, C., Qu, J., Ao, S., Li, J., Song, D., & Yong, Y. (2012). Provenance and tectonic settings of Permian turbidites from the Beishan Mountains, NW China: Implications for the Late Paleozoic accretionary tectonics of the southern Altaids. Journal of Asian Earth Sciences, 49, 54–68. https://doi.org/10.1016/j.jseaes.2011.03.013

Han, Y., Zhao, G., Cawood, P. A., Sun, M., Eizenhöfer, P. R., Hou, W., Zhang, X., & Liu, Q. (2016). Tarim and North China cratons linked to northern Gondwana through switching accretionary tectonics and collisional orogenesis. Geology, 44(2), 95–98. https://doi.org/10.1130/G37399.1

He, Z. Y., Klemd, R., Yan, L. L., & Zhang, Z. M. (2018a). The origin and crustal evolution of microcontinents in the Beishan orogen of the southern Central Asian Orogenic Belt. Earth-Science Reviews, 185, 1–14. https://doi.org/10.1016/J.EARSCIREV.2018.05.012

He, Z. Y., Klemd, R., Yan, L. L., Lu, T. Y., & Zhang, Z. M. (2018b). Mesoproterozoic juvenile crust in microcontinents of the Central Asian Orogenic Belt: evidence from oxygen and hafnium isotopes in zircon. Scientific Reports, 8(1), 5054.

He, Z. Y., Zhang, Z. M., Zong, K. Q., & Dong, X. (2013). Paleoproterozoic crustal evolution of the Tarim Craton: constrained by zircon U–Pb and Hf isotopes of meta-igneous rocks from Korla and Dunhuang. Journal of Asian Earth Sciences, 78, 54-70.

Hollocher, K., Robinson, P., Walsh, E., & Roberts, D. (2012). Geochemistry of amphibolite-facies volcanics and gabbros of the Støren Nappe in extensions west and southwest of Trondheim, Western Gneiss Region, Norway: a key to correlations and paleotectonic settings. American Journal of Science, 312(4), 357-416.

Hong, T., Santos, G. S., van Staal, C. R., Ji, W., & Lin, S. (2022). Mapping uncovered a multi-phase arc—back-arc system in southern Beishan during the Permian. National Science Review. DOI: 10.1093/nsr/nwac204

Hong, T., van Staal, C., Lin, S., Santos, G.S., Wang, K. (2023). Evolving Permian magmatism associated with arc migration in the southern Beishan Orogenic Collage, Central Asian orogenic belt, NW China. Geological Society, London, Special Publications. DOI: 10.1144/SP542-2022-346

Iizuka, T., Komiya, T., Rino, S., Maruyama, S., & Hirata, T. (2010). Detrital zircon evidence for Hf isotopic evolution of granitoid crust and continental growth. Geochimica et Cosmochimica Acta, 74(8), 2450-2472.

Irvine, T. N., & Baragar, W. R. A. (1971). A guide to the chemical classification of the common volcanic rocks. Canadian journal of earth sciences, 8(5), 523-548.

Khain, E. v., Bibikova, E. v., Kröner, A., Zhuravlev, D. Z., Sklyarov, E. v., Fedotova, A. A., & Kravchenko-Berezhnoy, I. R. (2002). The most ancient ophiolite of the Central Asian fold belt: U-Pb and Pb-Pb zircon ages for the Dunzhugur Complex, Eastern Sayan, Siberia, and geodynamic implications. Earth and Planetary Science Letters, 199(3–4), 311–325. https://doi.org/10.1016/S0012-821X(02)00587-3

Khukhuudei, U., Kusky, T., Otgonbayar, O., & Wang, L. (2020). The Early Palaeozoic mega-thrusting of the Gondwana-derived Altay–Lake zone in western Mongolia: Implications for the development of the Central Asian Orogenic Belt and Paleo-Asian Ocean evolution. Geological Journal, 55(3), 2129–2149. https://doi.org/10.1002/GJ.3753

Klepeis, K. A., Schwartz, J. J., Miranda, E., Lindquist, P., Jongens, R., Turnbull, R., & Stowell, H. (2022). The initiation and growth of transpressional shear zones through continental arc lithosphere, southwest New Zealand. Tectonics, 41(9), e2021TC007097.

Kröner, A., Kovach, V., Belousova, E., Hegner, E., Armstrong, R., Dolgopolova, A., ... & Rytsk, E. (2014). Reassessment of continental growth during the accretionary history of the Central Asian Orogenic Belt. Gondwana Research, 25(1), 103-125.

Kroner, A., Windley, B. F., Badarch, G., Tomurtogoo, O., Hegner, E., Jahn, B. M., ... & Wingate, M. T. D. (2007). Accretionary growth and crust formation in the Central Asian Orogenic Belt and comparison with the Arabian-Nubian shield.

Kuzmichev, A. B., & Larionov, A. N. (2013). Neoproterozoic island arcs in East Sayan: Duration of magmatism (from U-Pb zircon dating of volcanic clastics). Russian Geology and Geophysics, 54(1), 34–43. https://doi.org/10.1016/j.rgg.2012.12.003

Li P.F., Sun M., Shu C.T., Yuan C., Jiang Y.D., Zhang L., Cai K. (2019). Evolution of the Central Asian Orogenic Belt along the Siberian margin from Neoproterozoic-Early Paleozoic accretion to Devonian trench retreat and a comparison with Phanerozoic eastern Australia. Earth-Science Reviews, doi.org/10.1016/j.earscirev.2019.102951

Li, S., Zhao, S., Liu, X., Cao, H., Yu, S., Li, X., ... & Suo, Y. (2018). Closure of the Proto-Tethys Ocean and Early Paleozoic amalgamation of microcontinental blocks in East Asia. Earth-Science Reviews, 186, 37-75.

Lu, S.N., Li, H.K., Zhang, C.L., Niu, G.H. (2008) Geological and geochronological evidence for the Precambrian evolution of the Tarim Craton and surrounding continental fragments Precambrian Res., 160, pp. 94-107

Mao, Q., Xiao, W.J., Windley, B. F., Han, C., Qu, J., Ao, S., Zhang, J., & Guo, Q. (2012). The Liuyuan complex in the Beishan, NW China: a Carboniferous–Permian ophiolitic fore-arc sliver in the southern Altaids. Geological Magazine, 149(3), 483–506. https://doi.org/10.1017/S0016756811000811

Merdith, A.S., Williams, S.E., Collins, A.S., Tetley, M.G., Mulder, J.A., Blades, M.L., Young, A., Armistead, S.E., Cannon, J., Zahirovic, S., and Müller, R.D., 2021, Extending full-plate tectonic models into deep time: Linking the Neoproterozoic and the Phanerozoic: Earth-Science Reviews, v. 214, doi.org/10.1016/j.earscirev.2020.103477.

Metcalfe, I. (2021). Multiple Tethyan ocean basins and orogenic belts in Asia. Gondwana Research, 100, 87–130. https://doi.org/10.1016/J.GR.2021.01.012

Niu, Y. Z., Shi, G. R., Ji, W. H., Zhou, J. L., Wang, J. Q., Wang, K., ... & Yang, B. (2021). Paleogeographic evolution of a Carboniferous–Permian sea in the southernmost part of the Central Asian Orogenic Belt, NW China: Evidence from microfacies, provenance and paleobiogeography. Earth-Science Reviews, 220, 103738.

Niu, Y., Lu, J., Liu, C., Xu, W., Shi, J., & Song, B. (2018). Geochronology and Distribution of the Upper Carbonifeous—Lower Permian Ganquan Formation in the Beishan Region, Northwestern China, and Its Tectonic Implication. Geological Review, 64(4), 806–827.

Pearce, J. (1996). Sources and settings of granitic rocks. Episodes, 19(4), 120–125. doi.org/10.18814/EPIIUGS/1996/V19I4/005

Pearce, J. A. (1983). Role of the sub-continental lithosphere in magma genesis at active continental margins.

Pearce, J. A., Harris, N. B., & Tindle, A. G. (1984). Trace element discrimination diagrams for the tectonic interpretation of granitic rocks. Journal of petrology, 25(4), 956-983.

Pearce, J. A., Stern, R. J., Bloomer, S. H., & Fryer, P. (2005). Geochemical mapping of the Mariana arc-basin system: Implications for the nature and distribution of subduction components. Geochemistry, Geophysics, Geosystems, 6(7). doi.org/10.1029/2004GC000895

Rojas-Agramonte, Y., Kröner, A., Alexeiev, D. V., Jeffreys, T., Khudoley, A. K., Wong, J., ... & Seltmann, R. (2014). Detrital and igneous zircon ages for supracrustal rocks of the Kyrgyz Tianshan and palaeogeographic implications. Gondwana Research, 26(3-4), 957-974.

Ross, P. S., & Bédard, J. H. (2009). Magmatic affinity of modern and ancient subalkaline volcanic rocks determined from trace-element discriminant diagrams. Canadian Journal of Earth Sciences, 46(11), 823-839.

Rudnick, R.L. and Gao, S. (2003). The composition of the continental crust. In: Treatise on Geochemistry - The Crust. Rudnick, R.L., Holland, H.D. and Turekian, K.K. (Editors), Elsevier, Oxford. 1-64.

Saktura, W. M., Buckman, S., Nutman, A. P., Belousova, E. A., Yan, Z., & Aitchison, J. C. (2017). Continental origin of the Gubaoquan eclogite and implications for evolution of the Beishan Orogen, Central Asian Orogenic Belt, NW China. Lithos, 294–295, 20–38. https://doi.org/10.1016/J.LITHOS.2017.10.004

Santos, G. S., Hong, T., van Staal, C. R., Bedard, J., Lin, S., & Wang, K. (2022). Permian back-arc basin formation and arc migration in the southern Central Asian Orogenic Belt, Northwest China. Geological Journal. DOI: 10.1002/gj.4609

Santos, G.S., (2022). Petrology, tectonic setting, and regional implications of the ophiolitic Liuyuan Complex, NW China. PhD thesis, University of Waterloo.

Santos, G.S., Bedard, J., van Staal, C., Lin S., Hong, T., and Wang, K. (2023). Geology of the Liuyuan Complex, NW China: a Permian back-arc basin ophiolite at the southern edge of the Central Asian Orogenic Belt. GSA bulletin. DOI: 10.1130/B36736.1

Schwartz, J. J., Stowell, H. H., Klepeis, K. A., Tulloch, A. J., Kylander-Clark, A. R., Hacker, B. R., & Coble, M. A. (2016). Thermochronology of extensional orogenic collapse in the deep crust of Zealandia. Geosphere, 12(3), 647-677.

Shaw, S. E., & Flood, R. H. (2009). Zircon Hf isotopic evidence for mixing of crustal and silicic mantle-derived magmas in a zoned granite pluton, eastern Australia. Journal of Petrology, 50(1), 147-168.

Soldner 2022: Two distinct Paleozoic metamorphic events in the Tarim-North China Collage. National Science Review, Volume 10, Issue 2, February 2023, nwac133, https://doi.org/10.1093/nsr/nwac133

Soldner, J., Štípská, P., Schulmann, K., Yuan, C., Anczkiewicz, R., Sala, D., Jiang, Y., Zhang, Y., & Wang, X. (2020). Coupling of P–T–t–D histories of eclogite and metagreywacke—Insights to late Ordovician–Silurian crustal folding events recorded in the Beishan Orogen (NW China). Journal of Metamorphic Geology, 38(6), 555–591. https://doi.org/10.1111/JMG.12531

Soldner, J., Yuan, C., Schulmann, K., Jiang, Y., Štípská, P., Zhang, Y., ... & Wang, X. (2022). Early Paleozoic Cascadia-type active-margin evolution of the Dunhuang block (NW China): Geochemical and geochronological constraints. Bulletin, 134(9-10), 2503-2530.

Spencer, C. J., Kirkland, C. L., Prave, A. R., Strachan, R. A., & Pease, V. (2019). Crustal reworking and orogenic styles inferred from zircon Hf isotopes: Proterozoic examples from the North Atlantic region. Geoscience Frontiers, 10(2), 417-424.

Stampfli, G. M., Hochard, C., Vérard, C., Wilhem, C., & vonRaumer, J. (2013). The formation of Pangea. Tectonophysics, 593, 1–19. https://doi.org/10.1016/J.TECTO.2013.02.037

Stearns, M.A., Hacker, B.R., Ratschbacher, L., Rutte, D., Kylander-Clark, A.R.C., 2015. Titanite petrochronology of the Pamir gneiss domes: implications for middle to deep crust exhumation and titanite closure to Pb and Zr diffusion. Tectonics 34 (4), 784–802.

Tang, M., Wang, X.-L., Shu, X.-J., Wang, D., Yang, T., Gopon, P., 2014. Hafnium isotopic heterogeneity in zircons from granitic rocks: geochemical evaluation and modeling of“zircon effect” in crustal anatexis. Earth Planet. Sci. Lett. 389, 188–199.

Tian, Z., & Xiao, W.J. (2020). An Andean-type arc transferred into a Japanese-type arc at final closure stage of the Palaeo-Asian Ocean in the southernmost of Altaïds. Geological Journal, 55(3), 2023–2043. https://doi.org/10.1002/GJ.3700

Tian, Z., Xiao, W.J., Sun, J., Windley, B. F., Glen, R., Han, C., Zhang, Z., Zhang, J., Wan, B., Ao, S., & Song, D. (2014b). Triassic deformation of Permian Early Triassic arc-related sediments in the Beishan (NW China): Last pulse of the accretionary orogenesis in the southernmost Altaids. Tectonophysics, 662, 363–384. https://doi.org/10.1016/J.TECTO.2015.01.009

Tian, Z., Xiao, W.J., Windley, B. F., Huang, P., Zhang, J., Ao, S., Zhang, Z., Song, D., & Liu, F. (2021). Two key switches in regional stress field during multi-stage deformation in the Carboniferous–Triassic southernmost Altaids (Beishan, NW China): Response to orocline-related roll-back processes. GSA Bulletin, 133(11–12), 2591–2611.

Tian, Z., Xiao, W.J., Windley, B. F., Lin, L., Han, C., Zhang, J., Wan, B., Ao, S., Song, D., & Feng, J. (2014a). Structure, age, and tectonic development of the Huoshishan-Niujuanzi ophiolitic mélange, Beishan, southernmost Altaids. Gondwana Research, 25(2), 820–841.

Tikoff, B., & Teyssier, C. (1992). Crustal-scale, en echelon" P-shear" tensional bridges: A possible solution to the batholithic room problem. Geology, 20(10), 927-930.

van S taal, C.R., Hong, T., L in, S., Ji, W .H, 2021. Bedrock Geological Map of the Baidunzi-Heishankou Area, Guazhou, Gansu, China, scale 1:25,000: China Geological Survey, DOI: 10.35080/data.C.2021.P01.

Wang, B., Yang, X., Li, S., Teng, C., Yang, X., Huang, F., ... & Li, J. (2021). Geochronology, geochemistry, and tectonic implications of early Neoproterozoic granitic rocks from the eastern Beishan Orogenic Belt, southern Central Asian Orogenic Belt. Precambrian Research, 352, 106016.

Wang, P., Zhao, G., Cawood, P. A., Han, Y., Yu, S., Liu, Q., Yao, J., & Zhang, D. (2022). South Tarim tied to north India on the periphery of Rodinia and Gondwana and implications for the evolution of two supercontinents. Geology, 50(2), 131–136. https://doi.org/10.1130/G49238.1

Wang, X. S., Klemd, R., Gao, J., Jiang, T., Li, J. L., & Xue, S. C. (2018a). Final Assembly of the Southwestern Central Asian Orogenic Belt as Constrained by the Evolution of the South Tianshan Orogen: Links With Gondwana and Pangea. Journal of Geophysical Research: Solid Earth, 123(9), 7361–7388. https://doi.org/10.1029/2018JB015689

Wang, X., Yuan, C., Zhang, Y., Long, X., Sun, M., Wang, L., Soldner, J., & Lin, Z. (2018b). S-type granite from the Gongpoquan arc in the Beishan Orogenic Collage, southern Altaids: Implications for the tectonic transition. Journal of Asian Earth Sciences, 153, 206–222. https://doi.org/10.1016/J.JSEAES.2017.07.037

Wen, B., Evans, D. A., & Li, Y. X. (2017). Neoproterozoic paleogeography of the Tarim Block: An extended or alternative “missing-link” model for Rodinia?. Earth and Planetary Science Letters, 458, 92-106.

Wen, B., Evans, D. A., Wang, C., Li, Y. X., & Jing, X. (2018). A positive test for the Greater Tarim Block at the heart of Rodinia: Mega-dextral suturing of supercontinent assembly. Geology, 46(8), 687-690.

Whalen, J. B., & Hildebrand, R. S. (2019). Trace element discrimination of arc, slab failure, and A-type granitic rocks. Lithos, 348, 105179.

Wilhem, C., Windley, B. F., & Stampfli, G. M. (2012). The Altaids of Central Asia: A tectonic and evolutionary innovative review. Earth-Science Reviews, 113(3–4), 303–341. https://doi.org/10.1016/J.EARSCIREV.2012.04.001

Williams, I.S., Claesson, S., 1987. Isotopic evidence for the Precambrian provenance and Caledonian1039 metamorphism of high grade paragneisses from the Seve Nappes, Scandinavian1040 Caledonides: II. Ion microprobe zircon U-Th-Pb: Contributions to Mineralogy and Petrology1041 97, 205-217

Winchester, J. A., & Floyd, P. A. (1977). Geochemical discrimination of different magma series and their differentiation products using immobile elements. Chemical Geology, 20(C), 325–343. https://doi.org/10.1016/0009-2541(77)90057-2

Wooden, J.L., Barth, A.P., and Mueller, P.A., 2013, Crustal growth and tectonic evolution of the Mojave crustal province: Insights from hafnium isotope systematics in zircons: Lithosphere , v. 5, p. 17–28, https://doi.org/10.1130/L218.1.

Xiao, W. J., Mao, Q. G., Windley, B. F., Han, C. M., Qu, J. F., Zhang, J. E., Ao, S. J., Guo, Q. Q., Cleven, N. R., Lin, S. F., Shan, Y. H., & Li, J. L. (2010). Paleozoic multiple accretionary and collisional processes of the Beishan orogenic collage. American Journal of Science, 310(10), 1553–1594. https://doi.org/10.2475/10.2010.12

Xiao, W. J., Windley, B. F., Yuan, C., Sun, M., Han, C. M., Lin, S. F., Chen, H. L., Yan, Q. R., Liu, D. Y., Qin, K. Z., Li, J. L., & Sun, S. (2009). Paleozoic multiple subduction-accretion processes of the southern Altaids. American Journal of Science, 309(3), 221–270. https://doi.org/10.2475/03.2009.02

Xiao, W.J., Windley, B. F., Allen, M. B., & Han, C. (2013). Paleozoic multiple accretionary and collisional tectonics of the Chinese Tianshan orogenic collage. Gondwana Research, 23(4), 1316–1341. https://doi.org/10.1016/j.gr.2012.01.012

Xiao, W.J., Windley, B. F., Hao, J., & Zhai, M. (2003). Accretion leading to collision and the Permian Solonker suture, Inner Mongolia, China: Termination of the central Asian orogenic belt. Tectonics, 22(6). https://doi.org/10.1029/2002tc001484

Xu et al., 2013. Tectonic framework and crustal evolution of the Precambrian basement of the Tarim Block in NW China: New geochronological evidence from deep drilling samples https://doi.org/10.1016/j.precamres.2013.06.001

Yu, Y., Zong, K., Yuan, Y. et al. Crustal Contamination of the Mantle-Derived Liuyuan Basalts: Implications for the Permian Evolution of the Southern Central Asian Orogenic Belt. J. Earth Sci. 33, 1081–1094 (2022). DOI: 10.1007/s12583-022-1706-1

Yuan, Y., Zong, K., He, Z., Klemd, R., Liu, Y., Hu, Z., ... & Zhang, Z. (2015). Geochemical and geochronological evidence for a former early Neoproterozoic microcontinent in the South Beishan Orogenic Belt, southernmost Central Asian Orogenic Belt. Precambrian Research, 266, 409-424.

Zhao G.C. and Zhai M.G. (2013) Lithotectonic elements of Precambrian basement in the North China Craton: review and tectonic implications Gondwana Res., 23, pp. 1207-1240

Zhao, G., Wang, Y., Huang, B., Dong, Y., Li, S., Zhang, G., & Yu, S. (2018). Geological reconstructions of the East Asian blocks: From the breakup of Rodinia to the assembly of Pangea. Earth-Science Reviews, 186, 262–286. https://doi.org/10.1016/J.EARSCIREV.2018.10.003

Zhao, Y., Sun, Y., Ao, W., Zhang, H., & Zhu, T. (2019). Depositional age, provenance and tectonic significance of Precambrian metasedimentary rocks from the Dunhuang Complex, NW China: Evidence from field investigation, zircon U–Pb geochronology and whole–rock geochemistry. Precambrian Research, 326, 272-294.

Zhao, Y., Sun, Y., Diwu, C., Guo, A. L., Ao, W. H., & Zhu, T. (2016). The Dunhuang block is a Paleozoic orogenic belt and part of the Central Asian Orogenic Belt (CAOB), NW China. Gondwana Research, 30, 207–223. https://doi.org/10.1016/J.GR.2015.08.012

Zhao, Y., Sun, Y., Diwu, C., Zhu, T., Ao, W., Zhang, H., & Yan, J. (2017). Paleozoic intrusive rocks from the Dunhuang tectonic belt, NW China: Constraints on the tectonic evolution of the southernmost Central Asian Orogenic Belt. Journal of Asian Earth Sciences, 138, 562–587. doi.org/10.1016/J.JSEAES.2017.02.037

Zhao, Y., Sun, Y., Yan, J., & Diwu, C. (2015). The Archean-Paleoproterozoic crustal evolution in the Dunhuang region, NW China: Constraints from zircon U–Pb geochronology and in situ Hf isotopes. Precambrian Research, 271, 83-97.

Zheng, R., Li, J., Xiao, W.J., & Zhang, J. (2018). Nature and provenance of the Beishan Complex, southernmost Central Asian Orogenic Belt. International Journal of Earth Sciences, 107(2), 729–755.

Zheng, R., Li, J., Zhang, J., & Xiao, W.J. (2021). A prolonged subduction-accretion in the southern Central Asian Orogenic Belt: Insights from anatomy and tectonic affinity for the Beishan complex. Gondwana Research, 95, 88–112. https://doi.org/10.1016/J.GR.2021.02.022

Zheng, R., Li, J., Zhang, J., Xiao, W.J., & Wang, Q. (2020). Permian oceanic slab subduction in the southmost of Central Asian Orogenic Belt: Evidence from adakite and high-Mg diorite in the southern Beishan. Lithos, 358–359, 105406. doi.org/10.1016/J.LITHOS.2020.105406

Zong K, Klemd R, Yuan Y, et al. (2017) The assembly of Rodinia: The correlation of early Neoproterozoic (ca. 900Ma) high-grade metamorphism and continental arc formation in the southern Beishan Orogen, southern Central Asian Orogenic Belt (CAOB). Precambrian research. 290:32-48. doi:10.1016/j.precamres.2016.12.010

4.9 Figures and captions

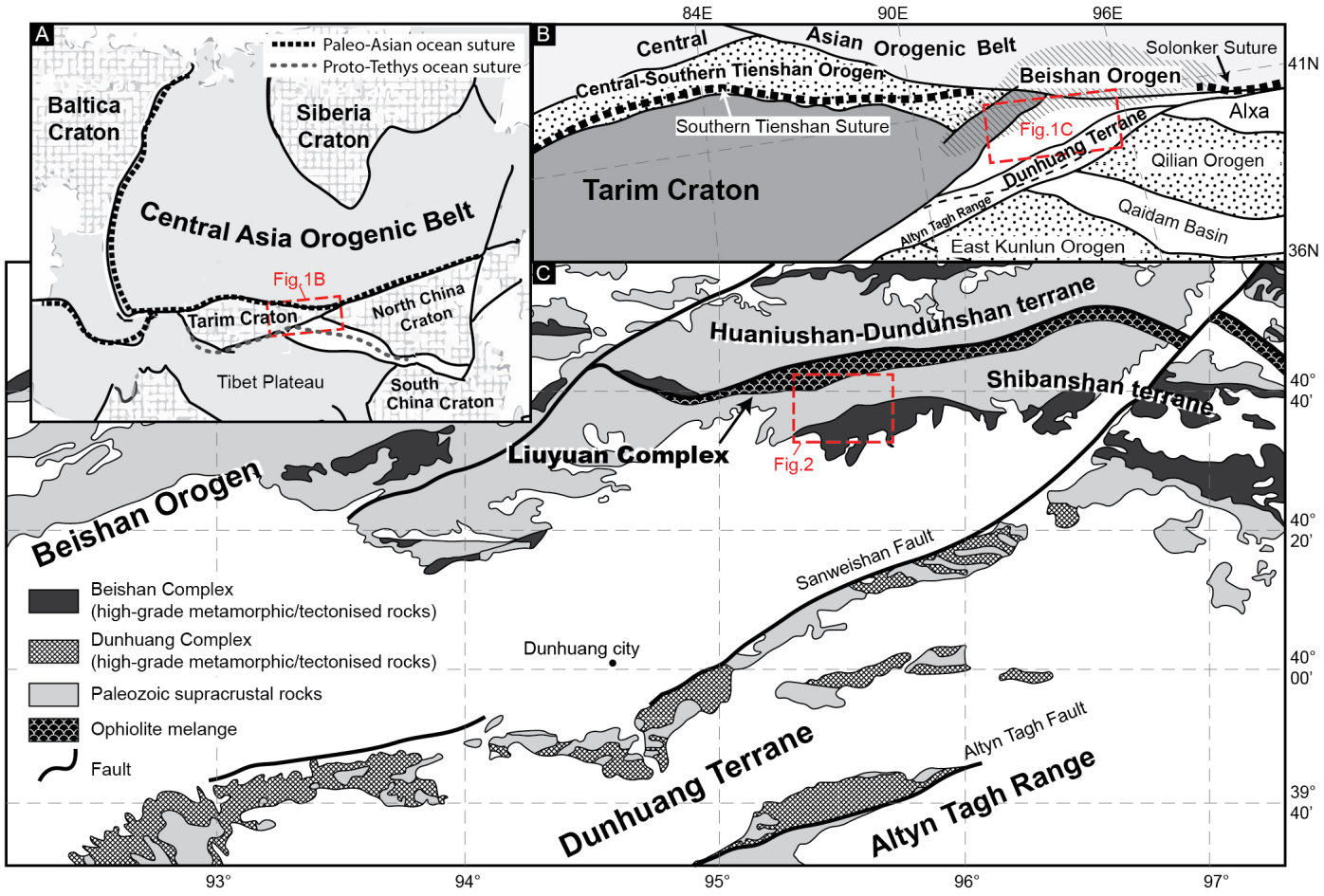


Figure 4-1: Tectonic context maps of Central Asia Orogenic Belt, Beishan Orogen and Liuyuan Complex. (A) Tectonic context of the Central Asia Orogenic Belt in Asia. (B) Sketch of tectonic context of the Beishan Orogen and its surrounding tectonic constituents: the Tarim Craton, Central-South Tienshan Orogen, Dunhuang Terrane, Alxa Block, Qilian Orogen, the Altyn Range, and the East Kunlun Orogen. (C) Tectonic context of the Liuyuan Complex between the Huaniushan-Dundunshan terrane and the Shibanshan terrane, as well as the southern Dunhuang Terrane. Modified from Mao et al. (2012).

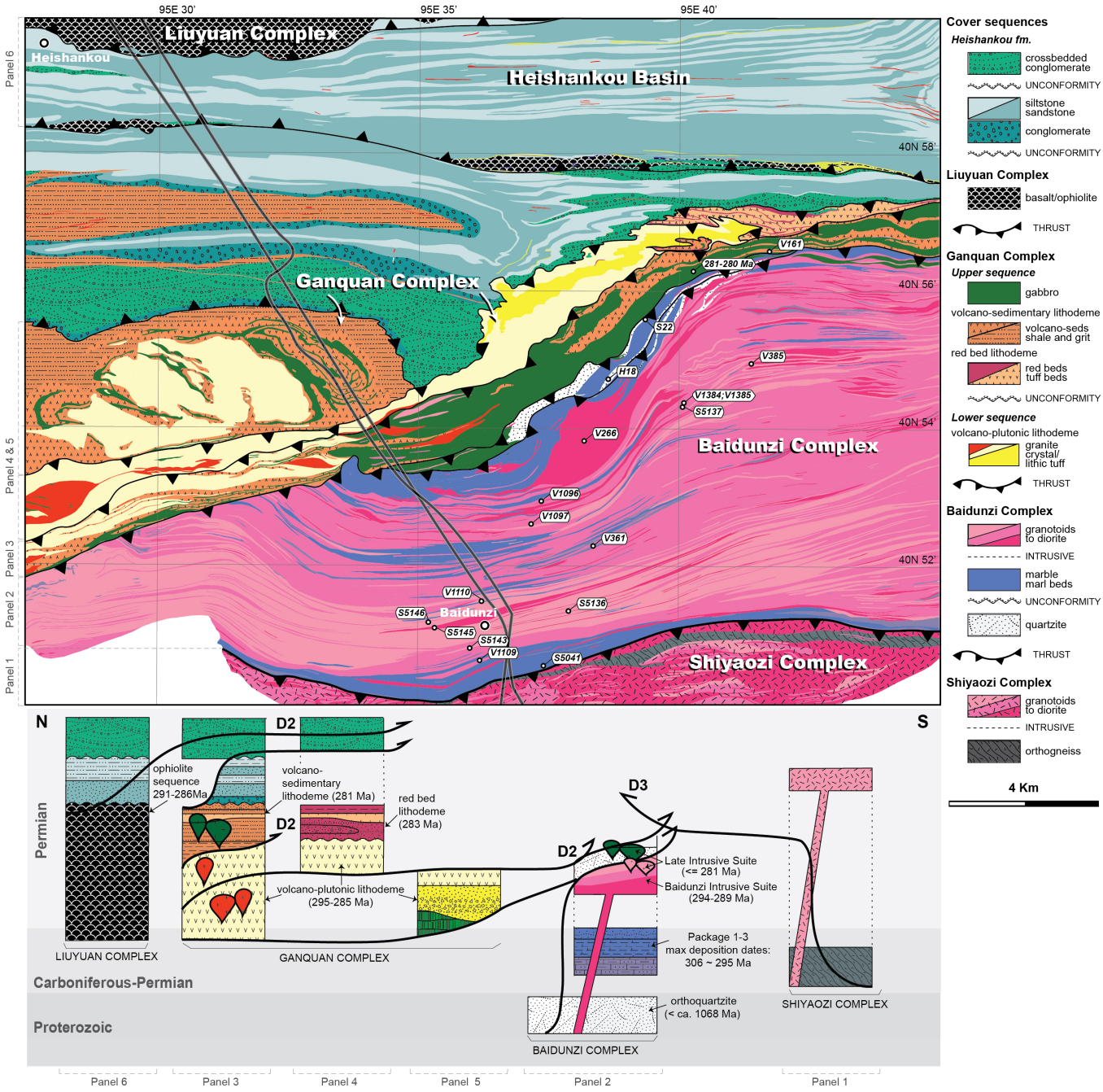


Figure 4-2: Geological map of Baidunzi Complex and surronding area.

Modified from van Staal et al. (2021) and Hong et al. (2022). The tectono-stratigraphic columns show comparative geology of tectono-stratigraphic packages bounded by major thrusts.

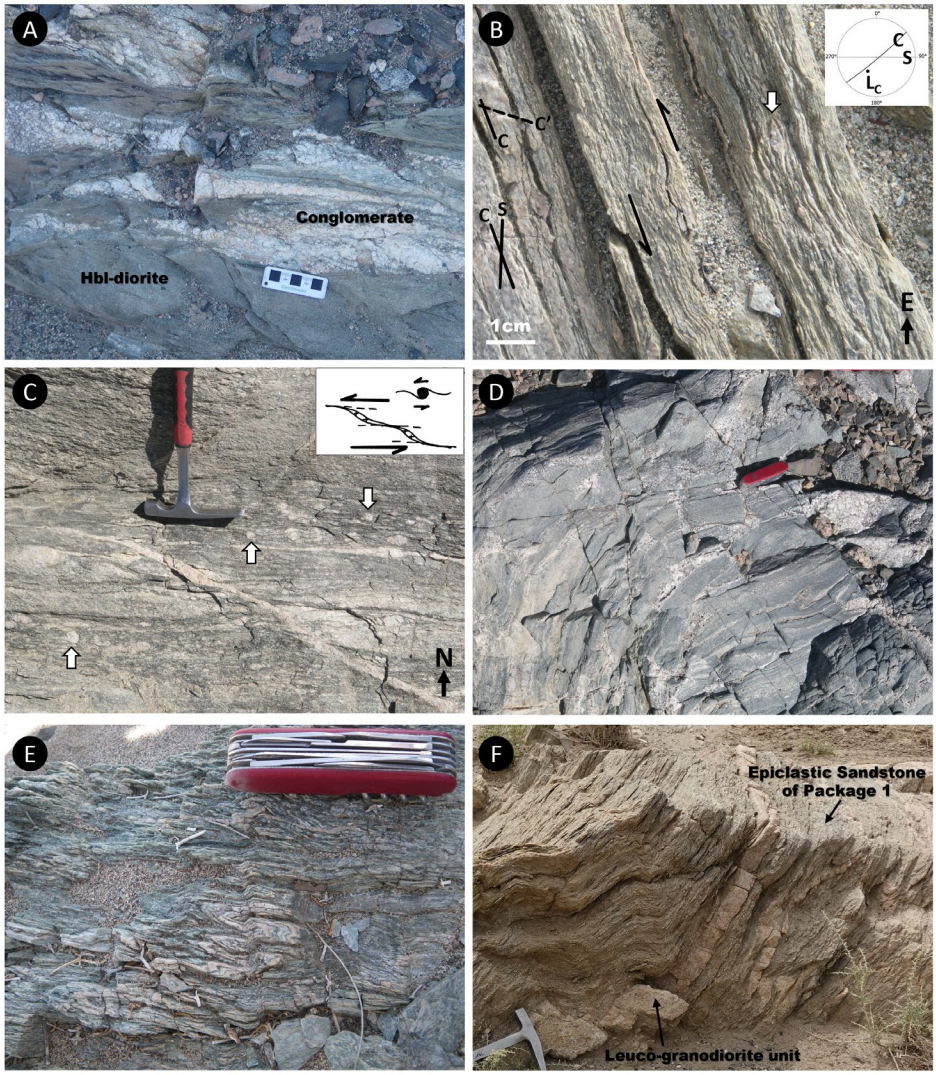


Figure 4-3: Field photos of Baidunzi Complex rocks.

Baidunzi Complex rocks showing cross-cutting relationships and kinematic senses. A) Strongly foliated diorite sill complex with numerous lenses of polyphase deformed grit and conglomerate in the Permian syn-tectonic Baidunzi Intrusive Suite. The conglomerate consists of large granitoid pebbles. B) A strongly foliated volcanogenic sandstone in the Baidunzi-Ganquan shear zone displaying mantled porphyroclasts, C-S fabrics and locally weak C' fabrics, indicative of sinistral kinematics. The inserted sketch shows the measurements indicate an oblique reversal shear with southside up (S0/Sm: 85, 140; Ls: 45, 212; S1: 90, 180). C) A tonalite injected by a quartz-rich granite vein and deformed into gneiss, indicating magma of Baidunzi Intrusive Suite intruded during a progressive deformation with sinistral kinematics in the late stage. D) Diorite melt banded quartzite with smeared-out pegmatite, suggesting syn-kinematic magmatism as melts go through foliated diorite but are also deformed by it. E) Strongly sheared gabbro (green) in the shear zone displays intrafolial folds of transposed foliation. F) A light pink granite of leuco-granodiorite unit intruded along foliation and brittlely deformed.

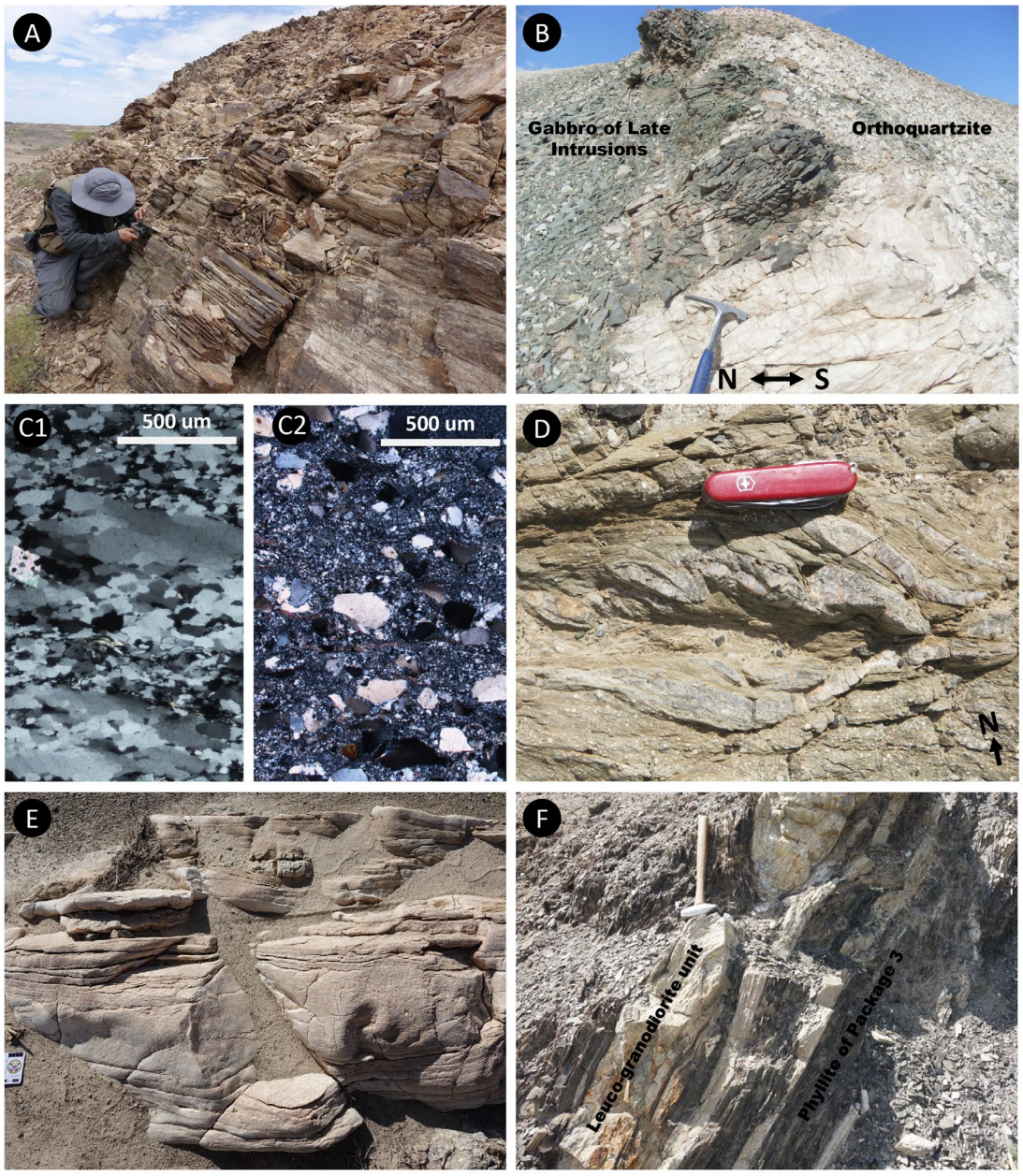


Figure 4-4: Field and petrographic photos of meta-sedimentary rocks.

(A) Bedded quartzite with foliations paralleled to beddings. B) Fault zone bounded by the gabbro of Late Intrusions Suite in the north and the orthoquartzite unit in the south, which also represents the shear zone boundary separated the Ganquan Complex in the north and the Baidunzi Complex in the south. C) Petrographic photo of the orthoquartzite; Petrographic photo of a monomict conglomerate with pebble-sized clasts. D) A quartz-rich granite vein intruded into an epiclastic psammite of package 1. E) Bedded marble of package 2. F) A tonalite of leuco-granitoid unit intruded into a strongly foliated black phyllite of package 3.

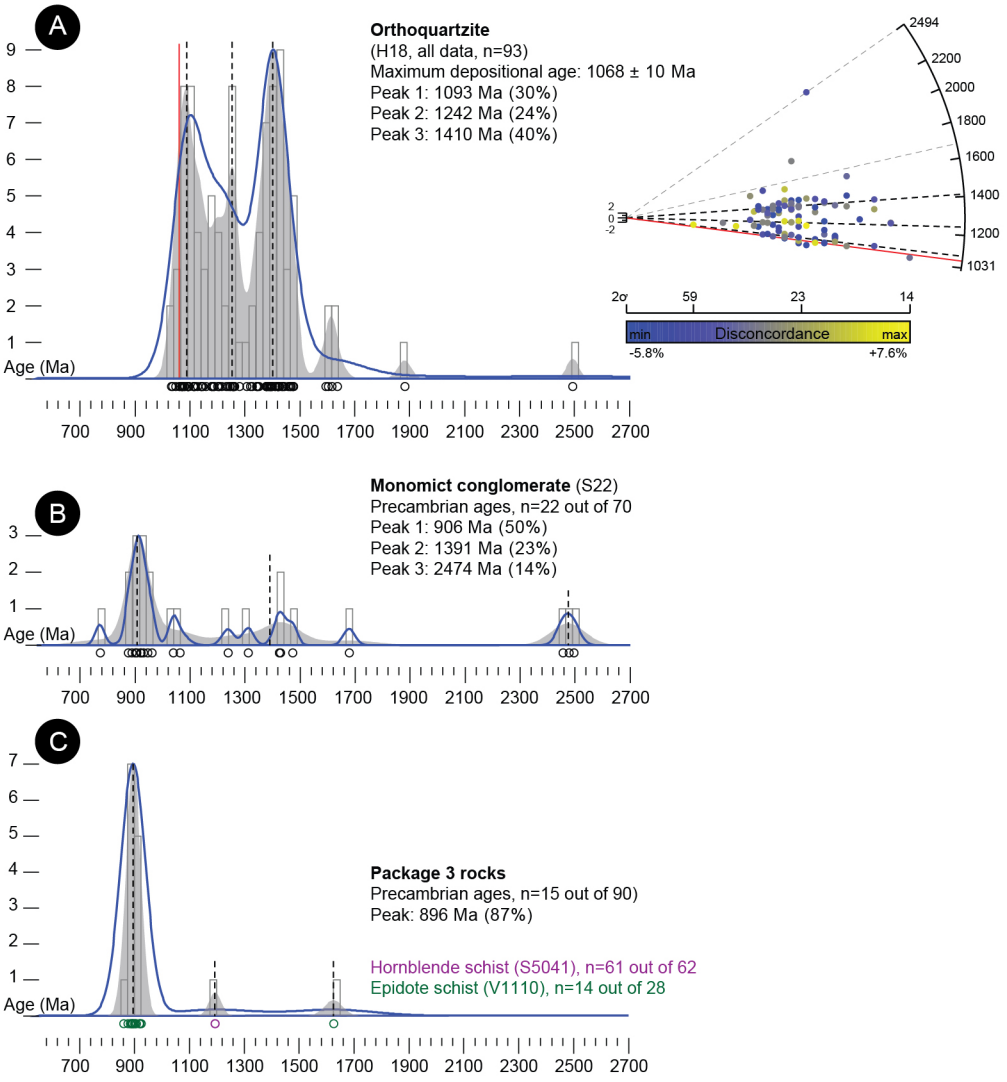


Figure 4-5: Precambrian U-Pb zircon detrital geochronology histograms with KDE plots.

Precambrian U-Pb zircon detrital geochronology histograms with overlain kernel density estimate (KDE) curves (Sircombe and Hazelton, 2004; Vermeesch, 2012) of (A) orthoquartzite, (B) monomict conglomerate, (C) meta-sedimentary rocks of package 3 rock units. Included in (A) are radial plots (Galbraith, 1990) of analytical error values and maximum depositional age (red line) estimated using the maximum likelihood algorithm model of Galbraith and Laslett (1993) and Galbraith (2005).

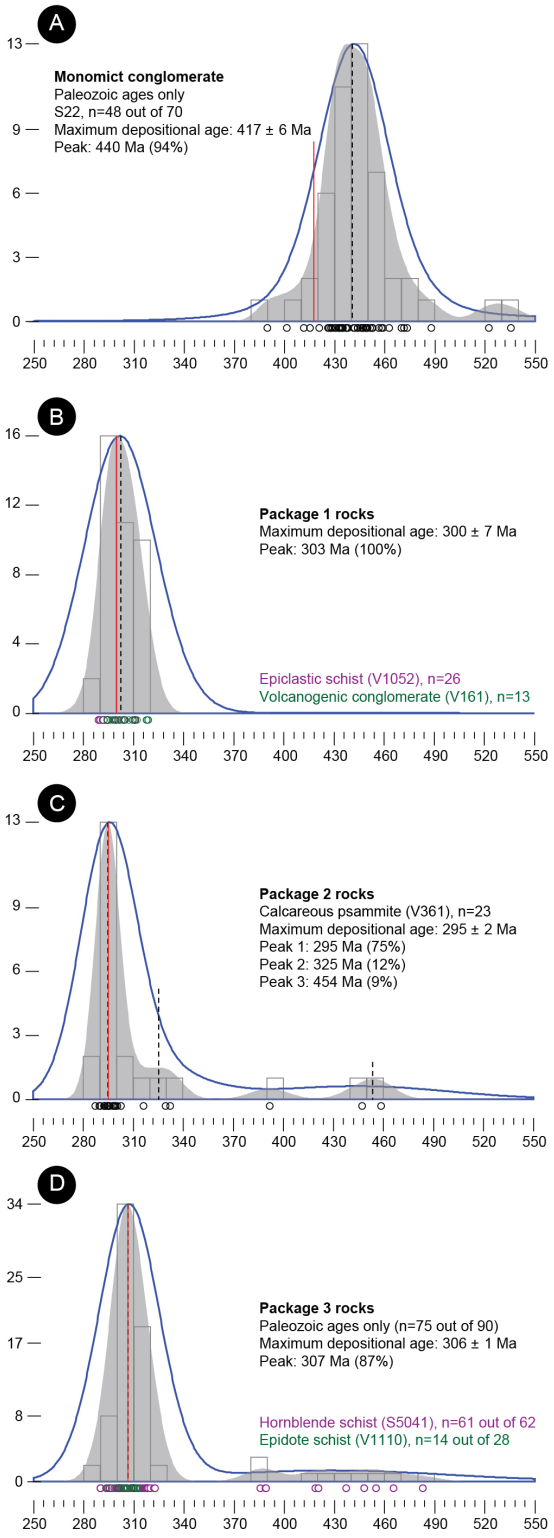


Figure 4-6: Paleozoic U-Pb zircon detrital geochronology histograms.

The Paleozoic U-Pb zircon detrital geochronology histograms with overlain kernel density estimate (KDE) curves (Sircombe and Hazelton, 2004; Vermeesch, 2012) of (A) monomict conglomerate, (B-D) meta-sedimentary rocks of package 1-3 rock units. The red line illustrates the estimation of the maximum depositional age using the maximum likelihood algorithm model of Galbraith and Laslett (1993) and Galbraith (2005).

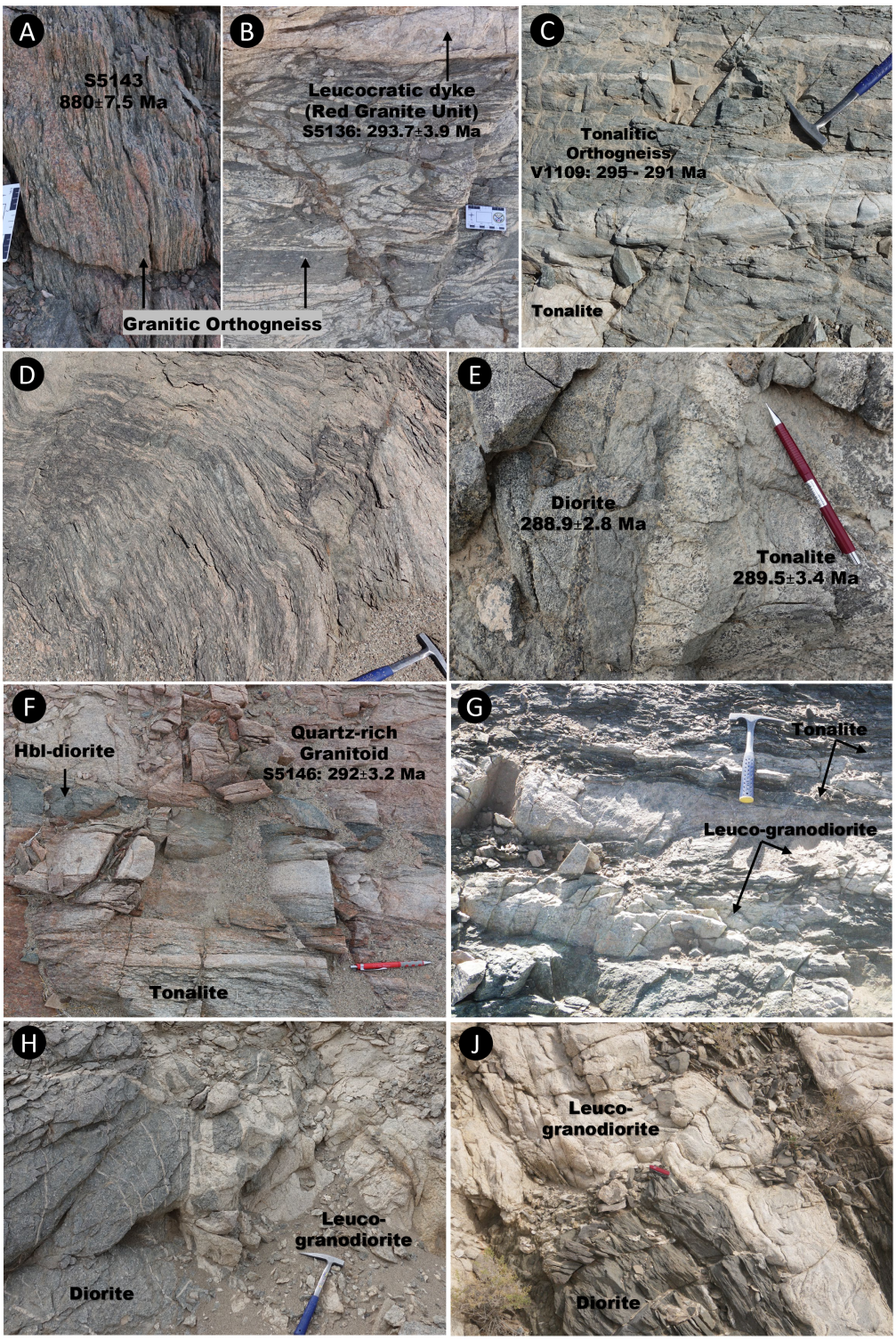


Figure 4-7: Field photos showing meta-plutonic units and their cross-cutting relations in the Baidunzi Complex.

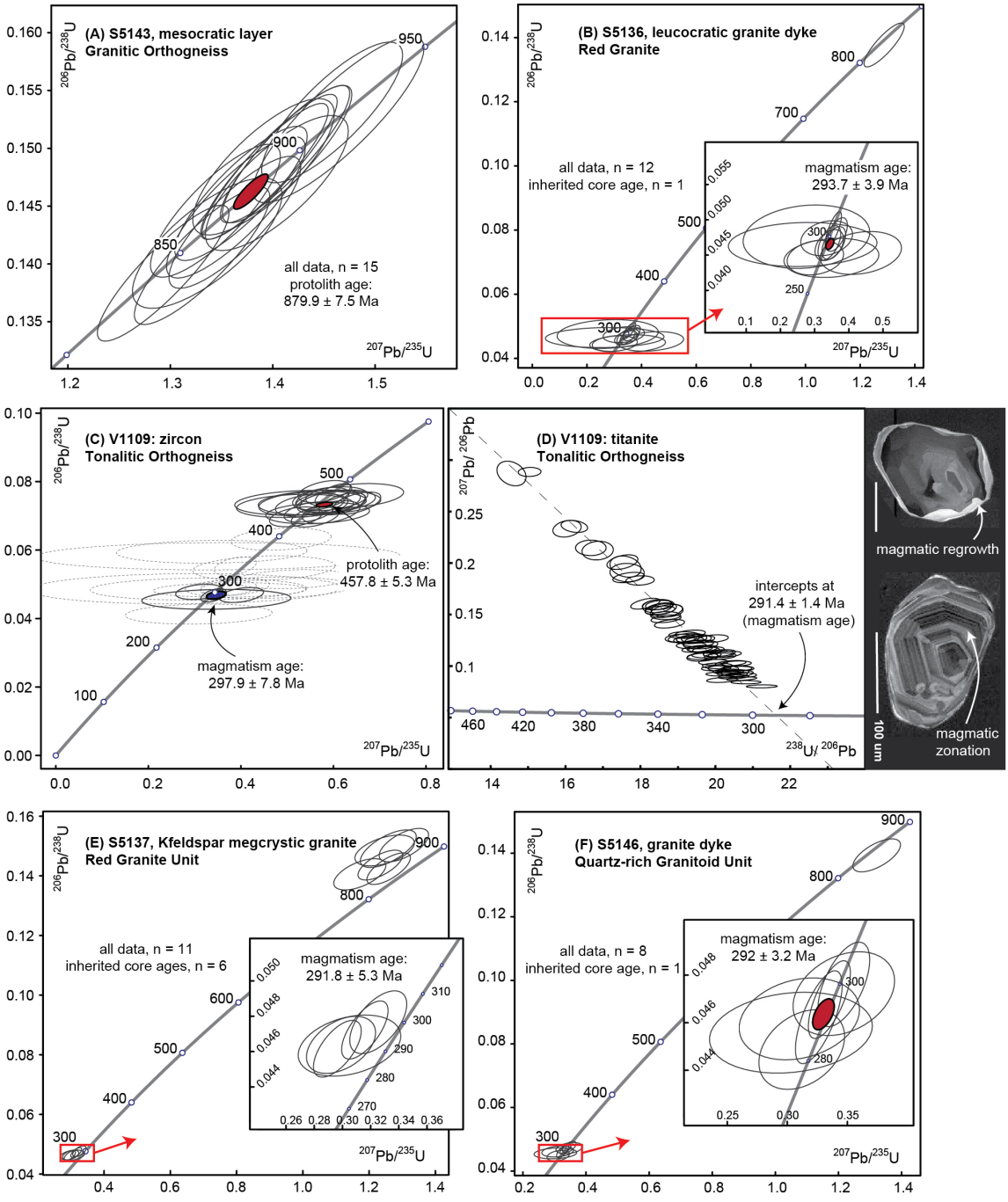
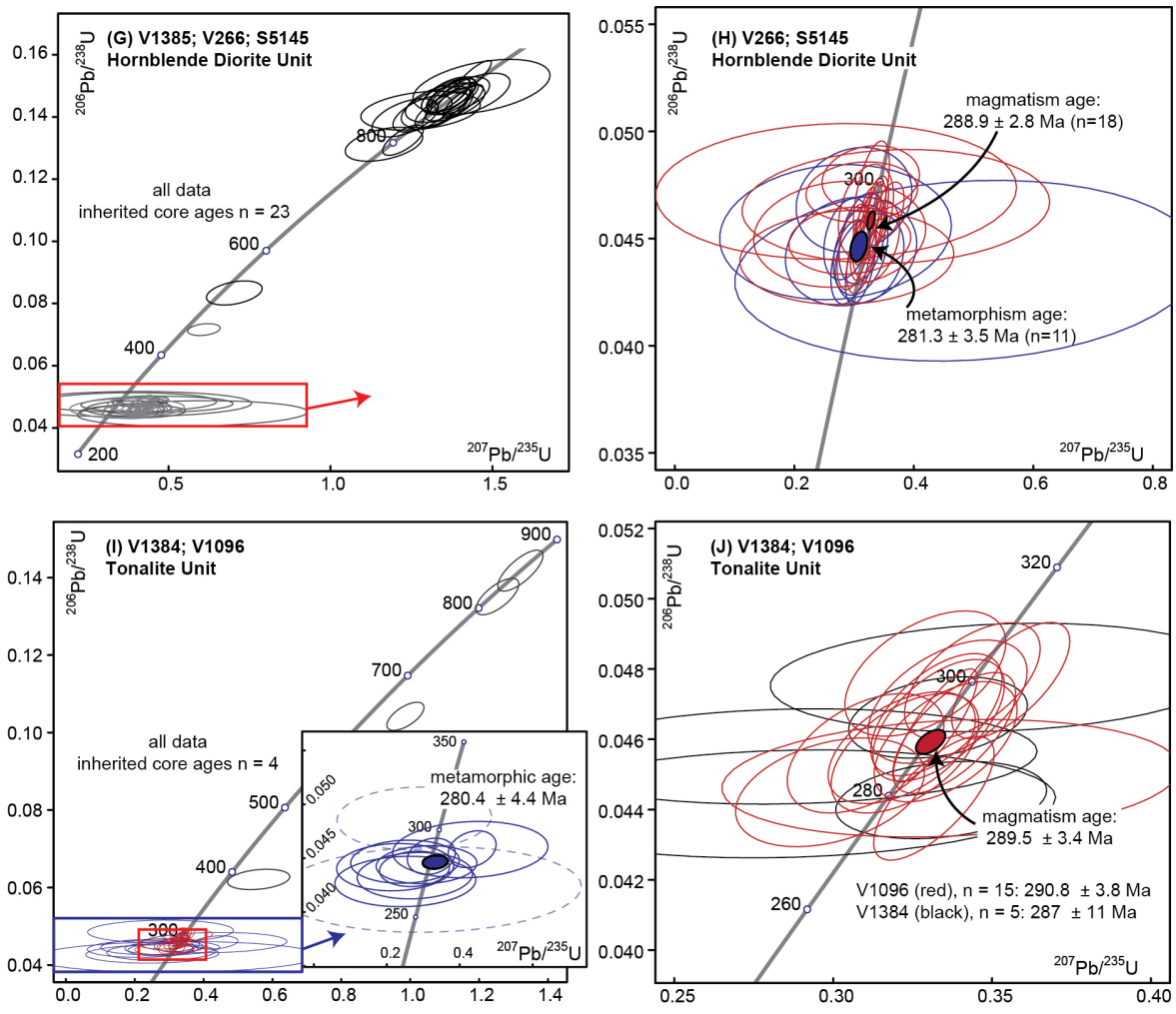


Figure 4-8: Concordia plots showing crystalline age results of orthogneiss and Baidunzi Intrusive Suite rocks.

Concordia plots showing crystalline age results of meta-plutonic rock units in the Orthogneiss and Baidunzi Intrusive Suite. Data circles (e.g., Fig. 8H) separated to blue and red-line groups to represent metamorphic and magmatic ages, respectively. Red rectangle inserted in Fig. 8I is zoomed in to Fig. 8J, and data circles in black and red represent different samples.

(**Figure 4-8** continued.)



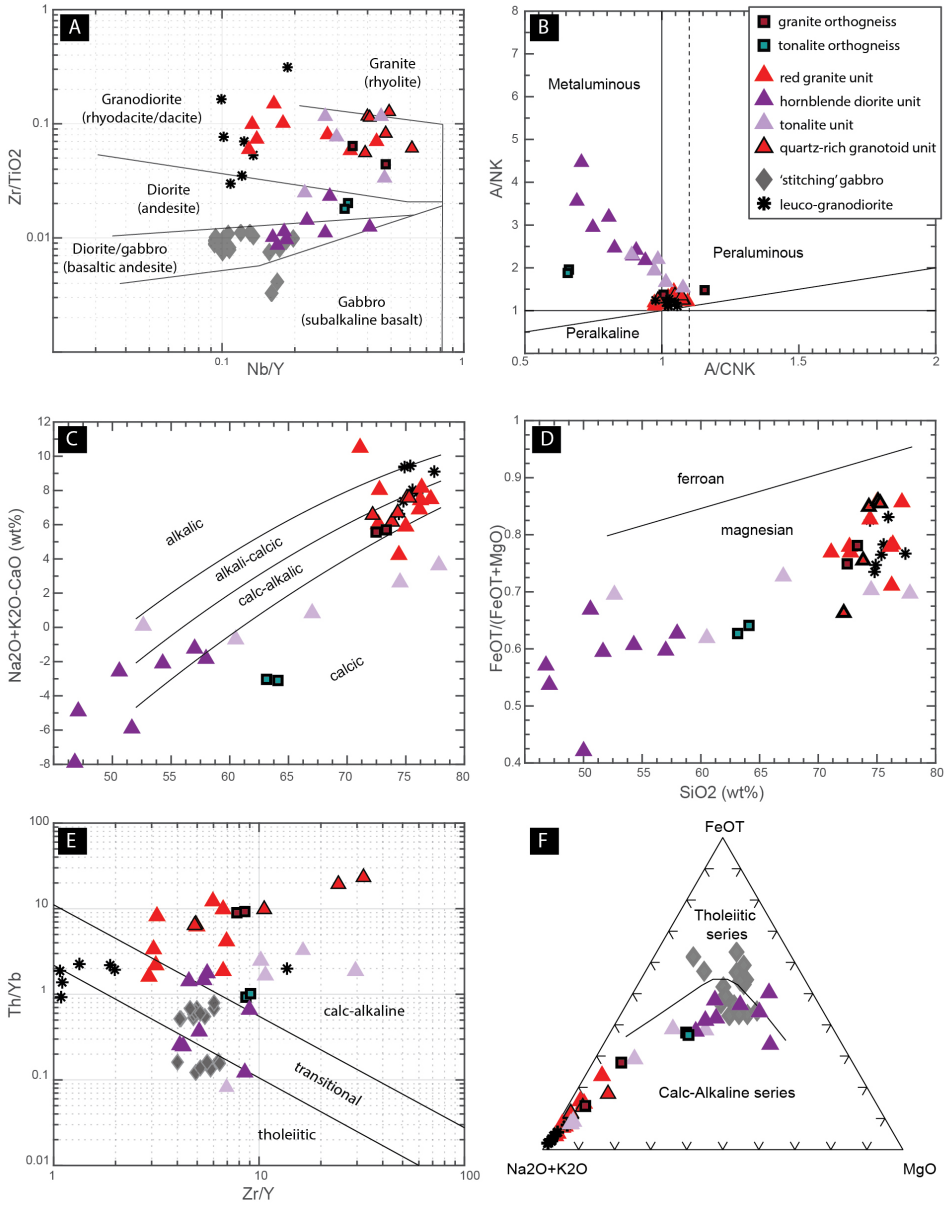


Figure 4-9: Major element geochemical plots of rock units from the Orthogneiss, Baidunzi Intrusive Suite and Late Intrusive Suite. Geochemical plots showing magma series and tectonic discriminations of rocks in the Orthogneiss, Baidunzi Intrusive Suite and Late Intrusion Suite. (A) Zr/TiO2 vs. Nb/Y classification diagram of Winchester and Floyd (1977). (B) A/NK vs. A/CNK plot (molar ratio of Al2O3/(Na2O+K2O) vs molar ratio of Al2O3/(CaO+Na2O+K2O)), aluminum saturation index (ASI), after Irvine and Baragar (1971). (C-D) The MALI (modified alkali-lime index) and Fe-index classification diagram from Frost et al. (2001, 2016). (E) Th/Yb vs. Zr/Y diagram for discrimination of magmatic affinities, after Ross and Bedard (2009). (F) The AFM diagram (relative proportions of the oxides of alkalis, iron, and magnesium) for discrimination of magmatic series by Irvine and Baragar (1971).

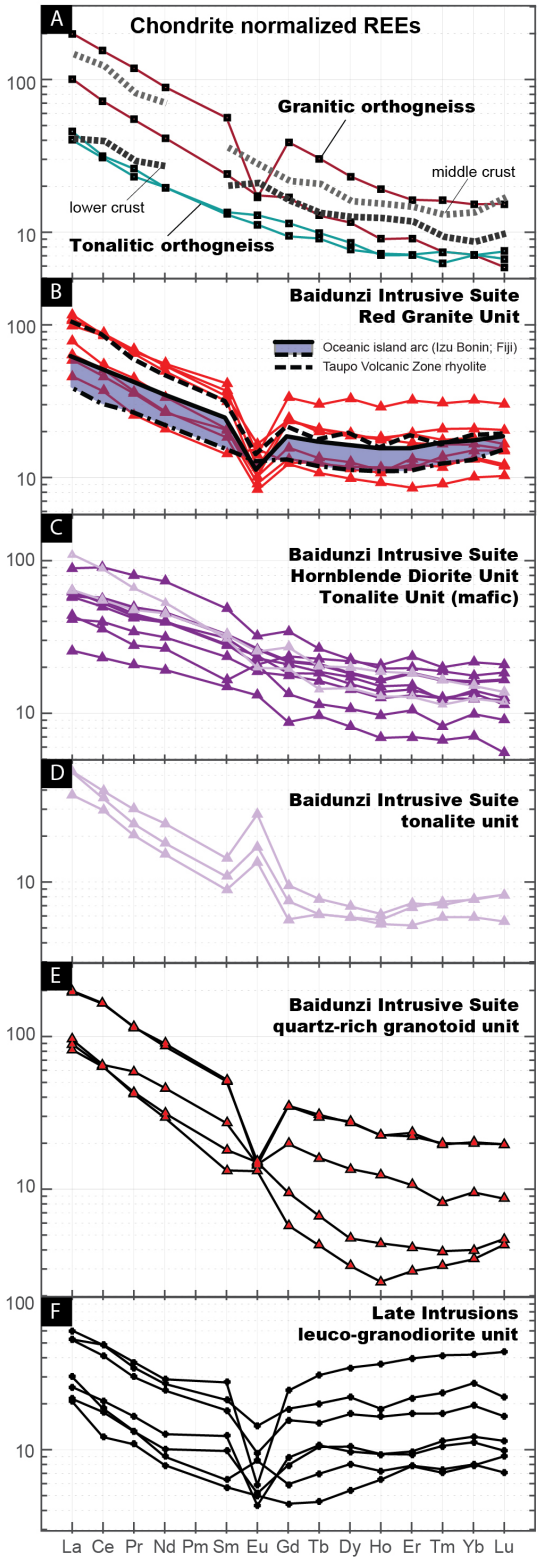


Figure 4-10: Chondrite normalized REE trace element patterns of rocks in the Orthogneiss, Baidunzi Intrusive Suite and Late Intrusion Suite.

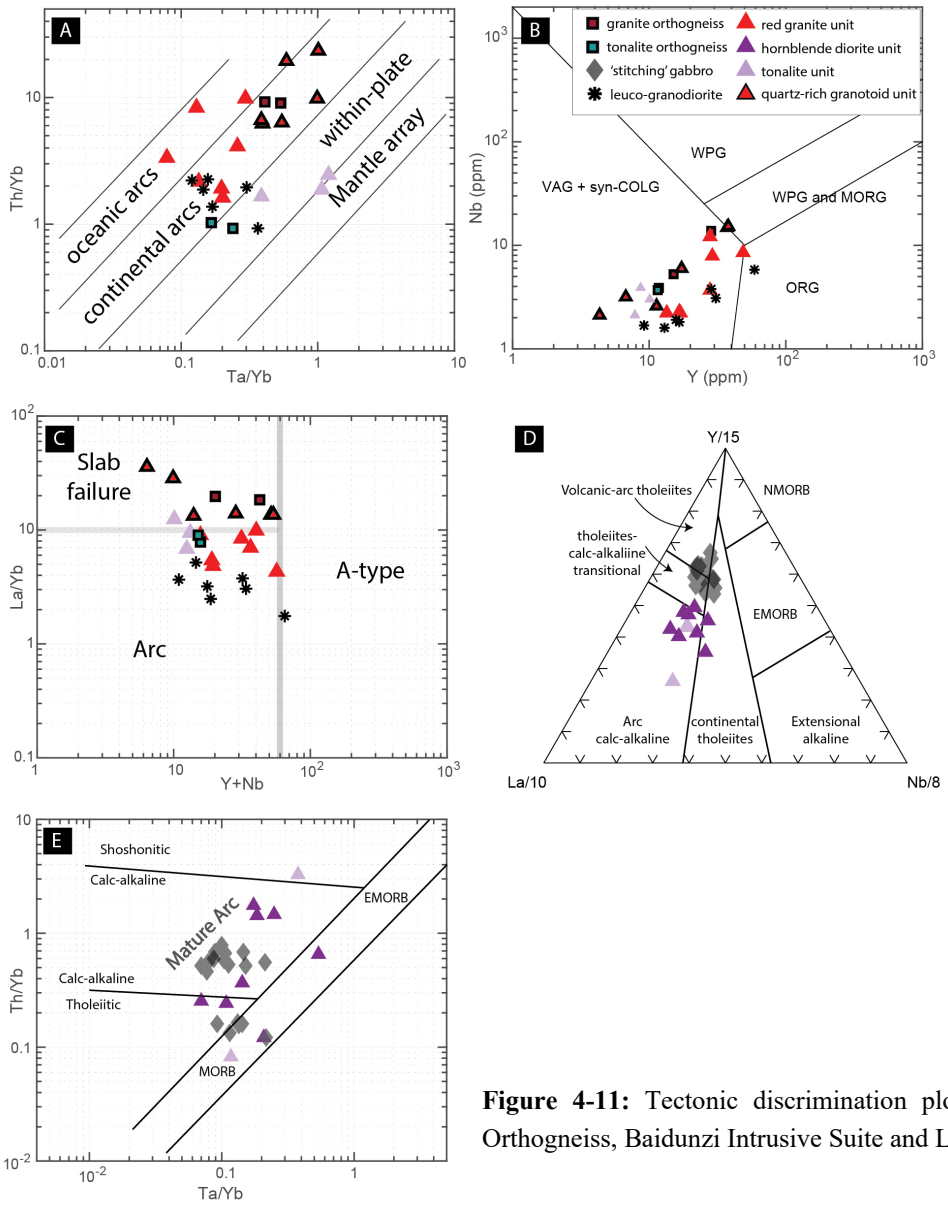


Figure 4-11: Tectonic discrimination plots of rocks in the Orthogneiss, Baidunzi Intrusive Suite and Late Intrusion Suite.

(A) Log-log plot of Th/Yb vs Ta/Yb (after Pearce 1984; 2005). (B) Selected tectonic discrimination diagrams of Pearce et al. (1984; 1996) for felsic rocks. Log-log plot of Nb vs Y. (C) Selected tectonic discrimination diagrams of Whalen & Hilderbrand (2019). Log-log plot of La/Yb vs (Y+Nb), all other plots of Whalen & Hilderbrand (2019) gave similar results, plotting in the arc field. (D) La/10 vs Y/15 vs Nb/8 ternary discrimination diagram (Cabanis and Lecolle, 1989) that shows mafic sample data. (E) Log-log plot of Th/Yb vs Ta/Yb (after Pearce 1984; 2005) for mafic sample data.

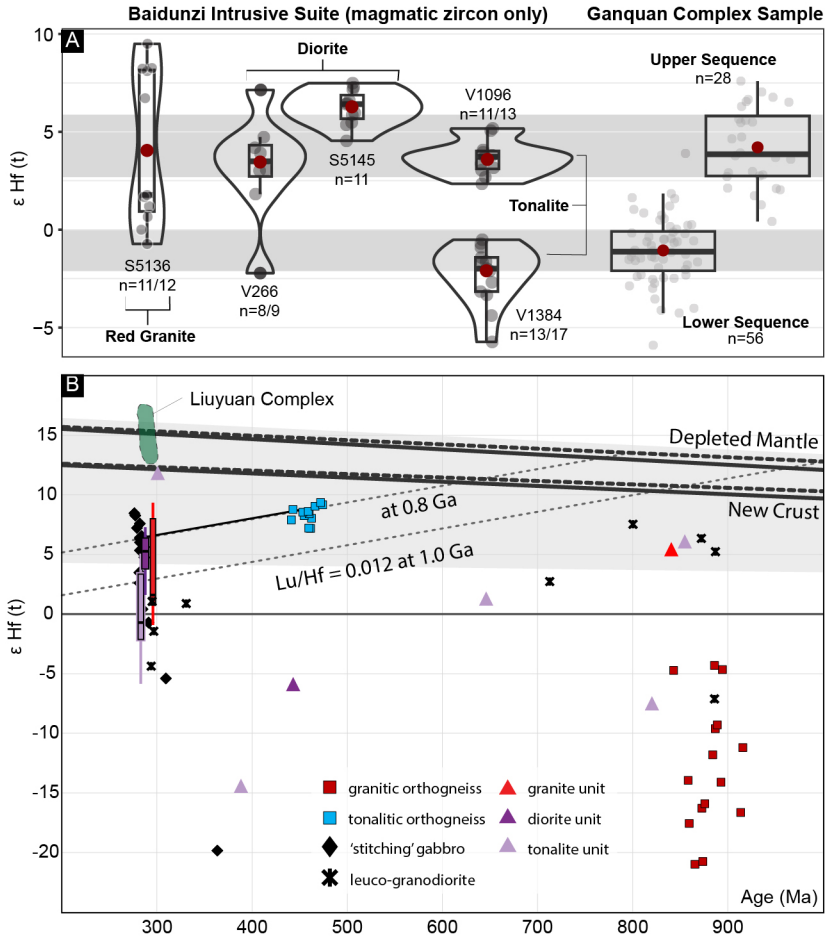


Figure 4-12: Hf isotope analytical results of igneous rocks from Baidunzi Intrusive Suite. (A) Box-violin plots of εHf (t) values showing distribution of εHf (t) spread of individual magmatic samples in Baidunzi Intrusive Suite and grouped volcanic and plutonic samples of Lower and Upper Sequences from Ganquan Complex (Hong et al., 2023). Robust type is used as the statistical approach to display sample spreads, with a confidence level at 95% (1 std). The red centrality point represents the trimmed mean value at a trim level of 0.2. (B) εHf (t) vs. single-grain zircon U-Pb age for all analyzed rocks from the Baidunzi Complex (inherited and magmatic). Symbols as in Fig. 9. Captured or inherited zircon data are displayed as individual symbols, and magmatic crystalline zircons are grouped together and displayed as error bar for each rock unit. The evolved model arc crustal trajectory is an isotopic reservoir with 176Lu/177Hf = 0.012 (Attia et al., 2020; Wooden et al., 2013). The Hf isotope evolution lines for arc mantle array, new crust and depleted mantle are obtained from Iizuka et al. (2010), Dhuime et al. (2011, 2012), and Griffin et al. (2000) and plotted back to the CHUR value (Bouvier et al., 2008) at either 3.8 Ga or 4.55 Ga. Liuyuan Complex basalt values are from Santos (2022) and Yu et al. (2022).

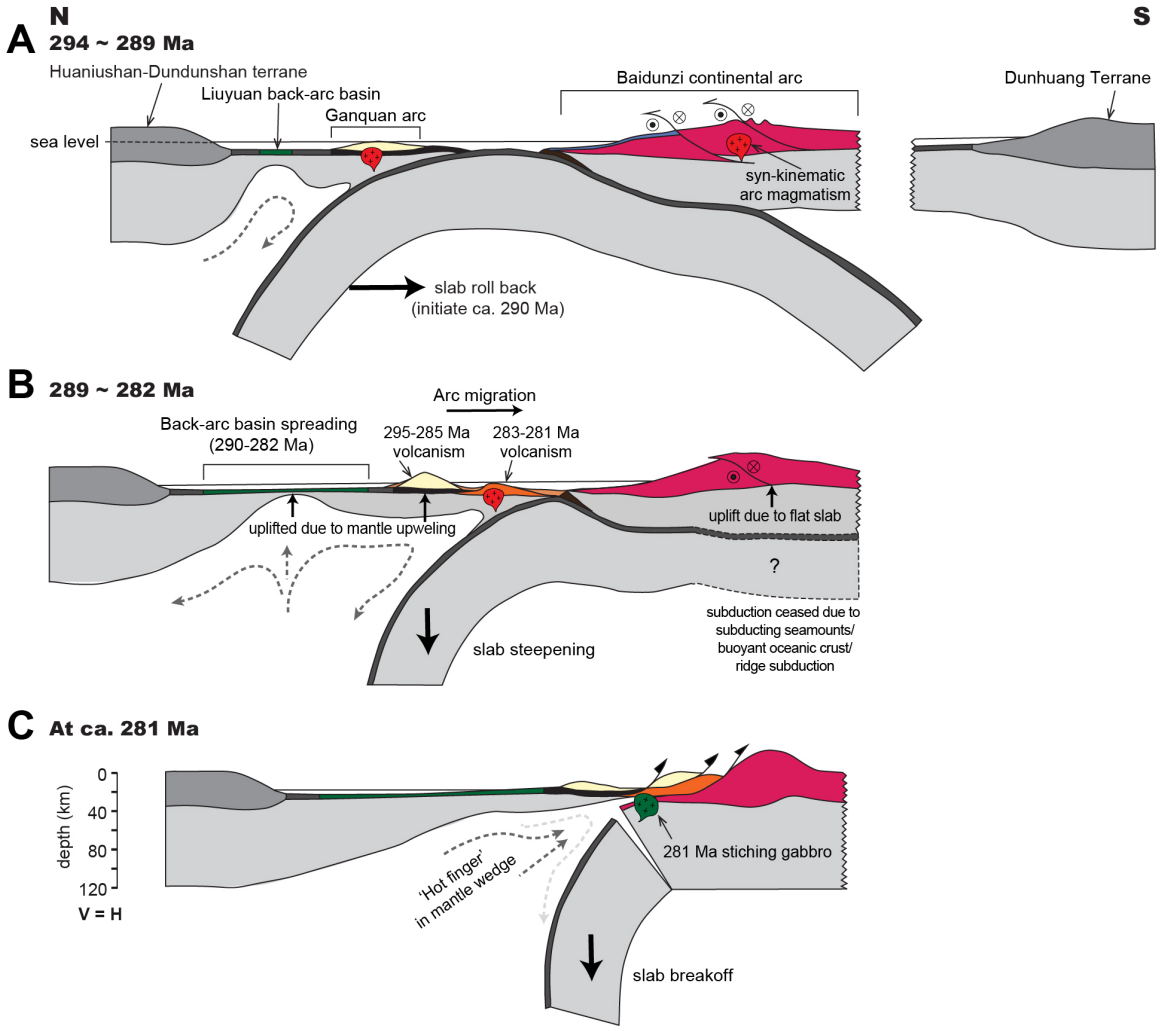


Figure 4-13: Cross section sketch for the proposed tectonic model of the coeval doubly vergent subduction scenario.

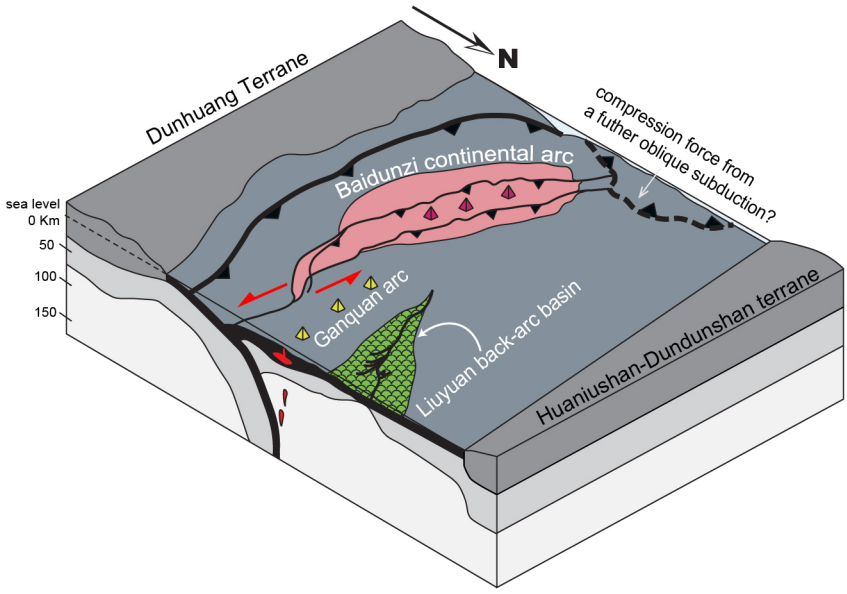


Figure 4-14: Block diagram sketch for the proposed tectonic model of the along-strike north-dipping subduction scenario in Late Carboniferous to Early Permian (ca. 294-289 Ma).

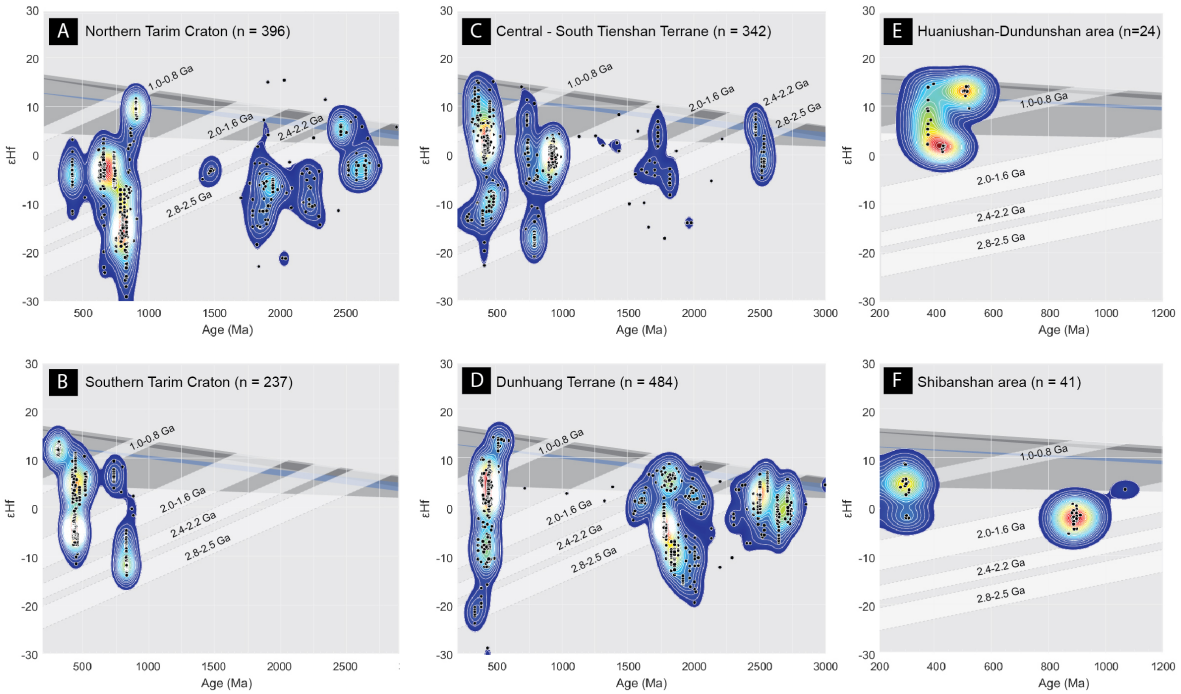


Figure 4-15: Epsilon Hf(t) versus age plots for crystalline, captured or inherited zircons of Archean to Triassic igneous rocks, from northern and southern Tarim Craton.

(A-B), Central-South Tienshan Terrane (C) and Dunhuang Terrane (D). (E-F) Epsilon Hf(t) versus age plots for crystalline, captured or inherited zircons of Mesoproterozoic to Triassic igneous rocks from Huaniushan-Dundunshan and Shibanshan terranes. Data sources are referenced in Data Repository of supplementary materials. The evolved model arc crustal assailant is an isotopic reservoir with 176Lu/177Hf = 0.012, and depleted mantle model age ranges correspond to the characteristic age ranges of continental crust in northern Tarim Craton (2.8-2.5 Ga), southern Tarim Craton (2.4-2.2 Ga) and Dunhuang Terrane (2.0-1.6 Ga), and the Grevillian ages during the Rodina assembly to breakup transition (1.0-0.8 Ga) (Wen et al., 2017; Zhao et al., 2019; Zhao et al., 2018).

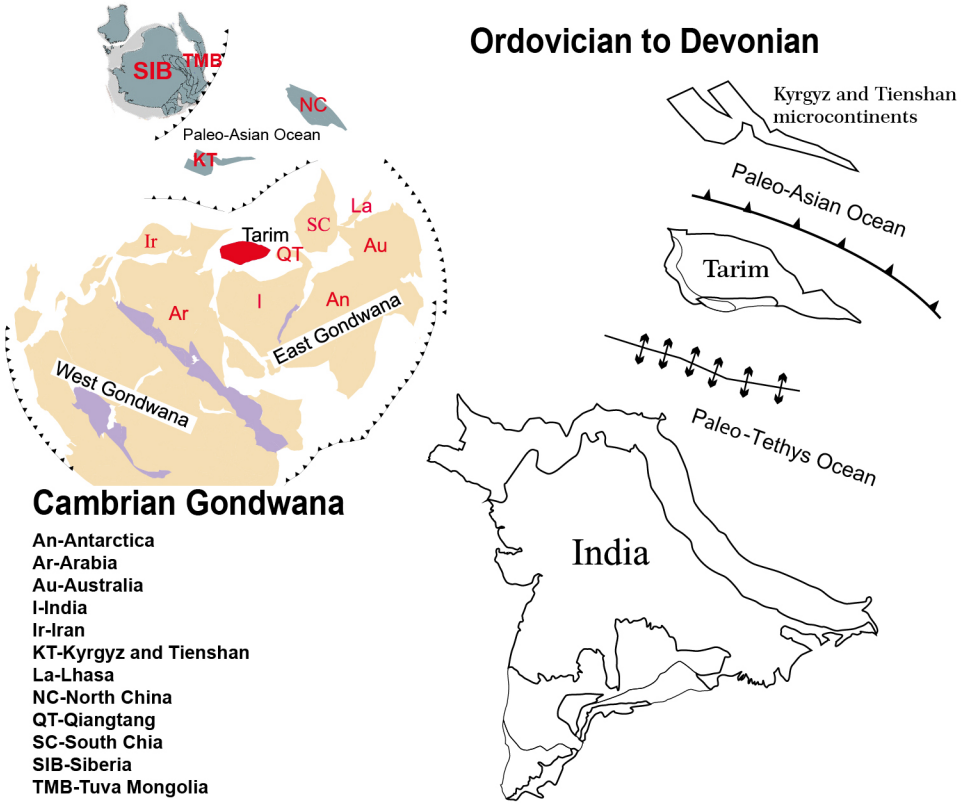


Figure 4-16: Sketch showing Gondwana breakup in Ordovician to Early Devonian.

Sketch showing Gondwana breakup in Ordovician to Early Devonian, resulting in opening of the Paleo-Tethys Ocean in south of the Tarim Craton, and active continental and island arc magmatism along the Kazahstan and Dunhuang block and in the Paleo-Asian Ocean in north of the Tarim Craton. Inserted displays GPlates reconstruction of Gondwana at ca. 500 Ma from Merdith et al. (2021).

Chapter 5: Summary of Conclusions

5.1 Summary

This thesis has focused on clarifying the Late Paleozoic tectono-magmatic history of the southern Beishan orogen before terminal orogenesis. In previous chapters the tectonic history of the Liuyuan BOC has been discussed, with particular reference to the proposed Liuyuan suture zone that separates the Huaniushan-Dundunshan and Shibanshan terranes. In this concluding chapter the main observations and interpretations from the thesis are summarized, and a framework of the Late Paleozoic tectonic history that focuses on the amalgamation of the multiple distinct arc-complexes in the southern Beishan is reviewed below.

5.1.1 Geology and tectonics of the Ganquan Complex

- The Ganquan Complex, a Permian volcanic complex, was identified within the Shibanshan continental terrane. Detailed field investigations revealed the presence of significant unconformities and thrust contacts, resulting in the division of the volcanic complex into distinct lower and upper sequences.
- The lower sequence, forming the volcano-plutonic lithodeme, is primarily composed of felsic volcanic rocks and subvolcanic intrusions of biotite granite. Notably, this lithodeme lacks continental-derived clastic sedimentary rocks. U-Pb zircon geochronology studies failed to demonstrate the presence of zircon inheritance, thereby providing precise volcanic emplacement dates ranging from 295 to 285 Ma.
- In contrast, the upper sequence is comprised of red beds and volcano-sedimentary lithodeme, both characterized by epiclastic sedimentary layers containing felsic volcanic clasts from previous volcanic activity or neighboring volcanoes. U-Pb detrital geochronology and Hf data

further affirmed that the volcano-plutonic lithodeme underlying the red bed lithodeme likely served as the source for the volcanogenic component in its sedimentary rocks. The observed thrust between the volcano-sedimentary and volcano-plutonic lithodemes validated the conclusion that the volcanism in the upper sequence was not built upon on the lower sequence. U-Pb geochronology studies of rocks from the upper sequence yielded consistent results, pinpointing the volcanic events between 283 and 281 Ma.

- Both the lower and upper sequences of the Ganquan Complex exhibit geochemical signatures characteristic of an island arc. The magmatic zircons found in these sequences display mantle-like δ18O values. Their U-Pb zircon ages range between 295 and 286 Ma and between 283 and 281 Ma, with corresponding εHf values varying from -4.2 to +1.9 and from +1.3 to +7.6, respectively, indicating a more juvenile magma source overtime.
- The Ganquan Complex of arc characteristics can be temporally and tectonically correlated with the neighboring back-arc ophiolitic rocks within the Liuyuan Complex. Collectively, these units are interpreted as components of an arc-back arc system. The initiation of back-arc opening is attributed to slab steepening and rollback processes. The observed progression of increasingly juvenile isotopic signatures within the Ganquan arc material is indicative of arc-trench migration, which gradually distanced the arc from the influence of an older arc basement contaminant.

5.1.2 Geology and tectonics of the Baidunzi Complex

- The multidisciplinary study integrates field observations with geochronological, geochemical, and isotopic analyses, leading to the identification of a Permian transpressional continental arc terrane, referred to as the Baidunzi Complex. This complex comprises a diverse assemblage of variably sheared and isoclinally folded metasedimentary and syn-kinematic plutonic rocks, which have undergone transformation into upper greenschist to amphibolite tectonites.

- The oldest rock found in the Baidunzi Complex is a unit of thick-bedded orthoquartzite. This unit exhibits no age signatures younger than 1.0 billion years, leading to the interpretation that it may represent basement rocks. Notably, the prevalent presence of Tonian-aged zircons within the orthoquartzite, as well as in the inherited zircon populations of the Baidunzi Intrusive Suite and Late Intrusive Suite rocks, suggest the Tarim Craton as the most plausible source region.
- The younger metasedimentary strata within the Baidunzi Complex encompass a diverse lithological assemblage, including volcaniclastic sedimentary rocks, marble, marl, interlayered psammite, and schist. The presence of young detrital zircon populations within these strata indicates a Kasimovian to Asselian maximum depositional age range of 306 to 295 Ma. This stratigraphic composition, coupled with the presence of basement fragments, serves as a key distinguishing factor, setting the Baidunzi Complex apart from the temporally overlapping adjacent Ganquan Complex.
- The Baidunzi Intrusive Suite encompasses hornblende diorite, tonalite, granodiorite, and granite with crystallization ages ranging from 294 to 289 Ma. They exhibit characteristics consistent with a continental arc tectonic setting for the Baidunzi Complex. These features include petrological attributes, pervasive zircon inheritance, trace element signatures, and a broad spectrum of $\varepsilon Hf(t)$ values spanning from -3 to +7.
- The late intrusive rocks including dykes and sills of leuco-granite to trondhjemite and a stitching gabbro unit, emplaced syn to post-tectonic with respect to the juxtaposition of the Baidunzi and Ganquan Complexes, sets amalgamation age at 281–280 Ma between the Baidunzi continental arc and the previously defined Ganquan island arc.
- The spatial and temporal connection between the Baidunzi continental arc and the Liuyuan backarc-Ganquan arc suggests two potential scenarios: either they developed within a coeval

doubly vergent subduction system or were products of the same north-vergent subduction system and subsequently structurally juxtaposed through continuing sinistral oblique convergence.

- The combined geochronological and Hf isotope evidence, coupled with the overall continental characteristics of the rock assemblages, suggests a close relationship between the Baidunzi Complex and the northern margin of the Tarim Craton. This relationship is integral to the understanding of the Gondwana breakup and the assembly of the Pangea supercontinent.

5.1.3 Structural amalgamation and syn-tectonic formation of Heishankou Basin

- The comprehensive geological and structural investigations of the Liuyuan BOC have revealed the presence of 6 structural panels and 5 distinct tectono-stratigraphic packages. From south to north these comprise the Shiyaozi Complex, the Baidunzi Complex, the Ganquan Complex, the Heishankou Basin and the Liuyuan Complex. The Heishankou Basin has provided valuable insights into the amalgamation history of the Liuyuan BOC.

- The geological makeup of the Heishankou Basin comprises a marine flysch-like sequence within the Heishankou Formation, characterized by an overall fining-upward trend, and deposition of a syn-tectonic sequence, represented by the Liuyuan conglomerate synthem.

- The Heishankou basin sediments share most of the polyphase deformation (D2 and D3) present in the Liuyuan, Ganquan, and Baidunzi complexes, although they lack the oldest structures which are exclusively observed in the Baidunzi Complex (D1).

- The lower members of the Heishankou Formation were deposited syn-tectonically during the uplift and exhumation of Ganquan and Baidunzi Complexes, representing an intramontane basin.

- The basin likely started forming as a foredeep during late D2, prior to southward thrusting of the Liuyuan Complex over the assembled units in D1 and/or D2. A pivotal aspect of this basin's

evolution is marked by the deposition of the Liuyuan conglomerate synthem, which is primarily characterized by the accumulation of detrital material eroded from the exposed Liuyuan Complex and the lower Heishankou Formation. This depositional phase aligns with the later stages of basin construction and signifies the point at which the Liuyuan Complex breached sea level, marking a critical transition in the basin's history.

- D2 deformation in the Heishankou Basin sedimentary rocks resembles a fold-and-thrust belt style of deformation, with imbricate thrusts, antiformal stacks, and local hanging wall cutoff's forming ramps. These features were partially overprinted or re-folded by the north-verging D3 when the Shiyaozi Complex accreted to the composite Ganquan-Baidunzi terrane.
- The deformation history of the Liuyuan Beishan Orogenic Collage (BOC) unravelled a complex tectonic evolution: The syn-D1 arc magmatism of the Baidunzi Intrusive Suite was emplaced within a transpressional tectonic setting. This phase was succeeded by the stepwise accretion of multiple segments of the Ganquan Arc and Liuyuan back-arc basin with the Baidunzi Complex, delineating a protracted period of south-verging D2 deformation. Accretion of the Liuyuan Complex followed accretion of the Ganquan arc and was achieved by terminal closure of the Liuyuan back-arc basin by north-directed subduction, which led to the establishment of an intermediate foreland basin during the late D2 deformation phase. This multiphase geological evolution culminated in the amalgamation and collision with the Shiyaozi Complex from the south, which in turn led to overprinting by the north-verging D3 deformation.

5.2 Future work

- **Extending the southern cross-section: Incorporating the Shiyaozi Complex**

Tectonic evolution of the poorly understood Shiyaozi Complex remains a gap in the regional tectonic model. Further field investigations are imperative to unravel its magmatic, structural, and metamorphic evolutionary history. These studies should aim to determine whether the Shiyaozi Complex could potentially serve as a continental basement from a specific source, providing insights into its possible connection to the Dunhuang Terrane. Moreover, such findings could significantly contribute to our understanding of the Late Permian to Triassic terminal orogenesis within the Central Asian Orogenic Belt (CAOB).

- **The missing strike-slip motions?**

Preserved crustal material in the Beishan Orogen and the broader southern CAOB exhibits penetrative transpressive deformation related to oblique convergence during subduction, collision, or accretion (He et al., 2021; Cleven, 2016; Yang et al., 2022). It is essential to investigate the role of strike-slip motion when modeling the late stages of collision and accretion in orogenesis. Many tectonic models have focused on the collision and attachment of terranes without considering the significant lateral transport of these terranes. This lateral motion may have a profound impact on the overall tectonic evolution and the formation of the present tectonic framework in the southern CAOB. Further exploration along shear zones in the Beishan Region to investigate the major transportation involved is warranted for a better understanding of regional tectonics.

- **Overestimation of juvenile continental growth?**

The CAOB has long been regarded as a significant accretionary orogen responsible for substantial continental growth. This perception primarily relies on the abundant Mesozoic and Paleozoic granitoid plutons characterized by low initial Sr isotopic ratios, positive εNd values, and young model ages (Jahn et al., 2000a; Jahn et al., 2000b). These granitoid plutons were thought to result from the melting of depleted mantle sources, contributing significantly to continental growth

during orogenesis (Jahn, 2004). However, mounting evidence suggests that many Mesozoic granitoids may be too young to be directly linked to the CAOB's evolution, and there are indications of significant volumes of pre-orogenic basement rocks and reworked basement signatures within arc complexes (Kröner et al., 2014).

This thesis explores the preservation of Precambrian basement fragments (Chapter 4) and characterizes radiogenic εHf values (< +10) in island and continental arcs (Chapter 3 and 4), indicating their lesser juvenile nature in comparison to depleted mantle sources (+12 to +15). The potential modeling of crustal reworking and mantle melting during magmatism is an intriguing avenue to explore, particularly in light of the high-resolution bedrock map available within the Baidunzi Complex (see published map in the Appendix). The findings could be important to refine the estimation of the predominant juvenile domains formed during orogenesis and to reassess the associated high rate of continental growth.

- **Incorporation of regional tectonic model into supercontinent cycles**

The Beishan Orogen preserved orthogneiss and paragneiss bodies dating from the late Stenian to early Tonian periods (1050 – 870 Ma, Liu et al., 2015), which potentially constitute Precambrian basement materials. These formations may be associated with the main Peri-Rodina accretion event (Song et al., 2015; Ge et al., 2016; Zhao et al., 2018; Soldner et al., 2020). Zhao et al. (2018) have highlighted the Ordovician to Devonian high-grade metamorphic rocks in the central parts of the Beishan Orogen, which highlights the earliest Early Paleozoic orogenic cycle linked to the assembly of Gondwana-derived micro-blocks. Conversely, Late Carboniferous to Permian high-grade metamorphic rocks in the southern Beishan Orogen serve as evidence for the second orogenic cycle, which is associated with the final closure of the Paleo-Asian Ocean and the amalgamation of Pangea.

Unfortunately, most regional tectonic models of the Beishan Orogen and the broader Central Asian Orogenic Belt have yet to be incorporated into the context of global supercontinent cycles and its components linked to potential source cratons. Integrating these interpretations and placing them within an evolving paleogeographic context would significantly contribute to constructing a more comprehensive framework for assembly of supercontinents such as Pangea.

References

Allen, M. B., B. F. Windley, and Z. Chi, 1992: Palaeozoic collisional tectonics and magmatism of the Chinese Tien Shan, central asia. Tectonophysics, 220, 89–115.

Anonymous. (1997). China Geological Map of the Tianshan and adjacent areas: 1: 1 000 000. Geology Publishing House, (in Chinese).

BGMRG, 1997. Stratigraphy (Lithostratic) of Gansu Province. China University of Geosciences Press, Wuhan, 314 pp. (in Chinese).

BGMRG (Bureau of Geology and Mineral Resources of Gansu Province), 2005. Report of 1: 250,000 Regional Geological Survey of Anxi (K47C004001) (in Chinese).

Chen, C.-M., H.-F. Lu, D. Jia, D.-S. Cai, and S.-M. Wu, 1999: Closing history of the southern Tianshan oceanic basin, western China: an oblique collisional orogeny. Tectonophysics, 302, 23–40.

Chen, S., Guo, Z., Qi, J., Zhang, Y., Pe-Piper, G., & Piper, D. J. (2016). Early Permian volcano-sedimentary successions, Beishan, NW China: Peperites demonstrate an evolving rift basin. Journal of Volcanology and Geothermal Research, 309, 31-44.

Cleven, N. R., Lin, S., Xiao, W., Davis, D. W., & Davis, B. (2018). Successive arc accretion in the southern Central Asian orogenic belt, NW China: Evidence from two Paleozoic arcs with offset magmatic periods. Bulletin of the Geological Society of America, 130(3–4), 537–557.

Cleven, N. R. (2016). Paleozoic transpressional tectonics in the Beishan orogenic collage, Northwest China: Evolution of the Hongliuhe suture zone. PhD thesis. UWSpace. http://hdl.handle.net/10012/10190

Fedorova, N. M., Levashova, N. M., Bazhenov, M. L., Meert, J. G., Sergeeva, N. D., Golovanova, I. v., Danukalov, K. N., Kuznetsov, N. B., Kadyrov, A. F., & Khidiyatov, M. M. (2013). The East European Platform in the late Ediacaran: New paleomagnetic and geochronological data. Russian Geology and Geophysics, 54(11), 1392–1401.

Filippova, I. B., Bush, V. A., & Didenko, A. N. (2001). Middle Paleozoic subduction belts: The leading factor in the formation of the Central Asian fold-and-thrust belt. Russian Journal of Earth Sciences, 3(6), 405–426.

Gao, J., M.-S. Li, X.-C. Xiao, Y.-Q. Tang, and G.-Q. He, 1998: Paleozoic tectonic evolution of the Tianshan Orogen, northwestern China. Tectonophysics, 287, 213–231.

Ge, R., Zhu, W., & Wilde, S. A. (2016). Mid‐Neoproterozoic (ca. 830–800 Ma) metamorphic P‐T paths link Tarim to the circum‐Rodinia subduction‐accretion system. Tectonics, 35(6), 1465-1488.

Gladkochub, D. P., Donskaya, T. v., Fedorovsky, V. S., Mazukabzov, A. M., Larionov, A. N., & Sergeev, S. A. (2010). The Olkhon metamorphic terrane in the Baikal region: An Early Paleozoic collage of Neoproterozoic active margin fragments. Russian Geology and Geophysics, 51(5), 447–460.

Guo, Q., Xiao, W., Windley, B. F., Mao, Q., Han, C., Qu, J., Ao, S., Li, J., Song, D., & Yong, Y. (2012). Provenance and tectonic settings of Permian turbidites from the Beishan Mountains, NW China: Implications for the Late Paleozoic accretionary tectonics of the southern Altaids.

Han, Y., & Zhao, G. (2018). Final amalgamation of the Tianshan and Junggar orogenic collage in the southwestern Central Asian Orogenic Belt: Constraints on the closure of the Paleo-Asian Ocean. Earth-Science Reviews, 186, 129-152.

He, Z. Y., Klemd, R., Yan, L. L., & Zhang, Z. M. (2018). The origin and crustal evolution of microcontinents in the Beishan orogen of the southern Central Asian Orogenic Belt. Earth-Science Reviews, 185(May), 1–14.

He, Z., Wang, B., Ni, X., De Grave, J., Scaillet, S., Chen, Y., ... & Zhu, X. (2021). Structural and kinematic evolution of strike-slip shear zones around and in the Central Tianshan: Insights for eastward tectonic wedging in the southwest Central Asian Orogenic Belt. Journal of Structural Geology, 144, 104279.

Hong, T., Santos, G. S., van Staal, C. R., Ji, W., & Lin, S. (2022). Mapping uncovered a multi-phase arc—back-arc system in southern Beishan during the Permian. National Science Review. .org/10.1093/nsr/nwac204

Jahn, B. M., Fuyuan, W. U., & Hong, D. (2000a). Important crustal growth in the Phanerozoic: Isotopic evidence of granitoids from east-central Asia. Proceedings of the Indian Academy of Sciences, Earth and Planetary Sciences, 109(1), 5–20.

Jahn, B. M., Wu, F., & Chen, B. (2000b). Massive granitoid generation in Central Asia: Nd isotope evidence and implication for continental growth in the Phanerozoic. Episodes, 23(2), 82–92.

Jahn, B. M. (2004). The Central Asian Orogenic Belt and growth of the continental crust in the Phanerozoic. Geological Society Special Publication, 226(1), 73–100.

Jin, S.Q., 1974. Subdivision and correlation of the lower Carboniferous of the Beishan region, Gansu. Acta Geol. Sin. 2, 159–174 (in Chinese with English abstract).

Khain, E. v., Bibikova, E. v., Kröner, A., Zhuravlev, D. Z., Sklyarov, E. v., Fedotova, A. A., & Kravchenko-Berezhnoy, I. R. (2002). The most ancient ophiolite of the Central Asian fold belt: U-Pb and Pb-Pb zircon ages for the Dunzhugur Complex, Eastern Sayan, Siberia, and geodynamic implications. Earth and Planetary Science Letters, 199(3–4), 311–325.

Kröner, A., Kovach, V., Belousova, E., Hegner, E., Armstrong, R., Dolgopolova, A., Seltmann, R., Alexeiev, D. v., Hoffmann, J. E., Wong, J., Sun, M., Cai, K., Wang, T., Tong, Y., Wilde, S. A., Degtyarev, K. E., & Rytsk, E. (2014). Reassessment of continental growth during the accretionary history of the Central Asian Orogenic Belt. Gondwana Research, 25(1), 103–125.

Kröner, A., Windley, B. F., Badarch, G., Tomurtogoo, O., Hegner, E., Jahn, B. M., ... & Wingate, M. T. D. (2007). Accretionary growth and crust formation in the Central Asian Orogenic Belt and comparison with the Arabian-Nubian shield.

Kröner, A., Alexeiev, D.V., Rojas-Agramonte, Y., Hegner, E., Wong, J., Xia, X., Belousova, E., Mikolaichuk, A.V., Seltmann, R., Liu, D., Kiselev, V.V., 2013. Mesoproterozoic (Grenville-age) terranes in the Kyrgyz North Tianshan: zircon ages and Nd–Hf isotopic constraints on the origin and evolution of basement blocks in the southern Central Asian Orogen. Gondwana Research 23, 272–295.

Kröner, Alfred, & Rojas-Agramonte, Y. (2014). The Altaids as seen by Eduard Suess, and present thinking on the late Mesoproterozoic to Paleozoic evolution of central Asia. Austrian Journal of Earth Sciences, 107(1), 156–168.

Kuzmichev, A. B., & Larionov, A. N. (2013). Neoproterozoic island arcs in East Sayan: Duration of magmatism (from U-Pb zircon dating of volcanic clastics). Russian Geology and Geophysics, 54(1), 34–43.

Laurent-Charvet, S., J. Charvet, L.-S. Shu, R.-S. Ma, and H.-F. Lu, 2002: Palaeozoic late collisional strike-slip deformations in Tianshan and Altay, Eastern Xinjiang, NW China. Terra-Nova, 14, 249–256.

Levashova, N. M., Degtyarev, K. E., Bazhenov, M. L., Collins, A. Q., & Van der Voo, R. (2003). Middle Paleozoic paleomagnetism of east Kazakhstan: post-Middle Devonian rotations in a large-scale orocline in the central Ural–Mongol belt. Tectonophysics, 377(3-4), 249-268.

Liu, Q., Zhao, G., Sun, M., Eizenhöfer, P. R., Han, Y., Hou, W., ... & Xu, B. (2015). Ages and tectonic implications of Neoproterozoic ortho-and paragneisses in the Beishan Orogenic Belt, China. Precambrian Research, 266, 551-578.

Mao, Q., Xiao, W., Windley, B. F., Han, C., Qu, J., Ao, S., Zhang, J., & Guo, Q. (2012). The Liuyuan complex in the Beishan, NW China: a Carboniferous–Permian ophiolitic fore-arc sliver in the southern Altaids. Geological Magazine, 149(3), 483–506. DOI:10.1017/S0016756811000811

McKerrow, W. S., Scotese, C. R., & Brasier, M. D. (1992). Early Cambrian continental reconstructions. Journal - Geological Society (London), 149(4), 599–606.

Meert, J. G., & Lieberman, B. S. (2008). The Neoproterozoic assembly of Gondwana and its relationship to the Ediacaran-Cambrian radiation. In Gondwana Research (Vol. 14, Issues 1–2, pp. 5–21).

Niu, Y., Liu, C., Shi, G. R., Lu, J., Xu, W., & Shi, J. (2018). Unconformity-bounded Upper Paleozoic megasequences in the Beishan Region (NW China) and implications for the timing of the Paleo-Asian Ocean closure. Journal of Asian Earth Sciences, 167, 11-32. https://doi.org/10.1016/j.jseaes.2018.06.019

Niu, W., Ren, B., Duan, L., Xin, H., Zhao, Z., Zhang, G., & Zhang, Y. (2020). 1 ： 50 000 Regional Geological Map Database of the Qinghegou Map-sheet, Inner Mongolia. Geology in China, 47(1), 106 – 118.

Rytsk, E. Y., Kovach, V. P., Yarmolyuk, V. v., Kovalenko, V. I., Bogomolov, E. S., & Kotov, A. B. (2011). Isotopic structure and evolution of the continental crust in the East Transbaikalian segment of the Central Asian Foldbelt. Geotectonics, 45(5), 349–377.

Şengör, A. M. C., Natal'In, B. A., & Burtman, V. S. (1993). Evolution of the Altaid tectonic collage and Palaeozoic crustal growth in Eurasia. Nature, 364(6435), 299–307.

Şengör, A. M. C., Natal'In, B. A., & Burtman, V. S. (1993). Evolution of the Altaid tectonic collage and Palaeozoic crustal growth in Eurasia. Nature, 364(6435), 299–307.

Suess, E. (1901). Das antlitz der erde (B. Dritter & H. Erste, Eds.; Vol. 3). F. Tempsky.

Suess, E. (1908). The Face of the Earth (Das Antlitz Der Erde) (W. J. Sollas & H. B. C. Sollas, Eds.; Vol. 3). Clarendon Press.

Song, D., Xiao, W., Han, C., Tian, Z., & Wang, Z. (2013). Provenance of metasedimentary rocks from the Beishan orogenic collage, southern Altaids: constraints from detrital zircon U–Pb and Hf isotopic data. Gondwana Research, 24(3-4), 1127-1151.

Song, S., Wang, M. M., Xu, X., Wang, C., Niu, Y., Allen, M. B., & Su, L. (2015). Ophiolites in the Xing'an - Inner Mongolia accretionary belt of the CAOB: Implications for two cycles of seafloor spreading and accretionary orogenic events. Tectonics, 34(10), 2221-2248.

Tian, Z., & Xiao, W. (2020). An Andean-type arc transferred into a Japanese-type arc at final closure stage of the Palaeo-Asian Ocean in the southernmost of Altaïds. Geological Journal, 55(3), 2023–2043. https://doi.org/10.1002/GJ.3700

Tian, Z., Xiao, W., Sun, J., Windley, B. F., Glen, R., Han, C., Zhang, Z., Zhang, J., Wan, B., Ao, S., & Song, D. (2014). Triassic deformation of Permian Early Triassic arc-related sediments in the Beishan (NW

China): Last pulse of the accretionary orogenesis in the southernmost Altaids. Tectonophysics, 662, 363–384. https://doi.org/10.1016/J.TECTO.2015.01.009

Wang, Y. U., Luo, Z., Santosh, M., Wang, S., & Wang, N. A. (2017). The Liuyuan Volcanic Belt in NW China revisited: evidence for Permian rifting associated with the assembly of continental blocks in the Central Asian Orogenic Belt. Geological Magazine, 154(2), 265-285.

Windley, B. F., M. B. Allen, C. Zhang, Z.-Y. Zhao, and G.-R. Wang, 1990: Palaeozoic accretion and Cenozoic redeformation of the Chinese Tien Shan range, Central Asia Earth Planetary Science Letters, 45, 326–336.

Windley, B. F., Alexeiev, D., Xiao, W., Kroner, A., & Badarch, G. (2007). Tectonic models for accretion of the Central Asian Orogenic Belt. Journal of the Geological Society, 164(1), 31–47.

Xiao, W., Windley, B. F., Hao, J., & Zhai, M. (2003). Accretion leading to collision and the Permian Solonker suture, Inner Mongolia, China: Termination of the central Asian orogenic belt. Tectonics, 22(6).

Xiao, W.J., L. Zhang, K.-Z. Qin, S. Sun, J., and Li, L., (2004): Paleozoic accretionary and collisional tectonics of the eastern Tianshan (China): implications for the continental growth of Central Asia. American Journal of Science, 304, 370–395.

Xiao, W.-J., B. F. Windley, C. Yuan, M. Sun, C.-M. Han, S.-F. Lin, H.-L. Chen, Q.-R. Yan, D.-Y. Liu, K.-Z. Qin, J.-L. Li, and S. Sun, (2009): Paleozoic multiple subduction accretion processes of the southern Altaids. American Journal of Science, 309, 221–270.

Xiao, W. J., Mao, Q. G., Windley, B. F., Han, C. M., Qu, J. F., Zhang, J. E., Ao, S. J., Guo, Q. Q., Cleven, N. R., Lin, S. F., Shan, Y. H., & Li, J. L. (2010). Paleozoic multiple accretionary and collisional processes of the Beishan orogenic collage. American Journal of Science, 310(10), 1553–1594.

Xiao, W., Windley, B. F., Sun, S., Li, J., Huang, B., Han, C., Yuan, C., Sun, M., & Chen, H. (2015). A Tale of Amalgamation of Three Permo-Triassic Collage Systems in Central Asia: Oroclines, Sutures, and Terminal Accretion. Annual Review of Earth and Planetary Sciences, 43(1), 477–507.

Yang, G., Li, Y., Tong, L., Wang, Z., Si, G., Lindagato, P., & Zeng, R. (2022). Natural observations of subduction initiation: Implications for the geodynamic evolution of the Paleo-Asian Ocean. Geosystems and Geoenvironment, 1(1), 100009.

Zhang, Y., Yuan, C., Sun, M., Long, X., Xia, X., Wang, X., & Huang, Z. (2015). Permian doleritic dikes in the Beishan Orogenic Belt, NW China: Asthenosphere–lithosphere interaction in response to slab break-off. Lithos, 233, 174-192.

Zhao, G., Wang, Y., Huang, B., Dong, Y., Li, S., Zhang, G., & Yu, S. (2018). Geological reconstructions of the East Asian blocks: From the breakup of Rodinia to the assembly of Pangea. Earth-Science Reviews, 186, 262–286. https://doi.org/10.1016/J.EARSCIREV.2018.10.003

Zuo, G., Liu, Y., Liu, C., 2003. Framework and evolution of the tectonic structure in Beishan area across Gansu Province, Xinjiang Autonomous Region and Inner Mongolia Autonomous Region. Acta Geologica Gansu 12, 1–15 (in Chinese with English abstract).

Appendix

1. Map Sheet of Baidunzi-Heishankou Area
2. Analytical methodologies and data repository of Chapter 3
3. Analytical methodologies and data repository of Chapter 4
4. Chapter 3 Table SM1
5. Chapter 3 Table SM2
6. Chapter 3 Table SM3
7. Chapter 4 Supplementary Table